VEHICLES, GROOMING, AND OTHER FACTORS AFFECTING SNOWROAD LONGEVITY IN YELLOWSTONE NATIONAL PARK

by

Molly McKellar Nelson

A thesis submitted in partial fulfillment
of the requirements for the degree

of

Master of Science

in

Civil Engineering

MONTANA STATE UNIVERSITY
Bozeman, Montana

April 2018

©COPYRIGHT

by

Molly McKellar Nelson

2018

All Rights Reserved

ACKNOWLEDGEMENTS

This study would not have been possible without the entire research team: Ry Phipps, Dr. Ed Adams, Dr. Dan Miller, and Robb Larson. I would especially like to thank Ry Phipps, who shared equally all of the work of the project, from soldering our equipment back together in the field to writing MATLAB codes back at the office. I would like to think Dr. Ed Adams for his guidance, involvement in all aspects of the project, and dedication to making it a success. Robb Larson built multiple custom instruments specifically for this study and ensured that they kept running in a difficult field environment. Dr. Dan Miller provided helpful insight throughout the process.

The National Park Service (NPS) provided funding for this project. I would like to thank Christina White for her support of the project and critical help with logistics. NPS staff throughout the park helped to provide us with resources, from snowmobiles and snowcoaches to assistance with data collection. Snowcoach operators generously donated their time and resources to provide vehicles for us to test. I would also like to thank Dr. Wade Vagias, who initially conceived of this project and encouraged me to consider graduate school.

Finally, I would like to thank my family and friends who have supported me throughout this process; your words of encouragement have been crucial. I am especially grateful to Matt for all of the love, support, and good perspectives provided throughout school. I could not have done it without you. And thanks to Ezzie for being great company during all my typing.

TABLE OF CONTENTS

1. INTRODUCTION 1

Background 1
Statement of Problem 4
Documents Regarding This Study 5

2. LITERATURE REVIEW 7

Snowroad Assessment and Maintenance 7
Snow as a Road Material 7
Snowroad Assessments (and Factors Considered) 12
Factors beyond Control Influencing Snowroad Conditions 15
Grooming Theory and Best Practice 18
Individual Vehicle Impacts on the Road 24
Vehicle Characteristics and Impact 24
Soil/Off-road Surface Characteristics and Impact 29
Types of Impact; How to Measure 33
Most Relevant Studies – Empirical Road Impact 37

3. METHODS 41

Overall Strategy 41
Road Conditions and Grooming – Causal Factors 42
Weather Patterns 42
Site Characteristics 44
Grooming Practices 45
Traffic Patterns 48
Road Conditions and Grooming – Condition Monitoring 49
Hardness 50
Temperature 52
Depth 54
Density 57
Sampling 59
Vehicle Pass-bys 62
Year 1 Pass-by Tests – General Setup 64
Year 2 Pass-by Tests – General Setup 67
Vehicle Loading 72
Subsurface Impacts 75
Surface Impacts 81

TABLE OF CONTENTS CONTINUED

Summary 86

3. Data and Discussion 88

Parkwide Hardness and Contributing Factors 88
Weather 91
Site Characteristics 97
Grooming 103
Traffic 114
Road Conditions – Other Measurements 119
Vehicle Pass-bys – Vehicle Loading 121
Vehicle Pass-bys – Subsurface Impacts 122
Aramis 122
Accelerometers 128
Vehicle Pass-bys – Loading vs. Subsurface Impacts 142
Vehicle Pass-bys – Surface Impacts 143
Quantified (Year 2 Methods) 143
Surface Video Observations 152

3. CONCLUSIONS AND RECOMMENDATIONS 155

General Conclusions 155
Recommendations and Management Implications 159
Suggestions for further Study 160

REFERENCES CITED 162

APPENDICES 169

APPENDIX A: Grooming Data Extraction and Analysis 170
APPENDIX B: Rammsonde Hardness 179
APPENDIX C: Load Cell Processing 186
APPENDIX D: Load Cell Data Sheets 205
APPENDIX E: Aramis 220
APPENDIX F: Accelerometer Processing 223
APPENDIX G: Accelerometer Data Sheets 238
APPENDIX H: Accelerometer cDAQ Data Sheets 255
APPENDIX I: Profilometer Processing 271

LIST OF TABLES

Table Page

1. Year 1 field test days....67

2. Year 2 test days and coaches (Abbreviations: Scenic Safaris (SS); Yellowstone Expeditions (Yell Exp); Buffalo Bus (BB); See Yellowstone (See Yell); Bombardier (Bomb); Teton Science School (TSS))....69

3. Vehicles tested, Year 2....70

4. Year 1 and Year 2 methods comparison....87

5. Maximum accelerations, maximum loads, and rutting recorded for all test vehicles (with highest daily values in red); note that on 1/29/17, the same test track was used for all vehicles, so each individual vehicle did not create a large rut....137

6. Hardening and softening of the road by vehicle type....151

A.1. Test locations, the categories determining which Excel formulas were used to identify groomer passes, and weather station data used for each site....175

A.2. Year 2 hardness test locations, the categories determining which Excel formulas were used to identify groomer passes, and weather station data used for each site....176

A.3. Grooming GPS data available by district and year....178

LIST OF FIGURES

Figure Page

1. Purpose-built and conversion snowcoaches 2

2. Strength of processed snow as a function of time and temperature, with temperature values marked on the appropriate lines (Abele, 1990) 9

3. A snow plane (Photo courtesy of NPS) 18

4. A tracked snowcoach (left), and wheeled/LPT snowcoach (right) 26

5. Shear, T, versus soil distortion, S, in three soil types (Laughery and others 1990) 30

6. Conceptual framework of research strategy 42

7. Weather stations used in this study, labeled (NRCS 2016, labels added) 43

8. Major snowroad grooming districts 46

9. (a), (b), and (c). Park groomers: (a) agricultural tractor (West District), (b) Prinoth groomer with tiller attachment (Old Faithful District), and (c) Prinoth groomers with various other attachments (Grant, Lake, Canyon, and North/ Mammoth Districts) 47

10. (a), (b), and (c). Drags used by groomers: (a) tiller (Old Faithful District), and (b), (c) Mogul Masters (other districts) 47

11. 30° Rammsonde penetrometer used in this study 51

12. Taking measurements with the Ramm penetrometer 52

13. Manual measurement of snowroad depth 55

14. Radar sled to measure snow depth 56

15. Weighing Year 1 density samples 57

LIST OF FIGURES CONTINUED

Figure Page

16. Year 2 density sampling equipment 59

17. (a), (b), and (c). Evolution of snow sampling devices: (a) corers, (b) sawed 60

18. Laboratory setup for compression tests 61

19. MSU Subzero Science and Engineering Research Facility CT scanner 62

20. (a) and (b). Test setup: (a) Year 1, roads throughout park, and (b) Year 2, Grant Village test track 63

21. Year 2 setup changes including separated lanes and additional instrumentation (shown in red boxes) 64

22. Year 2 test track in Grant Village 68

23. Load cell array 73

24. Example of each load cell reading (left) and sum of all load cell readings (right) 74

25. Distance between tires or bogey wheels (top) and time between vertical maximum forces (bottom) used in velocity estimates 75

26. Camera box for subsurface testing 77

27. Spraying a paint speckle pattern onto snow (left); resultant pattern (right) 78

28. Accelerometer orientations 79

29. Accelerometer array placement, February 12th, 2017 80

30. Hidden location for surface video filming 83

31. Marking whiskers used for scale in surface videos 84

LIST OF FIGURES CONTINUED

Figure Page

32. Profilometer 86

33. Hardness profiles throughout park, January 2017 radar trip 89

34. Hardness profiles throughout park, February 2017 radar trip 90

35. Year 1 and Year 2 precipitation compared to 30-year averages (1981-2010) 92

36. Average monthly temperatures, Years 1 and 2 94

37. Hardness vs. cumulative "degree days" at test sites 96

38. (a) and (b). Hardness vs. site elevation in the top (a) 10 cm and (b) 30 cm of the road 98

39. (a) and (b). Hardness versus "northness" of Year 2 site aspects (1 faces due north, -1 faces due south) for the top (a) 10 cm and (b) 30 cm 100

40. Average hardness in the top 10 cm versus site slope, by testing months 101

41. Average hardness in top 20 cm vs. average grooming speed for all months with more than two applicable data points 105

42. Average hardness in top 10 cm vs. time between grooming and hardness test 107

43. Hardness vs. temperature between the last grooming incident and the hardness test 109

44. Hardness vs. average daily precipitation and change in snow depth, Years 1 and 2 111

45. Hardness throughout season by grooming district 114

LIST OF FIGURES CONTINUED

Figure Page

46. Hardness vs. number of snowcoach photos captured by motion-sensor cameras 117

47. Aramis processing showing vertical strain (Feb. 12, 2016, Spring Creek test site) 123

48. Difference in "pressure bulb" for dry and wet soil (Corangamite Catchment Management Authority 2013) 125

49. Camera box positioned parallel to traffic, facing into traffic 126

50. Aramis analysis showing fracture (Mattracks, Jan. 29, 2017, Grant Test Track) 127

51. Acceleration plots versus time: LPT (left) and Bombardier (right) 129

52. Maximum acceleration values (left) and displacement values (right) for each pass, decreasing with depth 130

53. Vertical, longitudinal, and transverse maximum accelerations for different vehicles (Feb. 26, 2017, Grant Test Track); note larger scale for Bombardier 132

54. Maximum vertical acceleration versus vehicle velocity data from February 26, 2017 134

55. Increased tire pressures were associated with increased maximum vertical accelerations 136

56. Maximum vertical, longitudinal, and transverse accelerations caused by vehicles tested on January 29 and February 26 139

57. Vertical displacements at a 10-cm depth calculated from 2/12/2017 accelerometer readings 140

58. Change in vertical velocity direction at a 10-cm depth on 2/12/2017 141

LIST OF FIGURES CONTINUED

Figure Page

59. Area displaced after OSV passes ("#p" on axis label represents the number of passes, area displaced is cumulative for all tests of a given vehicle) 144

60. Cumulative area displaced by tires at different pressures 145

61. Maximum force and area displaced over time on 1/29/2017 146

62. Maximum force and area displaced over time on 2/12/2017 147

63. Maximum force and area displaced over time for a Scenic Safaris LPT coach on 2/27/2017 148

64. Rut depth (hollow outline), depth of the soft layer under the rut (penetrated by the placement of the penetrometer, shown by the grey section), and hardness underneath the soft layer (blue section, with hardness indicated by the graduated blue color bar) 150

65. Screenshot of an LPT traveling approximately 4.5 m/s (10 mph) 153

66. Screenshot of a tracked vehicle traveling approximately 4.5 m/s (10 mph) 154

B.1. Excel template required for input into MATLAB code; top left cell is positioned in Excel cell A1 181

C.1. Pass-by from the NPS LPT courier vehicle; note the high level of noise associated with the measurement 188

C.2. The same pass-by as Figure C.1, but with the Savitzky-Golay filter applied; significantly decreased noise 189

I.1. Profilometer picture processing 272

ABSTRACT

In winter, the National Park Service (NPS) at Yellowstone grooms snow that builds up on the park roads, making "snowroads" passable by snowmobiles and snowcoaches. The NPS has recently allowed experimental snowcoaches on low-pressure tires (LPTs) in addition to traditional tracks. As they consider a permanent policy on these LPTS, they want to understand these vehicles' impacts on snowroads compared with those of traditional tracked vehicles and snowmobiles. They also want to know how to optimize other operations (e.g., grooming) to maintain quality roads that support safe travel through the park.

This two-year field study investigated the snowroad quality in the park and factors influencing this quality. The approach involved data collection on both parkwide road conditions and individual vehicle passes. Both controllable and non-controllable factors were considered to provide information on their relative influence. Parkwide road quality analysis involved collecting GPS data on grooming activity, weather data from existing stations, road depth through radar measurements, traffic counts from motion-sensor cameras, hardness data, and snow sample analysis. The vehicle-by-vehicle impact study involved both subsurface and surface measurements in the road. Load cells, accelerometers, a high-speed, high-definition camera, a penetrometer, and a "profilometer" provided measurements.

Data analysis combined with existing literature provided insights into best practices for the NPS. Parkwide, snowroads harden throughout the season, with temperatures and traffic load being contributing factors. Grooming results in a harder road if snow disaggregation is followed by compaction, and with a longer set time between grooming and traffic. Individual vehicles' impacts are driven by surface interaction rather than motion at depth in the snowroad. On hard, groomed snowroads, both tracked and LPT snowcoaches can form ruts, but tracked vehicles continue to dig ruts deeper whereas LPT coaches' ruts level out and stop deepening with subsequent passes. This seems to be because LPTs form ruts primarily through compaction and tracked vehicles through snow displacement. Reduced tire pressures reduce rut formation and can harden the road.

Results from this study demonstrate that LPT coaches should not be disallowed from Yellowstone based on road impacts. Other results will inform NPS operations to optimize grooming practices.

INTRODUCTION

Background

The National Park Service (NPS) commissioned this study as part of its ongoing effort to use science to inform winter use operations. NPS policies regarding winter use in Yellowstone National Park have been the subject of heated debate since 1997. This controversy has only recently settled due to compromise in the Final Rule published in 2013. The rule instituted an adaptive management plan reliant on using best available science to inform policy. As operators work under this new paradigm and suggest ideas for improved technology that will make the park cleaner and quieter, the NPS is evaluating possible new technology for potential impacts on park resources like snowroads. The quality of the snowroads can have an impact on the safety of winter operations for park visitors and staff.

Each winter, Yellowstone National Park maintains approximately 320 kilometers of snowroads to support administrative and commercial snowmobile and snowcoach (collectively, oversnow vehicles or OSVs) use in the park. Snowroads are primary mainline roads in the interior of the park which, after accumulating sufficient snowfall, are packed and groomed flat by groomers or agricultural tractors towing a leveling and grooming device. Snowcoaches have been purpose-built for oversnow driving, but are most typically vans and mid-sized shuttle busses equipped with track systems (usually “Mattracks”) or large, low-pressure tires for floatation and propulsion on the snowroads (Figure 1). During the

last ten years, reports from park staff and OSV operators have indicated an increase in occurrence of ruts in the snowroads. These ruts can create dangerous driving conditions which compromise visitor experience and safety. Anecdotal reports indicate that ruts can range in depth up to over 20 cm.

Figure 1. Purpose-built and conversion snowcoaches

The National Park Service (NPS) started studying this issue in 2012, and Montana State University joined the research team through a Cooperative Ecosystems Studies Unit (CESU) research agreement starting in the winter of 2015-16. Faculty within the College of Engineering at MSU have a background in snow science and therefore the expertise the NPS believed was needed for this project. They also operate the MSU Subzero Research Facility, with capacity for examining snow microstructure through computerized tomography (CT) scans, producing snow for in-lab tests, and testing the mechanical properties of snow with compression tests and strain analysis software. The NPS and MSU agreed on conducting two seasons of fieldwork: the winters of 2015-2016 and 2016-2017.

The purpose of this study is to determine the primary factors contributing to the formation of ruts in Yellowstone National Park's snowroads and identify a suite of strategies to mitigate the phenomenon. The NPS is particularly interested in factors they can control, such grooming and the type of vehicles allowed on the road. The park's new rule is supposed to allow for innovative technologies that will reduce resource impacts. One idea that has gained traction in the last few years is allowing large, low-pressure-tire (LPT) snowcoaches. The NPS has allowed operators to experiment with these in recent years. The number of LPT coaches in use in Yellowstone has increased dramatically, starting with three in 2013-14, increasing to eight in 2014-15, over twenty in 2015-16, and finally just over 50 in 2016-17. As the park weighs whether to allow these into the future and with what constraints, they would like to understand how these vehicles impact the roads compared to tracked vehicles. While LPTs have the potential benefits of reduced operating noise and improved fuel efficiency, the NPS would like to understand the likelihood of their damaging roads.

Year 1 involved testing OSVs as they traveled through the park on their normal routes. A variety of testing equipment was developed during Fall 2015 specifically for this study and was used to collect data in the field. This yielded valuable information, but having no opportunity to measure vehicles on repeat passes limited opportunities to isolate variables. Therefore, researchers stressed the need for a controlled setup, with the opportunity to measure numerous runs by the same vehicle and alter variables of interest, in Year 2. The NPS worked with MSU to

provide a test track in Year 2 and recruited operators to bring vehicles to the track for a testing appointment in which they worked with researchers for one to two hours. Test methods used in Year 2 included many of those from Year 1 but also incorporated additional tests based on the results from Year 1.

This study supported completion of master's degrees in the field of engineering for two participating student researchers. This thesis describes part of the two-year study conducted by Montana State University (MSU) for Yellowstone National Park. Specifically, this report details methods, results from some of the methods, and possible implications of the data. The second thesis from this study, "A Yellowstone Snowroad Quality Investigation; a Comparison of Tracks vs. Tires and Other Contributing Factors" by Ry Phipps (2018), describes the results not included in this thesis. Results will inform management policies to ensure a safer experience for visitors, NPS employees, and concessioners, increase the longevity of snowroads, and inform future designs and styles of OSVs.

Statement of problem

The NPS wants to more thoroughly understand the factors that contribute to rutting so that they can mitigate factors within their control. Controllable factors include grooming practices and traffic (frequency and types of vehicles). Factors outside of administrative control include things like snowfall frequency and quantity, temperature throughout the winter, wind, and solar radiation.

This research has focused on two issues. The first, raised by the NPS's allowance of experiments with low pressure tire (LPT) snowcoaches in the park, is whether tires impact the roads differently than tracks. Since the NPS needs to make a decision on the long-term policy on these tires, they need more information on possible impacts.

The second issue is what grooming practices lead to the best road conditions. Operator comments from past years have indicated that road conditions vary throughout the park. Data gathered by MSU through groomer-operator interviews and a tour through the park in 2014 (prior to the beginning of this study) have indicated that grooming practices vary across districts. The NPS would like to understand whether any changes to grooming practices could be implemented to improve road conditions throughout the park.

Documents Regarding This Study

The research project described herein was comprehensive enough to necessitate work by two graduate students. The approach to the research was extremely collaborative and resulted in a comprehensive report produced by the research team for the National Park Service (NPS): "Snowroad Deterioration and Oversnow Vehicle Impact – Final Report, February 2018" (Nelson, Phipps, et al. 2018). This research was not easily separated into two theses. Therefore, this thesis will contain overlap with and many references to "A Yellowstone Snowroad Quality Investigation; a Comparison of Tracks vs. Tires and Other Contributing Factors"

(Phipps 2018). Both theses contain sections from the larger report written for the NPS. Together, these three documents describe the entirety of this project.

LITERATURE REVIEW

Planning for this study involved reviewing existing information about the topics of interest (snowroad conditions and vehicle interactions with a snowroad surface), identifying factors affecting road condition, determining measurable metrics providing insight into these factors and the road condition, and planning methodologies to relate influential factors with effects. Existing literature provided insight for each step of this process. Both the experiments in this study and the literature reviewed fell roughly into two categories: snowroad condition assessment and maintenance (grooming), and vehicle/snow interaction.

Snowroad Assessment and Maintenance

Snow as a Road Material

Snowflakes fall in many shapes and sizes and are fragile structures. When this structure is disturbed, the crystal will very likely break down ending up with less surface area. This can be achieved by grooming, wind transport or simply taking a handful of snow and pressing it together. This process of densification and compaction increases the opportunity for snow to strengthen through a process called sintering.

Ramseier and Sander (1965) found that sintering of snow is a function of temperature that is directly correlated to strengthening of snow. Colbeck (1987) defined this process by saying “crystal growth in dry snow is a process of continuous sublimation-evaporation from warmer and/or more curved surfaces

and condensation on colder and/or less curved surfaces". Basic thermodynamics dictates that water vapor moves from high to low pressures, as the water vapor is released into the air it condenses where the grains touch because the pressure is lower at these locations. This forming and strengthening of bonds is the processes of sintering and it is directly correlated to strengthening of the snowroad.

Abele (1990) took three snow samples of equivalent densities and allowed them to sinter for many days in a controlled laboratory environment (Figure 2). A disaggregated, compacted snow with a density of 0.5 g/cm^3 (comparable to densities seen in this study) was exposed to a constant temperature of -10 ^{o}C and reached an unconfined compressive strength of 10 kg/cm^2 in approximately 2-3 weeks. A sample of equivalent density was exposed to a constant temperature of -40 ^{o}C; this sample required more than 3 months for the snow to reach the same strength (Abele, 1990). This study implies that at colder temperatures a snow sample will require more time to sinter to equivalent strengths than a sample exposed to temperatures near freezing. The process of sintering does not occur at temperatures above freezing. Abele also found that snow at higher initial densities, achieved through compaction, would result in higher strengths after the sintering process.

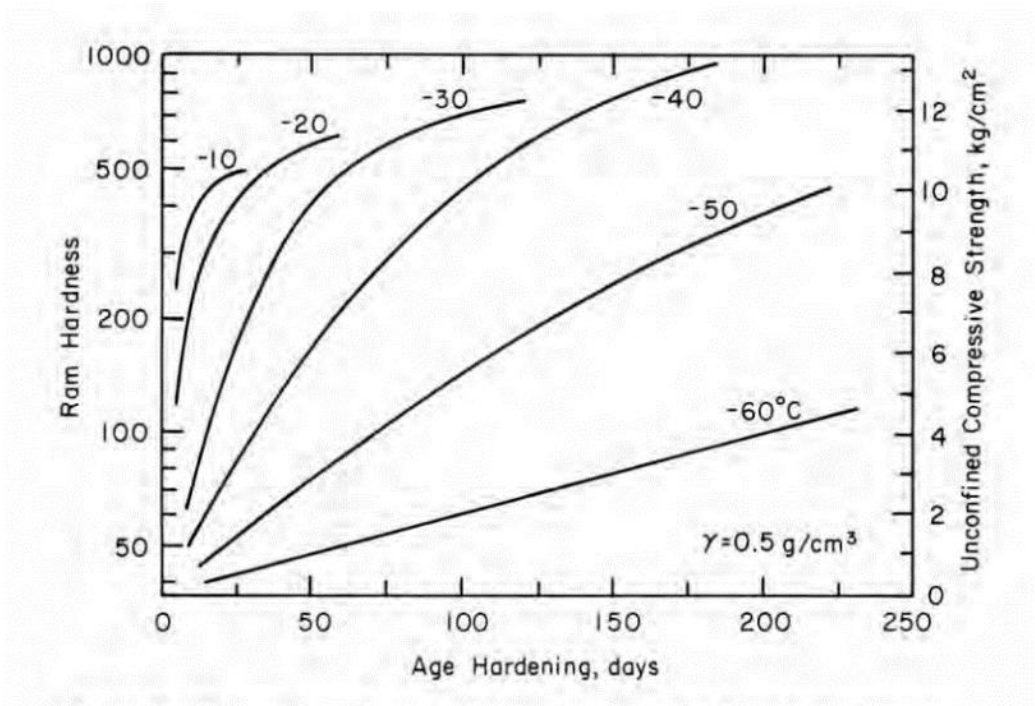

Figure 2. Strength of processed snow as a function of time and temperature, with temperature values marked on the appropriate lines (Abele, 1990)

Sintering and densification can occur in an undisturbed snowpack but occur significantly faster when the snow has been agitated or disaggregated (Lee and others, 1989). This is an important concept in relation to this project because the grooming and traffic on the snowroads could mean that the roads can sinter to higher strengths, faster. This process can be expedited even further by a melt-freeze event. When the temperature is above freezing the crystals will bear a slight amount of liquid water, then if the temperature drops to freezing this available water allows crystals to weld together. During warmer periods in the winter months this can become a diurnal process of melt in the day and freeze at night. The melting phase of

this process can significantly weaken the snowroad, but then ultimately makes the snowroad stronger when followed by the freeze phase.

Snow's strength is correlated with the number and size of bonds between grains (McCallum, 2012) and this microstructure dictates how the snow will deform. Mellor (1975) describes snow as a compressible non-linear viscoelastic material, which indicates that snow's deformation greatly depends on the rate at which it is loaded. Snow takes on both elastic (as a solid) and viscous (as a fluid) behaviors when loaded in different scenarios. When subject to a load, snow undergoes an immediate recoverable deformation (elastic component) as well as a time-dependent irreversible deformation, described as snow creep (viscous component) (Olagne & McClung, 1990). The stress exerted by a tracked snowcoach or an LPT snowcoach, at the velocities tested in this project, exerts a load to the snow in less than ~0.1 seconds, which is within the elastic time frame for snow (Olagne & McClung, 1990). For the purpose of this study, viscous behavior was not considered a significant factor and was not examined.

The most important environmental factor influencing the quality and survival of a snowroad is temperature (Barthelemy, 1975). Diurnal temperature changes majorly affect snow hardness around the park. With a relatively deep blanket of insulating snow, the ground temperature can typically be assumed to be near 0 ^{o}C. Geothermal energy maintains this temperature. In the winter months Yellowstone National Park's ambient air temperature stays quite cold. In this case the snowroad surface is much colder than the base of the snowroad. This

temperature gradient drives a vapor pressure flux throughout the depth of snow. With the warmer temperature near the ground, the vapor pressure is higher at depth in the snowpack, which drives upward heat and water vapor fluxes. Water vapor condenses to crystals as it moves upward, forming faceted crystals. This process results in an overall weaker snowpack configuration and is the process of temperature gradient metamorphism. In a relatively less dense homogeneous snowpack when the temperature gradient reaches -10 °C/m (14 °F/foot) or above, facet development can begin to take hold on a snowpack (LaChapelle & Armstrong, 1977). However, there are caveats with regards to higher snow densities (Akitaya, 1974).

Interestingly, with the snowroads being quite dense in Yellowstone (most areas near 0.5 g/cm^3), the temperature gradient metamorphism is slightly different than that described above. Akitaya (1974) found that a temperature gradient applied to higher density snow can actually increase hardness over time, which is the opposite of what happens in less dense snow. Based on Akitaya's 1974 research, snow of higher densities can be expected to strengthen when exposed to a relatively high temperature gradient where snow of lower densities could possibly weaken when exposed to a temperature gradient. Colbeck (1991) also conducted research on this topic and had similar conclusions. Based on Colbeck and Akitaya's findings most areas of the snowroads that consist of higher density snow (0.5 g/cm^3) are expected to harden with temperature gradients. However, it is still possible in less

dense areas, where there is insufficient compaction and disaggregation, for snow to become softer with an applied temperature gradient.

If snow falls beneath a certain strength threshold and vehicles are traveling on the snowroad, rutting will occur. Depending on temperature and traffic effects, the snowroad may deteriorate to the point of becoming impassable. When the road regains strength, through any of the above processes, it will act to 'lock in' the roughness, unless the road can be smoothed and recompacted simultaneously with the regaining of strength (Lee and others, 1989). This is a unique aspect to snow as a road material, and snow as a road material is greatly affected by environmental conditions.

Snowroad Assessments (and Factors Considered)

Hardness and density are the properties most indicative of snowroad loading capacity (Shoop and others, 2010), so are typically the parameters measured to assess road conditions. Since road systems can consist of many miles of multiple lanes, quick and portable testing methods can provide an advantage by allowing many tests to be taken throughout the road system.

Density is regularly collected in snow research of all kinds, including snowroad assessments. It is a straightforward measurement, requiring only the mass of a known volume of snow. Since only mass and initial volume are required to calculate the density, samples can be weighed on-site or transported from the field to the laboratory relatively simply, without a need for preserving the sample's microstructure.

Hardness of snow is of interest as an indicator of snow strength. The strength of the snow is important in understanding how it will support vehicles. Strength can be measured in several different ways; Abele (1990) provides a good explanation of the possible methods of strength assessment in snowroads. These methods range from in-situ plate bearing tests, in which a load is applied to a plate on the surface of the snow and displacement is measured, to laboratory compression tests of samples extracted from the road, to Rammsonde cone penetrometer in-situ measurements (Abele, 1990).

Rammsonde cone penetrometers are the most commonly used instrument to test snowroad hardness. They have the advantage of using easily portable equipment and being relatively fast and simple to use; this allows researchers to take more tests and therefore sample more points along the roads. A special version of the Rammsonde has been developed specifically for snowroad research. This version has a 30° cone instead of the original 60° cone so that it will more effectively penetrate the extremely hard snow produced through snowroad development (Lee and others, 1989).

The Rammsonde hardness measurement is so widespread in snowroad studies that standards have been established. Shoop and others (2010) cite two different sets of minimum snowroad standards that have been proposed targets for snowroad quality: Swiss Rammsonde hardness greater than 350, or Rammsonde hardness of 450 in the top 25.4 cm of snow and density of greater than 0.5 grams per cubic centimeter. Assuming that this 450 recommendation is a “Ramm hardness

number" in units of kg as measured with a 60° cone, this would equate to a Ramm resistance of 4415 N. Using a correction factor of 1.56 (Shoop and others, 2010) to convert readings from a smaller, 30° cone to readings from a larger, 60° cone, a 4415 N reading from a 60° cone would equate to a reading of 2830 N with a 30° Ramm cone. Lower hardness values may not be adequate to support oversnow vehicles and so may be at risk for rutting.

Another tool commonly used in snow science to characterize snow is a shear test. However, the tools typically used for this are not suited for the hard snow encountered on snowroads (Abele 1990). Shear testing therefore does not seem to be widely used in snowroad characterization. The one exception found was a specialized "confined shear strength test" developed especially for snow pavements and used by Abele (1990).

In recent years, ground-penetrating radar (GPR) has been employed to analyze snowroads. In 2009, Lee and Wang proposed a method to correlate GPR data with hardness as measured by a Rammsonde penetrometer. They worked on finding a correlation by using a layer-stripping method to gain information about the individual layers within the snowroad, and found that permittivity of the layers positively correlated with density, which also positively correlated with hardness. In 2016, Annan and others described use of GPR to assess the safety of winter roads by determining thickness of ice roads. GPRs capable of measuring snowroad characteristics are promising due to their portability and ability to take sample measurements over a large area easily.

Factors beyond Control Influencing Snowroad Conditions

Factors not controllable by the park include weather and site characteristics (e.g., aspect). Analysis included these factors so that the relative influences of controllable and non-controllable factors could be better understood. Since the formation of snowroads is dependent on snowfall, and the metamorphism of snow is influenced by temperature trends, weather factors are considered with respect to road conditions. Site characteristics like elevation, slope, and aspect are widely used in snow science and avalanche research, and will be investigated in this study to determine their relative importance on snowroad characteristics.

As noted in the Grooming Theory and Best Practice section, grooming smaller incremental depths of fresh snow at a given time leads to a more homogeneous hardness stratigraphy throughout the depth of the road. While the NPS can send groomers out during the middle of the day in the event of prolonged snowfall, this is not always feasible due to staff schedules and heavy traffic on the roads during the middle of the day. Therefore, amount of snow groomed at a time is often linked to daily snowfall amounts. Snowfall distribution throughout the park is considered in this report; however, some known concepts can help predict where high snowfall areas might be located.

While elevation is often presumed to be the predominant factor affecting the distribution of snow cover, this is generally only valid "within a given elevation interval at a specific location." This means that a higher elevation may only correspond with more snowfall within a small geographic region and over a small

variation in elevation because of snowfall's additional dependence on climate and slope, which can vary substantially over a small area (McKay & Gray, 1981). Within these constraints, higher elevation is typically linked with more snow.

Mizukami and Perica (2008) found that a snowpack with a higher mean seasonal density tends to have densification occurring at a higher rate mid-winter. Relating this to elevation, a trend of slower densification at higher elevations was demonstrated. They cite studies that have found correlation between denser newly fallen snow and warmer environments. They tracked the evolution of snow density throughout the season at various SNOTEL sites using data sets containing both snow depth and SWE values. According to the background information cited in their study, a snowpack at higher temperature experiences densification at a faster rate than a snowpack at a lower temperature due to the type of metamorphism predominant at warmer temperatures. Mizukami also used site aspects to define a "Northness" characteristic (cosine of azimuth) and "Eastness" characteristic (sine of azimuthal angle).

Wind is important in snow distribution for a couple of reasons. Combined with slope, it can be a dominant factor in snow distribution because of how it affects the movement of air masses over different elevations and over mountains which in turn determines precipitation (McKay & Gray, 1981). Wind can also affect snow cover through transporting and redistributing snow (McKay & Gray, 1981). Wind is also a factor that has been noted to negatively impact snowroad quality and present maintenance difficulties (Shoop and others, 2010). As seen frequently in certain

windy areas in Yellowstone, wind can cause drifts to build up on the road, making the surface uneven and requiring more grooming to maintain a flat and discernable road surface. Conversely, it can cause snow to blow off of the road which can leave an insufficient road base.

Aspect can impact snow cover in a variety of ways. McKay & Gray (1981) note that coastal mountain ranges see the impact of aspect in: "directional flow of snowfall-producing air masses", "frequency of snowfall", and "energy exchange processes influencing snowmelt and ablation." Sun on the south side of mountains in Yellowstone, for example, introduces more solar energy to snow cover on these southern aspects.

As noted in the Snow as a Road Material section, temperature is important to snowroad quality. Temperature is not only important for the initial formation and precipitation of snow but also snow metamorphism on the ground. This is true with snowroads as well as the ungroomed snowpack. According to Lang and others (1997), temperature gradients in the snowroad, driven by ambient temperature, are more influential on the daily quality of a snowroad than the processing.

McClung and Schweizer (1996) have examined the short- and long-term impacts of warm temperatures on snow hardness, showing that warmer temperatures cause softer snow in the immediate, short term but ultimately harden the snow over a long-term timeframe. This hardening comes in part from increased sintering in warm snow (McClung & Schweizer, 1996), as discussed in the Snow as a Road Material section.

Grooming Theory and Best Practice

Oversnow vehicles have operated in Yellowstone National Park for almost seventy years. Starting with snow planes in 1949 (Figure 3), oversnow operations have transitioned over time to include snowcoaches starting in the 1950s and snowmobiles in 1963. To support these operations, the NPS constructs and maintains snowroads throughout the park each winter. Over the same decades that the NPS has maintained Yellowstone's snowroads, collective knowledge about snowroad construction and maintenance has increased through studies in other locations throughout the world that depend on oversnow travel.

Figure 3. A snow plane (Photo courtesy of NPS)

Abele (1990) provides an overview of the evolution of modern snowroads, from expansive networks of rudimentary logging roads (over 50,000 km (31,000 mi) in Canada and 70,000 km (43,000 mi) in Finland by the 1950s), to military-constructed runways in cold regions in World War II, and finally to runways and roads for Antarctic research starting in 1947. Since the advent of research in

Antarctica, many studies have been conducted to increase knowledge about best practices for snowroad construction (Barthelemy, 1975; Blaisdell and others, 1998; Diemand and others, 1996; Lang and others, 1997; Lee & Haas, 1986; Lee and others, 1989; Russell-Head & Budd, 1989; Shoop and others, 2010; Shoop and others, 2014b). Shoop and others (2010) provide a good summary of the state of knowledge, incorporating many of the referenced studies.

An understanding of the snow metamorphism involved with snowroad formation helps explain the importance of different parts of the grooming procedure. According to Barthelemy (1975), the processes involved with construction and maintenance of snowroads "alter the state of natural metamorphism so that the rate at which density and hardness increase is accelerated". Snowroad construction and maintenance harness processes which already occur in snow in the right conditions.

Snow density and hardness are the parameters that construction and maintenance operations aim to optimize and maintain. The two main methods used for snowroad construction "processing" are disaggregation followed by compaction. These processes, in conjunction with one another, result in higher snow density and hardness. Breaking snow grains into smaller, non-uniform pieces creates thermodynamic instability, which increases the particles' ability to bond with one another (i.e., sinter). Compaction then presses the disaggregated particles together, maximizing contact between these particles and further encouraging sintering (Barthelemy, 1975). In addition, close packing that increases contact between the

grains helps distribute load throughout the snowpack (Lang and others, 1997). Effective snowroad grooming must incorporate these two components.

To achieve this processing and compaction, researchers have recommended a wide variety of equipment. Most of the relevant literature addresses the complete construction of snowroads, often starting on a deep snow or ice surface. While some of these practices may be beyond the scope of routine grooming, some of the equipment and processes used will be the same. If a deeper unconsolidated layer of snow has accumulated on the snowroad due to snowfall since the last grooming event, some methods regarding snowroad construction suggested in reviewed literature may be beneficial. Abele (1990) recommended the following construction scheme: 1) disaggregation with a tractor, harrow, and skid; 2) leveling compaction with a bulldozer and roller; 3) grading with a tractor and drag; 4) compaction finishing with a bulldozer, roller, and smooth drag; and 5) final grading with a road grader. Russell-Head and Budd (1989) found that pneumatic-tired rollers are most effective for the snow compaction needed for construction and maintenance of snowroads. Shoop and others (2010) compared rollers and drags, and found that both have different benefits. Data from this study further informed Antarctic testing of the Keweenaw Research Center "SnowPaver", which incorporates leveling blades, a unit that mills the snow, and a vibratory compaction plate into one unit (Shoop and others, 2014a). A history of the development of this unit is available in Alger and others (2011). Lang and others (1997) tested a variety of tillers followed by a drag bar for compaction, and achieved necessary snow strengths for a snow runway.

Russell-Head and Budd (1989) also noted that both the Soviets and Australians were using pneumatic-tired rollers to achieve compaction on their snowroads with success in Antarctica.

Compacting the road after each snowfall, in relatively thin layers (no more than a few centimeters), will produce the most uniform strength throughout the road profile. If compaction does not occur in this gradual manner, the entire depth of ungroomed snow should be processed and compacted all at once (Abele, 1990). If a large depth accumulates prior to the commencement of grooming, the compaction achieved will only compact to a certain depth from the top of the snowpack. According to Barthelemy (1975), "the enhancement of mechanical properties of snow" from compaction "is restricted to a limited depth below the surface". This can be overcome by "depth processing" (digging down to the bottom of the snow and processing the entire depth) of a deep layer of ungroomed snow that has accumulated (Barthelemy, 1975), but this may be logistically difficult. For Yellowstone, in which the snow processing equipment is mostly geared toward grooming the existing road, just processing the top layer, rather than constructing a new road in an existing snowpack, depth processing may not be possible.

After processing and compaction of the snowroad surface, the snowroad needs time to set up. According to Barthelemy (1975) "The importance of the age-hardening process in developing a trafficable surface and increasing the load-bearing capacity of a compacted snow mass cannot be overemphasized." Shoop and

others (2010) recommends that the McMurdo Station in Antarctica allow two to three weeks for age-hardening of its roads after snowroad compaction.

Some snowroad construction has involved the addition of various additives, ranging from water to sawdust (Abele, 1990). In 1989, Lee recommended more experiments with sawdust and other additives that could potentially strengthen snowroads. Lee specified that a sawdust additive had shown promise at the South Pole, where temperatures never got above freezing, but that the sawdust had not proven effective at McMurdo Station during its thawing season. In a climate in which temperatures near or above freezing are common, sawdust or other additives on the surface of the road surface can ultimately weaken the road. Debris on the road, which could include sawdust, can cause "melt holes" due to their low albedo which absorbs solar radiation, heating the snow (Abele, 1990; Lang and others, 1997).

Russell-Head noted in 1989 that Soviets, who were the most experienced snowroad-builders at the time, seemed to have learned that compaction is more efficient with warmer snow (though they had not published much information about their building techniques). Lee and others (1989) had drawn the same conclusion, recommending a heat treatment. Ramseier explained in 1966 that compacting snow at a high temperature (near the melting point) will lead to a higher density than compacting at a lower temperature, and that sintering near melting temperatures rapidly increases the strength of snow. However, while a higher temperature will lead to a faster rate of snow strengthening, it will result in a lower ultimate strength over a timeframe of several weeks to months (Abele, 1990).

The possibility for a rut to become frozen and preserved in a road surface due to temperature fluctuations (Lee and others, 1989) emphasizes the importance of processing any snow that has been disturbed from the flat surface during the grooming process; sintering that occurs in a rut will make the rut last longer. If processing is being achieved with a groomer's front blade, the bottom of the blade must reach down to the bottom of the rut at a minimum to break up a rut that has formed, then re-process and compact the snow so that it will bond in a flat surface again.

While processing the snow is critical to producing a strong snowroad, "overprocessing" of the snow can counteract this relationship. Reprocessing repeatedly increases the likelihood of contaminating the snow with exhaust fumes, oil, and hydraulic fluids. Hydrocarbons present in the snowpack prevent the snow grains from bonding (Lang and others, 1997).

Beyond the groomer, all vehicles passing over the road will impact it. This is addressed in the Individual Vehicle Impacts on the Road section, but is also mentioned in some of the studies on grooming. Shoop and others (2014b) cited tests from Canada that found that after snowroad construction and sintering, traffic can actually improve the road. Lee and Haas (1986) theorized that a buried ice layer in the McMurdo snowroad had formed from a combination of freeze-thaw cycles and traffic compaction. These observations indicate that the loading from vehicle traffic throughout the season may ultimately help to compact the road, though whether this packing could happen despite some surface damage is not discussed. Shoop and

others (2010) note that pneumatic tire rollers, used as drags in Antarctic snowroad grooming, increase density in the snowroad while disaggregating the top 10 cm of snow. This phenomenon could theoretically happen from vehicle traffic as well. Abele (1990) specifically mentions not to allow tracked vehicles on the snowroad unless they have smooth rubber tracks, and warns to avoid allowing high speeds, sudden stops, and sharp turns.

Individual Vehicle Impacts on the Road

Broadly, many of the concepts addressed in this study fall into the field of terramechanics. Terramechanics can be defined as "engineering science that studies the interaction between vehicles and (deformable) terrain", and is where the field of soil mechanics and vehicle mechanics overlap, according to Iagnemma (2011). Studies focus on vehicles on an off-road surface, in which the surface of interest is generally soil, and emphasize vehicle traction rather than influence on the terrain.

Vehicle Characteristics and Impact

Both wheeled and tracked vehicles are capable of negotiating rough terrain and obstacles that are not encountered on a typical roadway. The main difference between the two is that wheeled vehicles are typically more agile, but possess higher ground pressures than tracks. Lower ground pressure is typically only an advantage in soft terrain (Laughery and others, 1990). For travel on snowroads, which fall into this "soft terrain" category, low ground pressure is a desirable feature.

Compaction of soil or snow is directly related to the magnitude of applied normal (perpendicular to surface) stresses (force/area = pressure = stress). From engineering theory, a higher applied normal stress will theoretically cause more compaction of a soil that has reasonable bearing capacities. A simple method of reducing ground pressure is increasing the load-bearing surface area of a track or tire. For a tire, this is achieved by decreasing inflation pressure, increasing wheel diameter or incorporating more wheels into the vehicle (Håkansson and others, 1988). Tracked vehicles have multiple bogey wheels that support the weight of the vehicle, along with the track. A vehicle equipped with four tires will have higher ground pressure than the same vehicle equipped with tracks. However, there is more to road degradation than just ground pressure. The shearing phenomenon is an important variable to explore before declaring a tracked or wheeled vehicle superior with respect to impacts to snowroads.

Tracks and tires both have tractive "lugs" that run along the outside circumference of the track/tire. These lugs are in place to generate additional traction, which increases vehicle performance and control. In this report, the tractive lugs on a track will be denoted as grousers, and the lugs on a tire referred to as tread (Figure 4).

Figure 4. A tracked snowcoach (left), and wheeled/LPT snowcoach (right)

Ansorge and Godwin (2008) developed a technique to determine the effects of tires and tracks on longitudinal soil movement. This study revealed that tracks caused a backward movement of the soil at or near the surface, whereas the tires tended to provoke a forward movement of the soil in the same depth range (Ansorge & Godwin, 2008). In addition to these differences, a tracked vehicle applies shear for a longer period of time, leading to increased shear displacement beneath the tracks (Ansorge & Godwin, 2008). Although the tracks are applying shear for more time they are also applying a vibration for more time, which may cause more snow disaggregation. For these to be accurately compared, the tread and grousers must be of comparable dimensions and rigidity.

As a grouser moves around the track, it changes angles at the front and rear of the track, and at intermediate bogey wheel locations (depending on the tension in the track). Less tension results in a larger relative angle change of grouser to the road surface, as the track follows the contours of the bogey wheels. As a grouser embedded in the road surface changes angles, this can cause additional deformation. The soil (or snow, extrapolating findings of the study to snowroad applications) is

not only pushed backwards by the horizontal forces and the change of the lug angles, but is also lifted as the hindmost lug is lifted obliquely from the soil (Kevan, 1971). This principle pertains to tire rotation as well; however, the radius of curvature of the tire or track is important to consider. A track/tire with a larger radius of curvature will decrease the angle of contact with the surface and decrease the effect mentioned above by reducing the drastic nature of the lug changing angles at the front and rear of the track/tire.

This leads to the topic of wheel diameter as it pertains to road degradation. It is widely documented in the field of terramechanics that increased wheel diameter allows a vehicle to navigate through rougher terrain with a “smoother ride”. This “smoother ride” is due to reduction in magnitude and change of direction of the reactions transmitted to the vehicle as a result of a larger diameter wheel. As it pertains to road degradation, Antille and others (2013) found that smaller width tires can reduce soil compaction provided that the contact patch area is maintained (or increased) by means of a larger tire diameter (Bekker, 1956; Håkansson and others, 1988). With the combination of performance needs, passenger comfort, and road degradation issues, a balance between wheel diameter, width and lug pattern exists for a particular vehicle mission.

As a wheel or track rotates and the grouser/tread is embedded in a surface, the lugs push against the soil/snow horizontally, which is partially how traction is generated (Laughery and others, 1990). When this tractive force exceeds the shearing strength of the surface, the lug will slip. When this slip occurs it causes

additional permanent deformation to the road surface. The severity of this distortion is proportional to shearing strength of the surface and the magnitude of torque produced by the track. If a tracked and wheeled vehicle are traveling at equivalent velocities, the tracked vehicle's grousers are implanted in the surface for a longer time than a tread of a tire. This applies a shearing force to the surface for longer which can cause more soil distortion (Laughery and others, 1990).

A notable difference between tracks and tires occurs while turning a vehicle in soft terrain. When a tracked vehicle turns, one of the vehicle's tracks must slow as the advance of the other side pivots the vehicle about the slower track (Kevan, 1971). As a result of this "skid steer" technique for directional change, the road surface can become badly scoured from the slower track, especially as turn radius decreases. This phenomenon was not specifically studied in this project, but this scouring of the surface while turning is a disadvantage of tracked vehicles in their impact to snowroads like their impact to soil.

A unique benefit of low pressure tires (LPTs) is that the operator can adjust tire pressure for needs of the mission. During this study, snowcoach operators reported improved performance from decreasing inflation pressure in their tires. Literature confirms this concept and, simply put by Raper and others (1995), it is "putting more rubber on the road". Reducing tire pressure increases the patch size of the tire in contact with the surface and increases the traction of the vehicle. Raper and others (1995) found that the total cross-sectional area of the road surface deformation was not affected by inflation pressure; they observed that increased

inflation pressure caused decreased rut width but increased rut depth. These two parameters tended to cancel as each affects rut area in a different manner (Raper and others, 1995).

Soil/Off-road Surface Characteristics and Impact

Vehicles more often drive on road surfaces other than snow, so it is unsurprising that most literature pertains to vehicles traveling on these other surfaces. This literature is important to relate to this project because other soils that have been studied in depth can be related to snow. Snow is, in many instances, more sensitive to environmental factors than soil. But many findings of soil studies are also pertinent to snow studies. Laughery and others (1990) examined three soil types and their characteristics with respect to soil deformation (Figure 5). Laughery found that Soil Type B could be related to dense snow at very cold temperatures.

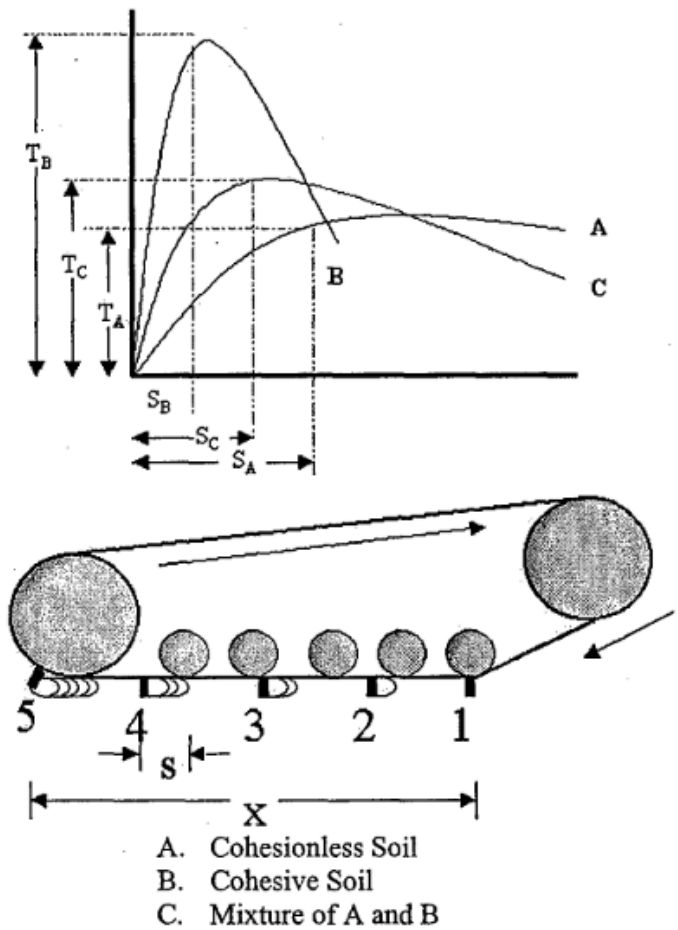

Figure 5. Shear, T, versus soil distortion, S, in three soil types (Laughery and others 1990)

Soil A refers to a cohesionless soil, B is a cohesive soil, and C a mixture of A and B. Comparing the three soil types depicts soil deformation characteristics with regards to the shearing stress. These curves were formed empirically and show the motion of soil under the plotted shear. Curve A represents a loose frictional or plastic soil such as wet clay. For this soil the shearing strength T_A is reached after the initial period of compaction, which takes place over a distance S_A. After this point the stress remains practically the same irrespective of any slip. Soil B consists

of a dry coherent mass, dry clay or snow at very low temperatures. This soil quickly reaches its maximum shearing strength and then tapers off considerably. Curve C is a combination of the two soil types and this soil reaches its shearing strength in-between soil types A and B (Laughery and others, 1990). This figure shows that a snow at cold temperatures (Soil B) will reach its shearing strength faster than the other two soil types, which indicates the highest tendency to deform from shear.

In addition to shearing tendencies, compaction is of interest when researching road degradation from vehicle traffic. Professionals throughout the soil mechanics field agree that if a higher stress is applied to a soil, more compaction will result. However, hardness and density of the material will dictate how much compaction a vehicle pass causes. A dense, hard road surface will resist compaction better than a relatively less dense, soft road surface. In the two years of testing in Yellowstone it seemed that compaction was much less of a factor than shear but in soft conditions, compaction can be a large contributor to rutting.

As a vehicle moves through a deformable surface and its vertical load is high enough, it will sink. This sinking causes compaction at and just below the surface of the road and can affect performance of the vehicle. Richmond and others (1990) found that "compaction is partially the result of vertical forces (vehicle weight) applied to the snow surface by the tire; however, it takes place along a curved path and, therefore, horizontal forces are also applied. When compaction occurs, it can be witnessed by the presence of a rut in the snow following vehicle passage". In these conditions a vehicle must push through the soil on the leading edge of the tire or

track; this is the concept of "bulldozing." Bulldozing resists movement and it leaves a trench or "rut" in the wake of the vehicle's path (Janarthanan and others, 2012). This deformation in combination with shear are the two primary causes of ruts in snow and many soil types.

A common misconception of tracks is that the weight of the vehicle is being supported by the entirety of the track's surface area in all conditions. This is not the case in certain road surface conditions; the tracked vehicle's weight is mainly supported by the bogey wheels on relatively stiff surfaces. The sinkage characteristics of a tracked vehicle depend on vehicle weight, track dimensions, track tension and the soil characteristics (Janarthanan and others, 2012). If the surface is extremely hard, the road experiences higher stresses due to concentration of load under the bogey wheels. In such a case, however, deformation may be limited despite the higher stresses. In the case of a softer surface, the portion of the track which is stretched between the sinking bogey wheels supports a portion of the load. This increased load-bearing surface area reduces the magnitudes of stresses seen by the road surface. In this case, deformation may be limited.

If a vehicle is exceptionally heavy it will apply relatively high normal (perpendicular to surface) stresses which can induce more sinkage and compaction. The track's tension contributes to how much of the track will take up load on a deformable surface. A tighter track can support more load as the bogey wheels press through the surface from vertical plastic deformation (Janarthanan and others, 2012); as this process occurs, the track tightens further and supports even more

load. Additionally, track dimensions are important to consider for ground pressures, a larger surface area track will distribute its load over more area which reduces pressure on the road surface. Tracks' ground pressures are heavily reliant on soil/snow strength properties, whereas tires have a unique advantage of controlling inflation pressure which controls load bearing surface area independent of soil/snow characteristics.

Types of Impact; How to Measure

The Wisconsin Department of Natural Resources, in its Forest Management Guidelines, breaks soil degradation into categories (Wisconsin Department of Natural Resources, 2011); the two modes they define that would apply to a snowroad are "compaction and rutting" and displacement. In snowroads, a rut—or depression in the road surface—could form due to either compaction or removal of snow. Additionally, the dependence of snow hardness on bonds within the snowpack means that impacts which break bonds in the snowpack (such as treads cutting through the snow) may reduce the snowroad's hardness, making it easier for a vehicle to displace snow, effectively making the road more vulnerable to rutting. Shoop and others (2014b) recognized this mode of weakening when using surface strength measurements to determine whether "vehicle traffic changed the snow either through compaction or by weakening through breaking the bonds of the prepared snow surface."

Understanding rut formation on snowroads involves understanding how snow might be compacted, displaced, or made less hard by passing vehicles. This

could involve motion at both the snow-vehicle interface and underneath the surface of the snow as it is compacted and moved. A variety of methods have been used previously to explore these mechanisms in studies concerning vehicle impacts on both soil and snow.

A number of studies have addressed changes to snow or soil surfaces during the passage of a vehicle. Instruments called “profile meters” or “profilometers” can measure depth, width, and total cross-sectional area of a rut and any snow piles adjacent to the rut. Raper and others (1995) employed a “profile meter” to measure both width and the “total deformed area” of ruts, compare those caused by tractor tires at different pressures. The U.S. Army Corps of Engineers Cold Regions Research and Engineering Laboratory (CRREL) has incorporated this type of instrument into several studies. Kestler and others (1999) and Affleck (2005) both used a profilometer to investigate vehicle impacts on thawing soil. Buck and others (2012) used a profilometer to examine vehicle impacts on vegetated soil. Finally, Shoop and others (2014b) applied this instrument to an Antarctic snowroad while comparing the impacts of tracked and wheeled vehicles.

Several instruments can be employed to indicate compaction caused by vehicles on a snow or soil surface. Some studies compare tire and track impacts with soil compaction to aid in vehicle selection for agricultural uses. For agricultural purposes, compaction and resultant increased density and resistance to penetration are undesirable effects as they generally result in decreased soil productivity due to reduced pore volume and size (Wisconsin Department of Natural Resources, 2011;

Sutherland, 2003). For snow, however, compaction is more complicated and can have both positive and negative impacts on snowroads. Compacting snow increases its density, encouraging sintering and making it harder. When this is localized to one set of tracks, however, it can cause ruts in the road surface.

Compaction to a road and the road's resistance to penetration are often measured using a cone penetrometer test. As discussed in the Snowroad Assessments section, the Rammsonde penetrometer ("Ramm penetrometer") is commonly used to measure snowroad hardness. Both 30° and 60° Ramm penetrometers have been used in snowroad studies, typically to measure overall road conditions (Lee and others, 1989; Russell-Head & Budd, 1989; Shoop and others, 2010; Shoop and others, 2014b). They have often been used in conjunction with a Clegg Impact Hammer to characterize the surface hardness of snow, both on untouched road and with regard to vehicle impacts (Lee and others, 1989; Russell-Head & Budd, 1989; Shoop and others, 2010; Shoop and others, 2014b; Shoop and others, 2014a). Tests of vehicle impacts in soils have also used a variety of cone penetrometer tests (Antille and others, 2013; Raper and others, 1995). In both snowroad and soil test, density has been measured as an indicator of compaction from grooming and/or other vehicle impact (Abele, 1990; Russell-Head & Budd, 1989; Shoop and others, 2010; Antille and others, 2013).

Beyond tests of deformation and compaction at a road's surface, subsurface motion can indicate the impact that vehicles are having on the road. Pytka (2010) used stress-state transducers buried at depths of 10, 20, 30, and 40 cms below a

snow surface to measure stresses at these depths as vehicles passed. Horn and others (2007) employed a similar stress-state-transducer setup to look at the stresses under logging vehicles on dirt logging roads. Keller and others (2002) used stress state transducers in conjunction with displacement transducers in an agricultural field to compare subsurface stress and motion caused by rubber-tracked and wheeled tractors. Arvidsson used this method to collect data under tracked and wheeled agricultural equipment in 2013 (Arvidsson & Keller, 2014). The stress state under a vehicle on a deformable surface provides insight into both the stress on the deformable material (snow or soil) and the motion within the soil or snowpack.

Snow scientists at Montana State University have previously used accelerometers to measure acceleration in snow during blasting for avalanche mitigation (Bones, 2012). Acceleration data can be integrated to give both velocity and displacement, though this processing can involve some error propagation (Stiros, 2008) and require correction. Yang and others (2006) provide an overview of previously proposed correction methods and the reasons behind them, and then propose an alternative correction method.

Another type of road disturbance measurement, used most typically on asphalt, is the distribution of stress at the tire-road interface. Coutermarsh and Shoop (2009) investigated this for snow and ice surfaces, using the CRREL Instrumented Vehicle to record vertical, longitudinal, and lateral/transverse forces at the tire contact patches (where the vehicle's wheels touch the ground surface).

These tests took place on a variety of snow surfaces, including packed, hardened snow. More commonly, these tests are conducted for vehicles on asphalt to test the difference in stress or force distribution in different directions for tires with different configurations (bias vs. radial, different pressures, etc.). Beer (1996) developed a measurement system specifically to determine the interface stresses in vertical, transverse, and longitudinal directions since "tyre/pavement interface stresses is one of the most important inputs in any pavement design system". The distribution of stress in different directions has been linked to specific types of road degradation in asphalt roads (Myers and others, 1999; Weissman, 1999).

Most Relevant Studies – Empirical Road Impact

CRREL has conducted the studies most closely related to the current study. Most recently, Shoop and others (2014b) describe a study in Antarctica in which they measured impacts from a variety of different oversnow vehicles (all on tires) making a variety of different maneuvers (turning, braking, etc.). They found that vehicles travelling at higher speeds (25 miles per hour or greater) and vehicles accelerating quickly tended to cause more damage to the road in terms of rutting. They recommend the use of large, wide tires when operating wheeled coaches on the snowroads.

In 2010, Shoop and others published a study on the snowroads at McMurdo Base in Antarctica, in which they monitored snowroad conditions and related these to construction, maintenance, and traffic loading. They note that the two major routes at McMurdo are each divided into three lanes: inbound, outbound, and

"construction/maintenance" or "sintering" (not used). They observed vehicle impacts based on the separation of vehicles into different lanes. They found a harder road surface in the tracked lane, but that lower in the road (20-50 cm, 7.9-20 in), the tracked lane strength decreased "faster and to a lower level" than the wheeled lanes.

One study has previously been conducted to examine impacts to the snowroads in Yellowstone National Park. Alger and others (2000) examined the formation of moguls ("bump formation") on Yellowstone's snowroads when traffic was predominantly snowmobiles and snowcoaches were relatively few in comparison. This study found that "the effect of coaches on the overall bump formation appears to be negligible." However, they did investigate snowcoach impact by running a Bombardier over a stretch of road in two sets of 50 passes and measuring the profile of the snow after these passes. They found that the effect of snowcoach passes on the snowroad surface differed from that of snowmobile passes, as "the snowcoaches do tend to rut the surface parallel to the line of travel and also loosen up the surface considerably. It is uncertain whether or not this would cause problems to extended heavy use by coaches." While the mechanism of mogul formation, which was the focus of this report, does not seem to apply to snowcoaches, the rutting that Alger and others noticed and predicted could potentially be a problem with increased snowcoach traffic on the roads is precisely the impetus for this study.

As discussed earlier, many of the studies relevant to this project address vehicles on a soil surface rather than snow since reducing rutting is of interest in the

agricultural industry. Ansorge and Godwin (2007) used lines of talcum powder layered at known depths and widths throughout a soil pack to test deformation after passage of a tire or track. They found that for a given loading, a tire would cause more deformation in the soil than a track, with the tire causing deformation comparable to that of a track with two to three time the load. They found that using a lower tire pressure with the same load would significantly reduce the tire's deformation and the resultant increase in soil density, but that the low-pressure tire still caused more deformation and density increase than a track.

Antille and others (2013) tested the change in soil's bulk density after a vehicle pass as related to tire size and inflation pressure. The main factor influencing soil displacement and density changes was found to be the initial soil density. Larger tire sizes and lower tire inflation pressures were both found to reduce soil displacement and density change. They also saw that higher pressure tires cause more of an increase in cone penetrometer test hardness readings.

Keller and others (2002) compared tracked and wheeled tractors to determine which caused more vertical stress and associated soil compaction. They found that wheeled tractors caused significantly larger vertical soil displacement. However, they also noted that an incorrect attachment of a plow implement (or other trailer) could cause an uneven distribution of stress under the tracks; they say that tires would be less susceptible to this type of problem since tire contact area will increase in response to increased loading.

Other studies deal with frozen and thawing ground surfaces which may be more relevant to a snowroad than other soils. CRREL has investigated vehicle impacts in soils subjected to freeze/thaw (Affleck, 2005) .

METHODS

Overall Strategy

Since this study addressed questions about both long-term issues (i.e., evolution of the snowroads throughout the season based on grooming and other factors) and more acute impacts (i.e., comparative impacts of different vehicle types passing over the snowroad), a multi-faceted research strategy was implemented. Automatically collected data, from both existing weather stations and instruments deployed for this study (GPS units recording groomer activity and motion-sensor cameras recording traffic), provided information throughout the winter on an ongoing basis. This weather, groomer, and traffic data provided useful information on its own, and was also useful when incorporated with data collected during active fieldwork. Active testing involved: 1) measuring snowroad conditions throughout the park on periodic monitoring trips, and 2) analyzing the instantaneous impact of individual vehicle pass-bys on the roads. The parkwide measurements were intended to give insight into grooming, weather, and traffic pattern impacts, while the pass-by measurements would provide information on comparative road impacts from different vehicles. Figure 6 shows a conceptual framework of the project that includes both causal factors and resultant conditions measured.

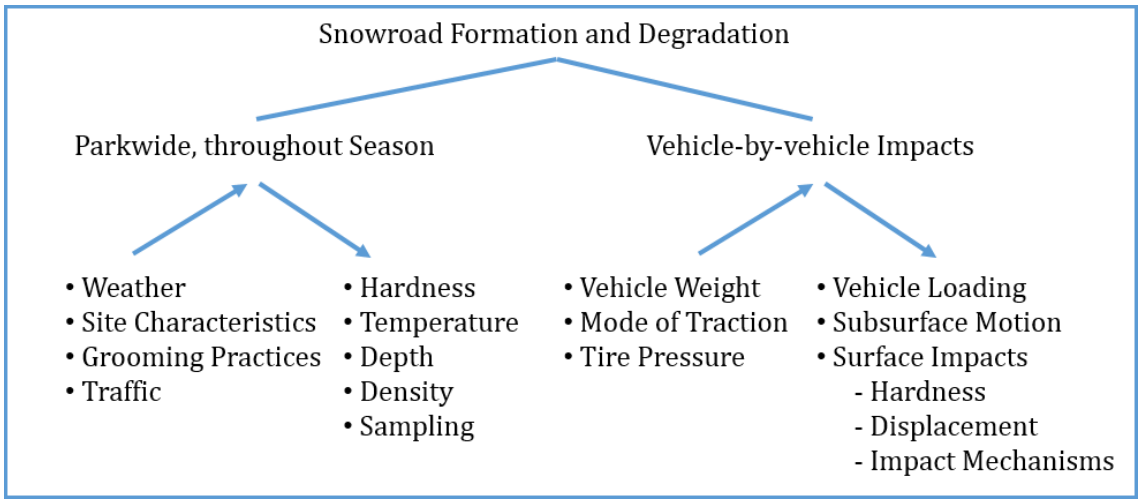

Figure 6. Conceptual framework of research strategy

Methods evolved from Year 1 to Year 2 as data analysis demonstrated what tests yielded the most useful results.

Road Conditions and Grooming – Causal Factors

Factors impacting road condition throughout the park include weather patterns, site characteristics, grooming practices, and traffic patterns (both quantity and type). Weather and grooming data were collected remotely throughout both test seasons. Traffic data was remotely collected during Year 1. Site characteristics are unchanging over the timeframe of two winters, so were determined using existing maps.

Weather Patterns

A number of weather stations operate both within and near the park. Available weather information was gathered from Snow Telemetry (SNOTEL) sites and other types of weather stations. This facilitated comparisons of how weather

during the two testing seasons compared with weather from previous years, how weather varied throughout the park, and possibly what weather was linked to rutting, harder roads, or other trends.

Figure 7 shows locations of various types of weather stations in the park that measure snow depth, snow-water equivalent (SWE), precipitation, temperature, or more than one of these parameters. Labels denote weather stations that provided data used in this project.

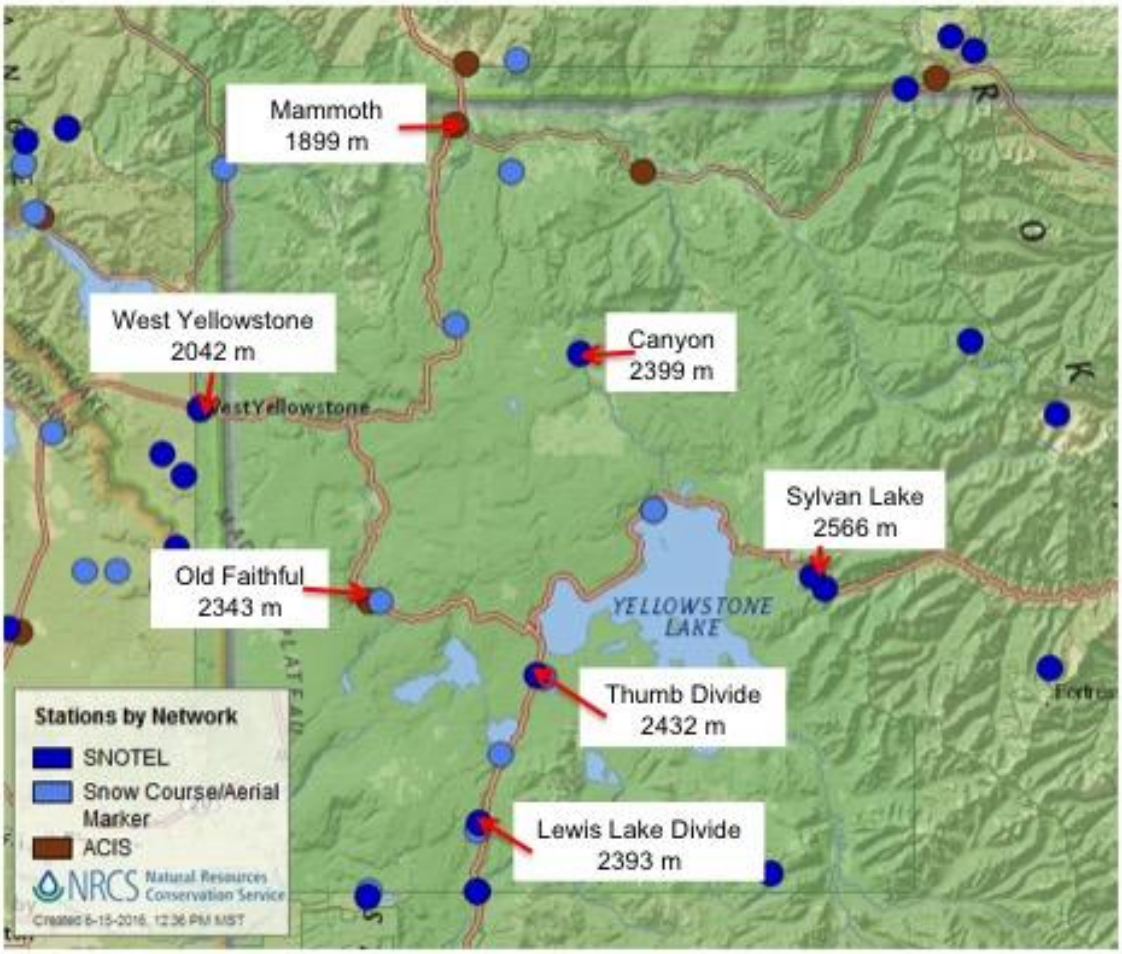

Figure 7. Weather stations used in this study, labeled (NRCS 2016, labels added)

Some weather data was collected through a site called Climate Analyzer, http://www.climateanalyzer.org. Climate Analyzer is a website offered by Walking Shadow Ecology, and the data they offer comes from the National Weather Service, the Natural Resource Conservation Service, the U.S. Geological Survey, Remote Automated Weather Stations, and The Hydrological Data System. The site allows instant access to data from all these sites in one location, which allows for easier data collection. In other cases, data was drawn straight from the primary sources.

Site Characteristics

"Site characteristics" traditionally thought to impact snow, and therefore snowroad quality, are generally unchanging on a small scale of time (i.e. two years). Elevation, aspect, and slope values have previously been calculated and are known for points throughout the park. The NPS Spatial Analysis Laboratory at Yellowstone provided this information for this project in the form of files compatible with ArcGIS software.

The range of snowroad hardness across the park changes throughout the season. Therefore, considering the dates of hardness measurements provides better insight into how site characteristics may impact the hardness between sites. As various site characteristics were graphed along with hardness readings, data was split up into date ranges and these ranges are shown in Figures 38 through Figure 40 in the Site Characteristics section.

Additional characteristics, like road orientation, were calculated within ArcMap as needed.

Grooming Practices

The components of snowroad grooming include what equipment is used and how it is used. In winter of 2014-2015, the winter season prior to commencement of this study, researchers who would ultimately become involved with this study and NPS staff traveled through the park to interview groomer operators and gather information on the types of groomers and grooming implements used by different park districts. While groomer operators can change their grooming attachments (drags, tillers, etc.) day-to-day, understanding the attachments available to each district and the strategies specific to each grooming district provides insight into equipment generally used by each district. Figure 8 shows a map of the major grooming districts. Major grooming districts in the park correspond with NPS maintenance districts, and groomers are based out of the park's major developed areas. One additional grooming district exists on the government snowmobile road out of Mammoth, but this road is only a few miles, only allows snowmobiles, and is not open to the public so was not considered in this study.

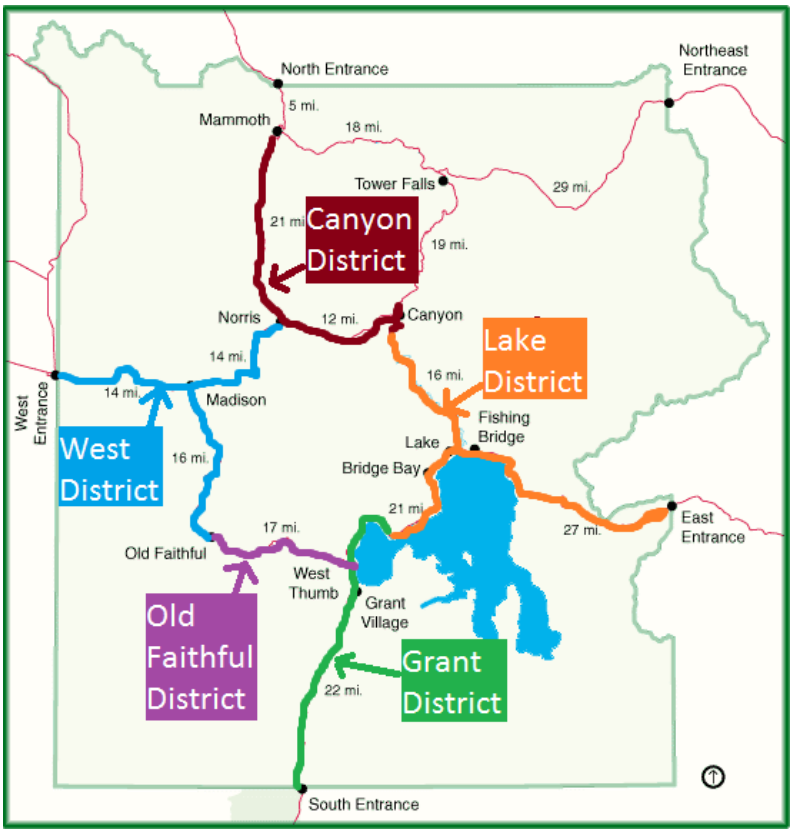

Figure 8. Major snowroad grooming districts

To track how each groomer is used, the NPS outfitted groomers with tracking devices from GPS Insight. These data loggers recorded information about each groomer at 2-minute intervals. An NPS account on the GPS Insight website provided access to all of this data. Each data point for these trackers records a time stamp, location of the groomer, speed of the groomer, distance traveled in the current trip, and distance traveled since the tracker has been installed.

During Year 1, the NPS outfitted 5 of the 6 park groomers with these GPS devices. These five groomers included the West Yellowstone agricultural tractor, the Old Faithful groomer, the Grant groomer, the Lake groomer, and the Canyon groomer. Some of these groomers and the drag implements they use are shown in

Figures 9(a), (b), and (c) and Figures 10(a), (b), and (c). The only groomer that was not tracked was the groomer that is based in Mammoth and is used only to groom the NPS employee snowmobile road, a two-mile back road that leaves the garage in Mammoth and joins the main road near Golden Gate. Due to difficultly with getting these units installed on park groomers, they were not in place in time to record any pre-season grooming information during Year 1. So, for Year 1, groomer data is only available from early January on for most groomers.

(a) (b) (c)

Figures 9(a), (b), and (c). Park groomers: (a) agricultural tractor (West District), (b) Prinoth groomer with tiller attachment (Old Faithful District), and (c) Prinoth groomers with various other attachments (Grant, Lake, Canyon, and North/Mammoth Districts)

(a) (b) (c)

Figures 10(a), (b), and (c). Drags used by groomers: (a) tiller (Old Faithful District), and (b), (c) Mogul Masters (other districts)

During Year 2, the Lake District got a new groomer but its GPS was not moved to the new groomer. This resulted in a loss of Lake groomer data. Additionally, the Old Faithful GPS unit had a malfunction through the beginning of

the season, resulting in minimal data from that groomer from the beginning of the season through February 22nd. An additional factor complicating grooming data analysis for Year 2 was that grooming equipment across the park experienced breakdowns. As the NPS worked to fix a broken groomer, they would often send another groomer to cover some of the broken groomer's district in the meantime. This Year 2 trend prompted analysis of every groomer's GPS data for passes by all designated test points, not just the points within the groomer's normal district. With this method, all recorded passes by hardness test points were captured.

For Year 1, all test sites were set as "landmarks" in the GPS Insight software. This allowed extraction of all data points collected within a selected distance of each specific site. Site-specific grooming data could then be compared with road conditions and other observations. For Year 2, this analysis was done in Excel after all GPS points for each groomer throughout the season had been downloaded. The analysis in Year 2 indicated that the original "landmark" data collection from Year 1 might have missed some passes, so the same processing from Year 2 was applied to all Year 1 data in the final analysis. Appendix A describes the grooming data analysis in more detail.

Traffic Patterns

During Year 1, motion-activated, Reconyx cameras were deployed at three of the testing sites on the main roads: along the Firehole River a few miles south of Madison Junction, near the entrance to the Virginia Cascades Drive on the Norris-Canyon road, and near Kepler Cascades, east of Old Faithful. Each of these sites lies

along a different popular trip route. These cameras captured and saved photos of passing traffic. Photos provided information on relative traffic loading patterns on the different road sections. Because of the assumption that traffic patterns would remain fairly similar from Year 1 to Year 2, these traffic cameras were not re-deployed in Year 2.

Road Conditions and Grooming – Condition Monitoring

During each of the seasons, a testing plan to monitor road conditions during the season was implemented. In Year 1, both NPS researchers and MSU researchers regularly monitored road conditions. NPS researchers conducted weekly testing at six predetermined test sites, with at least one test site in each of the major grooming districts. Additionally, MSU researchers conducted road condition testing during their trips to the park. During all pass-by tests, road conditions at the testing location were assessed. MSU researchers travelled throughout the entire park on two occasions to measure the snow depth (described in the Depth section) and assessed road conditions at sites along the way. During Year 2, only MSU researchers collected information during trips into the park, which was not on a strict weekly basis. In this second season, pass-by tests took place at a test track in Grant Village, so condition measurements were taken during all testing at this test track. Additionally, the second season incorporated two trips solely involving measurement of road conditions throughout the park.

In Year 1, NPS researchers stopped at the pre-determined test sites once per week, though not necessarily on the same day each week. Test sites were not all visited on the same day. They were provided with instructions for a testing procedure that involved recording: weather conditions at the time of testing, ambient temperature and snow surface temperature, hardness profile throughout the road depth, and snow temperature profile throughout the road depth. MSU researchers collected this same data set at each test site where pass-by testing was conducted, additionally measuring density and collecting snow samples on many occasions.

Additionally, in Year 1, two trips were conducted specifically to measure road conditions throughout the park. During these trips, researchers measured snow depth continually throughout the road system and stopped along the way to conduct testing similar to that from the weekly tests and to collect snow samples.

During Year 2, road condition assessments at both the pass-by test track and parkwide locations involved recording a road hardness profile, ambient temperature, depth, and density measurements. During parkwide road assessments, snow samples were also collected at some sites.

Methods for measuring road hardness, temperature, depth, and density, as well as collecting and processing samples, are described below.

Hardness

A Rammsonde penetrometer was used to measure hardness throughout the depth of the snowroad at each site. The Rammsonde (Ramm) penetrometer is an

instrument commonly used in snow science to characterize hardness throughout the depth of a snowpack. Figure 11 shows the instrument. It consists of a cone-shaped tip, with the cone end at an angle of thirty degrees, that increases in diameter for 5.5 cm (2.2 in) and then narrows back down, reaching a smaller diameter 10 cm (3.9 in) from the cone tip. A rod 20 cm (7.9 in) long is attached to this cone. Both of these are marked at 1.0-cm (0.39-in) increments. A smaller-diameter rod, 30 cm (12 in) long and marked at 10-cm (3.9-in) increments, is attached to the top of that. A "hammer" fits around the smaller-diameter rod. Penetrometers with other dimensions and cone angles are also available, but the sharper cone of the 30° Rammsonde penetrometer, like that used in this study, is the preferable model for use on harder snow like the snowroads encountered throughout this study.

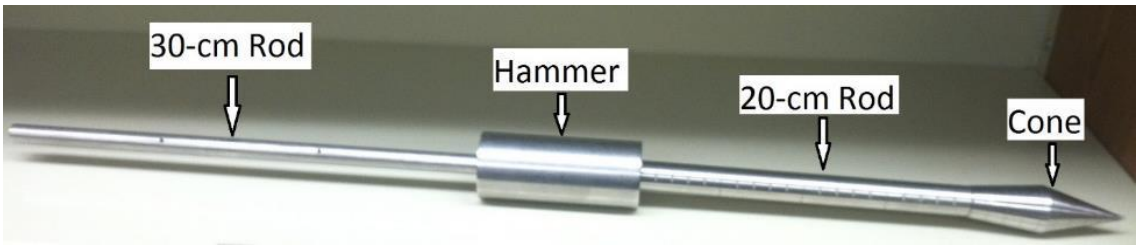

Figure 11. 30° Rammsonde penetrometer used in this study

To take measurements, researchers gently set the assembled instrument on the ground and measure how far it sinks. They then place the hammer on the assembly, again marking how far it sinks. They then drop the hammer from certain heights, defined by the 10-cm (3.9-in) increment marks, and measure how far the instrument penetrates. Standard equations translate these tests into hardness

values for layers throughout the snowpack. Appendix B presents details on these equations and the hardness calculations. Figure 12 shows the penetrometer in use in the field.

Figure 12. Taking measurements with the Ramm penetrometer

For each hardness reading, an average hardness was calculated for the 0 to 10 cm range, the 0 to 15 cm range, the 0 to 20 cm range, the 0 to 25 cm range, and the 0 to 30 cm range. For road sections that are less than 30 cm deep, only increments within the total depth were calculated. These average values allowed comparison between the hardness readings for different test sites since they could capture many layers of different hardness with one summary number for a depth range.

Temperature

Researchers initially planned to measure temperature both in the ambient air and throughout the snowroad snowpack. In Year 1, these measurements were taken with a variety of instruments as researchers learned what did and did not

work (described below). During Year 2, however, only ambient temperature was collected.

During Year 1, after testing hardness, researchers used the hole left in the snowroad from the hardness test to measure temperature throughout the depth of the road snowpack. A variety of instruments were used to take these measurements throughout the season.

Initially, everyone used a thermocouple probe (a metal rod with marks at 5-cm/2-in increments) with an Ampere reader to get temperature throughout the snowroad layers, as far down in the hardness hole as possible. From the beginning, the probe would not quite fit into the very narrow holes left behind by the hardness testing, so researchers tried to figure out better ways to get the temperature probe down into the snow. Then, early in the season, some readings seemed obviously incorrect. Due to the possibility of problems in the thermocouple probe wiring, the instrument was taken back to MSU and rewired. When returned to the field, however, the thermocouple setup once again started to give questionable readings. Finally, the Ampere thermocouple reader's temperature rating was discovered to be inadequate for the ambient temperatures encountered in the field.

An infrared (IR) thermometer initially measured temperatures on the surface of the road. A probe attachment, connected to the same instrument, measured the ambient temperature. This instrument eventually started showing problematic readings, however, much like the thermocouple setup. This turned out

to be for the same reason: ambient temperatures in the field were outside of the instrument's rated operating environment.

After these problems surfaced throughout the season, very simple digital thermometer probes that would consistently give good readings were employed for all temperature readings. These probes, however, were only 10 cm (3.9 in) long. This meant that obtaining temperatures throughout the depth of the road involved digging a pit instead of just sticking a probe into the hardness hole. The logistical difficulty of this process and the competing priorities during testing resulted in no such temperature profiles being measured in pits.

Due to these difficulties, most temperature readings from Year 1 are unusable. For this reason, in Year 2, the simple but reliable 10 cm-probe digital thermometers were used throughout the season. These were used to measure ambient temperature. During road condition assessments, the probe was laid on a bag of research equipment, out of the sun, until the thermometer had reached equilibrium. Readings consistently matched researcher's expectations for ambient air temperature, lending credence to the measurements. During pass-by tests, the thermometer would be used in a similar manner to measure ambient temperature at the test site throughout the day.

Depth

During both seasons, snow depth on the roads was measured in two ways: manually and using radar. Manual readings were taken either by digging a hole to the asphalt surface and measuring its depth (for shallower snow; shown in Figure

13) or by driving a stake into the road surface until hitting the asphalt, and measuring the length of the stake driven into the snow (for deeper snow). These methods were used during both road condition assessments and pass-by testing in both field seasons.

Figure 13. Manual measurement of snowroad depth

While manual checking provided accurate depth readings for test sites throughout the park, these could be completed for only a small number of sites throughout the park, so provided a blunt measure of the variation in snowroad depth between districts and locations within each district.

So that a more complete picture of snowroad depth variation throughout the park could be ascertained, Flat Earth, Inc., a Bozeman-based company specializing in radar technology, provided a snow depth sensor and mount for the project. The NPS supplied the MSU team with an old snowmobile trailer, and MSU combined these to create a trailer that could be towed by a snowmobile and collect snow depth data.

Flat Earth's products had previously been used at Bridger Bowl near Bozeman, MT, and elsewhere to measure snow depth. The trailer created for this project uses a radar instrument to take continual depth measurements as it is towed behind a snowmobile, and a GPS device to mark the location of each depth measurement.

Figure 14 shows the radar sled. In the figure, the orange equipment sticking out from the back of the sled is the location of the radar. The taller item sticking up from the trailer is a Trimble device tracking the sled's GPS location. The yellow box houses the electronic controls and SD card where information is stored. A car battery, in a plastic bag at the front of the sled, powers the setup. This radar sled was used to record snowroad depth throughout the park on two different trips during each of the two test seasons.

Figure 14. Radar sled to measure snow depth

Density

Snow density readings were taken at some test sites during both pass-by test days and road-condition-assessment trips both seasons, but the method changed from Year 1 to Year 2.

During Year 1, a metal tube of known inner diameter was pushed down into the snow until the surface of the snow was at one of the lines marked on the tube. A sample bag with the date and time of the sample collection as well as which line marking had been used was prepared. Then the sample was extracted when researchers dug snow out from around the tube, and slid a flat object under the sample tube so that the sample would come out intact without snow falling out the bottom. The sample was placed over the labeled bag, the flat object was slid out from under the sample, the bag was placed up around the tube, and all snow was shaken from the sample into the bag. The samples were transported to researchers' field housing and weighed, as shown in Figure 15. Density of each sample was calculated as the mass divided by the volume of that sample as determined by measurements of the tube.

Figure 15. Weighing Year 1 density samples

Due to the difficulty of digging snow out from around the density tube and potential problems associated with this in Year 1, in Year 2 a different method was used. A snow density testing kit, designed to capture a 100-cubic-centimeter segment of snow more quickly and uniformly than the original density tube, was incorporated into Year 2 testing. This main part of this kit consists of a metal rectangular box with a handle (Figure 16). This box has openings on the smallest sides of the rectangle so that it can be pushed into the snow and the box will fill with snow. After the box has been inserted into the snow, a sharper rectangular piece fits over the box to seal off the open sides of the box, precisely separating the snow sample from the surrounding snow. The sample is then deposited into a Ziploc bag, which has been pre-weighed, and the bag and sample are weighed together using a spring scale included in the testing kit. Then the weight of the sample plus bag minus the weight of the empty bag gives the density in grams per hundred cubic centimeters. A density reading was taken at all road-condition-assessment-trip sample sites except when the snow was too hard for the density tester to be inserted.

Figure 16. Year 2 density sampling equipment

Sampling

During testing, snow samples were collected and transported back to the Subzero Science and Engineering Research Facility at MSU. Samples were taken at different test sites and different grooming districts throughout the course of pass-by tests. Samples were transported in coolers with snow and ice packed around them to ensure that they stayed frozen, keeping their microstructures as intact as possible. Once in the lab at MSU, the samples were placed in a cooler at -25 °C (-13 °F) and sealed in plastic to avoid sublimation during storage.

During planning for Year 1 of this project, corers were developed for use collecting samples in this project. As researchers started taking them into the field and working with the snowroad snow, however, it was evident that the corers were not strong enough to go through the very hard snowroads, so a different sampling method was employed. Snow saws proved to be the most effective way to extract the very hard samples. These were taken in the form of blocks of snow. Because of

the ultimate difficulty of getting the samples and also the logistics of transferring samples from them to the MSU cold storage rooms in Bozeman, in both Year 1 and Year 2 only MSU collected samples, not asking the NPS researchers to collect samples during their weekly tests in Year 1. Figures 17(a) shows one of the corers, (b) shows a sample collected using the final method, and (c) shows a sample packaged and ready for transport.

(a) (b) (c)

Figures 17(a), (b), and (c). Evolution of snow sampling devices: (a) corers, (b) sawed, (c) sawed and packaged for transport

Samples were collected with the plan of processing them using compression tests to determine their mechanical strength and properties, and using computerized tomography (CT) scanning to investigate their microstructure. For testing mechanical properties, an experimental setup in the lab (pictured in Figure 18) was constructed so that a measured, downward vertical force could be applied to a sample and the associated displacement (compression) of the top of the sample could be measured. A GeoTac GeoJac was used to apply force to the top of the sample, while a linear variable differential transformer (LVDT) device measured downward movement at the top of the sample. During this testing, a high-speed,

high-definition camera recorded a video to be analyzed by a computer program called Aramis (described in more detail later in this report), which could analyze motion in the sample, the front of which had been flecked with black paint to facilitate particle tracking.

Figure 18. Laboratory setup for compression tests

The force and displacement recorded in these tests, along with the size of the sample and area over which the force is applied, could potentially give the sample material's modulus of elasticity and Poisson Ratio.

Researchers planned to perform CT scans on snow samples that had been brought back to the lab. CT scanning produces three-dimensional imagery of the scanned sample. In snow research, CT scans can provide insight into the

microstructure of the snow. The subzero labs at MSU have a CT scanner located in a cold room (shown in Figure 19), allowing scanning to take place in a below-freezing environment at a controlled temperature.

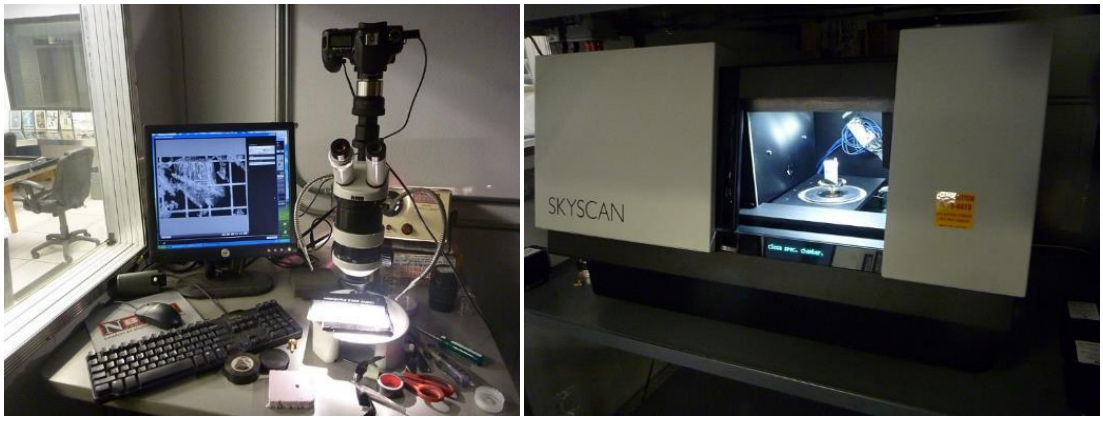

Figure 19. MSU Subzero Science and Engineering Research Facility CT scanner

Vehicle Pass-bys

In both test seasons, individual vehicles were tested as they drove along a test track. Various measurements, described below, were taken as each vehicle passed. This information was gathered so that the relative impacts of different vehicle types and configurations could be compared. Measurable impacts included loading (vertical force on the road), subsurface disturbance (displacement and/or acceleration beneath the road surface), and surface disturbance. During each season, testing generally involved instrumentation, mostly buried in the snowroad but sometimes out above the snow, with cables transferring the gathered data to one or more computers. A tent was set up to protect the computers and keep them warm and operational. Additionally, a generator was deployed to power the

electronics used in this study. During pass-bys, one or more researchers would remain in the tent, remotely controlling the testing equipment, while the other researchers remained outside of the tent directing the test vehicle and any other traffic, and taking additional measurements as needed. Figure 20 shows this setup in both years. General descriptions of pass-by testing conducted during Year 1 and Year 2 are provided below and followed by detailed descriptions of the testing equipment used.

(a) (b)

Figure 20, (a) and (b). Test setup: (a) Year 1, roads throughout park, and (b) Year 2, Grant Village test track

Figure 21 shows a schematic of testing in Year 1 and Year 2, with additions in the Year 2 testing season outlined in red.

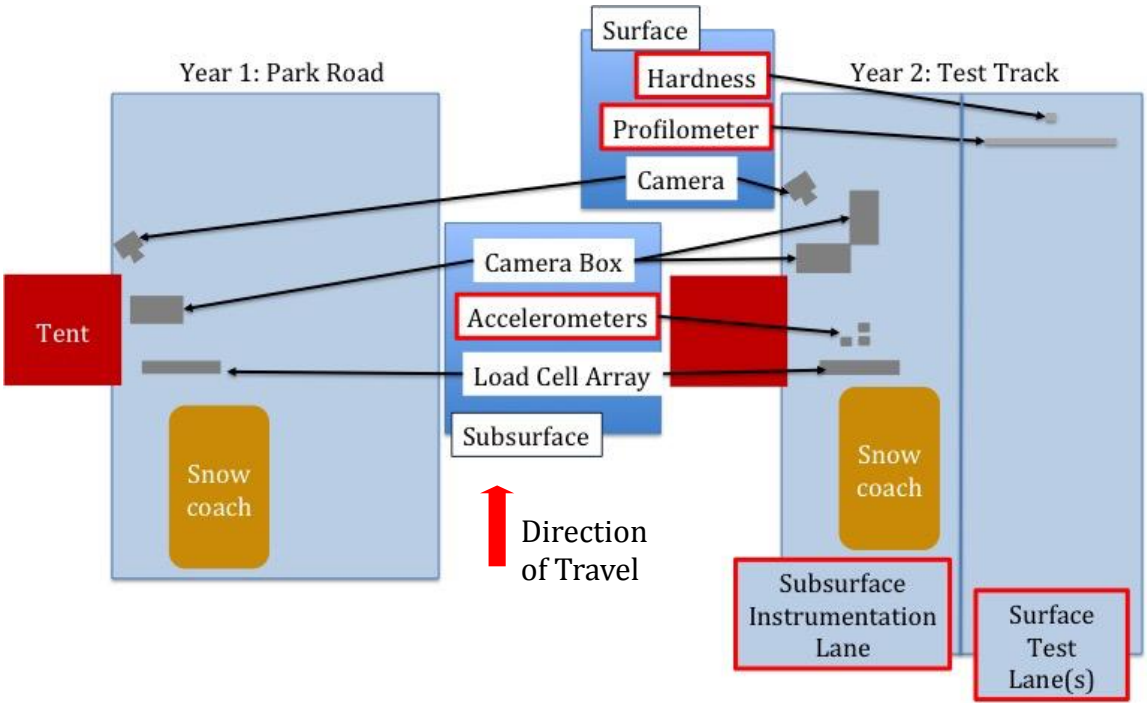

Figure 21. Year 2 setup changes including separated lanes and additional instrumentation (shown in red boxes)

Year 1 Pass-by Tests – General Setup

OSV testing during Year 1 mostly involved testing vehicles opportunistically as they were traveling through the park rather than having control of vehicles to test repeatedly. Only on the last two testing days (March 4th and 5th) of Year 1 did researchers have control over a vehicle that could be used for numerous pass-bys. As a result, Year 1 data generally only involves one pass-by from any particular vehicle on a given day.

During Year 1, test sites were set up along the snowroads already in-use in the park. During testing, researchers designated a lane for coaches to go through (marked by spray painted lines and cones and/or whiskers) while being recorded. They would then stop coaches, allowing one to go through the course at a time. If

this created a traffic back-up, some vehicles would be waved through without getting tested.

For all of the pass-by testing, vehicle information was collected to facilitate comparison of impacts and snow disturbance associated with different vehicle characteristics. The NPS conducts a snowcoach census each year, gathering information from snowcoach operators about each of their vehicles. Therefore, comprehensive vehicle information was not collected during pass-by tests, but rather basic information about vehicles for later cross-referencing with the census.

Information collected during pass-bys included the unique identifier for the coach (company and snowcoach name or number), a photo of the coach as backup verification of the coach's identity and basic characteristics, and the number of people on board the coach during testing.

Vehicles for which information had been collected proceeded through the test track. The research team member communicating with the snowcoach driver would communicate with the team in the tent via radio to ensure that the instruments were ready to collect data. The driver was provided with instructions on speed and/or acceleration/deceleration. In most tests, the driver was asked to drive at their regular cruising speed; in a few, they were asked to accelerate. These instructions were noted in records for each of the pass-bys. The vehicle would then drive along a previously marked line that routed it over buried load cells and right next to the camera location (surface or subsurface).

Testing days during Year 1 focused either on “surface” or “subsurface” data collection. Table 1 shows the breakdown of pass-by test data collection throughout Year 1. “Surface” data collection involved recording videos of pass-bys with a high-speed, high-definition camera. These videos could then be studied to provide information on the nature of the interaction between the vehicle tracks or tires and the road surface. “Subsurface” data collection involved burying the high-speed, high-definition camera in the snow in a protective box to record a high-speed series of images showing if and how the snow in the road was changing under the surface when a vehicle passed by. The snow wall adjacent to the box was flecked with black paint prior to testing to make motion detectable. Back in the lab, these videos were processed using Aramis, software that detects strain and motion in a series of images and is described in more detail below. During some test days, whether surface or subsurface analysis was taking place, an array of load cells was deployed below the road surface to measure the vertical force encountered during vehicle pass-bys.

Table 1. Year 1 field test days

Date	Day of Week	Location	Surf/Subsurf.	Load Cells (Y/N)	No. Pass-bys
2016 01 15	Friday	Kepler	Subsurface	Yes	9
2016 01 16	Saturday	VA Cascades	Subsurface	Yes	15
2016 01 17	Sunday	Firehole	Surface	Yes	37
2016 01 28	Thursday	VA Cascades	Surface	Yes	5
2016 01 29	Friday	W of Sprg Crk	Subsurface	Yes	11
2016 01 30	Saturday	Firehole	Surface	Yes	6
2016 02 11	Thursday	MJ Campground	Surface	No	16
2016 02 12	Friday	W of Sprg Crk	Subsurface	Yes	18
2016 02 13	Saturday	CA S Rim Drive	Subsurface	Yes	13
2016 02 19	Friday	W of Kepler	Surface	No	2
2016 02 20	Saturday	Blanding	Surface	No	11
2016 02 20	Saturday	Firehole Picnic Area	Surface	No	19
2016 02 21	Sunday	Gibbon Meadows	Surface	No	14
2016 03 04	Friday	Kepler	Subsurface	Yes	28
2016 03 05	Saturday	Lewis Lake	Subsurface	Yes	52

Year 2 Pass-by Tests – General Setup

The "opportunistic" nature of testing in Year 1, and the associated lack of control over variables, led researchers to request a more controlled setting in Year 2. Therefore, in Year 2, the NPS worked with researchers to provide a test track and to recruit operators who would volunteer their vehicles for testing.

Researchers were provided with a test track at Grant Village, near the Grant Visitor Center (Figure 22). This stretch of road is not normally used during the winter, so was groomed especially for this study. On each of the days during which pass-by testing was conducted, one or more operators signed up to bring a snowcoach for a test period of approximately two hours. This allowed data

collection for numerous runs by the same vehicle. Researchers used this opportunity to do repeat measurements with all of the controllable variables (speed, tire pressure) held constant and/or varied between runs.

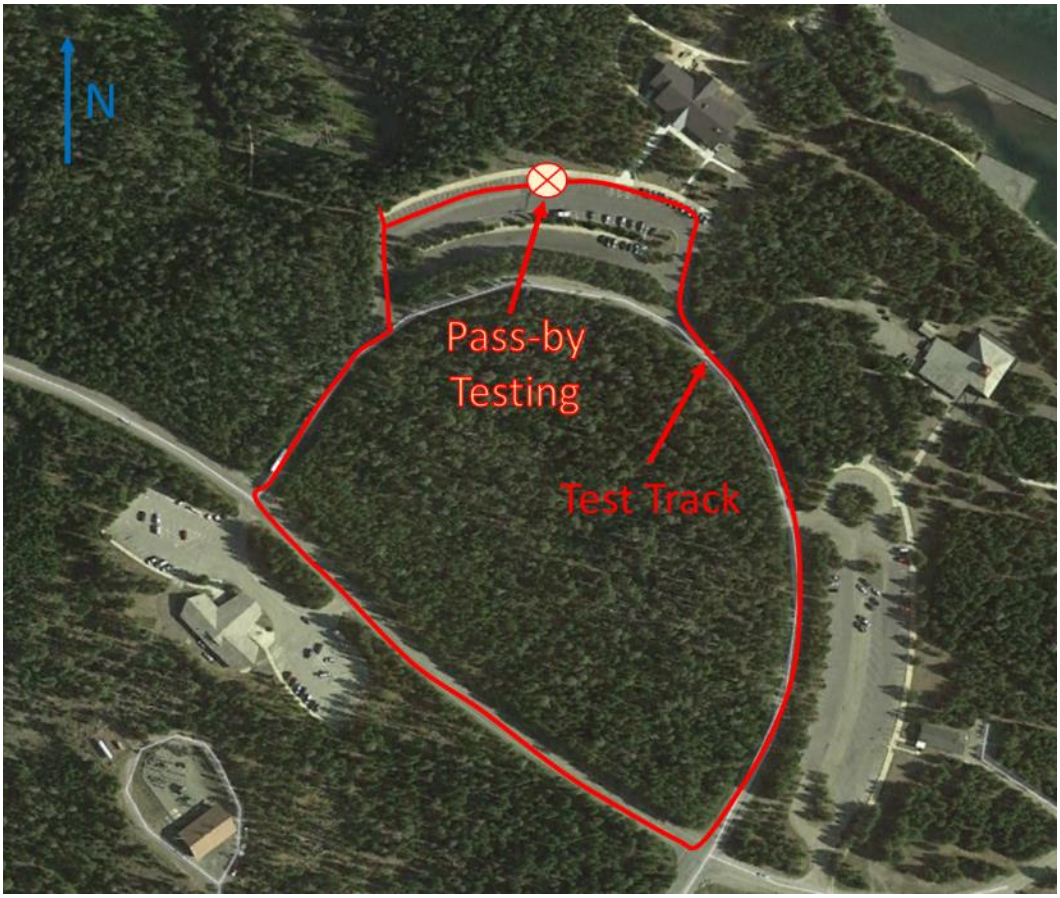

Figure 22. Year 2 test track in Grant Village

As in Year 1, researchers directed test vehicles through a predefined test track under which measurement instruments were buried. In Year 2, buried instruments included a load cell array, the high-speed camera and protective box (during some tests early in the season), and an array of accelerometers. Unlike in Year 1, in Year 2 none of these instruments (like the camera box) stuck out above

the snow at all, to avoid problems with drivers' tendencies to shy away from any equipment visible on the ground. Table 2 shows the Year 2 test dates, which vehicles were tested on these dates, and at what depths the subsurface instruments were deployed.

Table 3 provides further detail on the tracks or tires used by each vehicle. While ideally the instrument burial depths would have remained the same throughout the season, early season data provided insight into what depths would work best, so depths of testing were adjusted accordingly.

Table 2. Year 2 test days and coaches (Abbreviations: Scenic Safaris (SS); Yellowstone Expeditions (Yell Exp); Buffalo Bus (BB); See Yellowstone (See Yell); Bombardier (Bomb); Teton Science School (TSS))

Date	Top of Load Cell Depth (cm)	Accelerometer Depths (cm)	Vehicle(s) Tested
1/15/2017	10	NA	Mattracks (SS), Tires (NPS Suburban)
1/28/2017	8	5, 8, 12	Snowbuster (Yell Exp)
1/29/2017	10	10, 15	Mattracks (SS), Tires (XPR), Tires (NPS)
2/12/2017	20	10, 15, 20, 25	Tires (BB), Bomb (See Yell), SMs (NPS)
2/25/2017	20	10, 20, 30, 40	Tires (NPS)
2/26/2017	20	10, 20, 30, 40	Mattracks (TSS), Bomb (See Yell), Tires (NPS)
2/27/2017	20	10, 20, 30, 40	Tires (SS), Tires (NPS)

Table 3. Vehicles tested, Year 2

			Width of Tracks/Tires×		Tire Diameter	
Date	Vehicle(s)	Type of Tracks/Tires	cm	in	cm	in
1/15/17	SS Mattracks	Mattracks 150s (articulating on front, non-articulating on back)	41	16	NA	NA
	NPS Suburban	BF Goodrich Krawler T/A 40x14.50 R 17 LR 121 L M+S	37	14.7	101	39.8
1/28/17	Snowbuster	Snowbuster; 6 bogey wheels, 1 drive wheel (not touching ground)	61	24	NA	NA
1/29/17	SS Mattracks	Mattracks (articulated in front, not in back; 4 wheels in front, 5 in back)	40.5	16	NA	NA
	XPR Tires	Alliance FloTruck 600/50R22.5 MPT; Steel Radial	60	23.6	117	46.1
	NPS Tires	Michelin CargoXBib 600/50R22.5	60	23.6	117	46.1
2/12/17	BB Tires	Nokian Country King 560/60R22.5	56	22	124	49
	Bomb	Bomb	43*	17	NA	NA
	Snowmobiles	Snowmobile	not measured	not measured	NA	NA
2/25/17	NPS Tires	Michelin CargoXBib 600/50R22.5	60	23.6	117	46.1
2/26/17	TSS Mattracks	YS3s (front and back)	45.6	18	NA	NA
	Bomb	Bomb	43	17	NA	NA
	NPS Tires	Michelin CargoXBib 600/50R22.5	60	23.6	117	46.1
2/27/17	SS Tires	Alliance FlotMaster 381 620/50R22.5 IMP	62	24.4	119	46.9
	NPS Tires	Michelin CargoXBib 600/50R22.5	60	23.6	117	46.1
×Widths for ski/track vehicles are listed for the tracks rather than the ski.						
*A width was not taken specifically on Griz's tracks, so it is assumed to be equivalent to that from Sally.						

For each vehicle, researchers would work with the driver to define a testing plan, which involved varying the speed of the vehicle and, if the vehicle had tires, the

pressure of the tires. The test plans always involved runs through the test track at a steady speed, with initial runs generally at a low speed, usually 2.2 meters per second (m/s) (or 5 miles per hour (mph)), and later runs at higher speeds, usually increased at 4.4 m/s (10mph) increments, until making final runs at 11 m/s (25 mph). For LPT vehicles, drivers generally did the first set of runs, ranging across all of the speeds, at a high pressure, then aired down to another typical set of running pressures for another set of testing across the different velocities. Each different tire pressure setting at which a vehicle was tested was considered to be a separate "vehicle configuration", being considered separately from the same vehicle with different tire pressures in data analysis so that the effect of pressure on the vehicle's impacts could be tested. Variables were adjusted and tests repeated as time allowed.

Prior to commencement of pass-bys, hardness measurements of the untouched test track were taken. After the baseline had been established, the vehicle would make 5 to 7 passes through the test area at a given speed and tire pressure, if applicable. These passes included at least two passes through the test track over the buried instrumentation so that subsurface impacts could be measured. Then a lane would be designated for the vehicle to pass over 5 times specifically to test surface impacts. In many cases, the vehicle's 5 passes would be in a separate, untouched lane designated for that particular vehicle's surface passes; in other cases, in which snow conditions and/or vehicle configurations meant that passes were causing negligible surface impacts, the same instrumentation lane was used for all surface disturbance passes as well.

During the two instrumentation passes, researchers would record data from all of the buried instruments. After each set of five passes through the surface testing lane, researchers would take a profilometer reading in that lane and measure hardness in the top 10 centimeters.

The control granted by the testing setup of Year 2 allowed researchers to experiment with the comparative surface and subsurface impacts of different vehicles, and then to explore the influence that vehicle speed and variables like tire pressure can have on these impacts.

Vehicle Loading

Vertical forces within the snowroad were measured for each vehicle during pass-by testing. An array of twelve load cells (OMEGA Engineering, Inc.'s LC304-500s) buried under the snow provided these measurements. Figure 23 shows this array. As shown, the load cells are set up in line, and a 10.5 cm by 10.5 cm (4.13 in by 4.13 in) metal cover goes over the top of each load cell to protect it. Appendix C provides details on how this load data was processed, and Appendix D shows the data sheets for the specific load cells used in this project.

Figure 23. Load cell array

Two compact data acquisition (cDAQ) units recorded data from the load cells in real-time as vehicles passed. Each cDAQ read six load cells, and fed this information into a laptop through a LabVIEW software interface. A program in LabVIEW operated the cDAQ, defining the reading interval (2,000 readings per second), starting the data acquisition process, recording the data for all channels (i.e., load cells), stopping the data recording, and saving the data in both Technical Data Management Streaming (TDMS) and comma-separated values (CSV) format. This was all controlled on a laptop computer during testing.

In the processed files, the reading at each point in time showed the force on each load cell, for a total of twelve force readings. To show the total force from each

passing track, tire, or ski, researchers calculated an additional value for each point in time equal to the sum of all the load cell forces (Figure 24).

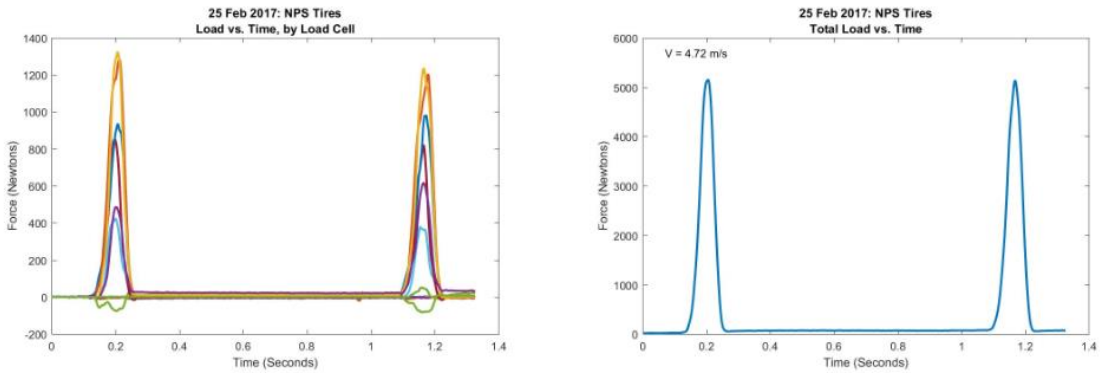

Figure 24. Example of each load cell reading (left) and sum of all load cell readings (right)

The load cells were also used to determine exact velocities of the snowcoaches during Year 2. The distance between two load-bearing points on a snowcoach was measured. Using the load events from that vehicle pass, a velocity was solved using the time between the loading events (in seconds) as calculated using the sample frequency (Figure 25). This distance over time measurement solved for exact velocity.

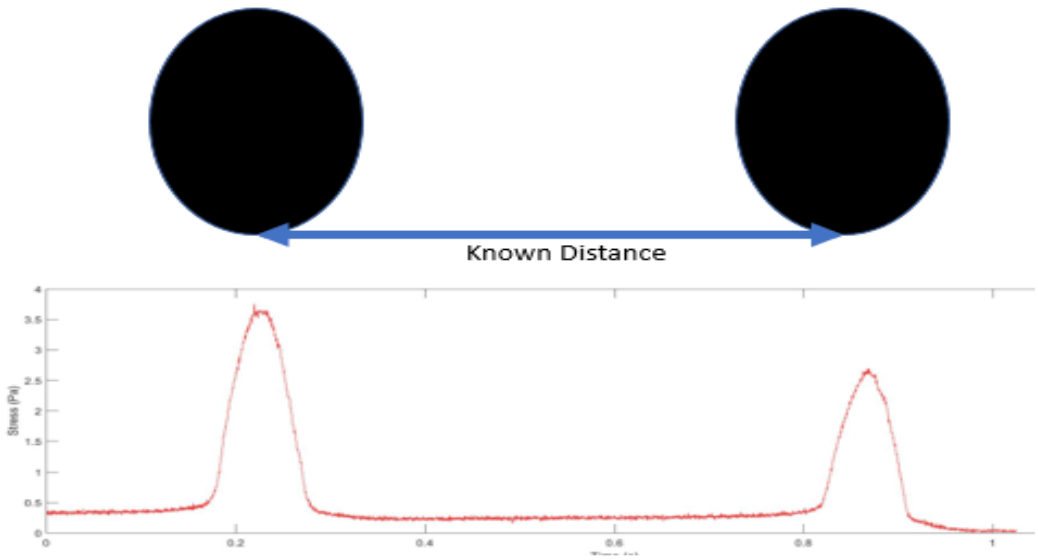

Figure 25. Distance between tires or bogey wheels (top) and time between vertical maximum forces (bottom) used in velocity estimates

During most measurements in the field, the load cell array was set up perpendicular to the direction of vehicle travel to show force across the entire width of the track, tire, or ski. In a few tests, the load cell array was positioned parallel to the direction of traffic to determine if this would provide any other insights.

Subsurface Impacts

During Year 1 and the beginning of Year 2, subsurface deformation was measured using Aramis, an optical strain measurement program. During Year 2, an array of accelerometers was implemented to capture similar and additional information.

Aramis is a software system manufactured by GOM, a German company. Aramis tracks points in a series of photos, analyzing how they move with respect to one another throughout the series, to calculate parameters such as vertical strain,

horizontal strain, and shear angle. In this study, Aramis was used to analyze series of images of pit walls within the road in order to demonstrate deformation taking place beneath the road surface.

During pass-by testing, a camera was positioned in a pit, usually facing perpendicular to the direction of traffic travel, in order to get images of a snow wall. Snowcoach drivers were asked to drive as close to this pit as they were comfortable doing so that the images would show the influences of vehicle loading as close to directly under the vehicle as possible. Because of this, the camera needed protection, and the snow wall needed support to prevent its collapse. A protective box, able to withstand the force of a snowcoach running over it, was designed and built for this purpose. The box frame has inner dimensions of 26.0 cm by 46.5 cm by 122 cm (10.2 in by 18.3 in, with a length of 48.0 in). These dimensions were designed to provide a window into a depth ranging from immediately under the snowroad surface to significantly beneath it and to facilitate using the camera's field of view at a given distance. On the end of the box, adjacent to the snow wall, a piece of Plexiglas confined the snow and prevented its falling out into the box. Figure 26 shows this box positioned in the snow.

Figure 26. Camera box for subsurface testing

During testing, a plywood board covered the box to prevent snow falling onto the camera. During some test days, snow was placed over the board so that drivers would not see the box and shy away from approaching it. When the box was totally covered in snow, a series of LED lights illuminated the snow wall during filming.

To calculate strain information, Aramis needs to be able to track points from image to image to see how they move relative to one another. Snow does not naturally have distinct optical features that would facilitate this analysis. So that Aramis would have points to analyze, snow was speckled with black paint prior to the box being placed into the snow pit. Black paint was diluted with water and the mixture applied to the snow wall in a speckle-pattern. Figure 27 shows the application process and a resultant pattern.

Figure 27. Spraying a paint speckle pattern onto snow (left); resultant pattern (right)

To provide high quality images to be used in Aramis, a Fastec TS3—a high-speed, high-definition camera—was used to capture images. The camera connected to a platform in the box (visible in Figure 26). A Gig-E cable ran from the camera to a laptop so that the camera could be armed and triggered from the laptop, meaning that no one needed to be next to the box during testing. This also allowed some remote adjustment of camera settings. For most subsurface videos, videos were saved as stacks of images, to facilitate easy processing in Aramis, and taken at a rate of 250 frames per second (fps).

Back at MSU, subsurface videos were analyzed in Aramis. Aramis returned a series of images with strain and other parameters calculated. This was then exported into a series of images or a video file showing how the parameter of interest varied throughout the duration of the vehicle pass-by using a color scale. Throughout Year 1, the camera setup was adjusted to improve image quality (i.e., speckling and lighting) to improve Aramis' ability to process the images. Appendix E: Aramis provides more details on these adjustments.

During Year 2, an array of Analog Devices ADXL327 small, low-power, 3-axis 2g accelerometers was implemented to measure acceleration throughout the depth of the snowroad during pass-bys. Accelerometers measure acceleration in one or more directions, so were set up in this study to measure acceleration in three different directions. Figure 28 illustrates: vertical, "longitudinal" (in the direction of traffic), and "transverse" (horizontal and perpendicular to the direction of traffic travel) accelerations. Accelerometer readings can be post-processed to give displacement, telling researchers how much the accelerometers are moving (in distance, mm or inches) as a vehicle passes, and whether they return to the original position after the pass. This possibility meant that accelerometer data would theoretically provide more insight into the motion detected by Aramis.

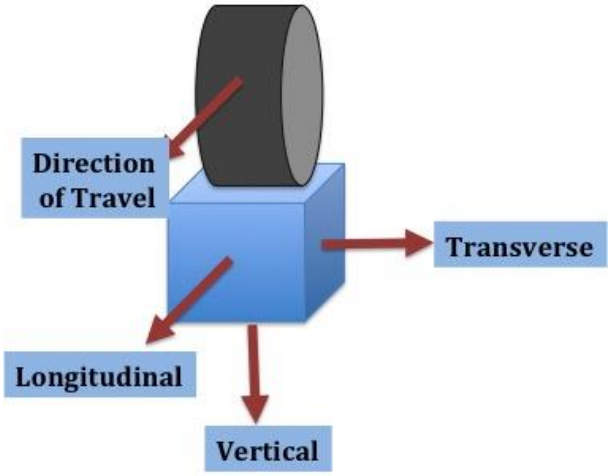

Figure 28. Accelerometer orientations

The accelerometers were buried at various depths to measure acceleration near the surface and provide information on how it differed deeper in the snowpack. Figure 29 shows the array of accelerometers on February 12th, 2017.

Figure 29. Accelerometer array placement, February 12th, 2017

The process of digging down into the snow to place the accelerometers necessarily disrupts the state of the snow so the disturbed snow is different than the snow in the rest of the road. Researchers attempted to minimize this disruption as much as possible while placing the accelerometers. To place the accelerometers, a large pit was initially dug to allow access to a vertical wall in to which the accelerometers could be inserted. On this vertical wall, researchers dug small holes approximately 5 cm (~2 in) back into the wall to attempt to get to less disturbed snow, and placed an accelerometer in the desired orientation at the back end of each hole. Snow and water were then combined to make a slush that was placed in the hole to hold the accelerometers in place and prevent them from moving as the pit next to the vertical wall was filled back in.

An accelerometer measurement kit constructed by a previous Masters student in the MSU snow science program (Bones, 2012) was used to wire the accelerometers to a computer that could record the readings. This kit involved a box into which accelerometer arrays could be plugged using 15-pin connectors, a cDAQ system (National Instruments NI cDAQ-9188) into which all of the accelerometer data was channeled, and then an Ethernet cable coming out that could relay the accelerometer readings to a computer through a LabView interface. The LabView program recorded acceleration values at a rate of 5,000 readings per second. Accelerometer data was saved after each pass using this program. The files were then post-processed back at MSU, as Appendix F describes in detail. Appendix G provides data sheets for the accelerometers used, and Appendix H provides data sheets for the accompanying cDAQ used in accelerometer data collection.

Surface Impacts

Since this study included snow disturbance on the surface of the road as well as under the surface, the Fastec camera was also used to film the surface of the snow as coaches passed. These test days usually involved a setup similar to that of subsurface testing, recording load cell data and also videos, and using the tent, generator, and heater to keep electronics warm. Passing vehicles were also stopped to get their information.

In the beginning of surface filming in Year 1, the camera was positioned on a tripod. However, a lower angle seemed to give better images of the tracks and snow displacement. Therefore, on later dates, the camera was placed inside its protective

box but on top of the snow rather than subsurface. This cut down on glare as well as providing a better viewing angle.

During pass-by tests in which vehicles were stopped for information, the vehicles would rarely go at or near normal cruising speeds once waved on to the test track. Because of the unwieldy nature of snowcoaches, drivers are hesitant to drive fast with any people or equipment on or near the road out of consideration for safety. However, since one of the questions of this study was whether snow displacement varied with speed, methods were adapted to get some videos at higher speeds. Researchers therefore conducted some tests standing by the road without a tent and not stopping the coaches (waving them on by if they stopped) and some tests hiding in trees, out of sight, attempting to film vehicles at full speed. Figure 30 shows the hidden setup, with the camera on a tripod up closer to the road and the laptop and table set back in the trees out of view of the road.

Figure 30. Hidden location for surface video filming

Another variation on surface videos during one test day was videos taken with a head-on view of oncoming coaches. These were intended to better show how OSVs throw snow out to the sides.

These different methods of testing resulted in videos taken at a range of speeds. No test equipment was recording speeds during the pass-bys, but vehicle speeds could prove to be important during data analysis. Therefore, during Year 1, scale objects were selected or set up at each test site. These objects were placed or recorded as being at measured distances from each other and the camera. Vehicle speeds could then be calculated using the vehicles' positions relative to these objects. For example, Figure 31 shows a frame from a pass-by where two marking whiskers set 31 cm (12 in) from each other and 2.59 m (102 in) from the camera lens provided scale.

Figure 31. Marking whiskers used for scale in surface videos

In surface videos, the distance between the whiskers, the distance between the camera and the whiskers, the approximate distance between the whiskers and the snowcoaches, the number of frames between the snowcoach reaching the first feather and reaching the second feather, and the number of frames recorded per second can provide the approximate snowcoach speed.

In Year 2, surface videos were not taken for every pass since each vehicle did so many passes, but rather were recorded for a small sampling of the test runs at a variety of speeds. During this year, all surface videos were accompanied by subsurface tests. The distance between tires or bogey wheels on each vehicle was also measured so that the time between force spikes as measured by the load cells could be used in conjunction with the distance between tires or wheels to calculate vehicle speed.

Additionally, in both years, researchers used a profilometer (Figure 32). The NPS constructed the profilometer after a design they had seen described in papers

by Rosa Affleck and Sally Shoop (Affleck, 2005; Kestler and others, 1999). Affleck lent the original instrument to the NPS for one of their previous years of testing, and after seeing its utility the NPS constructed their own, slightly modified version. The NPS lent the profilometer to MSU for the duration of this project.

The profilometer is ideally suited to record and quantify aberrations from a smooth road surface. Placing the profilometer vertically over any abnormality in the road (e.g., a rut or peak) and photographing it allows researchers to model a profile of the abnormality. Plans for the profilometer in this study included characterizing ruts (depth, width, etc.) by placing the profilometer across the road, as shown in Figure 32, and also investigating the "slip-stick" track phenomenon often observed on park roads by taking measurements along the length of the tracks. In Year 1, the profilometer was used to characterize instances of the slip-stick phenomenon encountered on the road. In Year 2, the profilometer was used to measure changes in the road surface after set numbers of passes by different vehicles, as discussed in the Year 2 procedure description, above. Appendix I provides details on how profilometer data was processed.

Figure 32. Profilometer

Summary

Table 4 summarizes test methods used in each year of the study.

Table 4. Year 1 and Year 2 methods comparison

	Parameter	Year 1 Methods	Year 2 Methods
Factors Impacting Roads	Weather	Weather Station Readings	Weather Station Readings
	Grooming	GPS on Groomers, Equipment Inventory	GPS on Groomers, Equipment Inventory
	Traffic Patterns	Traffic Cameras	N/A
	Site Characteristics	GIS Files	GIS Files
Snow Conditions throughout Park	Depth	Radar Sled, Spot-checks with Rulers	Radar Sled, Spot-checks with Rulers
	Density	Density Tube	Density Kit
	Hardness	Rammsonde Penetrometer (weekly and research trips)	Rammsonde Penetrometer (research trips)
	Slip-stick phenomenon	Profilometer	N/A
	Snow Strength, Composition	Lab Analysis of Samples	N/A
Vehicle Pass-by Impacts	Snow State	Rammsonde Penetrometer, Density Tube	Rammsonde Penetrometer, Density Kit
	Road Surface Profile		Profilometer
	Vertical Force	Load Cells	Load Cells
	Road Sub-surface Motion	Aramis	Aramis, Accelerometers

DATA AND DISCUSSION

Parkwide Hardness and Contributing Factors

The hardness readings taken throughout the park during radar runs provide a snapshot of road conditions throughout the park on a given weekend. Figure 33 shows hardness readings from the weekend of January 21-22, 2017, and Figure 34 shows hardness readings from the weekend of February 18-19, 2017. Note that the scale on the hardness graphs for the February weekend is six times that of the scale for the January weekend (60,000 N vs. 10,000 N), as all roads were harder by the February trip.

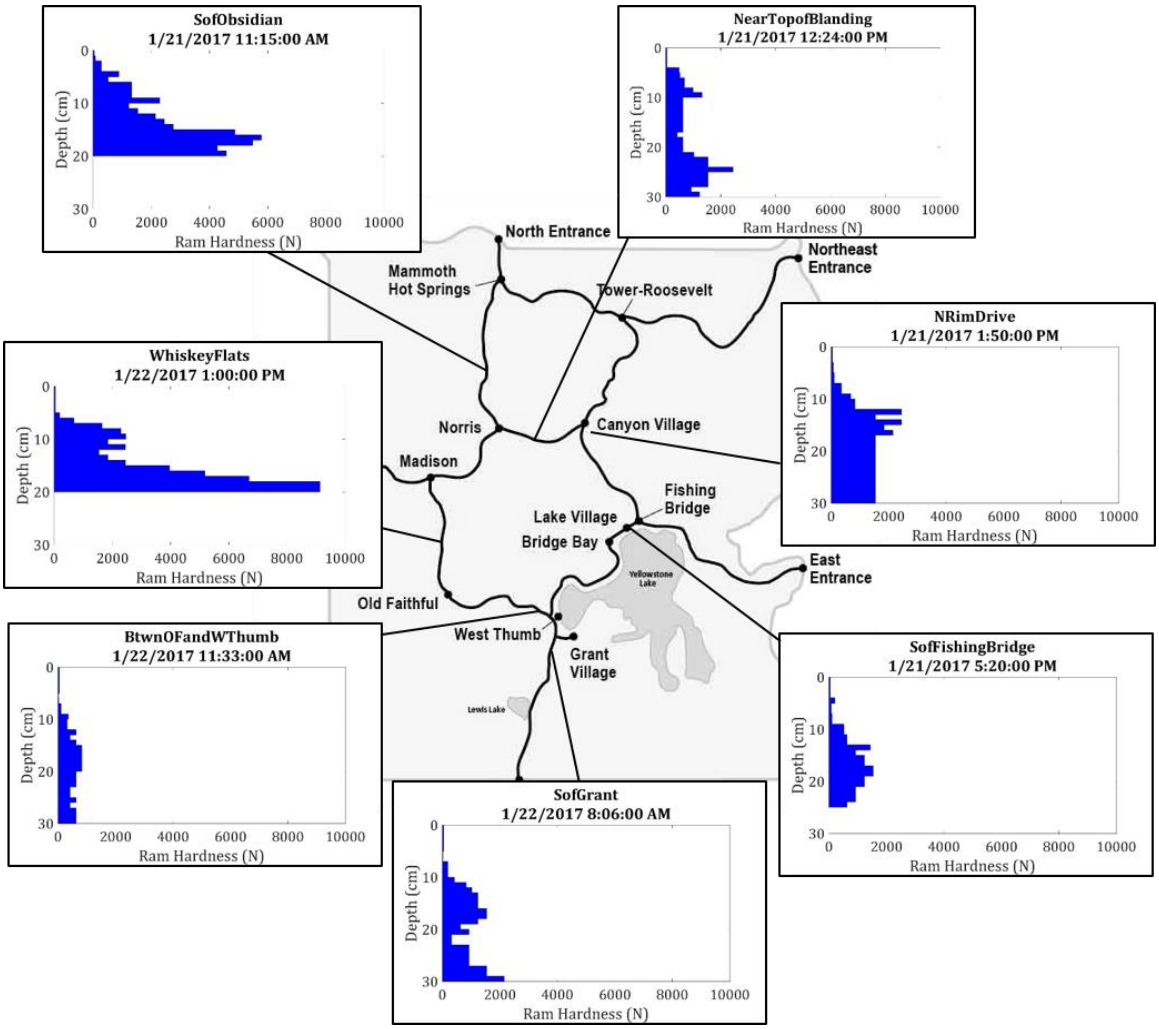

Figure 33. Hardness profiles throughout park, January 2017 radar trip

During the January trip, the hardest road layers measured were near the ground at Whiskey Flats and then near the ground south of Obsidian Cliff, between Mammoth and Norris. The measurement location with the softest snow throughout the road depth was between Old Faithful and West Thumb.

Prior to the radar trip in February 2017, a major freeze-thaw cycle occurred. This likely contributed to the extremely hard layer encountered at the test site between Mammoth and Norris, as shown in Figure 34. The location with the hardest

layer during the February trip is between Norris and Mammoth, which is consistent with the January trip. Also in both trips the softest road conditions throughout the road depth were seen in the Old Faithful to West Thumb stretch.

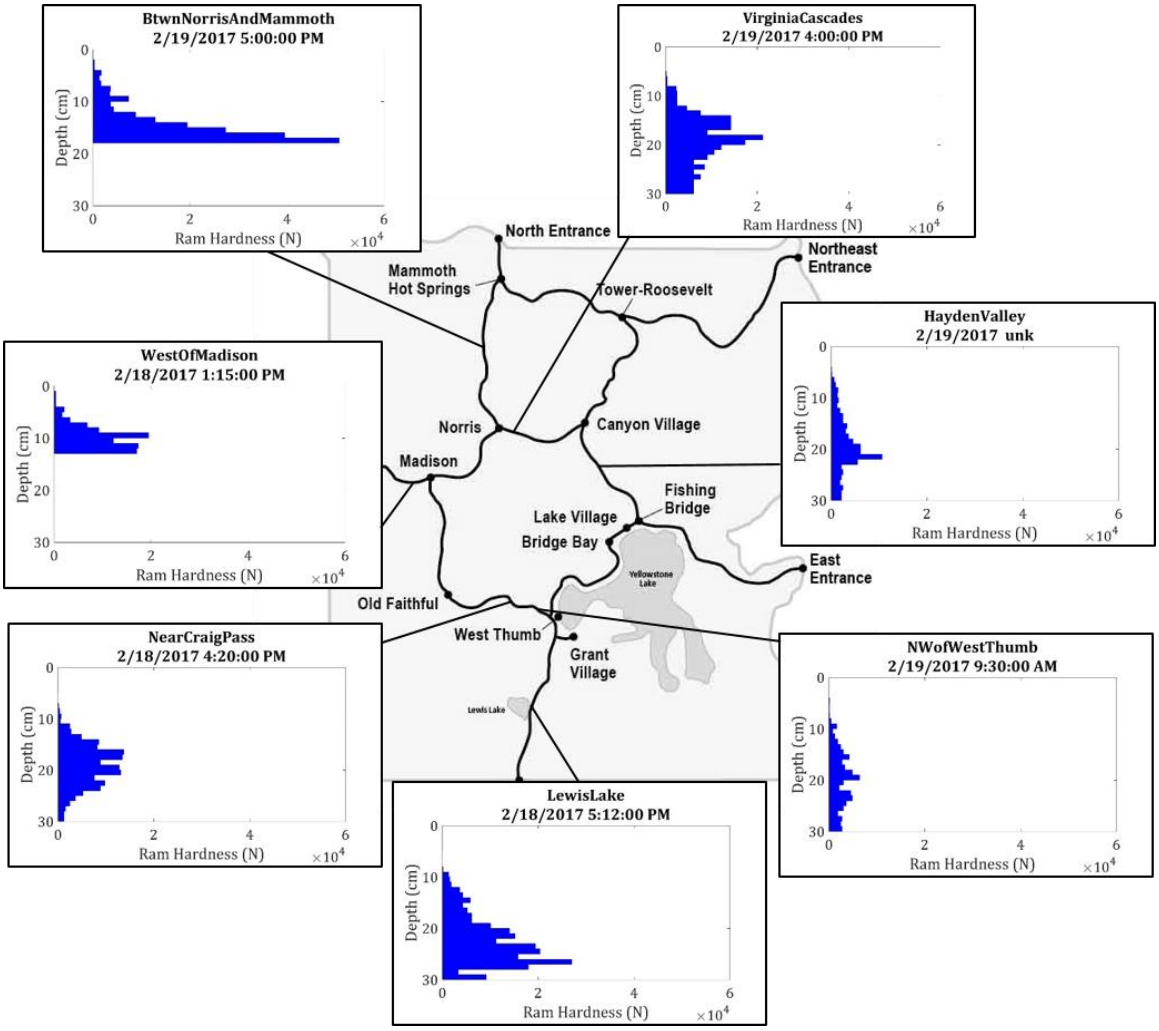

Figure 34. Hardness profiles throughout park, February 2017 radar trip

The hardness shown in the above figures provided road condition information that is related to factors possibly influencing road conditions in the following sections. Similar hardness data was taken throughout the park in Year 1, but not frequently on the same days. Therefore, hardness readings taken throughout

the park during Year 1 are not mapped like those above, but rather will be compared against site characteristics. In the following sections, hardness readings—both those shown above and others gathered throughout the study—will be correlated with potentially causal factors.

Weather

To track trends in the park's snow accumulation, the precipitation in Year 1 (2015-2016) and Year 2 (2016-2017) were compared to the 30-year precipitation average, 1981 – 2010 (Figure 35). Season 1 was a relatively dry winter with most sites showing below average precipitation. The exception to this was Sylvan Lake which has the highest elevation of all of the sites selected. Season 2 proved to be well above average for most sites throughout the winter with the exception of November. The difference between the two seasons' precipitation trends led to large variation in road conditions. Overall, there were few incidences of ruts during Year 1, whereas in Year 2 after large snowfall events there were many occurrences of significant rutting and snowcoaches struggling to stay on the road. Regarding the noticeable differences in vehicle performance between Year 1 and 2, the most obvious environmental difference is snowfall between these two seasons.

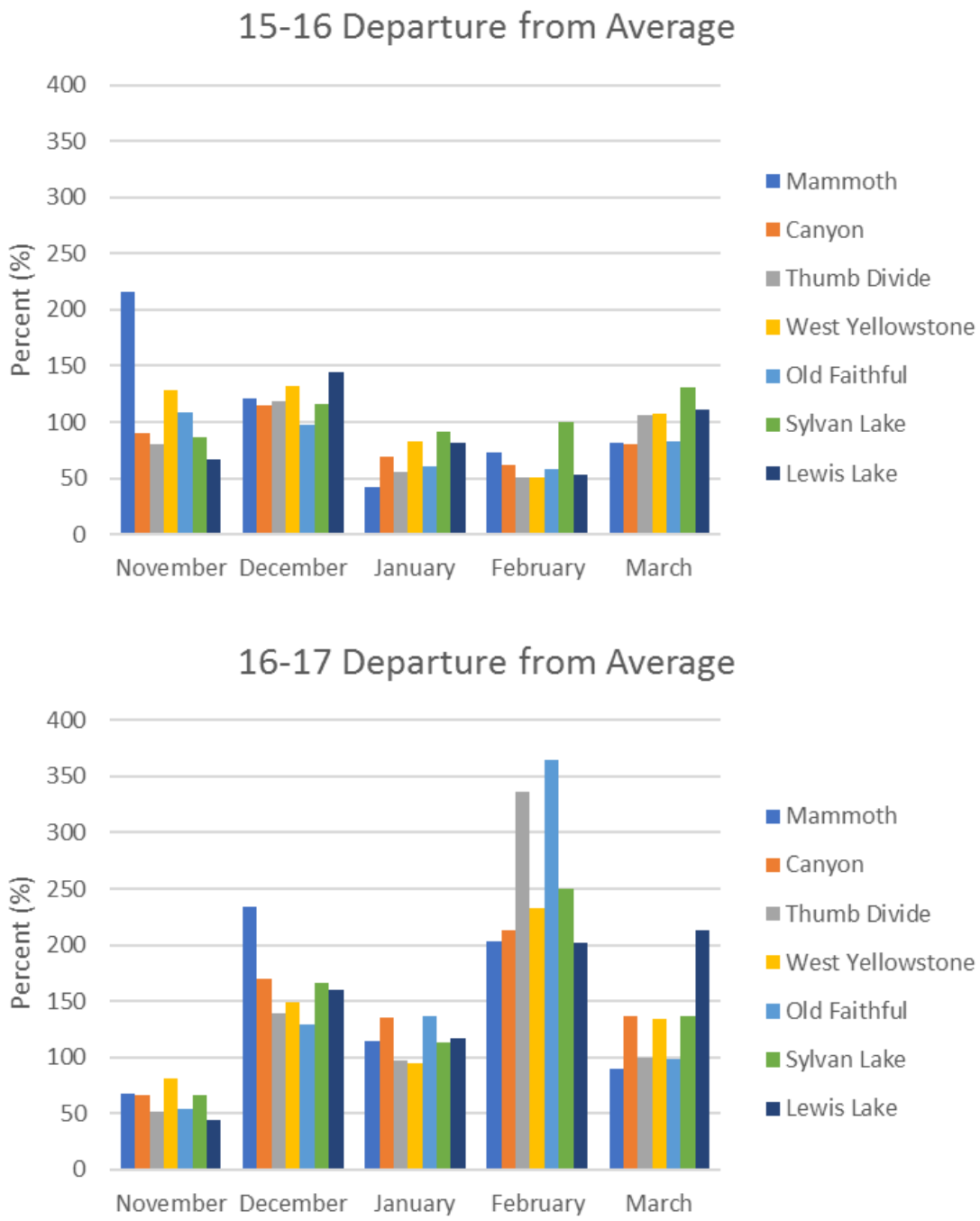

Figure 35. Year 1 and Year 2 precipitation compared to 30-year averages (1981-2010)

In addition to snowfall, it is important to examine temperature trends because of the influence of temperature on snow metamorphism. Figure 36 shows

the monthly average temperature for Year 1 and Year 2 for sites throughout YNP. Year 1 data shows a more uniform distribution of month-to-month temperature averages where Year 2 data shows colder temperatures for December and January and relatively warmer average monthly temperatures for November and March. Although there was not a drastic difference in monthly temperature averages between the two seasons, there were many events in Year 2 where daily average temperatures were significantly colder compared with Year 1. From literature it is known that at colder temperatures it takes longer for snow to sinter and gain strength. So on these colder days it is assumed that reduced sintering rates were present in the snowroads, resulting in reduced strengthening of the roads. Based on the large difference in snowfall amounts and slightly colder temperatures in Year 2, it is unsurprising that more rutting was observed in Year 2.

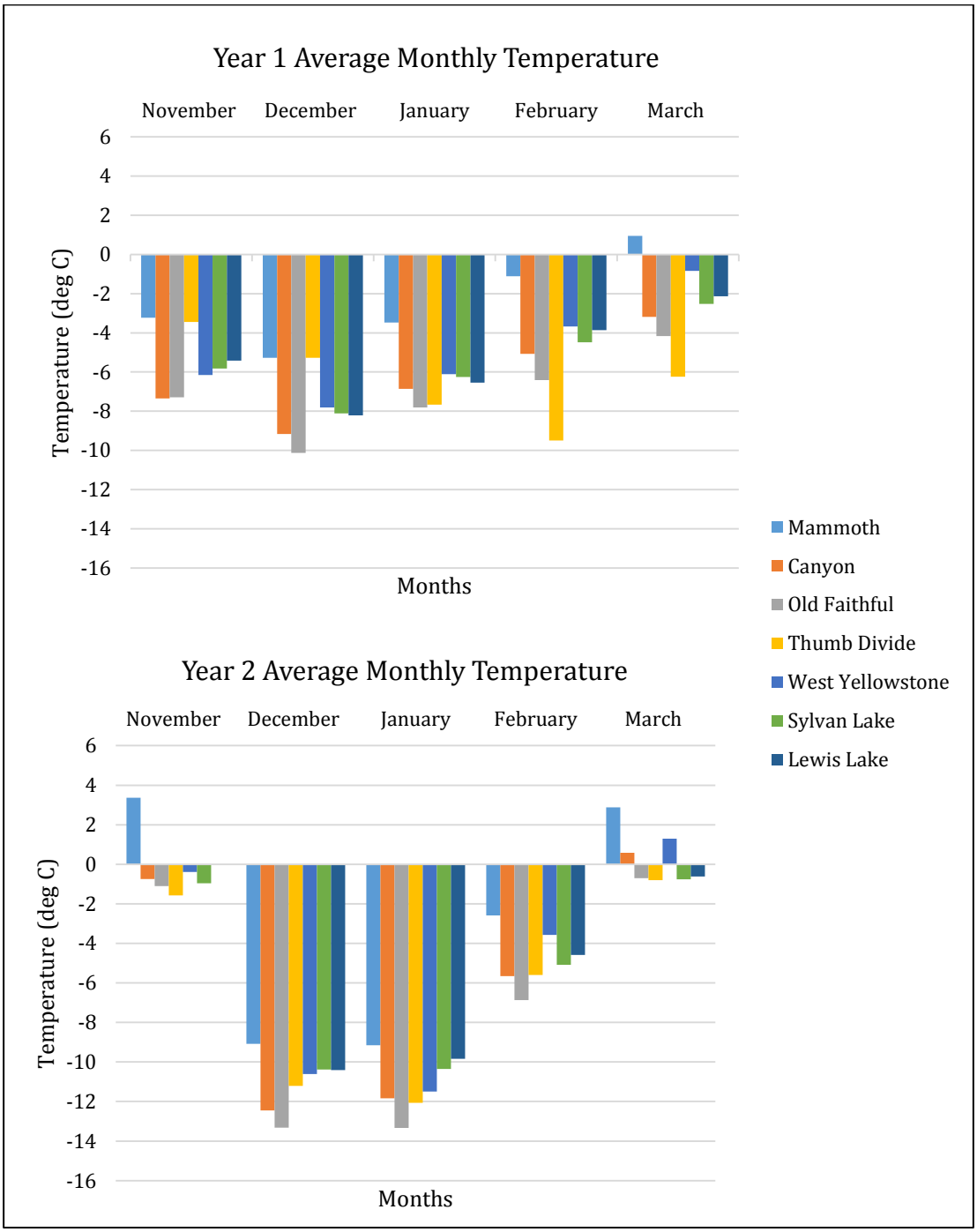

Figure 36. Average monthly temperatures, Years 1 and 2

Temperature can be quantitatively compared with hardness through a parameter called degree-days, used by Kozak and others (2002), and based on the

fact that "sintering increases rapidly at temperatures above -10 °C." This degree-day parameter finds the difference between maximum temperature and -10 °C (14 °F) for every day with a maximum temperature over -10 °C. This adds up throughout the season. Test sites in warmer areas with higher daily maximum temperatures on most days will have higher daily degree-day values than test sites in colder areas. Therefore a warmer test site will experience more "degree-days" throughout the season than a colder test site. For the hardness test sites, degree-days were calculated from December 1st, which is generally around the time that all districts in the park start to allow snow to build up for the snowroads.

Hardness at all tests sites versus degree-days since December 1st showed a positive correlation in this study. Sites with a higher number of degree-days since December 1st were harder than sites with less degree-days (Figure 37). This relationship was more pronounced deeper in the snowroad. This makes sense because snow deeper in the snowpack has been exposed to temperatures for a longer period, and exposure to warmer temperatures will have facilitated more sintering.

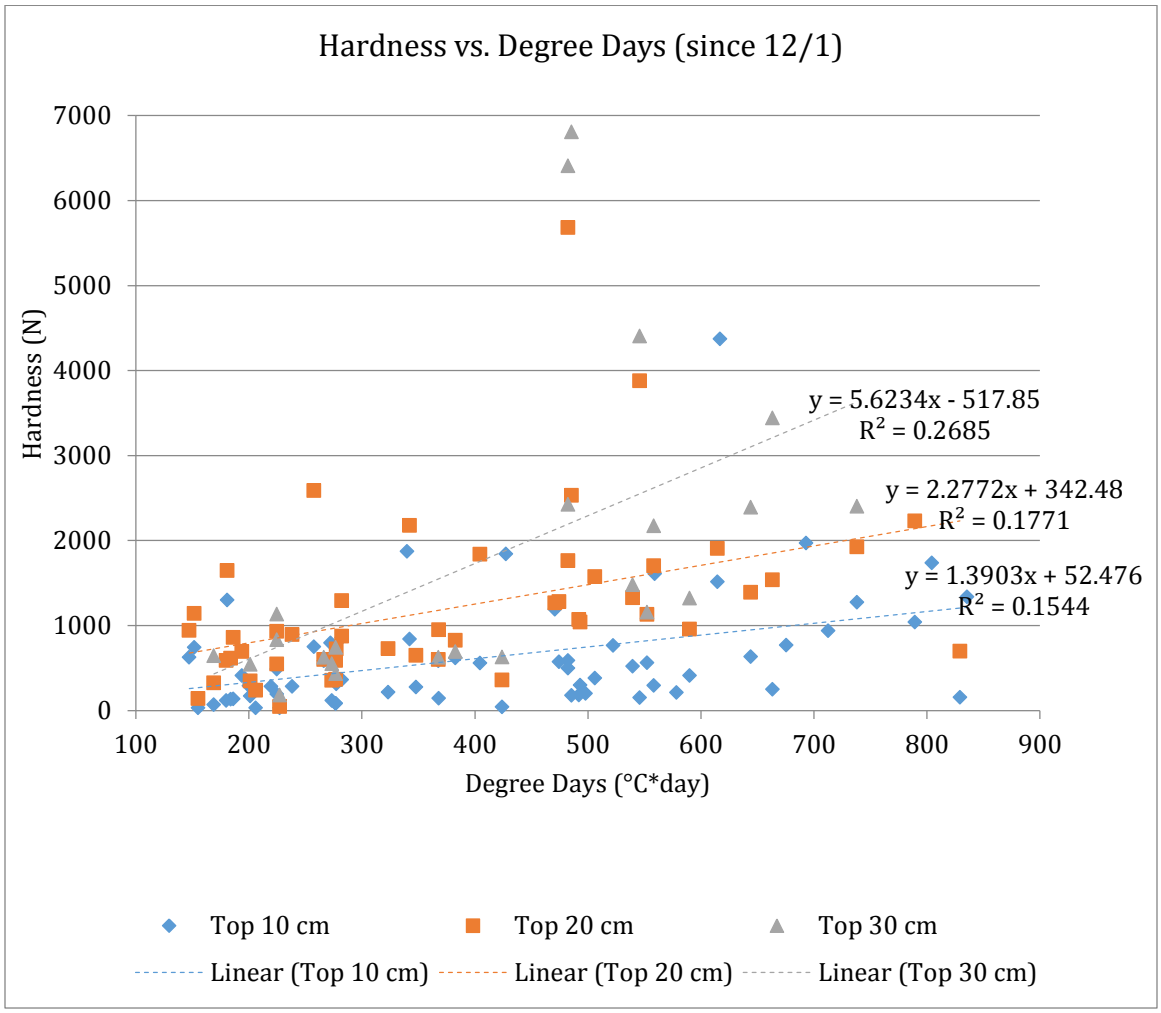

Figure 37. Hardness vs. cumulative "degree days" at test sites

This relationship between degree-days and hardness supports McClung's concept that warmer temperatures actually increase snow hardness over time (McClung & Schweizer, 1996). Supporting data for the second part of McClung's claim—that warmer temperatures have the immediate effect of making roads less hard—is discussed in the Grooming section, with respect to hardness versus temperature since grooming. However, researchers did note observationally that roads were harder at colder temperatures.

Site Characteristics

Hardness readings from both test years have been compared with site characteristics like elevation, aspect, and slope. Understanding correlation between hardness and non-controllable factors like site characteristics can help park management understand the relative impact of controllable versus non-controllable factors and where to focus their efforts. The hardness readings compared in these analyses include all readings from main park roads. This means that readings from the Grant Test Track are not included in the following graphs since it is not open to the public and was groomed especially for this project rather than along with the main line roads.

Figures 38(a) and (b) show that for hardness in the top 10 cm (~ 4 in) of the road, site elevation negatively correlates with hardness from both testing periods (January 21-22 and February 18-19), so the top 10 cm of snow is less hard at higher elevations. Figures 38(b) shows that this trend holds true at deeper depths for hardness data from earlier in the season (January 21-22), but that the correlation is less consistent at deeper depths later in the season (February 18-19).

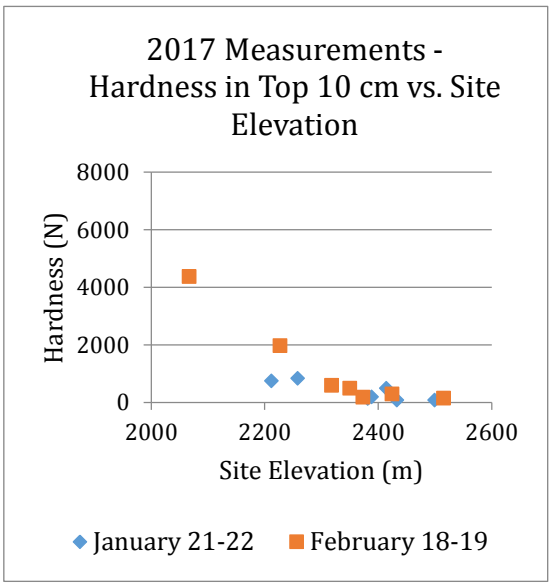

(a)

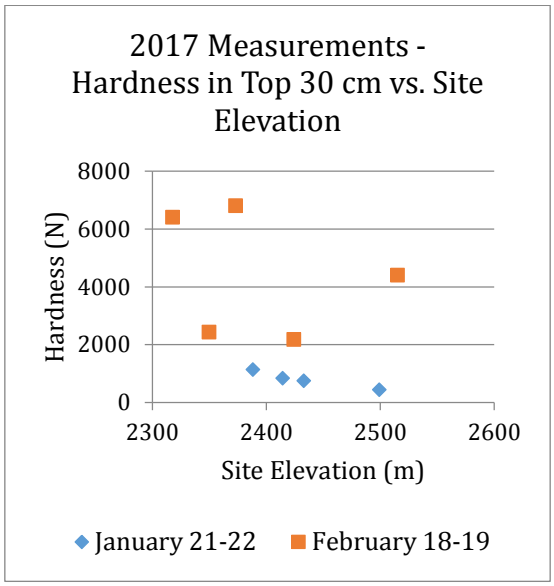

(b)

Figures 38(a) and (b). Hardness vs. site elevation in the top (a) 10 cm and (b) 30 cm of the road

These comparisons show hardness rather than density. While density does not necessarily dictate hardness, higher density snow has generally been observed to exhibit higher hardness, as noted in McCallum (2012). The elevation trend shown in Figures 38(a) and (b) are compatible with trends observed by Mizukami and Perica (2008) in a study of SNOTEL sites throughout the western US. Data demonstrated a relationship between the rate at which snow density increases in the natural snowpack during the winter and the site elevation. Both initial snowfall density and the rate at which density increases during mid-winter are less at higher elevations than at lower elevations. The higher hardness at lower elevations both in January and February may be linked to higher density snow associated with these lower elevations.

A couple of factors could influence this relationship. Higher elevations tend to remain at a colder temperature than lower elevations, and consistent colder temperatures can mean less sintering of the snow. As noted in the literature review, McClung and Schweizer (1996) found that while higher temperatures can cause immediate decrease in the hardness of a snowpack, high temperatures have the delayed effect of increasing the rate bond formation and therefore snow strength. This rapid bond formation results in snow exposed to warmer temperatures exhibiting faster hardening than snow exposed to consistently colder temperatures. The negative correlation between elevation and hardness could also be a result of higher elevations getting more snowfall on average than lower elevations, and therefore a larger depth of snow falling between grooming runs at the higher elevation. The Road Conditions – Other Measurements section of this paper notes that during this study higher elevation roads corresponded with deeper snowroad depth. This may be resulting in less compaction of the new snow at these high elevations, and is discussed further in the Grooming section.

Whichever factors are influencing this correlation, the relationship seems to be strong at the snow surface throughout the season, but less strong if including the hardness average over both the surface and deeper layers in the snow later in the season. This could be a result of other factors that impact the snowroad as time passes. Deeper layers in the snowroad have been impacted by additional factors (traffic and grooming patterns) for a longer period of time than the shallow layers. The reduced correlation of elevation and hardness at deeper depths later in the

season indicates that factors not related to the site elevation become more influential to the existing snowpack in the road as the season progresses.

Figures 39(a) and (b) show the average hardness in the top 10 cm (~4 in) and 30 cm (~12 in) of the snowroad measured at various sites versus the "northness" of the aspect of those sites, a concept used by Mizukami and Perica (2008). The aspect of a site is the direction its slope faces, with a zero-degree aspect facing north. The aspect values here have been translated to a factor of "northness" (or the cosine of the aspect value), with one being due north and negative one being due south. Due east and due west would both have a value of zero. This comparison shows a possible positive correlation between hardness and northness in the top 10cm of the road during the January measurements. The February readings show a more negative correlation, but this is less consistent.

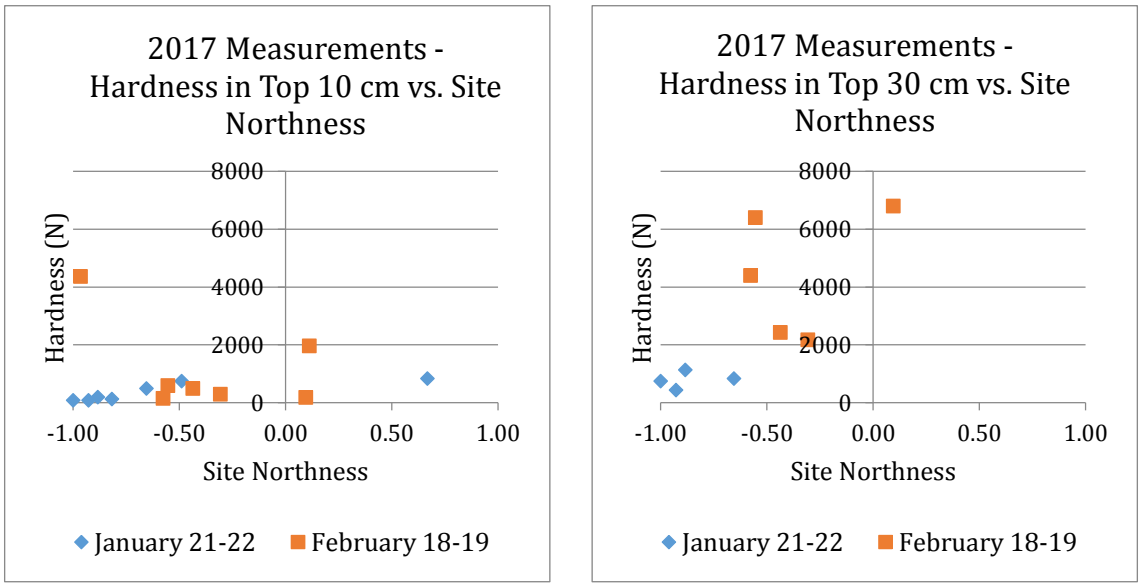

(a) (b)

Figures 39(a) and (b). Hardness versus "northness" of Year 2 site aspects (1 faces due north, -1 faces due south) for the top (a) 10 cm and (b) 30 cm

Figure 40 shows average hardness of the top 10 cm of the snowroad versus site slope, grouped by month of testing. No patterns are clear, though trendlines for each month's data points all seem to trend upward (increased hardness with increased slope), with the exception of December 2015. Note that slope values mostly fall within the one- to five-degree range, so do not vary significantly.

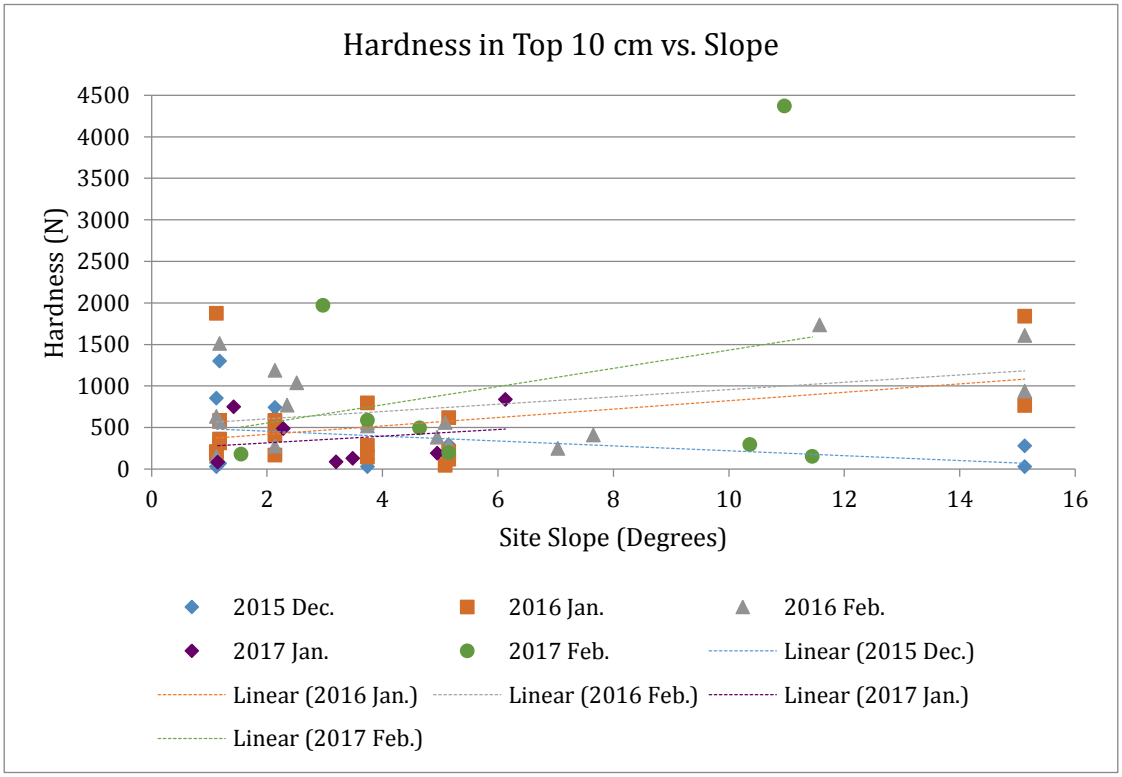

Figure 40. Average hardness in the top 10 cm versus site slope, by testing months

In snow science and avalanche forecasting, slope and aspect are of great importance. Mountain terrain includes a variety of slopes and aspects, so their impact on snow results in a wide range of snow conditions. However, because roads are constructed to minimize slope, the slope of roads varies over a relatively small range. Aspect is less influential for smaller slopes, so the small slopes on the road

could be part of why the trends between hardness and slope and hardness and aspect are not very strong.

Because of the reduced variation of site characteristics on roads and the associated reduced impact of these factors, another site characteristic unique to roads was examined. Because roads are relatively flat, any surrounding trees are likely to cast shadows on the roads. However, the road corridor itself provides a break in the trees through which the road may be exposed to the sun. Therefore, a site characteristic of "road orientation" was compared to hardness. This parameter was calculated by breaking the road into 200-meter segments (656 feet) using ArcMap and calculating the orientation of these road segments using the latitude and longitude of their end points. The resultant number was in degrees, with 0° being a west-to-east road orientation, and -90° (or +90°) being north-to-south. However, no hardness trend was apparent for this parameter either.

Last, "land cover", as defined in an ArcMap file provided by the Yellowstone Spatial Analysis Lab, was compared with hardness to determine whether the proximity of tree cover would have a discernable influence on hardness. However, only a handful of test sites were out of tree cover, so this parameter did not provide enough differentiation between shade at various test sites to provide a useful comparison.

Of the site characteristics compared in this study, only elevation seemed to have a noteworthy relationship with road hardness, with higher elevations corresponding with less hard snowroads. This could be due to the consistently

colder temperatures encountered at higher elevations; the increased amount of snowfall; and the different quality, less dense, snow that falls at higher elevations, and the slower rate of densification that goes along with this. Site slope and aspect seem to have negligible importance, likely because of the minimal slope of constructed roads.

Grooming

Many existing studies examine the relationship between grooming and snow hardness, providing detailed analysis of hardness produced by different grooming implements running side-by-side in controlled experiments. Due to limited field time and numerous priorities, no side-by-side grooming tests were conducted as part of this study. Rather, existing knowledge about grooming practices and their expected influences on road quality were used to inform analysis of the GPS groomer data in conjunction with weather station data from SNOTEL and NOAA stations throughout the park, all compared with hardness readings.

Since grooming influences the road throughout the entirety of the season, the hardness average over a 20-cm depth was used for many of these comparisons to represent the overall quality of the snowroad packing (beyond just the surface). Evidence in this study, discussed in the Vehicle Pass-bys – Subsurface Impacts section, indicates that day-to-day vehicle impacts occur in the top section of the road, so the top-10-cm-hardness average is likely influenced by day-to-day operations while the top-20-cm-hardness average is less so. Therefore, 10-cm-depth average hardness was examined for most day-to-day factors (e.g., time between

grooming and hardness) and 20-cm-depth average hardness was used to analyze impacts from season-wide grooming practices (e.g., average grooming speed throughout the season).

Grooming guides and studies, like those listed in the literature review, indicate that factors influencing snowroad hardness include setup time after grooming, temperature during grooming and the setup time, and fresh snow depth prior to grooming. Grooming data was coupled with time and weather data to determine which of these factors demonstrated a relationship with hardness. Hardness increases parkwide throughout the winter season, so data series are grouped into months of testing in an attempt to minimize the impact of this seasonal variation on the analysis.

The variable completely dependent on grooming practices and independent of weather is the speed of the groomer. Researchers hypothesized that a slower grooming pass would result in harder roads for the groomer using a tiller, but not necessarily for the other groomers which use a front blade and drag or just a drag in the case of the West District groomer. A comparison of average grooming speed with hardness in the top 20 cm of the snowroad, grouped by month (Figure 41) indicated a positive relationship between grooming speed and hardness, which does not match expectations. Examination of groomer speeds shows that speeds were fairly consistent within each district, though districts differed from one another in grooming speed. This consistency meant that data points clustered together with similar grooming speeds often all come from a single district. Therefore, the range of

hardness represented by a cluster of points may also reflect the other factors influencing this district's roads. For example, the grooming district with consistently higher grooming speeds may also be a district with a more effective grooming drag setup, colder temperatures on average, or some other confounding factor.

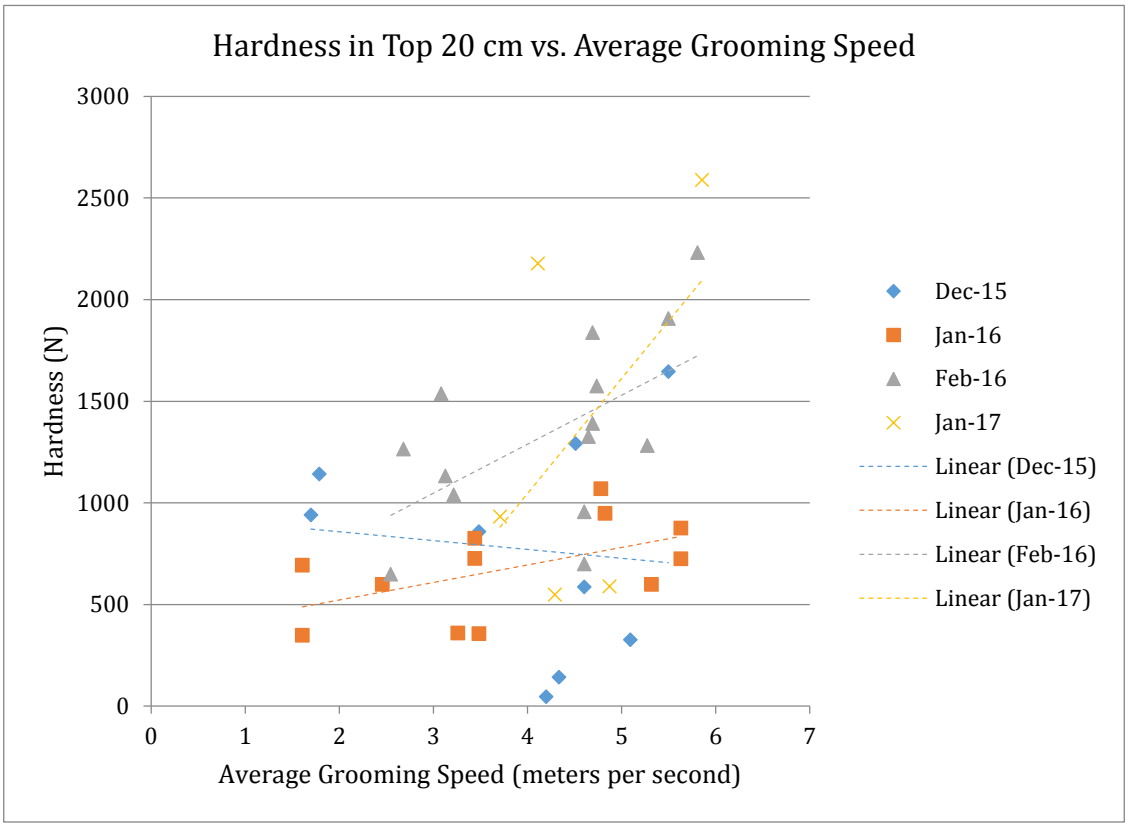

Figure 41. Average hardness in top 20 cm vs. average grooming speed for all months with more than two applicable data points

The positive correlation between average grooming speed and hardness in this data set runs counter to researchers' expectations and may not represent a consistent relationship. Interestingly, Shoop and others (2010) had similar findings about grooming (specifically, grooming with pneumatic-tired load cart), with data indicating better density increase in the snowroad at a higher grooming speed. As in

this study, Shoop and others posited that this relationship may be more indicative of temperature or other factors than the actual grooming speed.

Time of grooming and subsequent "setup" time for the road to harden as grains bond together can also be considered independently of weather, though the weather during that set time certainly impacts road quality. According to grooming literature, more time for the road to sit, untouched, is better for the road's strength. Figure 42 shows a positive relationship between "set time" (or the time between the groomer passing and the hardness test) and the hardness reading for the top 10 cm of the road, indicating that a longer time for the road to sinter after the grooming allows for a harder road. This trend was not evident for the hardness values in the top 20 cm of the road, indicating that this effect primarily impacts the surface of the road. This could be due to the deeper snow already having been compacted many times, meaning that additional compaction events increase the density (and encourage sintering) to a lesser degree than for shallower layers. The positive trend between set time and hardness at the snowroad surface underscores the importance of allowing as much time as possible between grooming and the onset of traffic to ensure the quality of the surface of the road.

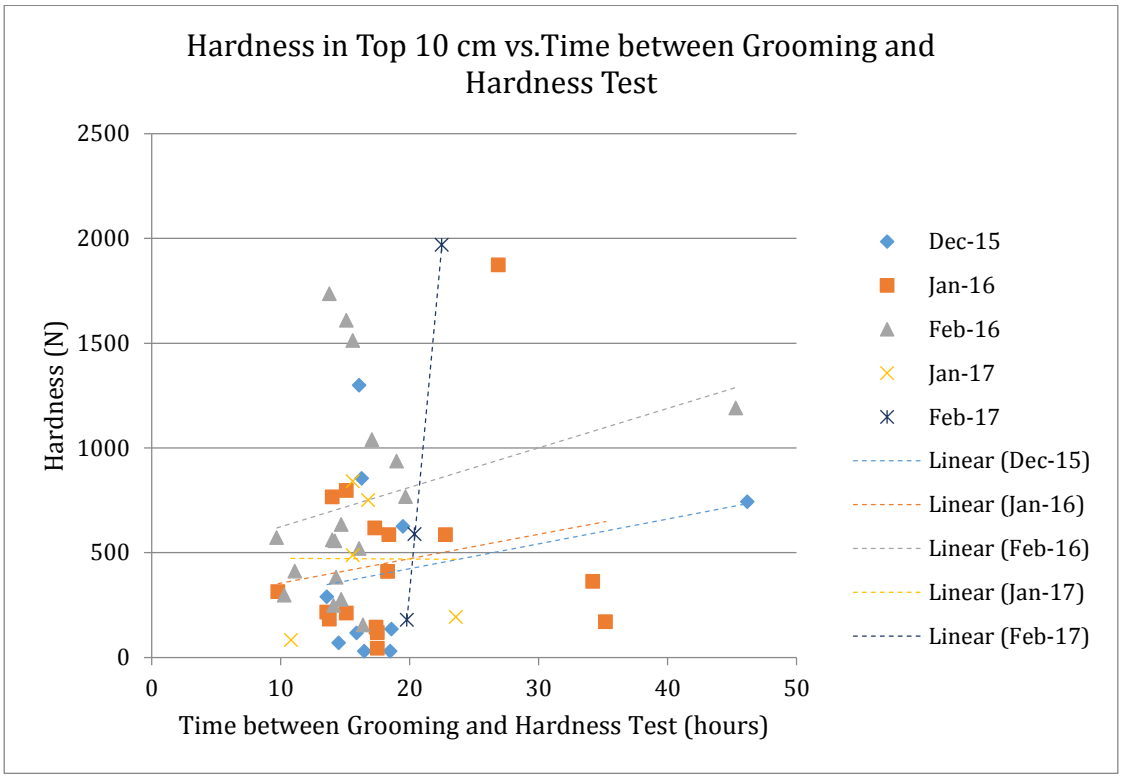

Figure 42. Average hardness in top 10 cm vs. time between grooming and hardness test

Temperature between grooming and the hardness test could also impact snowroad hardness, since sintering and metamorphism are driven in part by temperature. As mentioned in the literature review, previous studies (McClung & Schweizer, 1996; Kozak and others, 2002) have noted that warmer temperatures encourage snow bonding and hardening over a long timeframe, but that colder temperatures cause harder, stronger snow in the short term. Therefore both temperature at the time of the hardness test and the average temperature between the last grooming event and the hardness test were examined. Average temperature between grooming and hardness test showed a slightly negative correlation between temperature and hardness in the top 20 cm of the road, but less so in the

top 10 cm (Figure 43). The temperature at the time of testing did not show a correlation with hardness. This indicates that temperature in the hours leading up to the hardness test impacts the hardness within the snowpack, but that the temperature impact occurs over time as sintering and other processes take place rather than instantaneously. Van Herwijnen and Miller (2013) demonstrated that at -10 °C, both rounded grains and depth hoar increased in hardness rapidly within the first few hours of being left undisturbed, on average doubling their resistance to penetration within the first hour and then tripling it within six to seven hours. The temperature's impact on deeper layers of the snowpack but not as much on the surface also indicates that other factors (like traffic) may have more impact on the top layer of the snow.

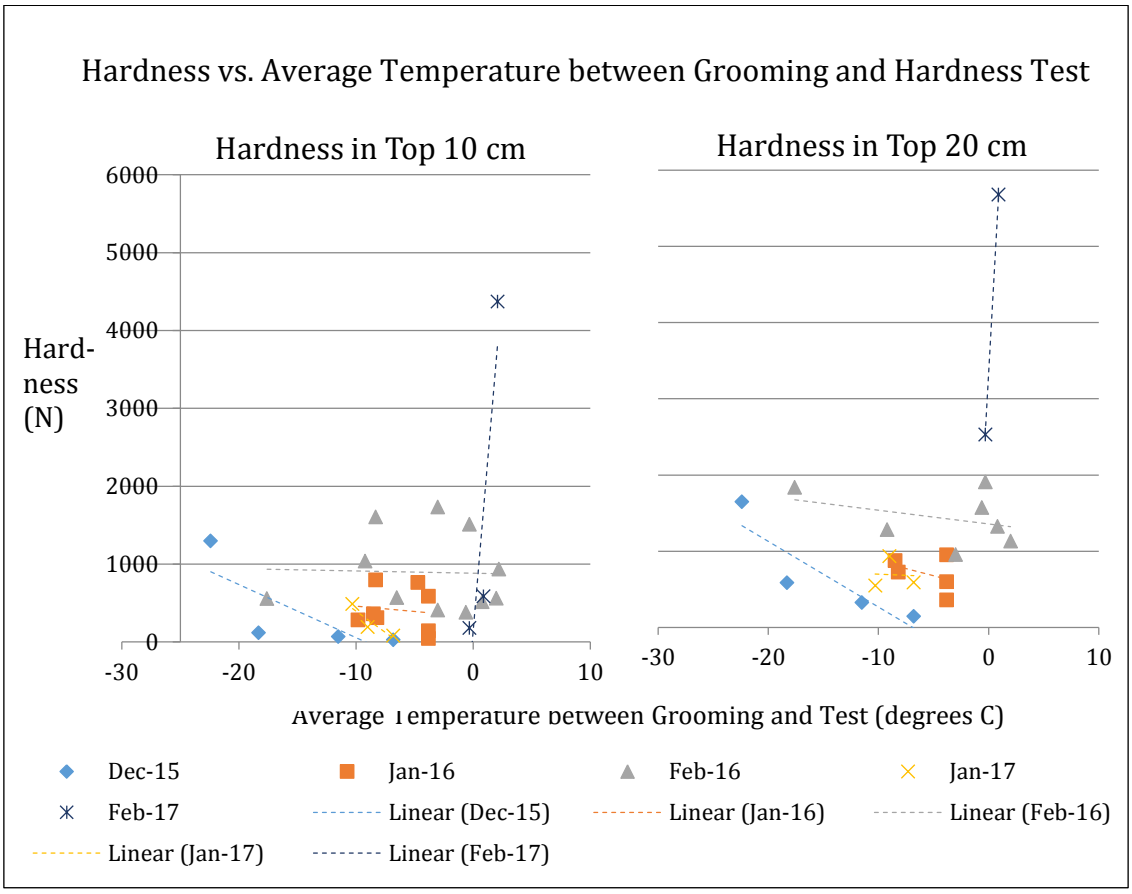

Figure 43. Hardness vs. temperature between the last grooming incident and the hardness test

One of the main hypotheses being tested regarding grooming and road quality was that a higher amount of snowfall between grooming runs would result in softer roads. For test sites comparable to a nearby SNOTEL site, hourly SNOTEL snow depth and precipitation data could be used to calculate the change in these parameters between grooming runs. This was calculated for all applicable sites. The amount of precipitation or change in snow depth from one grooming event to the next was generally very close to the daily totals calculated from midnight to midnight with SNOTEL data and those reported as daily totals at NOAA stations.

Data demonstrated that the vast majority of test sites were consistently groomed nightly, meaning that the precipitation between grooming runs would be approximately equal to the daily precipitation values at that test site.

Test sites for which SNOTEL sites were considered to be representative only accounted for 57% of hardness data points, and various gaps in the GPS data (described in Appendix A) further reduced the number of hardness tests that could be compared to hourly data with hours defined by grooming times. Further, hardness readings in shallow sections of the snowroad might not go to a depth of 20 cm, reducing the data points that could be used for a comparison of hardness deeper in the snowpack. Only 65 hardness tests on main park roads were available to begin with and all of these limitations decreased the number of points that could be used to demonstrate trends. Therefore, daily precipitation and snowfall values were deemed to be an adequate representation of those values calculated exactly from grooming run to grooming run, so were used in comparisons with hardness so that more data points (including those using NOAA data or having grooming data gaps) could be compared with hardness to test the grooming and precipitation hypothesis.

During Year 2, average hardness in both the top 10 cm of the road and the top 20 cm of the road was lower for sites with higher average daily precipitation and change in snow depth (Figure 44), which is the expected relationship. This was expected because of previous research that suggests grooming very small increments of snowfall (a few centimeters) will create a much more uniform and

quality road surface (Abele, 1990). This trend does not show up in Year 1 data. This could be due to the low amount of snowfall during Year 1.

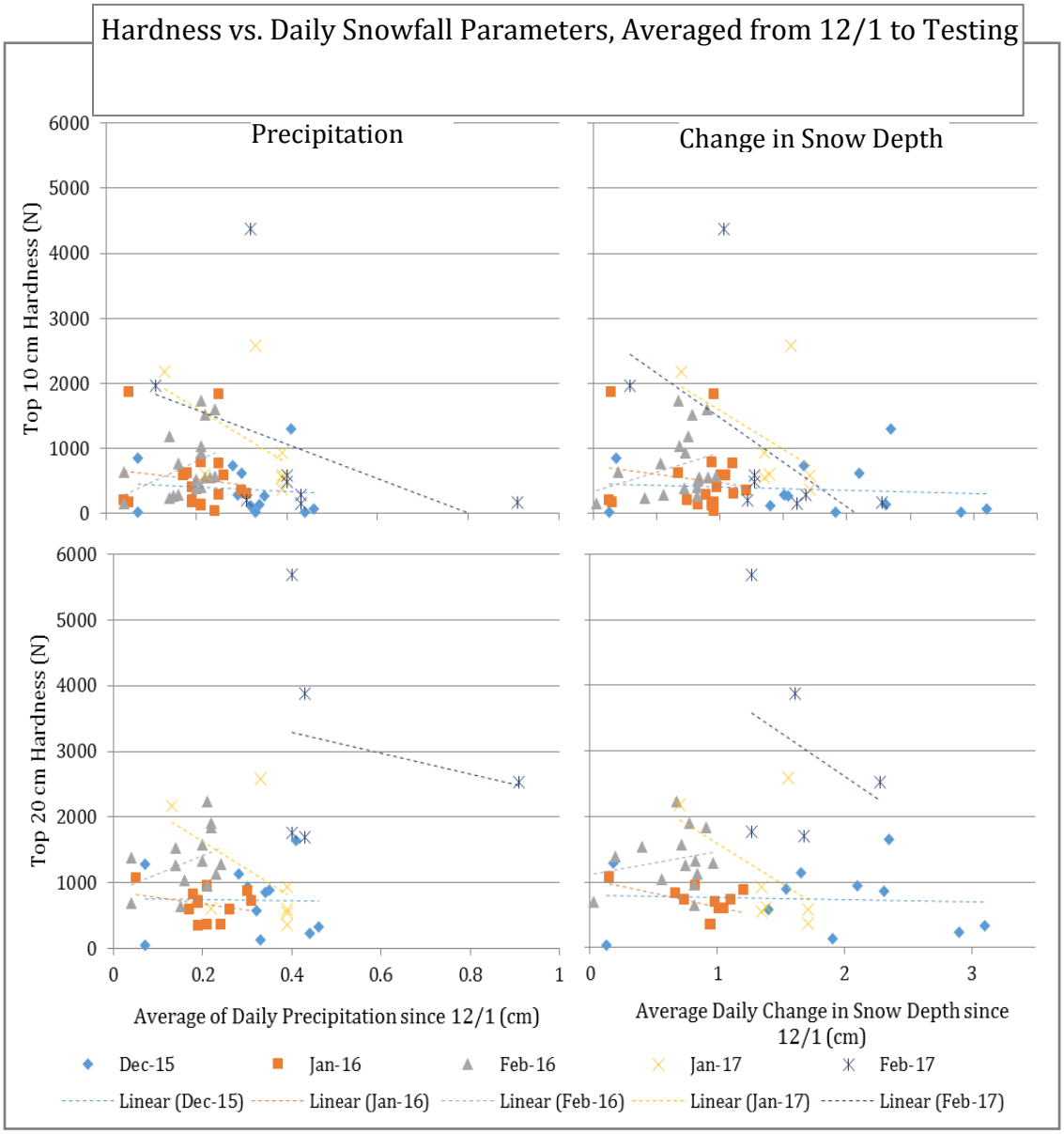

Figure 44. Hardness vs. average daily precipitation and change in snow depth, Years 1 and 2

Precipitation and snow depth ranges seen in the two years vary accordingly. While December 2015 data has some higher values for snow depth change than

January and February 2017 values, this reflects the concentration of snow in the beginning of Year 1. While the average daily snowfall during December 2015 had some high values, these average numbers only represented an average of days during December. Later that winter, as the average included more days (from December 1st through the hardness test date), the average snow depth increase dropped down, reflecting inclusion of all of the low- or no-snow days later in the season. Note that the difference between "precipitation" and "snow depth" data from SNOTEL is that the precipitation value represents the precipitation as water (much like the snow-water-equivalent) throughout the season, and snow depth represents the snow depth on the ground, which is impacted by both snowfall and evaporation/melting/etc.

The negative correlation between average daily snow depth increase and precipitation in bigger snow years with hardness indicates that a larger amount of snowfall between grooming runs may limit the effectiveness of those runs. Trying to compact a larger snow depth may reduce the overall compaction effectiveness and not result in as much bonding within the snowroad. This may be mitigated operationally by grooming multiple times per day during large snowfall events. GPS data indicated that groomer operators already implement this strategy occasionally, particularly in the Grant District.

One last comparison providing insight into the grooming districts is looking at change in hardness by district across seasons. Hardness increases throughout the winter season across the park, but the rate of change (change in hardness over time)

differs by district. Figure 45 shows hardness throughout Year 1 and Year 2, grouped by grooming district. In both years, Lake District has the lowest rate of hardness increase and Grant and Old Faithful Districts have rates of change within 30% of one another. In Year 1, West has the highest rate, but in Year 2 West doesn't have enough data points with the snow at least 20 cm deep to have an average hardness value for the top 20 cm. Canyon has a rate between Old Faithful and Grant in Year 1, but in Year 2 has twice the rate of either Old Faithful or Grant. Year 2 has so few data points compared with Year 1 that the data is less meaningful.

Many factors could be influencing these rates of hardness increase, but one stands out. Grooming speed does not seem to be the key factor, as Grant and Old Faithful Districts generally operate in different speed ranges but see similar rates of hardness increase throughout the season. Grooming method also differs between Old Faithful and Grant, with Old Faithful often using a tiller and Grant using a drag. Canyon and Lake, like Grant, also use drags but do not seem to be as similar in rate of hardness increase as Old Faithful and Grant. Climate could be an influencing factor, as described in the Weather Patterns section. The other major factor that obviously differs between the districts, however, is traffic. Grant and Old Faithful consistently carry a very similar traffic load with most tours out of the South Entrance heading to Old Faithful, passing through these two grooming districts. Lake consistently has the lowest traffic loading, and West has the highest. This will be discussed further in the next section.

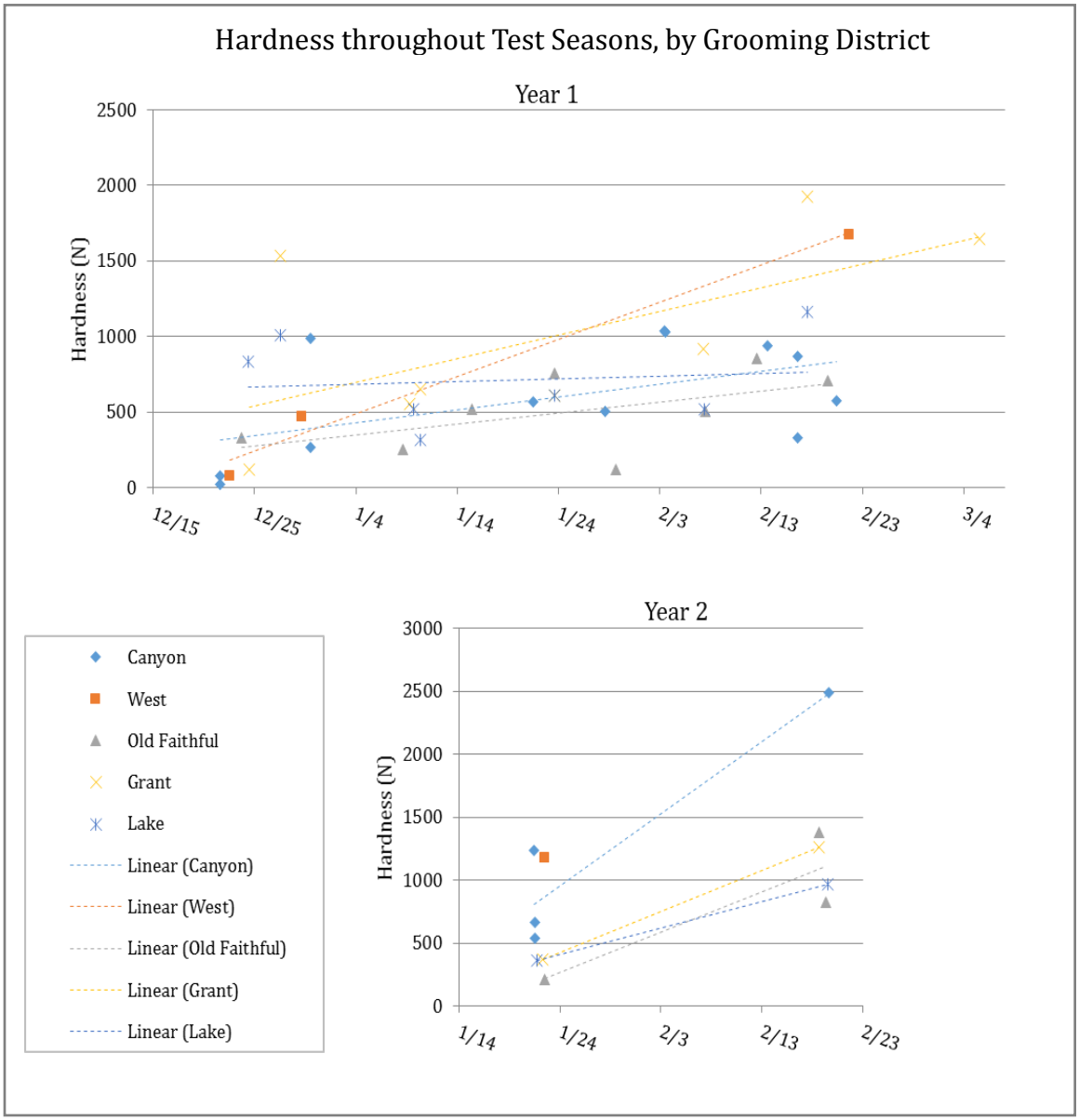

Figure 45. Hardness throughout season by grooming district

<u>Traffic</u>

As discussed above, the increase in hardness across different grooming districts in Year 1 and Year 2 seems possibly related to the traffic in that district, based on 1) Old Faithful and Grant districts experiencing very similar rates of

hardening, 2) Lake District experiencing the lowest rates of hardening, and 3) West District experiencing the most hardening in Year 1.

While exact amounts of traffic on each road section are not quantified, traffic on different road sections can be estimated using both the photographs from motion-sensor cameras deployed in Year 1 and general impression of traffic loads gleaned during trips into the park.

The photos collected from the motion-sensor cameras in Year 1 provide a rough estimate of relative traffic loads between the three test sites where the cameras were sited. Figure 46 shows the number of snowcoach photos captured by the motion-sensor camera at each test site and how those relate to hardness. Note that this is not the exact number of snowcoaches that passed the site, but the number of photographs showing snowcoaches. Some snowcoaches that went by cameras slowly were captured in multiple photographs so are counted multiple times in the "snowcoach photos" number. Additionally, the ability of the camera to capture passing coaches in its photos is very dependent on the camera's position, namely its proximity to the road. For example, Virginia Cascades test site has a fairly narrow road corridor through dense trees, so the camera at that site was positioned quite close to one of the lanes. The majority of trips going to the Canyon area via Norris (thus passing through the Virginia Cascades test site) are day trips that return through the same route on the same day. However, photos often showed many more coaches heading east than west. The eastbound lane was further from the camera, so coaches going that direction were more likely to still be in the

camera's frame of view, making it into a photograph, in the time it took the camera to detect motion and snap a picture. The proximity of the westbound lane to the camera seems to have prevented some snowcoaches traveling in this lane from being photographed. Therefore, Virginia Cascades daily photo totals were calculated by multiplying the number of eastbound coach photos by two rather than using any of the westbound coach photos.

Trendlines relating hardness to the number of snowcoach photos for the test sites show a positive relationship, and have a relatively consistent slope (change in hardness to change in number of snowcoach photos) for hardness in the top 10 cm (~4 in) of the road, as seen in the left graph of Figure 46. Trendlines for this relationship in the top 20 cm (~8 in) of the road are not consistent between test sites or with the top 10 cm (~4 in) averages. The top 20 cm (~8 in) would be expected to be more representative of the season-wide impact of something like cumulative traffic load, so the meaning of this lack of consistency is unknown. However, the consistent relationship between traffic and hardening of the top 10 cm (~4 in)—indicating that traffic throughout the season leads to harder roads—is worth noting.

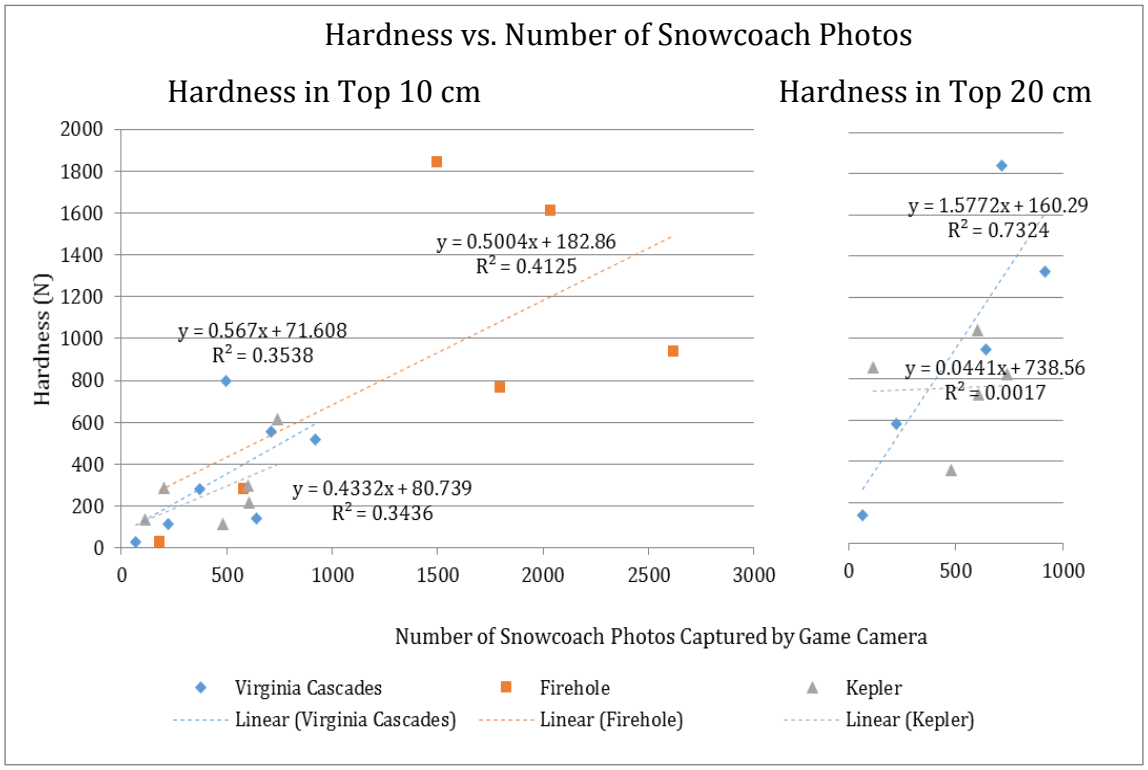

Figure 46. Hardness vs. number of snowcoach photos captured by motion-sensor cameras

The 10-cm-depth data in Figure 46 hints at the relationships further indicated by Figure 45. Figure 45 shows the West district hardening throughout the season having roughly twice the slope as the average of the slopes of Old Faithful and Grant, and Canyon having a slope between that of Old Faithful and Grant. The estimates of relative traffic loading provided by the traffic cameras indicate that in Year 1, the Firehole test site (in the West District) had approximately twice the snowcoach traffic as the Kepler test site (in the Old Faithful District), with snowcoach photo totals of 3141 and 1463, respectively, for the period of photo data collection (12/8/15 to 2/24/16). The slope for the Lake District is approximately one tenth of the average of the slopes of Old Faithful and Grant. In Year 2, the slope

for the Lake District is half that of the average of Old Faithful and Grant, and that for the Canyon District is twice the average of Old Faithful and Grant. While no traffic data is available for Year 2, the relationship of the slopes between the different districts again seems to relate to the typical amounts of traffic for the respective grooming districts, with the exception of Canyon. These comparisons indicate that more snowcoach traffic loading ultimately leads to higher road hardness on a seasonal scale, and that the rate of hardness increase may be proportional to amount of snowcoach traffic.

Like the camera data, the season-wide change (Figure 45) contains some conflicting trends. The hardening throughout the season at the Canyon test sites, for example, was comparable with that of the Grant and Old Faithful districts in Year 1, but was far higher than all others (except West, for which a trendline could not be established due to limited data) in Year 2. The Canyon District is complex in that it has two separate sections with very different traffic patterns. The west part of the Canyon District, the road from Norris to Mammoth, receives a high volume of traffic, particularly Xanterra coaches travelling between Mammoth and Old Faithful. The east part of the Canyon District, Norris to Canyon Village, has much less traffic as it is primarily a day-trip destination receiving a much smaller amount of winter visitation than Old Faithful. Data points for Canyon were therefore broken out into "Canyon East" and "Canyon West" to determine whether seasonal hardening rates would be higher in the west section of the district based on its increased traffic load. For Year 1, this breakdown showed Canyon East to have a higher rate of hardening

by far. For Year 2, not enough data was available to compare the two. Canyon data therefore did not match the trends observed in data from the other districts.

While the increase of hardness in the roads throughout the season is compared with traffic here, there is also a correlation of accumulation of degree-days throughout the season. Since total degree-days experienced by test sites between December 1st and the date of testing has been linked with road hardening and this degree-day figure increases throughout the season, like the total snowcoach traffic experienced by the roads, understanding the relative contributions of these two factors is difficult. However, the correlation between traffic loading and the slope of average hardening rates indicate that traffic contributes to seasonal hardening and should be considered in addition to temperature patterns. This does not take into account the potential for snowroad surface disruption caused from vehicle traffic on a day where rutting may occur, but rather describes what seems to be a trend over the timeframe of the entire season.

Road Conditions – Other Measurements

Methods included measurement of snow characteristics other than hardness. Phipps (2008) describes these in detail, so this section provides just a brief overview. Other snow characteristics considered included snowroad depth, density, temperature, and mechanical properties.

The Flat Earth radar equipment measured snowroad depth throughout the park on multiple trips during both Year 1 and Year 2. Overall, snow depth on the

road was deeper during Year 2, as expected from weather patterns. Depth data from both years demonstrated a correlation between higher elevations and deeper snowroads (i.e., more snow built up on the road surfaces). The Sylvan Pass, South Road, and Canyon-to-Norris areas, all located at relatively high elevations, consistently contained some of the deepest snowroads in the park. Deeper roads also correlated with slightly softer (lower hardness) snow, which is likely related to the consistently lower temperatures and associated slower sintering rates.

While testing methods did involve collecting some density data, density measurements from the groomed roads consistently fell within a relatively small range: about 0.4-0.5 g/cc. In this range, hardness can vary drastically. Since hardness is more telling about the snowroad's resistance to penetration from snowcoach tracks or tires than just density, analysis in this study used hardness more than density.

The temperature gradient throughout the depth of the snowpack is important to the metamorphosis of the snow. Ambient air temperature plays a large part in driving that temperature gradient and was the main temperature component considered in this study, as described in the Weather section above.

Laboratory compression tests examined mechanical properties of snow samples retrieved from throughout the park on both radar sled trips and pass-by-testing trips, and CT scans were planned to provide insight into the snow microstructure. However, the extreme stiffness of the snow limited the information the compression tests yielded. Efforts were therefore focused primarily on in-situ

measurements and their analysis, which yielded a higher results-to-effort ratio than laboratory tests. This optimized research productivity for a study already challenged to produce enough data collection and analysis to adequately describe the road conditions throughout such a large area (i.e., the park). This focus followed conclusions from Lang et al. (1997) that microstructure image analysis is not an effective way to assess snowroads because of its time-consuming nature.

Vehicle Pass-bys – Vehicle Loading

Phipps (2018) addresses results from the load cell measurements at length. Trends in the load data included typical loading patterns associated with different types of vehicles. LPT vehicles consistently produced two large spikes in vertical load produced by the front tires and then the back tires. Tracked vehicles tended to produce vertical load spikes under each bogey wheel, with the track itself causing much less vertical loading. The lack of vertical load from the tracks of tracked vehicles was consistent on hard snow. On softer snow, the tracks carried slightly higher loads.

The maximum total magnitude of load was consistently higher for wheeled vehicles as they have less contact points among which the load is distributed. Lowering the tire pressure on wheeled vehicles decreased the maximum vertical load on the ground surface during a vehicle pass-by due to the increase in contact area from a more inflated to less inflated tire. This contact area increase spread the vertical force out over a larger area, decreasing its magnitude at any one point. For

both tracked and wheeled coaches, vertical load magnitude increased with increased velocity, possibly due to increased potential for dynamic loading at increased speeds.

No strong correlation between vertical load and road impacts (i.e., rutting) was evident. Additional processing of the load data facilitated supplementary ways to compare load data with road impacts. The impulse, which incorporates the time over which a load is applied, was examined. Despite the consistently higher magnitude of load for wheeled vehicles, impulse for wheeled and tracked vehicles travelling at similar speeds was generally comparable. Like vertical load, impulse did not obviously correlate with road impact.

Vehicle Pass-bys – Subsurface Impacts

Aramis

During both Year 1 and Year 2, subsurface videos processed using Aramis were used to investigate subsurface motion during passage of coaches. In Year 1, some processed videos showed promising results. The still frame in Figure 47 shows vertical strain measured in one video taken during passage of a Mattracks vehicle. This is the type of data expected from these tests. The strain calculated by Aramis and shown here could be compared with with the loading measured by the load cells to provide information about the snow's mechanical properties. This would also provide insight into how tracked and wheeled snowcoaches cause the snow to deform differently.

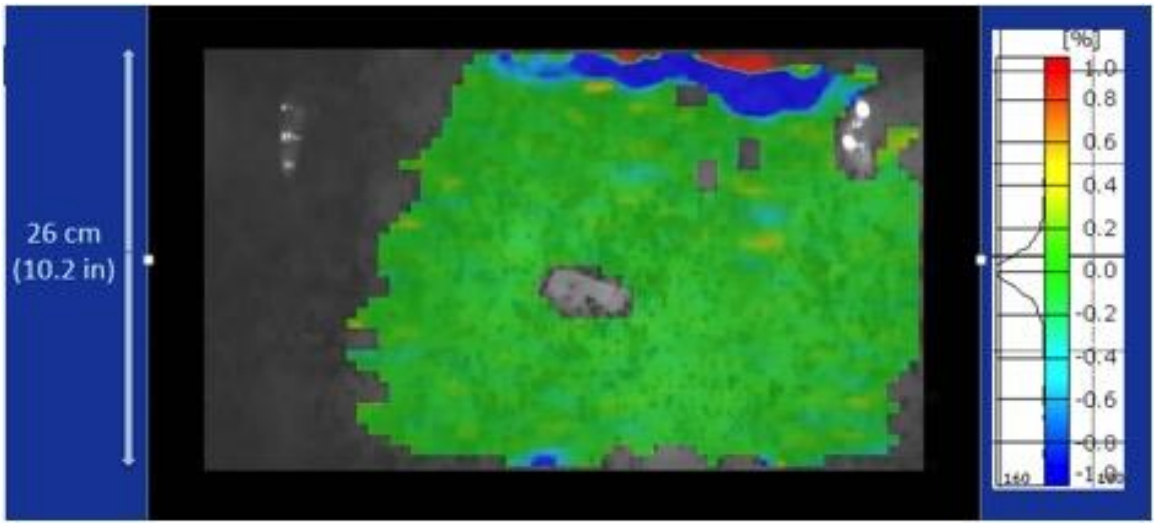

Figure 47. Aramis processing showing vertical strain (Feb. 12, 2016, Spring Creek test site)

Despite some promising processed images from Year 1, many image series did not show motion. This lack of motion could be due to a couple of factors: 1) many snowcoach drivers did not approach the box closely because they did not want to damage their vehicles, and 2) motion in the snow primarily only occurring at the very surface (the top several cm) of the snowpack, which was not captured in all video setups. Additionally, for images to be of sufficient quality for Aramis to track the motion of points in the images, both the lighting and paint flecks on the snow needed to meet precise standards. In some image series, the paint on the snow would start melting if the sun was shining on the snow above the wall; this would cause the paint flecks to melt into the pit wall and become impossible for Aramis to track.

Prior to Year 2, many more laboratory and field experiments were conducted to try to fix any controllable factors. Other snow markers (e.g., ground pepper) were

tested, and additional lights were ordered and tested. Museum-grade, glare-proof acrylic plexiglass was obtained to minimize the glare that could obscure the snow wall.

In Year 2, the subsurface camera setup had been improved, based on the laboratory testing, to remove any question that lighting or snow-marking practices could be the cause of no motion being detected. When these improvements were introduced into field testing in Year 2, the Aramis analysis showed a similar lack of motion, which indicated that subsurface deformation may actually be negligible. Additional literature review revealed that for soils, vehicle passage results in deformation primarily directly under the vehicle (Figure 48). Shoop and Alger (1999) confirmed that this is especially true in snow. The side-view Aramis technique was poorly suited to detect vertical motion in this location.

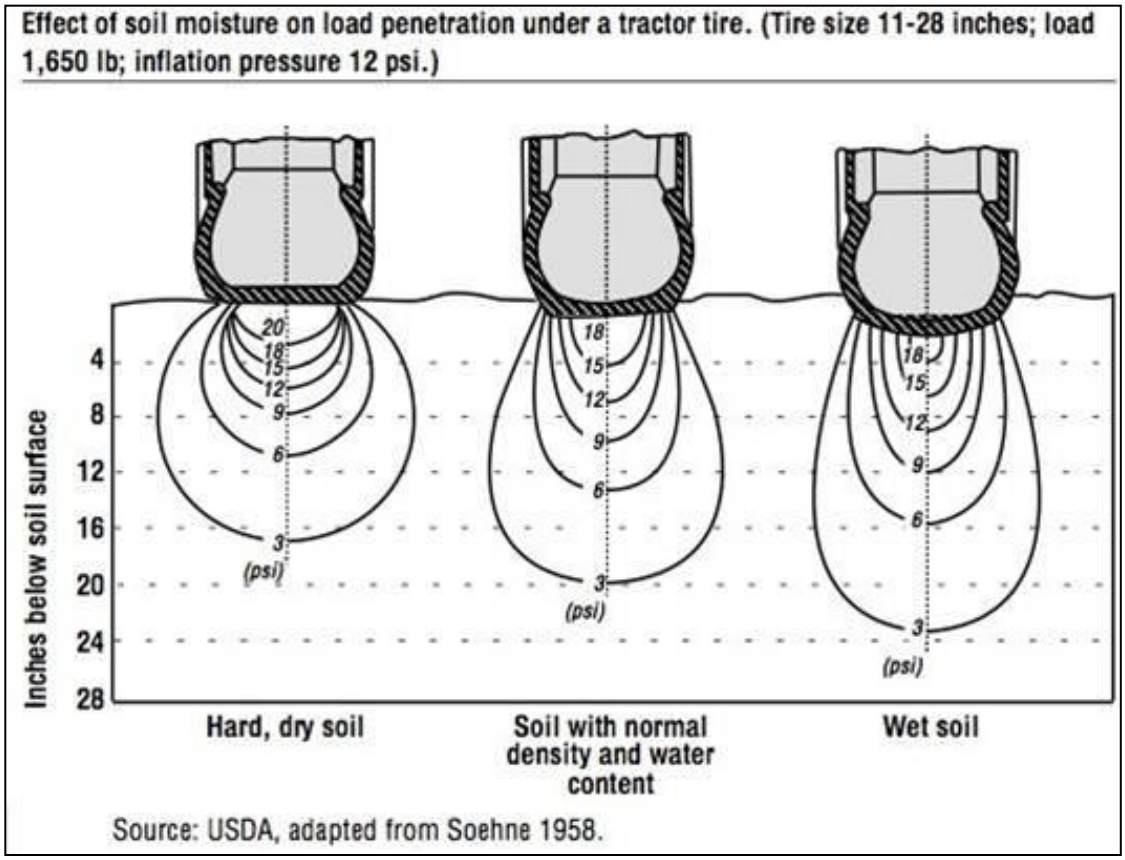

Figure 48. Difference in "pressure bulb" for dry and wet soil (Corangamite Catchment Management Authority 2013)

In light of this concept, the testing methodology was again adjusted during the second testing trip of Year 2. To capture a full picture of the potential motion under the vehicle, the camera box was set up parallel to the vehicle's direction of travel. With this setup, shown in Figure 49, the tracks or tires on one side of the vehicle would run directly over the length of the box which would allow for Aramis to view the pressure bulb.

Figure 49. Camera box positioned parallel to traffic, facing into traffic

Aramis was able to detect motion in the first few videos captured with the new test setup. However, one of the problems with using Aramis from the beginning had been the struggle to create a perfectly flat snow wall. In any location where there was a void between the snow wall and the plexiglass, the plexiglass was not confining the wall to prevent snow from moving horizontally. To analyze the deformation of the snow required an assumption that the plexiglass served as a confining wall. This would indicate that the only motion observed would be that within the snowpack, and not within an artificially-created hole in the snow. However, within the first few runs with the new camera setup, the force from the vehicle passing seems to have overwhelmed the capacity of the plexiglass, allowing it to flex and causing a large fracture to form in the snow wall (Figure 50). Once this

disconnect had formed in the snowpack, later passes would not show strain within the snowroad accurately.

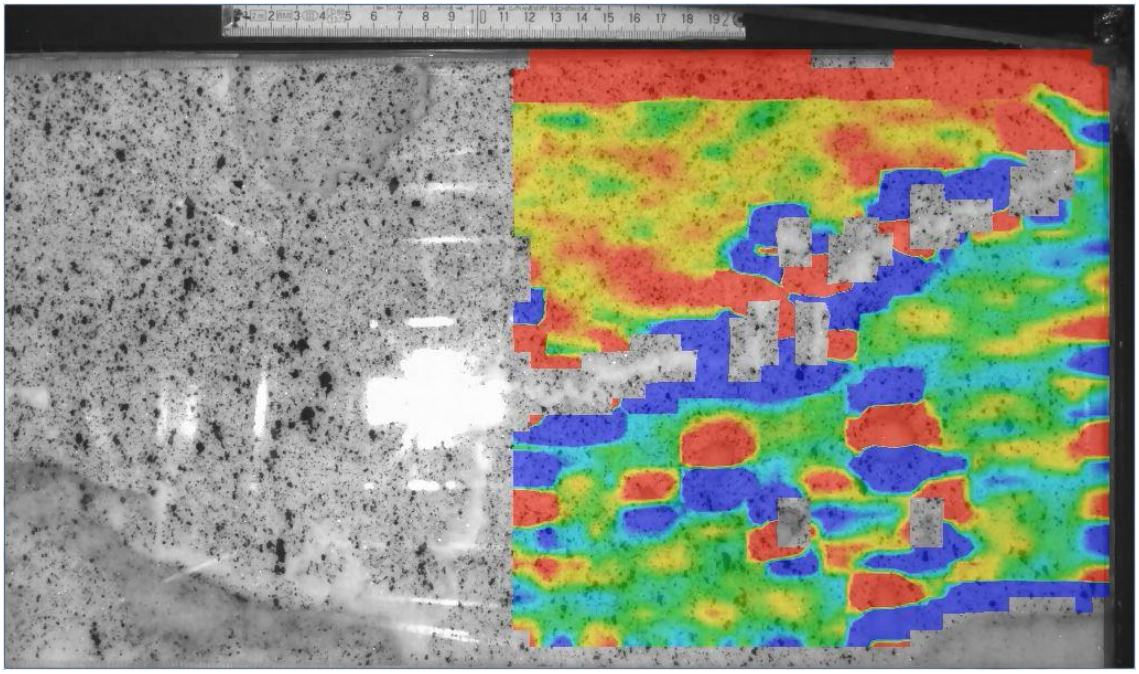

Figure 50. Aramis analysis showing fracture (Mattracks, Jan. 29, 2017, Grant Test Track)

Once a fracture has formed in the snow wall, the deformation occurring in successive passes does not necessarily represent the deformation happening the in the rest of the snowroad because it is separated. For testing to continue after this fracture, a new, undisturbed snow wall would need to be excavated and the camera set up again. This is a very time-consuming process, and this incident showed that the setup was vulnerable to fractures.

With this test, all options for improving the camera setup and getting substantial subsurface displacement measurements had been exhausted. While Aramis has been used successfully to measure strain in snow in a laboratory setting,

this series of experiments indicated that the difficulties of creating a highly visible and confined snow wall within a snowroad may prevent collection of substantial data in this situation. Anticipating this problem, a second method of measuring subsurface motion, an accelerometer array, was prepared between field seasons and implemented in Year 2.

Accelerometers

Acceleration describes the rate at which the velocity is changing. One "g" is the acceleration due to gravity, so would be the change in velocity over time (m/s/s or ft/s/s) for an object falling toward the earth (disregarding air resistance). Acceleration can also be negative, quantifying the change in velocity over a given time for something to stop. A car accident in which a vehicle goes from a high speed to stopped in a matter of seconds would involve high magnitude, negative accelerations. A study by Allen and others (1994) found that the action of "plopping backward into a chair" could cause momentary acceleration of 10.1 g to a person's head. The small accelerations measured in snowroads during this study therefore were surprising, but were consistent in magnitude across test days.

Accelerometer measurements provided the insight into the subsurface motion that Aramis did not. Accelerometers, like the load cells, provide raw readings of voltage, and processing converts this raw data into g's of acceleration. The data can then be processed to provide velocity and displacement. As discussed in the literature review, error propagates through this processing. Various methods have been developed to correct some of the known problems with accelerometer data,

and one of these was used in the processing for this project as described in Appendix F: Accelerometer Processing. However, the initial errors and extensive correction processing of the velocity and displacement data render their values less certain. Therefore analysis focused primarily on the accelerations; velocity and displacement numbers were considered secondarily.

Similarly to the load cell measurements, the acceleration data showed patterns particular to types of vehicles. LPT vehicles show two distinct oscillatory events where tracked vehicles show more than two events (i.e., one event per bogey wheel and/or ski) (Figure 51). This was the case for all vehicles. All vehicle patterns displayed the characteristics shown in the below graphs: acceleration did not happen as a positive or negative event, but rather oscillated back and forth from positive to negative acceleration at a rapid rate throughout the event.

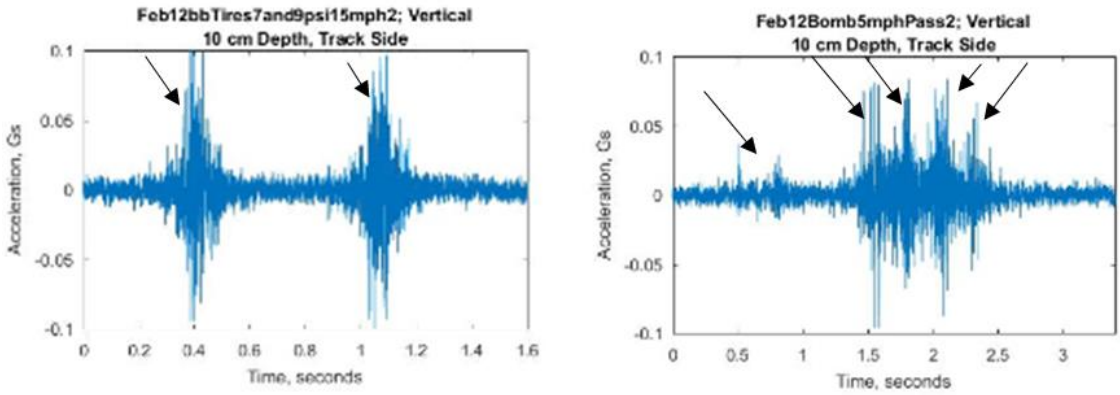

Figure 51. Acceleration plots versus time: LPT (left) and Bombardier (right)

The magnitude of these accelerations generally decreased with increased depth in the snowpack (Figure 52). Final displacement is not always in the same direction so varies between positive and negative in Figure 52, but for both

directions the magnitude of displacement decreases with depth. This aligns with the Aramis analysis, indicating that motion mostly occurred near the surface of the road.

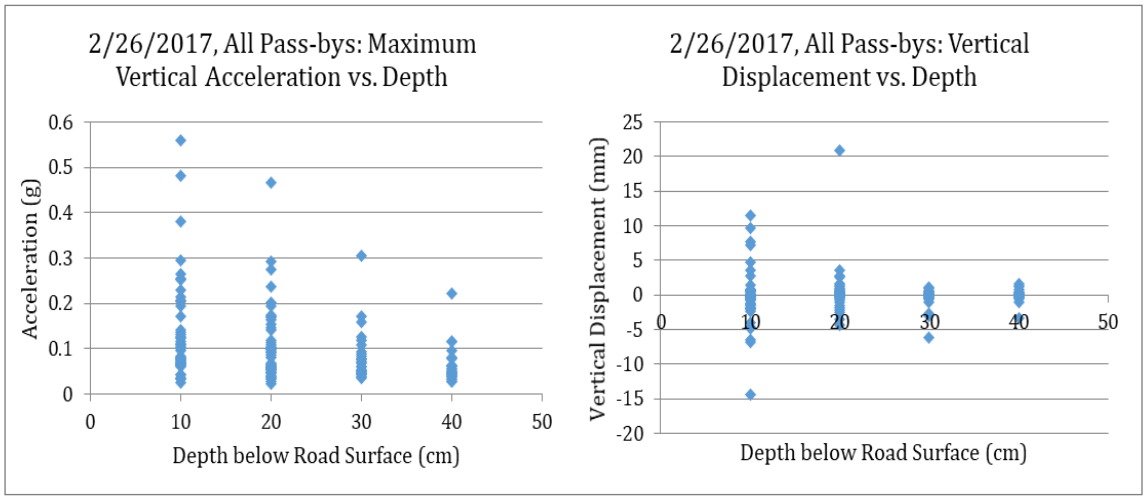

Figure 52. Maximum acceleration values (left) and displacement values (right) for each pass, decreasing with depth

Another characteristic of the graphs shown in Figure 52 is that both the accelerations and displacements were generally very small. Note that displacements, even close to the surface (at a 10 cm depth) were generally less than 15 mm. The example acceleration plots (Figure 52) were representative of numerous tests when acceleration levels were generally below 1 g (i.e., below 9.81 m/s^2).

The decrease in acceleration with depth held true for longitudinal (in the direction of traffic) and transverse (horizontal and perpendicular to the direction of traffic) acceleration as well as vertical accelerations. Figure 53 demonstrates this concept; all accelerations shown decrease with depth. Most vehicles tested exhibit this decrease, but some vehicles also showed a zig-zag pattern, in which

accelerations at a deeper depth would be higher than those at a shallower depth. Further research would be required to explain this phenomenon.

In the examples shown in Figure 53, the change in acceleration with depth is greater for vertical accelerations than longitudinal or transverse for tracked vehicles, but greater for longitudinal acceleration than vertical or transverse for the LPT snowcoach. Difference in motion between different layers of snow could significantly impact the snowpack, in theory. Large vertical acceleration near the surface that drops off deeper in the snowpack may be indicative of compacting, which would be beneficial for the snowroad because it encourages sintering. Large differences between longitudinal motion throughout the depth of the snow, however, would likely indicate shearing between the layers, breaking bonds between horizontal layers of snow. However, as discussion in the Vehicle Pass-bys – Surface Impacts section will show, surface impact measurements did not indicate that LPTs were shearing the surface more than tracks or that tracks were compacting the surface more than LPTs. This could indicate that the maximum accelerations measured do not necessarily correspond to permanent displacement from this motion. Researchers speculated that these readings may be more indicative of strong vibrations rather than permanent deformation.

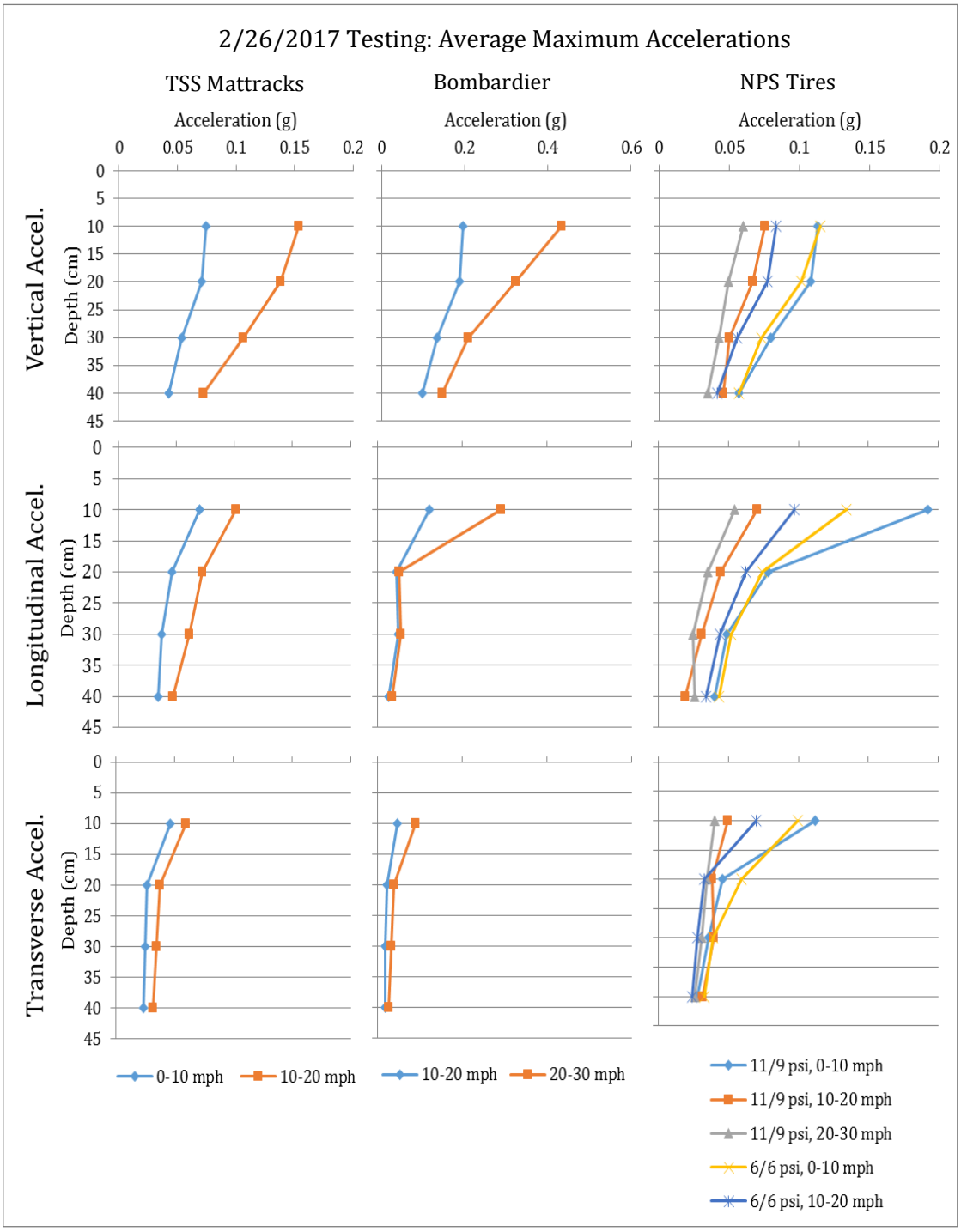

Figure 53. Vertical, longitudinal, and transverse maximum accelerations for different vehicles (Feb. 26, 2017, Grant Test Track); note larger scale for Bombardier

Vehicle velocity also seemed to play a role in the magnitude of acceleration, but this correlation was different for tracks and tires, and even for different tire pressures. Close examination of Figure 53 reveals the velocity trends, and Figure 54 shows an example of these correlations from another representative test day. Each graph shows the maximum vertical accelerations encountered during each run, with one reading from each different accelerometer (which were positioned in an array throughout the snow) from each run. Each fitted line shows the general direction of the trend for each individual accelerometer, as identified in the legend by its location in the snowpack. On this day, vehicles tested included a Mattracks coach, a Bombardier, and the NPS wheeled coach at two different tire pressure configurations. The tracked vehicles show mostly positive correlations between vertical acceleration and velocity (i.e., most of the trend lines have positive slopes), whereas the wheeled coaches show mostly negative correlations.

Of all vehicle configurations tested during the season, five out of six tracked vehicles (including one snowmobile) exhibited this mostly positive correlation between the magnitude of maximum vertical acceleration and the vehicle velocity. Nine out of eleven LPT configurations showed a negative correlation between maximum acceleration and vehicle velocity.

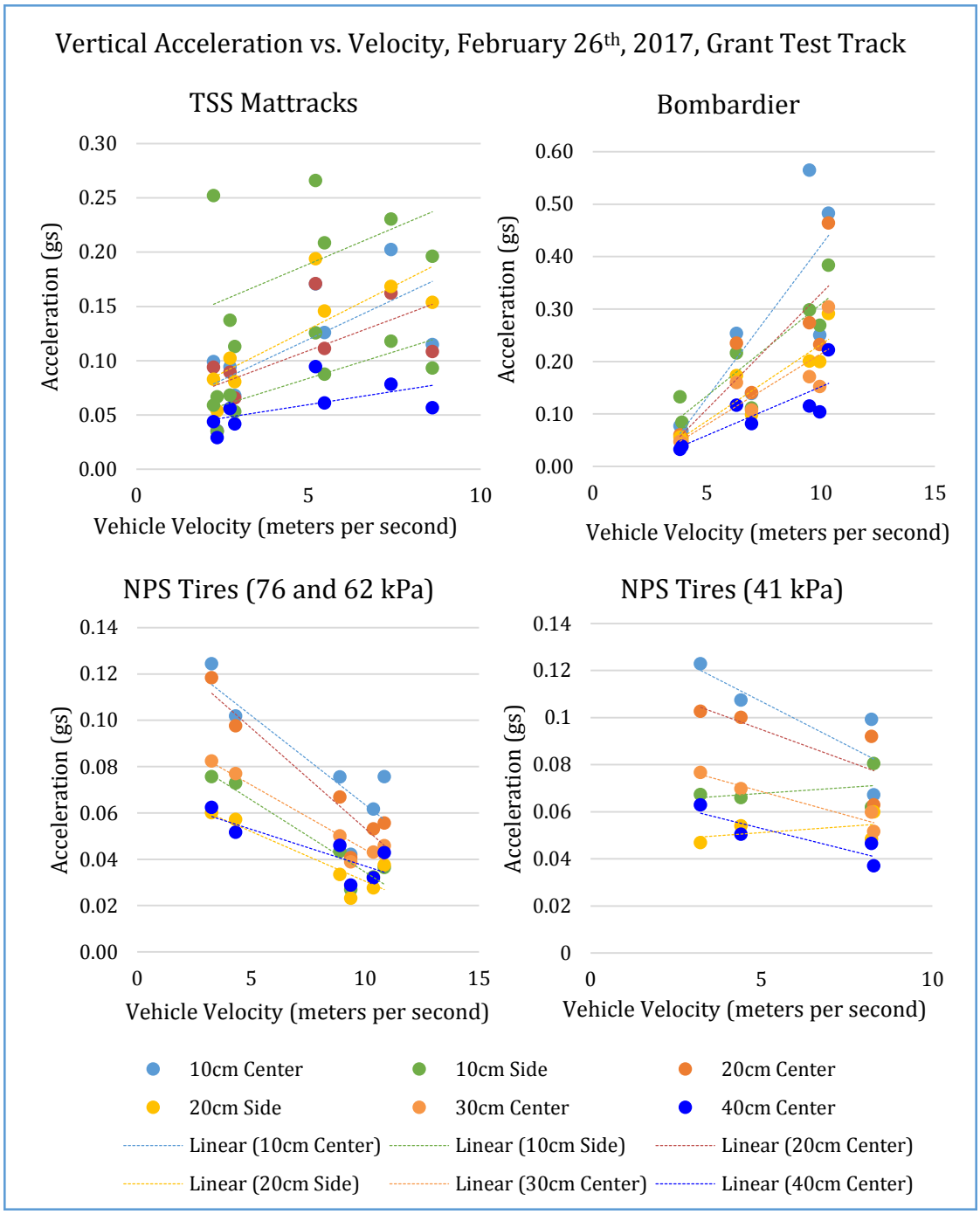

Figure 54. Maximum vertical acceleration versus vehicle velocity data from February 26, 2017

Wheeled coaches were also separated into "high pressure" (any tire having a pressure of 62 kPa (9 psi) or greater) and "low pressure" (all tires having pressures

less than 62 kPa (9 psi)). All snowcoaches operating on tires are referred to as "low-pressure tire" coaches in Yellowstone's winter operations. However, a distinction between the higher end of their operating pressure and the lower end of their operating pressure has been established for this study as differences in impacts and measurements have surfaced for these different categories. While all tires mostly showed a negative correlation between maximum acceleration and velocity, this trend was less strong for the lower pressure tires. As tire pressure decreases, the surface area of the tire increases and the vertical pressure of the tire on the snow surface decreases. In this way a lower pressure tire becomes more like a track in soft snow, with even pressure distribution across the track surface. If maximum acceleration is tied to vibration, as speculated earlier, the increase in surface area and contact with the snowroad caused by decreasing tire pressure could be contributing to increased vibration in the road.

Longitudinal and transverse accelerations generally follow similar trends to the vertical accelerations in relation to velocity. In most cases, one accelerometer that reads higher vertical accelerations than the others in the array for a given pass also reads higher longitudinal and transverse accelerations on that pass for both tracked and wheeled vehicles.

Beyond the correlation with velocity, tire pressure demonstrated a consistent association with vertical acceleration. Lower pressure tires had a lower maximum vertical acceleration than the same tires at higher pressures in most

cases. Figure 55 shows an example of this. Longitudinal and lateral accelerations did not demonstrate this trend as strongly.

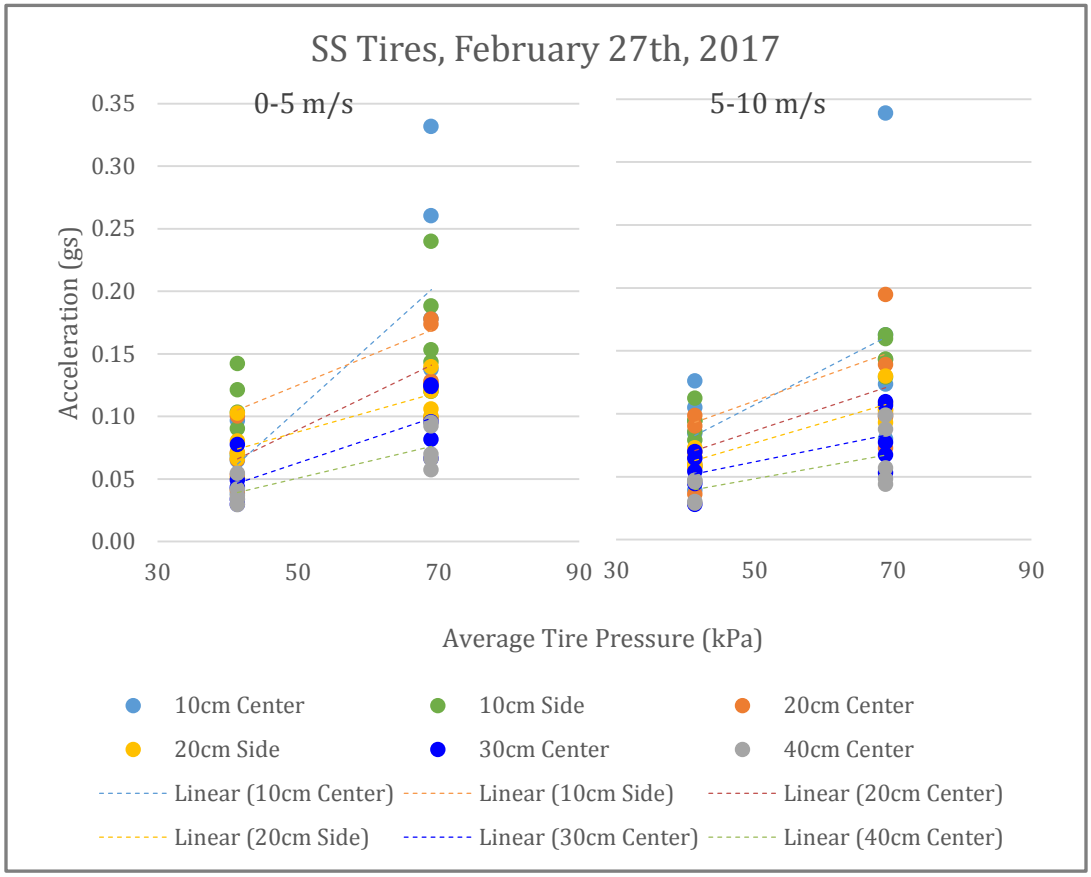

Figure 55. Increased tire pressures were associated with increased maximum vertical accelerations

The maximum accelerations were also compared with rut formation in an attempt to link the two. Table 5 shows the maximum acceleration encountered in each direction and the maximum vertical load during the vehicle's tests, and the final rutting observed after the vehicle is tested. If one of the acceleration values or the load was the driver of rutting, the vehicle for which that parameter is highest during a given day should cause the worst rutting on that day. However, no link is

evident. Neither the acceleration values nor the loading values show strong correlation with rutting.

Table 5. Maximum accelerations, maximum loads, and rutting recorded for all test vehicles (with highest daily values in red); note that on 1/29/17, the same test track was used for all vehicles, so each individual vehicle did not create a large rut

Date	Vehicle(s)	Vertical Center Range (gs) Max	Longitudinal Center Range (gs) Max	Transverse Center Range (gs) Max	Max Load (N)	Rutting Level
1/28/17	Snowbuster	0.357	0.411	0.075	5601	medium
1/29/17	SS Mattracks	0.291	0.123	0.068	3676	large
	XPR Tires (10/10 psi)	0.543	0.243	0.077	8320	large
	NPS Tires (10/10 psi)	0.217	0.268	0.140	6298	large
	NPS Tires (8/8 psi)	0.150	0.182	0.130	3899	large
	NPS Tires (6/6 psi)	0.140	0.175	0.140	3990	
2/12/17	BB Tires (7/9 psi)	0.111	0.056	N/A	2020	none
	BB Tires (4/5 psi)	0.075	0.056	N/A	1166	none
	BB Tires (2/2 psi)	0.064	0.064	N/A	814	NA
	Bomb	0.597	0.349	N/A	1026	small
	NPS SM	0.158	0.085	N/A	NA	medium
2/25/17	NPS Tires (11/9 psi)	0.247	0.197	0.130	5428	none
	NPS Tires (9/7 psi)	0.124	0.189	0.140	4735	none
2/26/17	TSS Mattracks	0.159	0.104	0.065	968	none
	Bomb	0.432	0.292	0.089	490	medium
	NPS Tires (11/9 psi)	0.113	0.193	0.112	2724	large
	NPS Tires (6/6 psi)	0.115	0.134	0.100	1448	medium
2/27/17	SS Tires (9/11 psi)	0.201	0.128	0.050	963	medium
	SS Tires (5/7 psi)	0.083	0.054	0.049	1250	medium
	NPS Tires (10/9 psi)	0.158	0.103	0.068	1109	NA

Table 5 reconfirms trends mentioned before (larger vertical acceleration for higher pressure tires) and introduces new ones. On each day that a Bombardier snowcoach ("bomb") was tested, the bomb had the highest maximum vertical acceleration by far. This was contrary to expectations as bombs are also fairly light so often caused smaller loading than other vehicles. However, bombs are known to have a high level of vibration, which is another indicator that acceleration spikes may be linked with vibration.

By showing the maximum accelerations encountered in all directions for each vehicle tested, Table 5 also demonstrates a pattern of acceleration distribution between different types of vehicles. Figure 56 provides a visual representation of this trend. Overall, tracked vehicles tended to have less evenly distributed accelerations than wheeled coaches. The maximum vertical acceleration associated with tracked vehicles tends to be substantially larger than the maximum accelerations in the other two directions, followed by the maximum longitudinal acceleration and finally the transverse acceleration. LPTs generally have the largest acceleration in the longitudinal direction, with vertical second but often close in magnitude to the transverse. An exception to this trend is the XPR LPT coach tested on January 29, 2017. This coach also had a very high maximum load, the highest load encountered in testing this season, and caused a substantial rut. To inform the design of asphalt for road surfaces, stress distribution among the different directions (vertical, longitudinal, transverse) is often used to help predict road degradation from different types of tires or vehicle loading (Beer, 1996; Myers et al., 1999; Weissman, 1999). This led researchers to investigate whether the distribution of maximum acceleration across the three different directions might be a factor contributing to ruts, but no definitive link could be demonstrated consistently through the data.

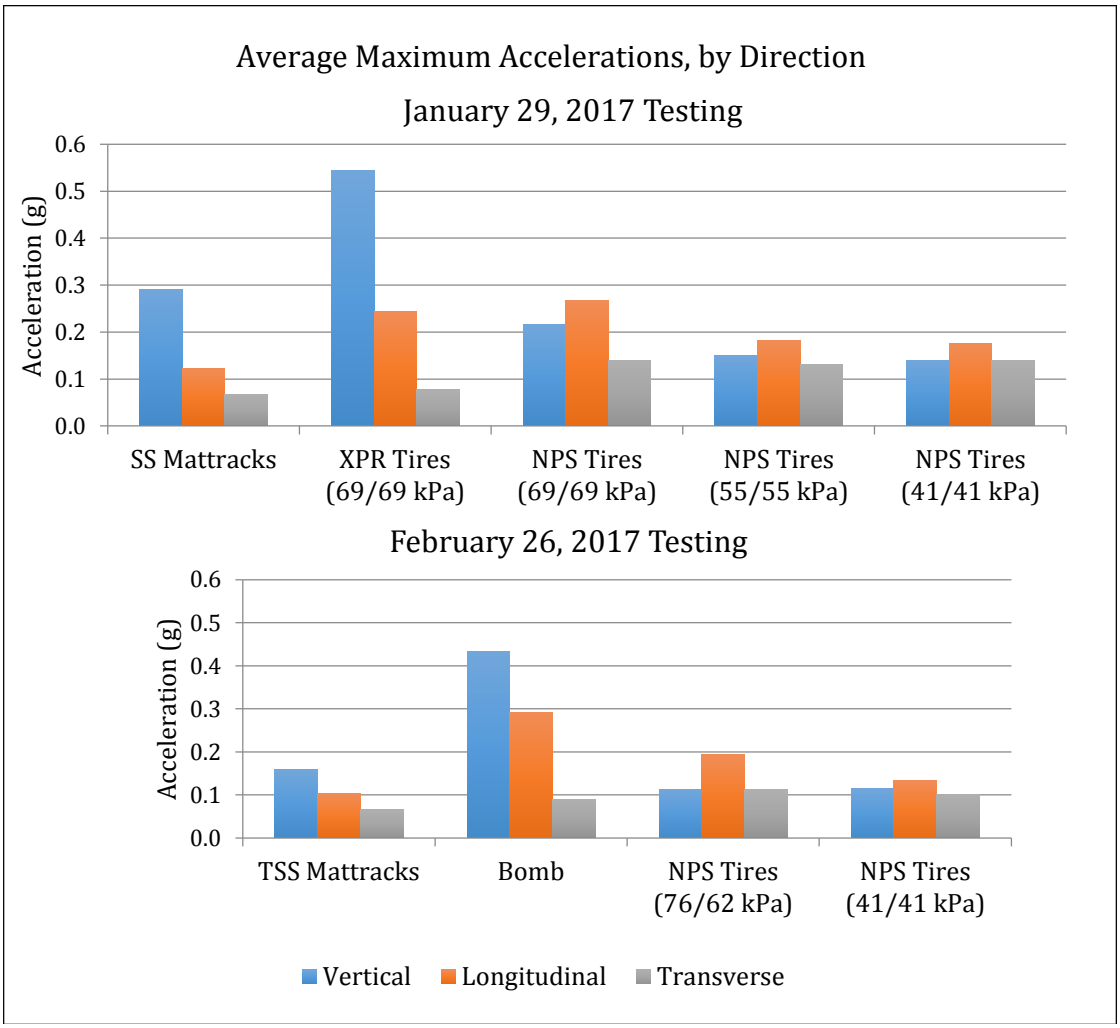

Figure 56. Maximum vertical, longitudinal, and transverse accelerations caused by vehicles tested on January 29 and February 26

Figure 57 shows an example set of displacements from one testing day. Researchers expected to see the accelerometers moving down as vehicle traffic pushed them down, but this was not a consistent pattern, which brought into question the accuracy of the displacements. The displacements could not ultimately be linked to any other parameter like rutting.

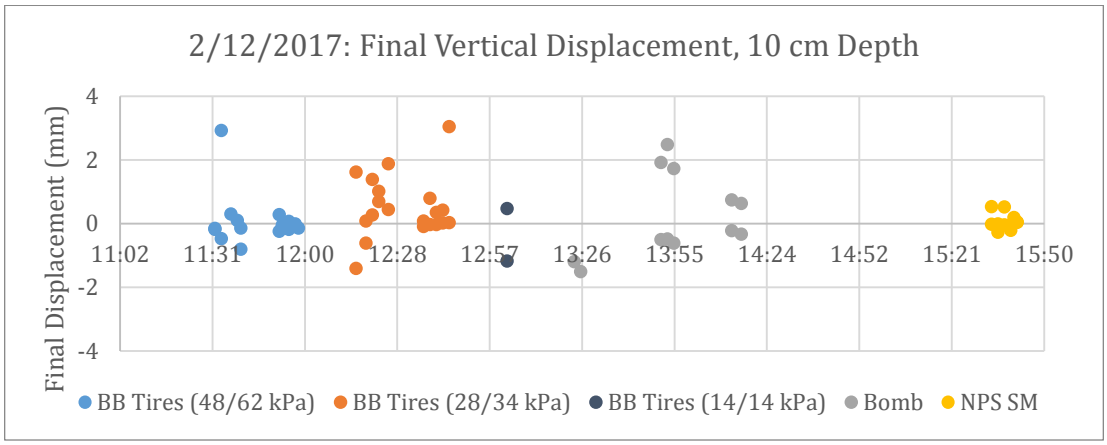

Figure 57. Vertical displacements at a 10-cm depth calculated from 2/12/2017 accelerometer readings

Due to suspicions about vibration influencing the accelerometers, a velocity-related parameter was developed as an indicator of vibration. The number of changes in the direction of the velocity was calculated for each pass-by. The hypothesis was that this might have higher values for pass-bys involving vibration, and specifically that Bombardiers would likely have high values of this parameter and that this might explain their high spikes in acceleration. Regarding road impact, a study by Podolskiy and others (2008) demonstrated that impulsive vibrations can decrease the stability of snow under stress. If high numbers of changes in velocity indicated vibration in the snowpack, then this could weaken the snowroad surface, making it more at-risk for shearing failure as vehicles travel over it. Change in velocity direction, however, could not be linked to rutting, and did not always correspond most to Bombardiers as expected (Figure 58).

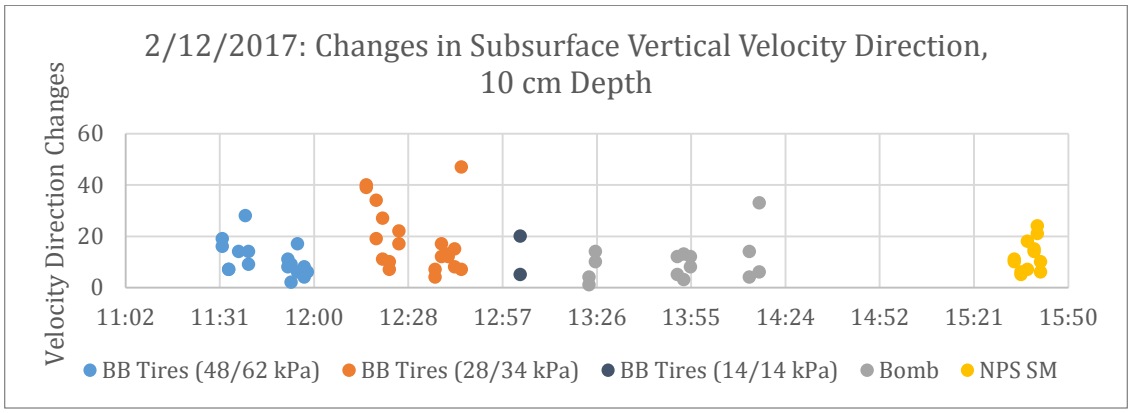

Figure 58. Change in vertical velocity direction at a 10-cm depth on 2/12/2017

A number of factors can impact the accuracy of acceleration and other parameters derived from accelerometer data. In these tests, the accelerometers were buried at various depths throughout the snowroad. The process of digging a pit in the road necessarily changes the hardness of the road adjacent to where the accelerometers are buried. To minimize the impact of this change, accelerometers were buried over 5 cm back horizontally into the relatively undisturbed snow wall, so the snow directly over the accelerometers would theoretically be representative of the hardness of the snow elsewhere. However, as with all other measurements taken during this project, the hardness of the snowroad varied day-to-day which would also impact acceleration readings.

The accelerometers were securely inserted into the snow wall within the road prior to testing, but as the vehicles passed over the accelerometer matrix, it is possible that the accelerometers could have rotated. While the accelerometers theoretically would have quantified any vertical, longitudinal, or transverse motion, these accelerometers are unable to measure rotation. While the baseline calculated

for each accelerometer for each test accounts for the direction of gravity based on the orientation of the accelerometer, a rotation during a measurement would cause the accelerometer's baseline gravity reading to shift, making the acceleration reading from the pass-by inaccurate.

Accelerometer readings often contain a substantial amount of noise. Because the accelerations in these tests were so small, the noise-to-data magnitude ratio may be high, making it more difficult to distinguish valid data from noise. One limitation of the accelerometer data is the sampling frequency limitations of the instrumentation. The "Frequency Response" bandwidths listed for the accelerometers (see Appendix G) are 1600 Hz, 1600 Hz, and 550 Hz for the X, Y, and Z directions, respectively. The sampling rate of 5,000 samples per second is higher than the accelerometer response frequency, which could increase the amount of noise in the readings. The 5,000 samples-per-second sample rate does fall within the cDAQ's capability to transmit (see Appendix H). Since the frequency of motion due to passing vehicles is unknown, the sampling rate cannot be compared with the sampling rate recommended by the Nyquist Theorem.

Vehicle Pass-bys – Loading vs. Subsurface Impacts

Phipps (2018) describes the attempts to correlate subsurface loading and acceleration data with ruts in the road surface. While attempted in countless comparisons, few repeatable trends between vertical loading and road impact were discerned. Trends between subsurface acceleration and road impact yielded

similarly little. Therefore focus shifted to analysis of raw surface measurements (cross-sectional area of snow displaced from the road, hardness at the road surface), as described in the next section.

Vehicle Pass-bys – Surface Impacts

Quantified (Year 2 Methods)

The profilometer and Rammsonde penetrometer measured the surface impacts of the snowroads for this project. These instruments were rudimentary, reliable, and produced the most dependable data. These tools allowed researchers to measure rut dimensions and hardness of the snow next to and in the vehicle path so that rut size and hardness could be quantified. Load, acceleration, profile, and hardness, among other data, were collected from pass-bys. The profilometer and hardness data would help to quantify if any of the other measurements contributed to rut evolution and snowroad hardness. Unfortunately, with Year 1's testing strategy the profilometer and Rammsonde penetrometer were not able to be used after each pass of a snowcoach. This was due to the lack of a noticeable change in rut dimension from a single pass of a snowcoach as well as the need to move coaches through and avoid traffic delays. The use of a test track in Year 2 allowed a coach to pass through the instrumentation multiple times and for these surface measurements to be taken.

By quantifying the surface disturbance (i.e., rut formation) of interest to the NPS, these surface measurements provide the dependent variable. All factors

contributing to road quality can be compared to these measurements to determine their relative impacts. This led researchers to focus on the surface measurement tools and used this data as a foundation for all other measurements.

Using the profilometer data, a displacement area of a rut was calculated. This provided a scalar value to score rut severity based on a two-dimensional area of a rut. It was found that both tracks and tires can form ruts in conditions that permit rutting; these ruts from tracks and tires can be of equal severity. However, it was discovered that once tires form a rut, a point would come where the rut would not significantly increase in dimensions. On the contrary, tracks would form a rut and continue to increase the rut size after more passes (Figure 59).

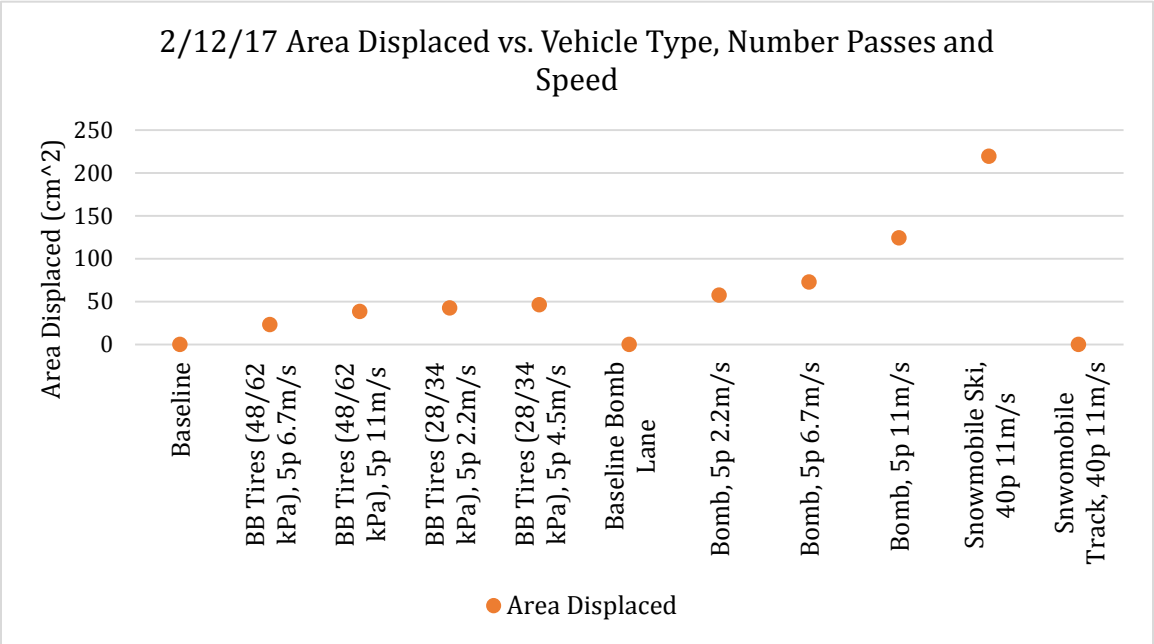

Figure 59. Area displaced after OSV passes ("#p" on axis label represents the number of passes, area displaced is cumulative for all tests of a given vehicle)

Due to vehicle testing time constraints, a relatively limited dataset was collected for each testing day, so it is unknown if this trend would hold with many more passes. Nevertheless, with the data that was collected, this trend did hold for almost all testing days.

Tire pressure proved to have an effect on rut size; tires of higher pressure can produce an initial rut but if tire pressure is decreased, the rate at which the rut formed decreased (Figure 60). This was the case in most scenarios on the test track in Grant.

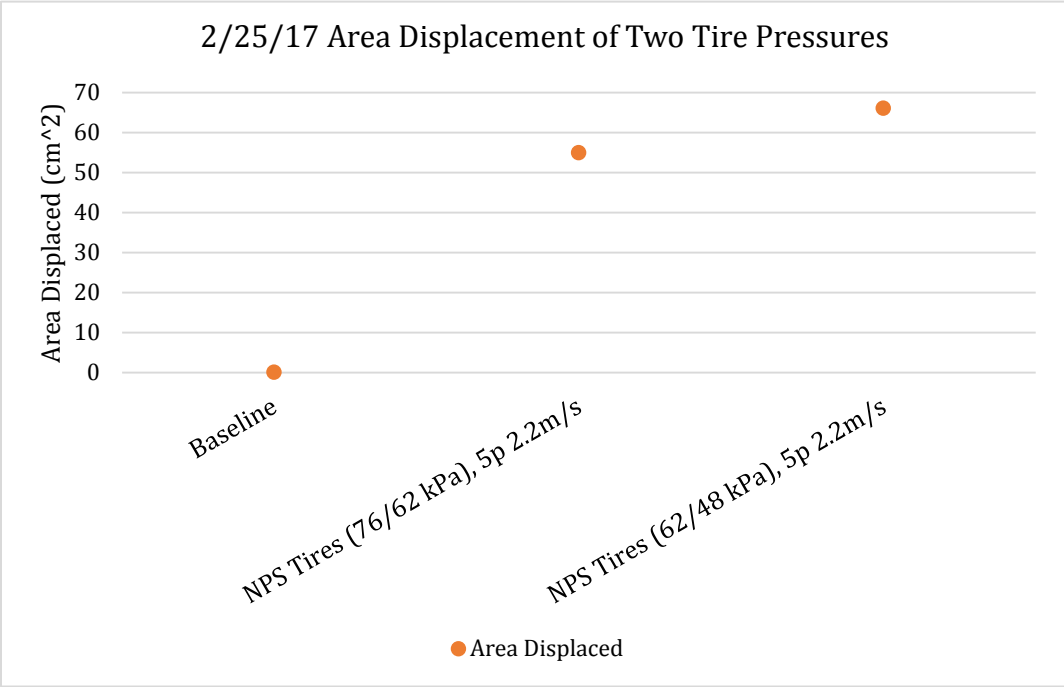

Figure 60: Cumulative area displaced by tires at different pressures

Area displacement was compared to impulse, maximum load, and maximum acceleration in the vertical, transverse, and longitudinal directions (Figure 28) and examined for trends. As explored in the vehicle loading section it was found the load

did not have a profound effect on rut size. This point is reiterated in Figure 61, in which the light blue dots represent maximum load measurements from passes from a Mattracks vehicle; the load remains relatively unchanged, yet the area displaced increases substantially. This indicates a driving factor of rut formation independent of load. The LPT tires represented by the dots after 14:00 cause an initial rut formation from a wheeled coach with tire pressures of 10 psi. This rut area increases only slightly after the second set of runs, from a different LPT vehicle with equal tire pressures. The tire pressure is then decreased represented by the grey and yellow dots shown before 16:48, and the area displacement levels off further.

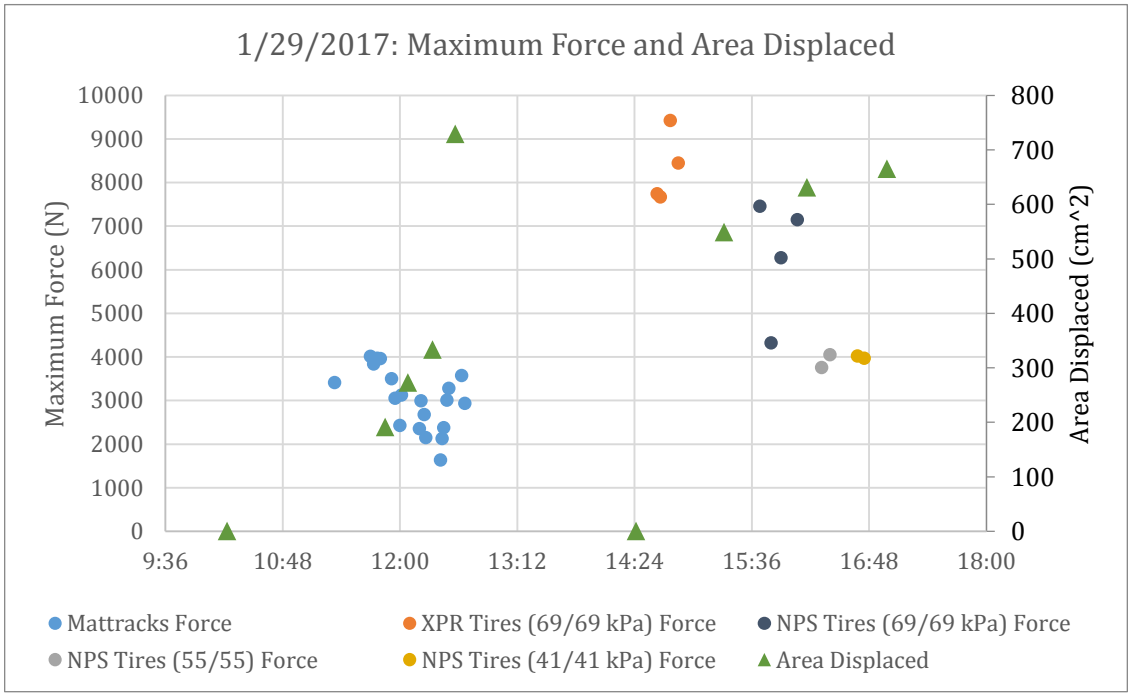

Figure 61. Maximum force and area displaced over time on 1/29/2017

Figure 62 shows similar patterns to Figure 61: the LPT tires cause an initial rut and when the tire pressure decreased, the rate at which the rut was forming

decreased. A Bombardier is then tested which had lower magnitude maximum forces and yet the area displacement diverges. This diverging pattern for tracked vehicles was seen in most other plots as well. These trends indicate that rut formation is mostly dictated by a surface interaction. The literature review and surface video observation sections go over shear concepts in detail.

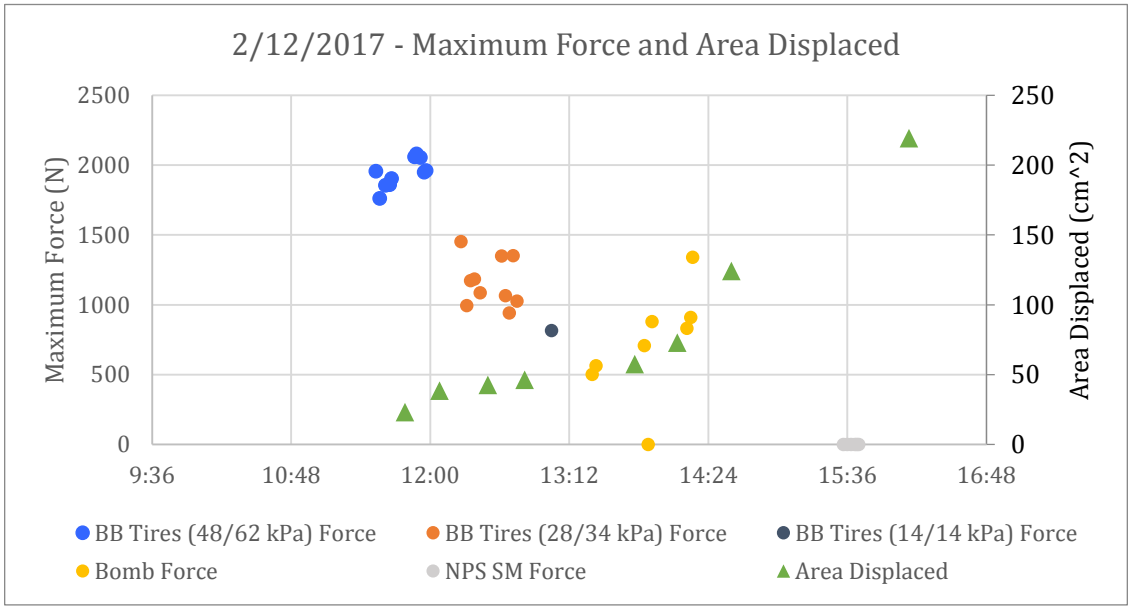

Figure 62. Maximum force and area displaced over time on 2/12/2017

Figure 63 shows a Scenic Safari's LPT coach tested at two tire pressures. This vehicle formed a rut but the rut growth is reduced after additional passes.

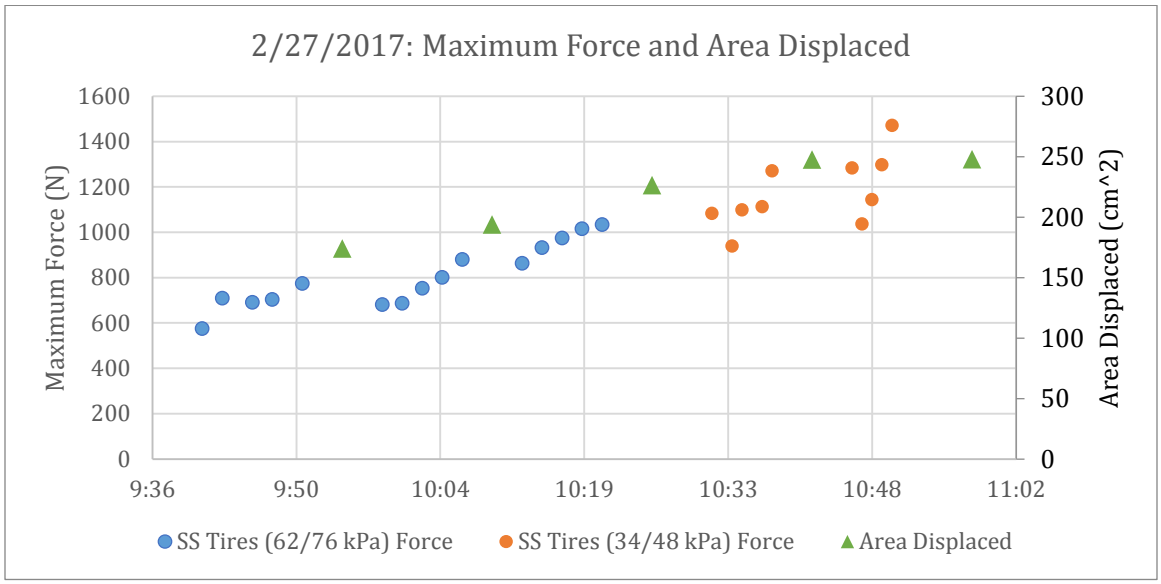

Figure 63. Maximum force and area displaced over time for a Scenic Safaris LPT coach on 2/27/2017

Max acceleration/displacement and impulse were analyzed in comparison to these surface measurements for all testing days from the test track in Grant, but no obvious trends were observed from these datasets. This reiterates the point that rutting is not closely tied to sub-surface interactions.

The next surface parameter analyzed was hardness; a baseline hardness measurement was taken before each new snowcoach testing period. The baseline measurement was taken in an untouched area of the test track. This measurement was used to compare hardness measurements taken in the rut in a coach's path after five passes at a specific velocity. This was completed for tracks and tires and while the results varied, some trends did surface.

Figure 64 shows rut depth, depth of the soft layer at the rut surface, and the hardness below the soft layer for passes on January 29, 2017, to give a picture of how the snowroad surface evolves during coach passes. While most impact occurs

at the surface, the surface of the road changes as rutting moves it down and changes the snow hardness . The figure shows results from testing of one Mattracks coach and two LPT vehicles. The first LPT coach was tested after one set of passes, and the second LPT coach was tested after two sets of passes, with the first at tire pressures equal to those of the first LPT coach and the second at lowered tire pressures.

In Figure 64, a Mattracks vehicle completed five passes at four different velocities: 2 m/s (5 mph), 4 m/s (10 mph), 7 m/s (15 mph), and 9 m/s (20 mph). Rut depth, shown by the hollow section at the top of each column, increases with all Mattracks test passes, at an increasing rate after later passes. The “soft section” under the rut, defined as the layer penetrated by initial, gentle placement of the penetrometer, also grows deeper or stays equal with Mattracks passes. The hardness of the snow below that soft layer tends to decrease after sets of Mattracks passes, with the exception of one set of passes in which the hardness increased (6.7 m/s passes). For the LPT coaches, the depth of the rut increased on all passes but at a decreasing rate (both at the initial, higher pressure and when the pressure was decreased). The soft layer increased then stayed equal after the higher pressure passes, then decreased after the lower pressure passes. The hardness under the soft layer decreased after the initial set of LPT passes, but then increased, both with more passes at the initial, higher pressure, and then with passes from tires with lowered pressure.

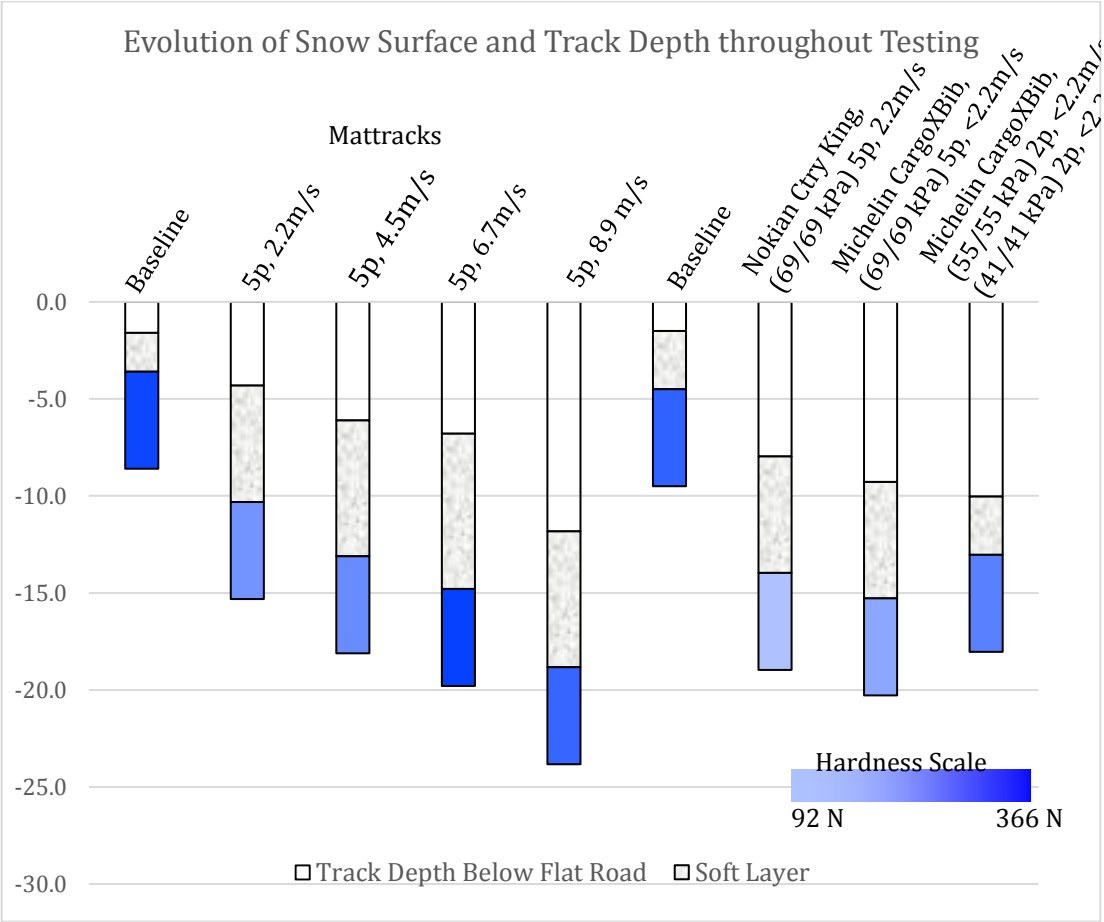

Figure 64. Rut depth (hollow outline), depth of the soft layer under the rut (penetrated by the placement of the penetrometer, shown by the grey section), and hardness underneath the soft layer (blue section, with hardness indicated by the graduated blue color bar)

Since the trend was not overwhelmingly obvious for all Year 2 testing days, researchers summed all events in which a track or tire (high pressure and low pressure) hardened the surface (Table 6). As mentioned in the Accelerometers section, tires at pressures of 62 kPa (9 psi) and above were designated as a high pressure tires and those with pressures below 62 kPa (9 psi) were considered to be low pressure tires.

Table 6. Hardening and softening of the road by vehicle type

	Tire Pressure	Hardens Surface	Number of Passes
High Pressure Tires	> 62 kPa (≥ 9 psi)	4	10
Low Pressure Tires	< 62 kPa (< 9 psi)	5	6
Tracks	N/A	6	15

This data demonstrated that high-pressure tires harden the surface 40% of the time, low-pressure tires harden the surface 85% of the time, and tracks harden the surface 40% of the time. This data shows high-pressure tires and tracks are equivalent in softening the road 60% of the time. Low-pressure tires appeared to be superior at hardening the snowroad surface.

Although the Rammsonde penetrometer was very reliable, there are some caveats to how this tool worked in field conditions. Snow is an extremely variable material, not just across a large area, but also locally. Snow has the ability to retain many different mechanical properties. An example of this would be that as a snowcoach or groomer drives, snow can be collected along the exterior and undercarriage of the vehicle. At some point this melted, slushy snow can slip off the coach and fall onto the snowroad which can form an irregularity from the surrounding surface. This inconsistency is then buried by new snow and groomed into the snowroad. If this location is unintentionally selected for a hardness measurement, the hardness reading would be misrepresentative of the adjacent snow hardness. A similar circumstance can arise with areas being softer due to inconsistencies of groomer mechanics or other environmental factors such as sun/shade throughout the day. Groomers cannot completely groom a surface to be

homogeneous in hardness. Because of these variances, there can be a small amount of error associated with the hardness measurements. This can also explain deviation of trends that cannot be explained through understood parameters.

Surface Video Observations

The high speed, high definition camera brought insight into the track and tire interactions at the surface by replaying the videos in slow motion. There was difficulty in quantifying the shear concept, so the camera was used to investigate this qualitatively. Researchers would film the coach passes from camera angles that proved to be beneficial for observing surface interactions and the differences between the tracks' and LPTs' interactions with the snowroad. Researchers noticed that just by watching and listening to the difference between tracks and tires as they move that there was an obvious difference between the two. After watching numerous surface videos in slow motion it was even more evident that there was a large difference in surface interaction between tracks and tires.

Tracks in general have larger dimension grousers than tread patterns on a LPT vehicle. As these large grousers contact the snowroad some deformation will occur; the severity of this deformation will largely depend on the snowroad hardness. This can be seen by comparing a tracked vehicle and a LPT vehicle traveling at comparable velocities in sequential passes when the snowroad has the same hardness (Figure 65 and Figure 66). Generally, the tracks kick up more snow than the LPTs. This snow that is being kicked up is due to a shearing load from the tractive effort of the grousers/tread of tire. Through video analysis researchers

believe that tracks are causing higher shearing loads to the snowroad. This is due to the grousers on tracks generally being larger than those on LPTs and the fact that the tracks' grousers stay embedded in the road for longer, applying a shearing load for more time. As discussed in the literature review, grousers embedded in the snowroad change angles most drastically at the front and rear of the track and also as the bogey wheels travel over the grouser; this causes the grouser to move while embedded in the snow. If a tire were to have grousers of equivalent size to a tracked vehicle it is believed that the shearing loads would be comparable, but tracks would still apply shearing load and the grouser movement over a longer time.

Figure 65. Screenshot of an LPT traveling approximately 4.5 m/s (10 mph)

Figure 66. Screenshot of a tracked vehicle traveling approximately 4.5 m/s (10 mph)

In the Vehicle Characteristics and Impact section of the literature review, numerous vehicle impact topics were covered. Due to the complexity of this project, not all of these phenomena could be addressed in testing. So by use of the camera, researchers hoped to document some of these that were not otherwise measured. However, due to relatively high strengths of the snowroad in Year 1 and 2, some types of vehicle impacts could not be captured by a single vehicle pass due to these having a small scale impact per vehicle pass on hard roads. This emphasized the fact that road degradation in Year 1 and Year 2 was generally caused from compounding vehicle effects, not a single pass. So repetition of vehicle passes significantly contributes to vehicles' impact to the snowroad surface.

CONCLUSIONS AND RECOMMENDATIONS

General Conclusions

Both tracked and wheeled snowcoaches can cause ruts. Ruts form through two primary modes: snow compaction and snow displacement. Additionally, both tracked and wheeled snowcoaches can soften snow at the surface as they pass, making the road more susceptible to both types of rutting.

When tracked vehicles form ruts, the ruts continue to deepen with subsequent passes. When wheeled vehicles form ruts, the ruts eventually reach a point at which they stop deepening, especially if tire inflation pressure is lowered. This difference implies that tires tend to cause ruts primarily through compaction whereas tracks form ruts through snow displacement. As snow is compacted and becomes denser, its resistance to compaction increases. Each additional instance of loading by the same vehicle will cause less compaction than previous passes. This compaction of the road will encourage sintering, which makes the road harder. The continually increasing rut depth of tracked vehicles implies that they cause ruts primarily through snow displacement.

Data showed that the snowroad surface often hardens after the passage of a wheeled snowcoach with tires at a very low pressure (less than 62 kPa (9 psi)). Snowcoaches with tires at higher pressure and tracks more often softened the road. While this implies that tires are not uniformly causing compaction in the road, Shoop and others (2010) provide an example of tires being used for a grooming

implement. In this example, the tires effectively compact deeper layers of the road but cause disaggregation in the top 10 cm of the road. Considering data from this study together with the literature, it seems likely that tires do cause road compaction at a 10 cm depth in the snow and below, but may cause softening at the road surface, especially when running at higher inflation pressures. A softer snow surface can leave the snowroad vulnerable to snow displacement.

The scope of this study included testing vehicles on groomed, prepared snowroads. These roads are hard to begin with, so compaction often does not cause a large depression in the road. On harder roads, ruts are more likely to form through snow displacement. On softer roads, compaction will cause a more substantial initial depression in the road. While the compaction can result in a harder surface, when this occurs just in one set of tracks it creates an uneven snow surface. This means that on softer roads tires may create more substantial ruts than tracks.

Also, on softer roads, a tracked vehicle sinks down into the snow more fully so that the vehicle's weight is more evenly distributed across the whole track. (On hard roads, the vehicle's weight is concentrated at the bogey wheels.) This weight distribution will cause a tracked vehicle to cause less compaction on a soft road than a wheeled vehicle of comparable weight.

The different impacts that vehicles have on soft roads and hard roads underscores the fact that vehicles perform differently in different conditions. While vehicle performance is outside the scope of this study, existing literature and

operator experience will confirm that different vehicles perform better in certain snow conditions.

The negligible degradation and possible benefits of tires to the groomed snowroad surface indicate no reason for NPS management to prevent park snowcoach operators from running wheeled coaches. This does not take into account vehicle performance and safety, which is outside the scope of the project. However, park staff and OSV operators can weigh in on this element.

The road hardening associated with tires at lower pressures (below 9 psi) indicates that lower pressure tires can be immediately beneficial to the roads. Additionally, lower pressure tires decrease the vertical pressure on the snowroad, likely causing less compaction on softer roads and decreasing uneven road surfaces experienced in soft snow. The ability to adjust pressure not only provides snowcoach operators the ability to adjust snowcoach capability when needed, but can also help reduce impacts to the road.

Differences between grooming districts are correlated with weather and traffic. The occurrence of days throughout the season with maximum temperature above -10 °C increases the road strength, though only to a point. Temperatures high enough to cause snowmelt that does not refreeze would counteract this pattern. Hardness readings indicated that traffic may actually be beneficial for road hardness below the surface.

Other factors that correlate to road hardness on a parkwide scale include snowfall between grooming events, which generally corresponds with daily

snowfall amounts. Grooming smaller amounts of fresh snow during each grooming run results in a more consistent quality throughout the depth of the road. Both elevation and snow depth showed a negative correlation with hardness. Both of these are also positively correlated with average daily snowfall. Grooming practices can be tailored to improve road quality in these vulnerable areas (deeper snow depth and higher elevation) by grooming frequently and during large snowfall events if possible.

Longer "set times" (in which the snowroad surface is undisturbed after grooming) are good for the road quality, so grooming as early as possible in the evening to leave maximum time before the roads experience morning traffic is beneficial. Groomers should not leave before most traffic has left their district for the day, though, as tracks in a freshly groomed snowroad will create an uneven, hard road surface.

Existing literature shows that grooming is most effective when incorporating both disaggregation of snow particles and then compaction with a drag. Most districts use a front blade to disaggregate and a drag to compact. As long as the blade is used to adequately break up the snow surface, these are a suitable option for the grooming needs of the park. Consider incorporating both elements into all park groomers if problems are noted in the other districts.

Results from this study indicate that the current traffic in the park and grooming practices can continue to support a quality road if some basic recommendations are followed. While this study attempted to address a large

variety of questions about this topic, many of the individual elements of this study can be and have been subject to multi-year studies, so this topic could be studied in much more detail. A similar study of vehicle impact on soft, ungroomed roads would be beneficial to the park in the future to provide further insight into how vehicles impact the road in different snow conditions.

Recommendations and Management Implications

The results of this study will help inform the NPS as they make a long-term decision on whether to allow LPT snowcoaches into the future. This study indicates that LPT coaches do not have more of an impact on a groomed road surface than tracks do. In some cases, especially when run at low pressures, tire seem to actually help the road. If the NPS is making a decision on whether to allow tires based on their impact to groomed road surfaces, this study indicates no reason not to allow tires. The results here do indicate the importance of varying tire pressure in accordance with weather conditions, and the NPS should stress this importance to operators.

However, while very soft roads were outside of the scope of this study, literature indicates that tires could rut more in soft snow due to their large vertical forces causing snow compaction. Additional study would be needed to verify the comparative impacts of tracks and tires on soft roads. This unknown indicates that disallowing tracks would not be justified at this point either.

The park's grooming operations will always be limited by the time limits imposed on snow setup by the daily traffic load on the park's roads. However, within this constraint, NPS grooming operators can take several actions to maximize the benefits of their grooming. They should start grooming as soon as possible when snow starts to accumulate on the road surface, since grooming smaller increments of fresh snow is better for road quality. Grooming should take place after traffic has passed for the day, but as early as possible after that to allow maximum set-up time. The NPS should review grooming equipment and outfit all groomers with equipment to accomplish both disaggregation of snow (could be achieved with a front blade, or tiller) and compaction (generally accomplished with a drag). This combination of processes maximizes effectiveness.

Suggestions for Further Study

The comprehensive nature of this investigation meant that many topics were only addressed briefly. The results of this study indicate the potential for many follow-up studies that could be of benefit to Yellowstone.

The NPS is interested in learning about what tire sizes are optimal for preserving their roads while providing adequate performance. A follow-up study could specifically look at how tire size (both length and width, and the ratio between these two) influences road impacts. Another study could look at how these parameters influence a vehicle's maneuverability.

Grooming data in this project provided a high-level overview of grooming practices and resultant road conditions. This could be studied in more depth. An intensive study with daily sampling and tests at regular intervals after grooming would provide more insight into how the road sets up and how this is affected by different factors like weather. Tests comparing the relatively efficacy of different grooming techniques have been conducted and have results available in existing literature. However, none of these tests have used the equipment ("Mogul Masters") common in the park. Side-by-side testing of NPS grooming equipment could potentially help the NPS optimize their current practices.

The challenges of remote field work and resultant small sample numbers in this study mean that more data collected using similar methods would be useful to help confirm that the trends in this study hold and are statistically significant. Future tests could involve less varying of vehicle velocity and tire pressure to remove the confounding effect of these variables and confirm that differences in road impact are specific to type of vehicle (tracks or tires) rather than being influenced by changing variables.

A focused study looking at the snow layers in the snowroad, correlated with weather and grooming conditions, would provide more insight into how the snow metamorphism is influenced by both the weather and the grooming. This was done to some degree in this study, but a more focused study with more frequent testing and sampling could provide more insight into the evolution of the snowroad throughout the season.

REFERENCES CITED

2011. Forest Soil Productivity. Wisconsin Forest Management Guidelines, Wisconsin Department of Natural Resources, 1 -13.

2016. Webmap. United States Depatment of Agriculture
Natural Resource Conservation Service (16 June).

Abele, G. 1990. Snow Roads and Runways. Technical Report.

Affleck, R.T. 2005. Disturbance Measurements from Off-Road Vehicles on Seasonal Terrain. U.S. Army Engineer research and Development Center.

Akitaya, E. 1974. Studies on depth hoar. Contributions from the Institute of Low Temperature Science, 26: 1-67.

Alger, R., S. Gruenberg and G. Gwaltney 2000. Snowmobile Trail Bump Formation Analysis, Prediction, and Modeling. Michigan Technological University.

Alger, R., S. Shoop, M. Knuth and G. Blaisdell 2011. Development of Processed Snow Roads in Antarctica. 17th International Conference of the ISTVS, Blacksburg, VA.

Allen, M.E., I. Weir-Jones, D.R. Motiuk, K.R. Flewin, R.D. Goring, R. Kobetitch and A. Broadhurst 1994. Acceleration perturbations of daily living. A comparison to'whiplash'. Spine, 19(11): 1285-1290.

Annan, A.P., N. Diamanti and S.R. Jackson 2016. Ground-penetrating Radar for Assessing Winter Roads. Geophysics, 81(1): WA101-WA109.

Ansorge, D. and R.J. Godwin 2007. Tracks and Tires: a Full Scale Laboratory Investigation. Landtechnik, 62(1): 30-31.

Ansorge, D. and R.J. Godwin 2008. The effect of tyres and a rubber track at high axle loads on soil compaction—Part 2: Multi-axle machine studies. Biosystems Engineering, 99(3): 338-347.

Antille, D.L., D. Ansorge, M.L. Dresser and R.J. Godwin 2013. Soil Displacement and Soil Bulk Density Changes as Affected by Tire Size. Transactions of the American Society of Agricultural and Biological Engineers, 56(5): 1683-1693.

Arvidsson, J. and T. Keller 2014. Soil Stresses Under Tracks and Tyres - Measurements and Model Developement. International Conference of Agricultural Engineering, Zurich, 7. (7).

Barthelemy, J.I. 1975. Snow-Road Construction - A Summary of technology From Past to Present. Naval facilities Engineering Command.

Beer, M.D. 1996. Measurement of tyre/pavement interface stresses under moving wheel loads. International Journal of Heavy Vehicle Systems, 3(1-4): 97-115.

Bekker, M.G. 1956. Theory of land locomotion.

Blaisdell, G.L., R.M. Lang, G. Crist, K. Kurtti, J. Harbin and D. Flora 1998. Construction, Maintenance, and Operation of a Glacial Runway, McMurdo Station, Antarctica. US Army Corps of Engineers Monograph 98-1.

Bones, J.A. 2012. Experimental Investigation of Interactions Between Explosive Detonations and the Resulting Snowpack Response. (Master of Science Montana State University.)

Buck, N.L., S.A. Shoop and T.J. Cary 2012. Initial Effects of Heavy Vehicle Trafficking on Vegetable Soils. U.S. Army Engineer Research and Developement Center.

Colbeck, S. 1987. Snow metamorphism and classification. Seasonal Snowcovers: Physics, Chemistry, Hydrology, Springer, 1-35.

Colbeck, S. 1991. The layered character of snow covers. Reviews of Geophysics, 29(1): 81-96.

Coutermarsh, B.A. and S.A. Shoop 2009. Tire slip-angle force measurements on winter surfaces. Journal of Terramechanics, 46(4): 157-163.

Diemand, D., R. Alger and V. Klokov 1996. Snow road enhancement. Transportation Research Record: Journal of the Transportation Research Board, (1534): 1-4.

Håkansson, I., W.B. Voorhees and H. Riley 1988. Vehicle and wheel factors influencing soil compaction and crop response in different traffic regimes. Soil and tillage research, 11(3-4): 239-282.

Horn, R., J. Vossbrink, S. Peth and S. Becker 2007. Impact of Modern Forest Vehicles on Soil Physical Properties. Forest Ecology and Management, 248: 56-63.

Iagnemma, K. 2011. Surface Interaction Modeling Engineering Methods. Massachusetts Institute of Technology.

Janarthanan, B., C. Padmanabhan and C. Sujatha 2012. Longitudinal dynamics of a tracked vehicle: Simulation and experiment. Journal of Terramechanics, 49(2): 63-72.

Keller, T., A. Trautner and J. Arvidsson 2002. Stress Distribution and Soil Displacement under a Rubber-tracked and a Wheeled Tractor during Ploughing, Both on-land and within Furrows. Soil & Tillage Research, 68: 39-47.

Kestler, M., A., S. Shoop, A., K. Henry, S., J. Stark, A. and R. Affleck, T. 1999. Rapid Stabilization of Thawing Soils for Enhanced Vehicle Mobility A field Demonstration Project. U.S. Army Corps of Engineers.

Kevan, P.G. 1971. Vehicle Tracks on High Arctic Tundra: an 11 Year Case History around Hazen Camp, Ellesmere Island, N.W.T. Defence Research Establishment Ottawa.

Kozak, M.C., K. Elder, K. Birkeland and P. Chapman 2002. Predicting Snow Layer Hardness with Meteorological Factors. International Snow Science Workshop, Penticton, British Columbia, 329-336.

LaChapelle, E.R. and R.L. Armstrong 1977. Temperature Patterns in an Alpine Snow Cover and Their Influence on Snow Metamorphism. COLORADO UNIV BOULDER INST OF ARCTIC AND ALPINE RESEARCH.

Lang, R.M., G.L. Blaisdell, C. D'Urso, G. Reinemer and M. Lesher 1997. Processing Snow for High Strength Roads and Runways. Cold Regions Science and Technology, 25: 17-31.

Laughery, S., G. Gerhart and R. Goetz 1990. Bekker's Terramechanics Model for Off-Road Vehicle.

Lee, J.H. and W. Wang 2009. Characterization of Snow Cover Using Ground Penetrating Radar for Vehicle Trafficability -- Experiments and Modeling. Journal of Terramechanics, 46: 189-202.

Lee, S.M. and W.M. Haas 1986. Development of Methodology for Improved Design of Snow Roads and Airstrips. Antarctic Journal of the United States, 21(5): 301-302.

Lee, S.M., W.M. Haas, R.L. Brown and A.F. Wuori 1989. Improving snow roads and airstrips in Antarctica. MICHIGAN TECHNOLOGICAL UNIV HOUGHTON.

McCallum, A.B. 2012. Cone Penetration Testing in Polar Snow. (Doctor of Philosophy Gonville and Caius College.)

McClung, D.M. and J. Schweizer 1996. Effect of Snow Temperatures on Skier Triggering of Dry Slab Avalanches. International Snow Science Workshop, Banff, Alberta, Canadian Avalanche Association, 113-117.

McKay, G. and D. Gray 1981. The distribution of snowcover. Handbook of snow: 153-190.

Mellor, M. 1975. A review of Basic Snow Mechanics. The International Symposium on Snow Mechanics, Grindelwald, Switzerland 251-291.

Mizukami, N. and S. Perica 2008. Spatiotemporal Characteristics of Snowpack Density in the Mountainous Regions of the Western United States. Journal of Hydrometeorology, 9(December 2008): 1416-1426.

Moschas, F., D. Mouzoulas and S. Stiros 2015. Phase errors in accelerometer arrays: An analysis based on collocated sensors and FEM. Soil Dynamics and Earthquake Engineering, 78: 32-45.

Myers, L., R. Roque, B. Ruth and C. Drakos 1999. Measurement of contact stresses for different truck tire types to evaluate their influence on near-surface cracking and rutting. Transportation Research Record: Journal of the Transportation Research Board, (1655): 175-184.

Nelson, M.M., Phipps, R.E., Adams, E., Miller, D., Larson, R. 2018. Snowroad Deterioration and Oversnow Vehicle Impact – Final Report, February 2018. College of Engineering, Montana State University.

Niedringhaus, L. 1965. Study of the Rammsonde for Use in Hard Snow. Technical Report 153.

Olagne, X. and D.M. McClung 1990. Nonlinear formulation of snow creep. Cold Regions Science and Technology, 19(1): 1-18.

Phipps, R.E. 2018. A Yellowstone Snowroad Quality Investigation; a Comparison of Tracks vs. Tires and Other Contributing Factors. (Master of Science Montana State University.)

Podolskiy, E., P. Chemous, O. Abe, N. Barashev and K. Nishimura 2008. Experimental Study of Short-term Loading Influence on Shear Strength. International Snow Science Workshop, Whistler, British Columbia, 701-708.

Pytka, J. 2010. Determination of snow stresses under vehicle loads. Cold Regions Science and Technology, 60(2): 137-145.

Ramseier, R., O. 1966. Role of Sintering in Snow Construction. Journal of Terramechanics, 3(3): 9.

Ramseier, R., O. and G. Sander, W. 1965. Sintering of Snow as a Function of Temperature. International Symposium on Scientific Aspects of Snow and Ice Avalanches.

Raper, R.L., A.C. Bailey, E.C. Burt, T.R. Way and P. Liberati 1995. Inflation Pressure and Dynamic Load Effects on Soil Deformation and Soil-Tire Interface Stresses. American Society of Agricultural Engineers, 38(3): 685-689.

Richmond, P.W., G.L. Blaisdell and C.E. Green 1990. Wheels and Tracks in Snow. Second Validation Study of the CRREL Shallow Snow Mobility Model. COLD REGIONS RESEARCH AND ENGINEERING LAB HANOVER NH.

Russell-Head, D., S. and W. Budd, F. 1989. Compacted-Snow Runways. U.S. Army Corps of Engineers.

Shoop, S., G. Phetteplace and W. Wieder 2010. Snow Roads at McMurdo Station, Antarctica.

Shoop, S.A., R. Alger, J. Kunnari and W.L. Wieder 2014a. Evaluation of a New SnowPaver at McMurdo Station, Antarctica. ENGINEER RESEARCH AND DEVELOPMENT CENTER HANOVER NH COLD REGIONS RESEARCH AND ENGINEERING LAB.

Shoop, S.A., M.A. Knuth, W.L. Wieder and M. Preston 2014b. Vehicle impact testing of snow roads at McMurdo Station, Antarctica. COLD REGIONS RESEARCH AND ENGINEERING LAB HANOVER NH.

Stiros, S.C. 2008. Errors in velocities and displacements deduced from accelerographs: An approach based on the theory of error propagation. Soil Dynamics and Earthquake Engineering, 28(5): 415-420.

Sutherland, B.J. 2003. Preventing soil compaction and rutting in the boreal forest of Western Canada: a practical guide to operating timber-harvesting equipment. FERIC.

Van Herwijnen, A. and D.A. Miller 2013. Experimental and numerical investigation of the sintering rate of snow. Journal of Glaciology, 59(214): 269-274.

Weissman, S. 1999. Influence of tire-pavement contact stress distribution on development of distress mechanisms in pavements. Transportation Research Record: Journal of the Transportation Research Board, (1655): 161-167.

Yang, J., J.B. Li and G. Lin 2006. A simple approach to integration of acceleration data for dynamic soil–structure interaction analysis. Soil Dynamics and Earthquake Engineering, 26(8): 725-734.

Zhang, P., J. Chang, B. Qu and Q. Zhao 2016. Denoising and Trend Terms Elimination Algorithm of Accelerometer Signals. Mathematical Problems in Engineering, 2016: 1-9.

APPENDICES

APPENDIX A

GROOMING DATA EXTRACTION AND ANALYSIS

All data from Yellowstone's GPS Insight account for all of Year 1 and Year 2 was downloaded. This included all locations recorded on each groomer from the time the GPS units were installed through the end of grooming during Year 2. This included a reading every 2 minutes when the groomer was running. The reading included: Vehicle, VIN, Date/Time, Ignition (on/off), Max Speed, Average Speed, Instantaneous Speed, Speed Limit, Odometer, Voltage, Distance, Latitude, Longitude, "Address", "Landmark" (for landmarks set in GPS Insight website by researchers), and "Run Time." A few other parameters (like Maximum Acceleration) were listed but the park's units did not have the correct instrumentation for these so they appeared blank.

Readings from each season were processed by listing all of the test sites from a given season in an Excel file, developing formulas to identify when a groomer passed one of these test sites, and using these formulas to identify groomer data points that indicated the groomer was passing a test point. In Year 1, researchers originally used a function on the GPS Insight website to set a "Landmark" at each test site and then have GPS Insight determine which points fell within a chosen distance from this landmark. This procedure worked for some test locations but gave false readings or missed readings for others. Some test sites are near an intersection, so readings on the other sections of road may appear as grooming of the test point even if the groomer did not actually come toward the test point side of the intersection. Other test sites might be located on a straightaway where the groomer goes faster than in other sections so its passes may not be picked up as

close enough to the test site to register. These sites required a more tailored approach to pull out relevant groomer points. Due to this complexity and the need to examine all the raw data for accuracy of identified groomer passes, formulas tailored to particular test sites were developed and used to process all raw data in Excel rather than relying on GPS Insight's "Landmark" feature. Formulas were developed by trial-and-error until they seemed to capture all grooming instances for the test points.

Since the majority of points on the road are groomed nightly, formulas were calibrated until they showed nightly grooming incidents for most test locations. The locations of groomer pass-bys identified as falling near these test sites were then spot-checked to verify their accuracy. For most sites, the grooming incidents were determined either by grooming GPS points that fell within a certain proximity to the test point or by two grooming GPS points that fell on either side of the test point. Excel cell references have been replaced with abbreviations here. The formulas used are shown below.

Abbreviations in Formulas

- TestPtLat: Latitude of the test site
- TestPtLong: Longitude of the test site
- GrmLat: Latitude of groomer GPS point reading
- GrmLong: Longitude of groomer GPS point reading
- NextGrmLat: Latitude of next chronological groomer GPS point reading

- NextGrmLong: Longitude of next chronological groomer GPS point reading

Formulas

- Test-location on a road with east-west orientation:

=IF(OR(AND(ABS(GrmLat-TestPtLat)<=0.001784, ABS(GrmLong-TestPtLong)<=0.0254), AND(OR(AND(GrmLong<TestPtLong, NxtGrmLong>TestPtLong), AND(NextGrmLong<TestPtLong, GrmLong>TestPtLong)), OR(ABS(GrmLat-TestPtLat)<=0.003568, ABS(NxtGrmLat-TestPtLat)<=0.003568))), "Yes", "-")

- Test location on a road with north-south orientation:

=IF(OR(AND(ABS(GrmLat-TestPtLat)<=0.001784, ABS(GrmLong-TestPtLong)<=0.00254), AND(OR(AND(GrmLat<TestPtLat, NxtGrmLat>TestPtLat), AND(NxtGrmLat<TestPtLat, GrmLat>TestPtLat)), OR(ABS(GrmLong-TestPtLong)<=0.003568, ABS(NextGrmLong-TestPtLong)<=0.003568))), "Yes", "-")

- Other, unique test locations (Oth):

- Grant Test Track (Year 2)

=IF(AND(ABS(GrmLat-TestPtLat)<=0.001784, ABS(GrmLong-TestPtLong)<=0.00254), "Yes", "-")

- North Rim Drive (Year 2)

=IF(AND(AND(ABS(GrmLat-TestPtLat)<=0.001784, ABS(GrmLong-TestPtLong)<=0.00762), NOT(OR(GrmLong<=-110.4997, AND(GrmLat>=44.72055, GrmLong<=-110.4948)))), "Yes", "-")

Groomer passes for each individual test point for each season were extracted into an additional Excel sheet. For each groomer pass, there were often several GPS points identified as being near the test site. Researchers read through each point identified and deleted duplicates (e.g., when multiple points 2 minutes from one another had all been identified). Also, groomers generally passed the test site twice each night, once going out on their grooming run and once on the way back. Since each lane was only being groomed once, the later of the two passes was selected for data analysis since this was presumably when grooming for that piece of road was completed, with both lanes having been groomed. The point(s) from the earlier pass was/were deleted from the spreadsheet.

For each site, the most representative weather station was selected, based on location and similarity to the weather station sites. Weather stations selected for the test sites are listed in the table below. Data from the relevant weather station was extracted for November through March of the relevant season(s) and placed on the same sheet as the grooming points for that year. Table A.1 provides information on the test sites for which road hardness data was collected, the category of the road used to determine the correct Excel formula for the point, and the weather station used for that site.

Table A.1. Year 1 hardness test locations, the categories determining which Excel formulas were used to identify groomer passes, and weather station data used for each site

	Test Site				Weather Station Used	
	Name	Latitude	Longitude	NS/EW/Oth	Type	Name
Year 1	Blanding	44.70813	-110.61749	EW	SNOTEL	Canyon
	Virginia Cascades	44.71917	-110.66633	EW	SNOTEL	Canyon
	Firehole	44.60736	-110.84596	NS	SNOTEL	West Yellowstone
	West of Spring Creek	44.43152	-110.76011	EW	SNOTEL	Thumb Divide
	Madison Junction Campground	44.64622	-110.86121	EW/Oth	SNOTEL	West Yellowstone
	Canyon South Rim	44.71446	-110.49263	EW	SNOTEL	Canyon
	Gibbon Meadows	44.71530	-110.72894	EW	SNOTEL	West Yellowstone
	Lewis Lake	44.31036	-110.60189	NS	SNOTEL	Lewis Lake
	Kepler	44.44906	-110.80829	NS	NOAA	OLD FAITHFUL, WY US
	West of Kepler	44.45121	-110.81086	NS	NOAA	OLD FAITHFUL, WY US
	Firehole Picnic	44.59503	-110.83084	NS	NOAA	OLD FAITHFUL, WY US
	Solfatara	44.80571	-110.7366667	NS	NOAA	YELLOWSTONE PARK MAMMOTH, WY US
	Riddle	44.35849	-110.5820333	NS	SNOTEL	Thumb Divide
	Pumice Point	44.45479	-110.4947028	EW	NOAA	LAKE YELLOWSTONE, WY US
	East of Madison	44.64873216	-110.7818332	EW	SNOTEL	West Yellowstone

Table A.2. Year 2 hardness test locations, the categories determining which Excel formulas were used to identify groomer passes, and weather station data used for each site

	Test Site				Weather Station Used	
	Name	Latitude	Longitude	NS/EW/Oth	Type	Name
Year 2	North Rim Drive	44.719769	-110.49683	Oth	SNOTEL	Canyon
	Blanding	44.717453	-110.639824	EW	SNOTEL	Canyon
	South of Fishing Bridge	44.5522	-110.4083	NS	NOAA	LAKE YELLOWSTONE, WY US
	South of Obsidian Cliff	44.8106	-110.7316	NS	NOAA	YELLOWSTONE PARK MAMMOTH, WY US
	South of Grant	44.3644	-110.5807	NS	SNOTEL	Thumb Divide
	Between Old Faithful and West Thumb	44.419411	-110.602089	EW	SNOTEL	Thumb Divide
	Whiskey Flats	44.532489	-110.828592	EW	NOAA	OLD FAITHFUL, WY US
	Lewis Lake	44.3104	-110.601814	NS	SNOTEL	Lewis Lake
	Near Craig Pass	44.4412	-110.676159	NS	SNOTEL	Thumb Divide
	Kepler	44.44906	-110.80829	NS	NOAA	OLD FAITHFUL, WY US
	West of Madison	44.644611	-110.919704	EW	SNOTEL	West Yellowstone
	Virginia Cascades	44.71922	-110.666268	EW	SNOTEL	Canyon
	Hayden Valley	44.643427	-110.457214	NS	SNOTEL	Canyon
	Northwest of West Thumb	44.421705	-110.586572	EW	SNOTEL	Thumb Divide
	Between Norris and Mammoth	44.861152	-110.736385	NS	NOAA	YELLOWSTONE PARK MAMMOTH, WY US
	Grant Test Track	44.393182	-110.557337	Oth	SNOTEL	Thumb Divide

Grooming and weather data for each test site was then used to calculate parameters for each site. These included: time between grooming and hardness test, temperature at the hardness test, average temperature between grooming and the hardness test, average precipitation between grooming events, average change in snow depth between grooming events, average daily precipitation, average daily change in snow depth, and average daily "degree-days" (maximum daily temperature minus -10 °C for every day on which the maximum temperature was above -10 °C).

Table A.3 shows dates for which data was available for each groomer during each year. The delay in data collection at the beginning of Year 1 was due to when the NPS was able to install the GPS devices. The data gaps in Year 2 come from malfunction of the Old Faithful Groomer GPS unit and the Lake District getting a new groomer without the GPS unit being moved from one to the other.

Table A.3. Grooming GPS data available by district and year

Year	Grooming District	Dates of Data
1	Canyon	12/16/15-3/3/16
	West	1/21/15-3/14/16
	Old Faithful	12/12/15-3/14/16
	Grant	12/16/15-4/1/16
	Lake	12/17/15-3/28/16
2	Canyon	12/6/16-3/9/17
	West	12/9/16-3/17/17
	Old Faithful	2/22/16-3/13/17
	Grant	11/28/16-3/17/17
	Lake	NA

APPENDIX B

RAMMSONDE HARDNESS

The equation for hardness is stated below, the Ramm number (RN) was solved for first then converted to a force (RR) by the equations below.

$$RN = T + H + \frac{nfH}{p}$$
$$RR = RN\ x\ 10$$

RN = Ramm number (kg)
RR = Ramm resistance (N)
n = number of hammer blows
f = fall height of the hammer (cm)
p = increment of penetration for *n* blows (cm)
T = mass of tubes including guide rod (kg)
H = mass of hammer (kg)

When the cone on the penetrometer enters the snowroad, the resistance varies due to the increasing diameter of the cone. To deal with this variance Niedringhaus (1965) developed a method to mitigate this issue. He developed a correction factor to be used in the top 10 cm. For the top 5 cm of penetration, a correction factor of 4 should be applied to the Ramm number. From 5 to 10 cm, this factor should be 1.6. Due to the importance of accurate hardness measurements in this study, Niedringhaus' correction factor was employed.

The MATLAB code used to process hardness data is shown on the following pages. This code takes the raw drop height, number of drops, and penetration depths for each Ramm reading, as entered into an Excel template (Figure B.1), and calculates and graphs the hardness for each layer. It gives the user an option of whether or not to use the correction factors.

Tube Wt. (kg):	1.075	Hammer Weight (kg):			1.0125	
		Raw Data				
Date	Time	Tester(s)	No. Drops	Fall Height (cm)	Total Penetration Depth (cm)	Notes
2/26/2017	2/26/2017 13:05	MSU	0	0	6	Tube
			0	0	8	Tube+ Hammer
Temp taken @	13:05		2	10	10	
Location:	TestTrackBomb5passes5mph					

Figure B.1. Excel template required for input into MATLAB code; top left cell is positioned in Excel cell A1

```
% Hardness Processor
% See paper
% http://journal.frontiersin.org/article/10.3389/feart.2016.00052/full
% for reference on this material
clear
clc

% Define Parameters
W  = 1.0125  ;      %Weight of Hammer (kg)
Q  = 1.075  ;       %Weight of tube (kg)

% Select file
currentFile = uigetfile('*.xlsx', 'Select file to process:');

%%% Raw Data
% Grab table of Drop #, Fall Ht, Penetration Depth Values
rdgsCols = xlsread(currentFile, 'Sheet1', 'D:F');
rdgs = rdgsCols(5:size(rdgsCols,1),:);

% Grab location and time and make graph title, output filename
[~, ~, loc] = xlsread(currentFile, 'Sheet1', 'B8');
[~, ~, time]  = xlsread(currentFile, 'Sheet1', 'B5');
gtitle = [loc; time];
l = char(loc);
t = char(time);

% Find the year, month, and date from the time to put in the graph
filename
if t(4)~= '/'
    y1 = 6;
    y2 = 9;
    m1 = 1;
    d1 = 3;
    d2 = 4;
else
    y1 = 5;
    y2 = 8;
    m1 = 1;
    d1 = 3;
    d2 = 3;
end

% Make the graph filename
gfilen = sprintf('%s_%s_%s_%s',t(y1:y2),t(m1),t(d1:d2),l);

% Prep Vectors for Data
DrHt        = [];      %Drop Heights
NumDr       = [];      %Number of Drops
S           = [];      %Penetration Depths

% Grab the columns of data from Excel hardness plots (has to be same
% format) but doesn't matter how many rows...
```

```
for i = 1:size(rdgs,1)
    NumDr(i)=rdgs(i,1);
end

for i = 1:size(rdgs,1)
    DrHt(i)=rdgs(i,2);
end

for i = 1:size(rdgs,1)
    S(i)=rdgs(i,3);
end

%%% Processing

% Prep vector for hardness data
R = [];

%Now solve for Ram Hardness

% For cases where the penetration depth is the same in two subsequent
% readings, assume the higher hardness for all readings at that depth.
Do
% that by setting the penetration for that reading (= change in depth
from
% last reading) equal to the difference between the current reading and
the
% depth reading two points earlier.

R(1)=Q ;
R(2)=Q+W ;

for i=3:length(S)
    dS = S(i)-S(i-1);
    % Then calculate R based on the dS value.
    R(i)=((W*DrHt(i)*NumDr(i))/dS)+(W+Q);
end

% Allow user to select if they would like to add the correction factors
% from
% http://www.dtic.mil/dtic/tr/fulltext/u2/a211588.pdf
% (Lee 1989, p.8)
[sel,okay] = listdlg('PromptString', 'Use correction factors?',...
    'SelectionMode','single','ListString',{'Yes','No'}, 'InitialValue',
2);
if sel == 1

    %% Split any intervals that cross 5 so appropriate CFs can
    %% be applied to the sections on either side.
    for i = 1:length(S)
        if i==1 && S(i)>5
            S = [5 S];
            R = [R(i) R];
        elseif S(i)<5 && S(i+1)>5
```

```
            S = [S(1:i) 5 S(i+1:end)];
            R = [R(1:i) R(i+1) R(i+1:end)];
        end
    end

    %% Split any intervals that cross over 10
    for i = 1:length(S)
        if i==1 && S(i)>10
            S = [10 S];
            R = [R(i) R];
        elseif S(i)<10 && S(i+1)>10
            S = [S(1:i) 10 S(i+1:end)];
            R = [R(1:i) R(i+1) R(i+1:end)];
        end
    end

    %% Apply correction factors
    for i = 1:length(S)
        if S(i) <= 5
            R(i) = 4*R(i);
        elseif and(S(i)>5, S(i)<=10)
            R(i) = 1.6*R(i);
        end
    end
    gfilen = sprintf('%s_CF',gfilen);
end

Sff=[0 0];
for i=1:length(R)
    Sff=[Sff S(i) S(i)];
end

Rff=[0];
for i=1:length(R)
    Rff=[Rff R(i) R(i)];
end
Rff=[Rff 0];

% Make final RR values in Newtons
RffN = 10*Rff;

clf
plot(RffN,Sff)
set(gca, 'YDir', 'Reverse')
xlabel('Ram Hardness (N)')
ylabel('Depth (cm)')
title(gtitle)

Fgfilen = sprintf('%s.jpg',gfilen);
set(gcf, 'PaperUnits', 'Inches');
set(gcf, 'PaperPosition', [0 0 8.5 5.5]);
set(gca, 'fontsize', 24);
saveas(gcf, Fgfilen);
```

```
% Make matrix of values to load into Excel
SumMat = zeros(length(S), 4);
Sw0 = [0, S(1:length(S)-1)];
SumMat(:,1) = Sw0;
SumMat(:,2) = S;
SumMat(:,3) = 10*R;
SumMat(:,4) = R;

% Make matrix of orig values to go next to proc vals
OrigData = zeros(length(DrHt), 3);
OrigData(:,1) = DrHt;
OrigData(:,2) = NumDr;
OrigData(:,3) = rdgs(:,3);

% Find weighted averages to add into Excel
AvgRng = [10, 15, 20, 25, 30];
WtdAvg = [];
for i = 1:length(AvgRng)
    SumAvg = 0;
    if S(length(S)) >= AvgRng(i)
        for j = 1:length(S)
            if and(S(j)<=AvgRng(i), S(j)~=0)
                SumAvg = SumAvg + (S(j)-Sw0(j))*10*R(j);
            elseif and(S(j)>AvgRng(i), Sw0(j)<AvgRng(i))
                SumAvg = SumAvg + (AvgRng(i)-Sw0(j))*10*R(j);
            end
        end
        Avg = SumAvg/AvgRng(i);
        WtdAvg = [WtdAvg Avg];
    elseif S(length(S)) < AvgRng(i)
        WtdAvg = [WtdAvg 0];
    end
end

% Write to Excel File
xlTitle = sprintf('Proc_%s',currentFile);
hdr = [time; loc; currentFile];
WtdAvgLabels = {'Weighted Average Over', '10cm', '15cm', '20cm',
'25cm', '30cm'};
hdrLabels = {'Top of Layer (depth, cm)', 'Bottom of Layer (depth, cm)',
...
    'Ramm Resistance (N)', 'Ramm Resistance (kg)', '', 'Drop Height
(cm)', ...
    'Number Drops', 'Total Penetration'};

sheet = 'Sheet1';
xlswrite(xlTitle,hdr,sheet,'A1');
xlswrite(xlTitle,WtdAvgLabels,sheet,'A4');
xlswrite(xlTitle,WtdAvg,sheet,'B5');
xlswrite(xlTitle,hdrLabels,sheet,'A6');
xlswrite(xlTitle,SumMat,sheet,'A7');
xlswrite(xlTitle,OrigData,sheet,'F7');
```

APPENDIX C

LOAD CELL PROCESSING

The twelve load cells that created the load cell array were LC304-500 load cells designed by Omega Engineering Inc. These load cells are designed to withstand loads of 2,225 N (500 lbs), however they are capable of withstanding loads of up to 150% of capacity. Each load cell comes with a unique specifications sheet and a calibration factor. With information from the specifications sheet, raw voltage readings from the load cells can be converted to load measurements. The data is then post-processed using various programs described below.

A LabVIEW program was created to trim the data and convert it into force (Newtons or pounds). The program trimmed the data before the first load event and after the last load event according to a set threshold (a force significant enough in magnitude to indicate a vehicle passing). The LabVIEW code was programmed to trim readings earlier than 2,000 points before the first time the threshold is reached and beyond 2,000 readings after the last time the threshold is reached. Calibration information specific to each load cell was entered to set the program to translate voltage readings from each load cell into the force represented by the voltage readings. This program saved the data in comma-separated values (CSV) format that could be opened in Excel, facilitating generation of graphs and investigation of the force data. Each load cell data file (one per pass-by) was processed using this trimming program.

Furthermore, once the data was saved as an .xlsx file (Excel file), the data was imported into MATLAB for more involved processing techniques. MATLAB was used

to make 3-dimensional plots, solve for vehicle velocity (see the Vehicle Loading methods section for details), and solve for impulse.

With possible damage to the load cells throughout use in this project, some days the load data was quite 'noisy'. This is not uncommon with the use of instruments in the field and there are commonly used methods to 'smooth' the data. The most advantageous method for researchers to smooth the data was a Savitzky-Golay filter in MATLAB. This is a built-in filter in MATLAB that smooths noisy data. It takes noisy data and increases the signal-to-noise ratio without greatly distorting the signal. This filtering method proved to be a good fit for use with this project's noisy load data. Figure C.1 shows unfiltered data from Year 2 and Figure C.2 shows the same data after the filter was applied.

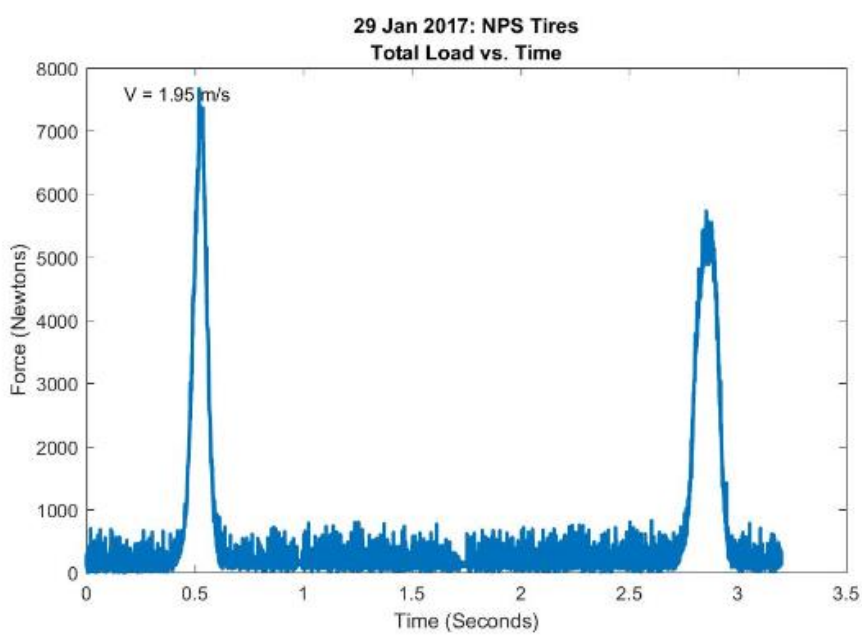

Figure C.1. Pass-by from the NPS LPT courier vehicle; note the high level of noise associated with the measurement

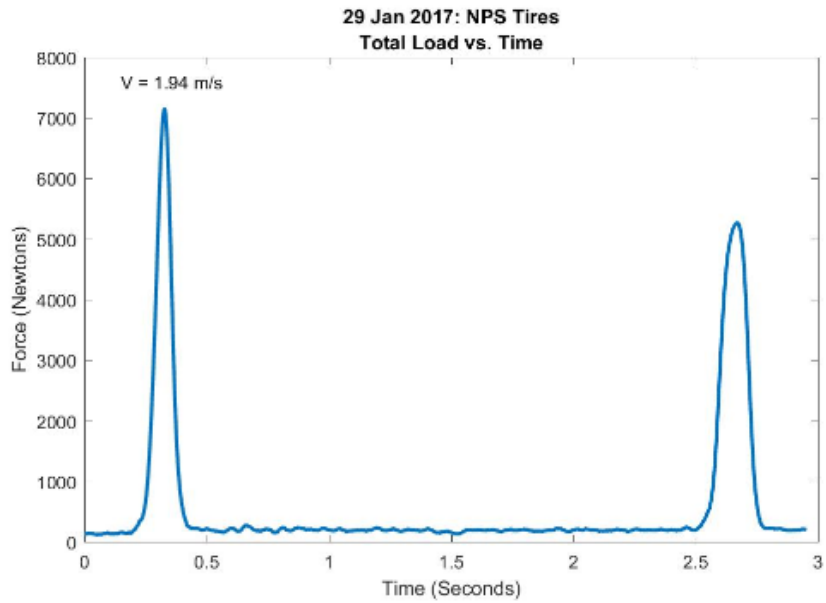

Figure C.2. The same pass-by as Figure C.1, but with the Savitzky-Golay filter applied; significantly decreased noise

To solve for impulse, a numerical integration was carried through in MATLAB. A trapezoidal integration method was used. This method sums the area under the load curve with respect to time. The equation for this method is seen below.

$$A_i = \frac{1}{2}(f_i + f_{i+1})h$$

$$A_T = A_0 + A_1 + \cdots A_{N-1}$$

A_i = incremental area
f_i = function value at point i
h = distance between points
A_T = total area

The MATLAB code used to process load cell data is shown on the following pages. This file takes input of an Excel file with 12 columns, with each column

containing raw voltage readings from one load cell. The code that calculates impulse is included after the original load cell processing code.

```
% MATLAB file to make load plots
% Used for Yellowstone Snowroad Project, this is a generic file that
% must changed for various vehicles. For example Tire width, distance
% between axles and other various changes must be made for accurate
% velocities and other parameters this code solves for.

clear; clc

% Set Pass Info
% Set date of pass-bys for plot titles
Dt = '29 Jan 2017';

% Vehic = '117cmx58cm Tires, 75 kPa,61 kPa'; Tire Dimension then
% inflation pressure.

Vehic = 'NPS Tires';     %  Vehicle Type

% Track width or anything to note
Tirewidth=60;       % Centimeters
Ttl = sprintf('%s: %s',Dt,Vehic);

ConversionFile = uigetfile('*.xlsx','Select conversion file:');
% Assign array a variable name
B = readtable(ConversionFile);
C = table2array(B);

% If data is 'noisy' apply Savitzky-Golay filter, this filter will
reduce % the noise to signal ratio.
% C = sgolayfilt(C,10,401);         % y = sgolayfilt(x,order,framelen)
                                    % framelen must be odd
C = sgolayfilt(C,2,41);

%Grab Columns
loadcell1= 4.448*C(:,1);    %4.448 is for newton conversions
loadcell2= 4.448*C(:,2);
loadcell3= 4.448*C(:,3);
loadcell4= 4.448*C(:,4);
loadcell5= 4.448*C(:,5);
loadcell6= 4.448*C(:,6);
loadcell7= 4.448*C(:,7);
loadcell8= 4.448*C(:,8);
loadcell9= 4.448*C(:,9);
loadcell10=4.448*C(:,10);
loadcell11=4.448*C(:,11);
loadcell12=4.448*C(:,12);
loadcellsum=4.448*C(:,13);

t(1)=1;

for i=1:length(loadcell1)
t1(i)= i;             %Time for stress
end
```

```
figure('units','normalized','outerposition',[0 0 1 1])
plot(t1,loadcellsum,'linewidth',2)
xlabel('t')
ylabel('N')
set(gca,'XTick',0:400:length(loadcell1));
PlotTitle2 = sprintf('%s; %s',ConversionFile,'Summed Load');
title(sprintf('%s; %s',ConversionFile,'load vs time'))
grid on
grid minor

% Ask user where to trim this file. i.e. Isolate wanted events.
begPromptAll = 'Enter the beginning trim value (at least 1): ';
beginAllLoad = input(begPromptAll);

endPromptAll = 'Enter the ending trim value (at least 1): ';
endAllLoad = input(endPromptAll);

loadcell1trim=   loadcell1(beginAllLoad:endAllLoad);
loadcell2trim=   loadcell2(beginAllLoad:endAllLoad);
loadcell3trim=   loadcell3(beginAllLoad:endAllLoad);
loadcell4trim=   loadcell4(beginAllLoad:endAllLoad);
loadcell5trim=   loadcell5(beginAllLoad:endAllLoad);
loadcell6trim=   loadcell6(beginAllLoad:endAllLoad);
loadcell7trim=   loadcell7(beginAllLoad:endAllLoad);
loadcell8trim=   loadcell8(beginAllLoad:endAllLoad);
loadcell9trim=   loadcell9(beginAllLoad:endAllLoad);
loadcell10trim=  loadcell10(beginAllLoad:endAllLoad);
loadcell11trim=  loadcell11(beginAllLoad:endAllLoad);
loadcell12trim=  loadcell12(beginAllLoad:endAllLoad);
loadcellsumtrim= loadcellsum(beginAllLoad:endAllLoad);

%Preallocate vectors of ones twos threes ect
one=zeros(length(loadcell1trim),1);
two=zeros(length(loadcell1trim),1);
three=zeros(length(loadcell1trim),1);
four=zeros(length(loadcell1trim),1);
five=zeros(length(loadcell1trim),1);
six=zeros(length(loadcell1trim),1);
seven=zeros(length(loadcell1trim),1);
eight=zeros(length(loadcell1trim),1);
nine=zeros(length(loadcell1trim),1);
ten=zeros(length(loadcell1trim),1);
eleven=zeros(length(loadcell1trim),1);
twelve=zeros(length(loadcell1trim),1);

%Create vectors of ones twos threes ect
for i=1:length(loadcell1trim)
  one(i)=1;
  two(i)=2;
  three(i)=3;
  four(i)=4;
  five(i)=5;
  six(i)=6;
  seven(i)=7;
```

```
  eight(i)=8;
  nine(i)=9;
  ten(i)=10;
  eleven(i)=11;
  twelve(i)=12;
end

% Number of points in trimmed data
TrimmedAllLoad = endAllLoad-beginAllLoad+1;

for i=1:TrimmedAllLoad
t(i)= i;              % Time for stress
end

figure('units','normalized','outerposition',[0 0 1 1])
plot(t,loadcellsumtrim,'linewidth',2)
xlabel('t')
ylabel('N')
set(gca,'XTick',0:100:length(loadcell1));
PlotTitle2 = sprintf('%s; %s',ConversionFile,'Summed Load');
title(sprintf('%s; %s',ConversionFile,'load vs time'))
grid on
grid minor

%% Have user enter the intervals where the two maxes are located
Prompt0 = 'How many spikes are there on this plot? ';
NumSpikes = input(Prompt0);
Mmax=zeros(1,NumSpikes);
tmax=zeros(1,NumSpikes);
firstMaxbegin=zeros(1,NumSpikes);
firstMaxend=zeros(1,NumSpikes);
for i=1:NumSpikes
    Prompt1 = 'Enter beginning of first maximum interval: ';
    firstMaxbegin(i) = input(Prompt1);
    Prompt2 = 'Enter end of first maximum interval: ';
    firstMaxend(i) = input(Prompt2);

   [Mmax(i),tmax(i)] = max(loadcellsumtrim(firstMaxbegin(i):...
                       firstMaxend(i)));
end

Prompt1 = ...
'Enter the number from left to right of the 1st spike you want for
velocity measurement: ';
firstspike = input(Prompt1);
Prompt2 = ...
'Enter the number from left to right of the 2nd spike you want for
velocity measurement: ';
secondspike = input(Prompt2);

tm1f = tmax(firstspike)+firstMaxbegin(firstspike);
tm2f = tmax(secondspike)+firstMaxbegin(secondspike);
```

```
%% Caculate Velocity from time interval -- UPDATE AXLES for specific
%  Vehicle

timeInt = tm2f-tm1f;
timeS = timeInt/2000;
% In centimeters (Distance between front to rear bogey) or dist between
% tires
axles = 455;
Vms = axles/(100*timeS);  % Vel in meters per second
Vmih = Vms*60*60/1609.34; % Vel in miles per hour

VelTitle = sprintf('V = %.2f m/s ', Vms);

%% Put time into seconds
tS = t/2000;

%% Plot load data in metric units
% By Load Cell, 3D Non-surface
figure(1); clf;
subplot(2,2,1);
plot3(tS,one,loadcell1trim,'linewidth',2)
hold on
plot3(tS,two,loadcell2trim,'linewidth',2)
plot3(tS,three,loadcell3trim,'linewidth',2)
plot3(tS,four,loadcell4trim,'linewidth',2)
plot3(tS,five,loadcell5trim,'linewidth',2)
plot3(tS,six,loadcell6trim,'linewidth',2)
plot3(tS,seven,loadcell7trim,'linewidth',2)
plot3(tS,eight,loadcell8trim,'linewidth',2)
plot3(tS,nine,loadcell9trim,'linewidth',2)
plot3(tS,ten,loadcell10trim,'linewidth',2)
plot3(tS,eleven,loadcell11trim,'linewidth',2)
plot3(tS,twelve,loadcell12trim,'linewidth',2)

xlabel('Time (Seconds)')
ylabel('Load Cell Number')
zlabel('Force (Newtons)')
PlotTitle1 = {Ttl,'Load vs. Time, by Load Cell';
title(PlotTitle1)
hold off

% Summed load plot
subplot(2,2,4)
plot(tS,loadcellsumtrim,'linewidth',2)
xlabel('Time (Seconds)')
ylabel('Force (Newtons)')
PlotTitle2 = {Ttl,'Total Load vs. Time'};
title(PlotTitle2)

% Write the velocity on the summed graph at specified position
yl=ylim;
xl=xlim;
text(.05*(xl(2)-xl(1))+xl(1),.95*(yl(2)-yl(1))+yl(1),VelTitle);
```

```
% By Load Cell, 2D
subplot(2,2,3)
plot(tS,loadcell1trim,'linewidth',2)
hold on
plot(tS,loadcell2trim,'linewidth',2)
plot(tS,loadcell3trim,'linewidth',2)
plot(tS,loadcell4trim,'linewidth',2)
plot(tS,loadcell5trim,'linewidth',2)
plot(tS,loadcell6trim,'linewidth',2)
plot(tS,loadcell7trim,'linewidth',2)
plot(tS,loadcell8trim,'linewidth',2)
plot(tS,loadcell9trim,'linewidth',2)
plot(tS,loadcell10trim,'linewidth',2)
plot(tS,loadcell11trim,'linewidth',2)
plot(tS,loadcell12trim,'linewidth',2)
xlabel('Time (Seconds)')
ylabel('Force (Newtons)')
PlotTitle3 = {Ttl,'Load vs. Time, by Load Cell'};
%legend()
title(PlotTitle3)

%% Select maximums for each loads cell to create bar graph
figure('units','normalized','outerposition',[0 0 1 1])
plot(t,loadcellsumtrim,'linewidth',2)
xlabel('t')
ylabel('N')
set(gca,'XTick',0:100:length(loadcell1trim));
PlotTitle2 = sprintf('%s; %s',ConversionFile,'Summed Load');
title(sprintf('%s; %s',ConversionFile,'load vs time'))
grid on
grid minor

Prompt3bar = 'Which spike has the highest magnitude? ';
BiggestspikeNum = input(Prompt3bar);

tForBar = firstMaxbegin(BiggestspikeNum) + tmax(BiggestspikeNum);

Mcell1  = loadcell1trim (tForBar);
Mcell2  = loadcell2trim (tForBar);
Mcell3  = loadcell3trim (tForBar);
Mcell4  = loadcell4trim (tForBar);
Mcell5  = loadcell5trim (tForBar);
Mcell6  = loadcell6trim (tForBar);
Mcell7  = loadcell7trim (tForBar);
Mcell8  = loadcell8trim (tForBar);
Mcell9  = loadcell9trim (tForBar);
Mcell10 = loadcell10trim(tForBar);
Mcell11 = loadcell11trim(tForBar);
Mcell12 = loadcell12trim(tForBar);
Mcellarray=[Mcell1  Mcell2  Mcell3  Mcell4 Mcell5 Mcell6 Mcell7...
Mcell8 Mcell9  Mcell10 Mcell11 Mcell12];
figure(1)
subplot(2,2,2)
bar(Mcellarray)
```

```
xlim([0 13])
ylabel('Force (Newtons)')
xlabel('Load Cell Number')
Bartitle = {Ttl,'At Max Summed Load'};
title(Bartitle)

%% Information for saving Figure 1
ThreePlotName = sprintf('%sPlotsmet.jpg', ConversionFile(1:end-5));
set(gcf, 'PaperUnits', 'Inches');
set(gcf, 'PaperPosition', [0 0 17 11]);
saveas(gcf, ThreePlotName);

%% Contour plot
figure(3); clf;
loadarray=cat(2,loadcell1trim,loadcell2trim,loadcell3trim,loadcell4trim
,...loadcell5trim,loadcell6trim,loadcell7trim,loadcell8trim,loadcell9tr
im,...loadcell10trim,loadcell11trim,loadcell12trim);

onestwosthrees=cat(2,one,two,three,four,five,six,seven,eight,nine,ten,.
..eleven,twelve);

tarray=zeros(length(loadcell1trim),12);

for i=1:12
    tarray(:,i)=tS;
end

mesh(tarray,onestwosthrees,loadarray)

ContourPlotName = sprintf('%sContourPlot.jpg', ConversionFile(1:end-
5));
set(gcf, 'PaperUnits', 'Inches');
set(gcf, 'PaperPosition', [0 0 17 11]);
xlabel('time')
ylabel('Load Cell Number')
zlabel('Force (Newtons)')
Contourtitle = {Ttl,'Surface Plot of Load Cells'};
title(Contourtitle)
saveas(gcf, ContourPlotName);




%% Solve for stress this vehicle produced
% This was an attempt to solve for stress however, through analysis
% this was not warranted as a accurate method. Additional information
% would be needed to solve for an accurate stress. This will be left
% here though in case the information is one day gathered and this code
% could be utilized.

% Area of load cell effected
```

```
Area=Tirewidth*10.16;
           % Tirewidth(4*2.54cm)=Area
% Solve for stress at each maximum load
Stress=zeros(1,NumSpikes);
for i=1:NumSpikes
Stress(i)=Mmax(i)/Area;       % First stress (max)     %second stress
(max)
end                           % For bomb and mattracks more than two
peaks

% Display stress results in command window
Stress

%% Select the Stress/Strain Excel file where you are storing
stress/strain
% info.
currentFile = uigetfile('*.xlsx', 'Select file to process:');
currentFileName = currentFile(1:end-5);

% Get the existing names of sheets in the Excel workbook.
[status,sheets] = xlsfinfo(currentFile);
sheets = [sheets 'Other'];

% Ask the user which Sheet to put the data on. If the vehicle is not
% listed yet, allow the user to select "Other". Then ask for the user
% to provide an appropriate name for the vehicle so that we can make a
% new sheet for it in the Excel file.
[sel,okay] = listdlg('PromptString', 'Select the Vehicle',
'SelectionMode',...
    'single','ListString',sheets);
if sel == length(sheets)
    vPrompt = 'Please enter the vehicle name (Snowbuster, SS Tires,
etc.): ';
    Vsheet = input(vPrompt, 's');
else
    Vsheet = sheets(sel);
end

% If you will be adding to an existing sheet, read the data from that
% sheet in so you know where the blank rows start.
if sel < length(sheets)
    [num,txt,raw] = xlsread(currentFile, char(Vsheet));
    SSrows = size(txt,1)+1;
    SSaddRow = SSrows(1)+2;
    StartCell = sprintf('A%d',SSaddRow);
    StartDataCell = sprintf('B%d',SSaddRow);okay
    StartDataCellNums = sprintf('B%d',SSaddRow+5);
else
    StartCell = 'A1';
    StartDataCell = 'B1';
    StartDataCellNums = 'B6';
end

% Find where the blank rows start and define 2 rows down as your start
```

```
% point.

%% Test vals (won't be needed when plugged into bigger file)
%Vehic = 'NPS Tires';
%ConversionFile = 'NPS Tires';
%Vms = 100;
%Vmih = 5;
StressTimes = (firstMaxbegin+tmax)/2000;
%Stress = [100, 200, 300, 400, 500];

% Make Column and Row Titles
Tc = {'Vehicle';'File';'Processed';'Velocity (m/s)';'Velocity
(mph)';...
    'Load Time (s)';'Load (N)'};

% Make partial column for file ID values
Mdc = {Vehic; ConversionFile; sprintf('Processed %s',...
    datestr(datetime('now'))); Vms; Vmih};
MdcVs = [StressTimes; Mmax];

xlswrite(currentFile, Tc, char(Vsheet), StartCell)
xlswrite(currentFile, Mdc, char(Vsheet), StartDataCell)
xlswrite(currentFile, MdcVs, char(Vsheet), StartDataCellNums)
```

The following MATLAB code solves for impulse. Many portions of this code are similar to the code above. For additional comments reference the code above.

```
%% File to go through load cell data and solve for impulse.
% This file is similar to Generic_Loadplots_Thesis however
% Impulse has been added to code

clear; clc

ConversionFile = uigetfile('*.xlsx','Select conversion file:');
B = readtable(ConversionFile); %Chg for real file
C = table2array(B);

%Grab Columns
loadcell1= 4.448*C(:,1);    %4.448 is for newton conversions
loadcell2= 4.448*C(:,2);
loadcell3= 4.448*C(:,3);
loadcell4= 4.448*C(:,4);
loadcell5= 4.448*C(:,5);
loadcell6= 4.448*C(:,6);
loadcell7= 4.448*C(:,7);
loadcell8= 4.448*C(:,8);
loadcell9= 4.448*C(:,9);
loadcell10=4.448*C(:,10);
loadcell11=4.448*C(:,11);
loadcell12=4.448*C(:,12);
loadcellsum=4.448*C(:,13);

t(1)=1;

for i=1:length(loadcell1)
t1(i)= i;             %Time for stress
end

figure('units','normalized','outerposition',[0 0 1 1])
plot(t1,loadcellsum,'linewidth',2)
xlabel('t')
ylabel('N')
set(gca,'XTick',0:400:length(loadcell1));
PlotTitle2 = sprintf('%s; %s',ConversionFile,'Summed Load');
title(sprintf('%s; %s',ConversionFile,'load vs time'))
grid on
grid minor

% Ask user where to trim this file.
begPromptAll = 'Enter the beginning trim value (at least 1) for all the
load cells: ';
beginAllLoad = input(begPromptAll);
endPromptAll = 'Enter the ending trim value (at least 1) for all the
load cells: ';
endAllLoad = input(endPromptAll);
```

```
% Enter Date the measurement was taken since we can only compare
% vehicles from same day
Dt = '5 Mar 2016';
%Vehicle Type
Vehic = 'TSS Mattracks';
Ttl = sprintf('%s: %s',Dt,Vehic);

% Trim the loadcell data from user specified inputs
loadcell1trim=   loadcell1(beginAllLoad:endAllLoad);
loadcell2trim=   loadcell2(beginAllLoad:endAllLoad);
loadcell3trim=   loadcell3(beginAllLoad:endAllLoad);
loadcell4trim=   loadcell4(beginAllLoad:endAllLoad);
loadcell5trim=   loadcell5(beginAllLoad:endAllLoad);
loadcell6trim=   loadcell6(beginAllLoad:endAllLoad);
loadcell7trim=   loadcell7(beginAllLoad:endAllLoad);
loadcell8trim=   loadcell8(beginAllLoad:endAllLoad);
loadcell9trim=   loadcell9(beginAllLoad:endAllLoad);
loadcell10trim=  loadcell10(beginAllLoad:endAllLoad);
loadcell11trim=  loadcell11(beginAllLoad:endAllLoad);
loadcell12trim=  loadcell12(beginAllLoad:endAllLoad);
loadcellsumtrim= loadcellsum(beginAllLoad:endAllLoad);

% Number of points in trimmed data
TrimmedAllLoad = endAllLoad-beginAllLoad+1;

for i=1:TrimmedAllLoad
t(i)= i;              %Time for Load
end

%Plot the trimmed summed data
figure('units','normalized','outerposition',[0 0 1 1])
plot(t,loadcellsumtrim,'linewidth',2)
xlabel('t')
ylabel('N')
set(gca,'XTick',0:100:length(loadcell1));
PlotTitle2 = sprintf('%s; %s',ConversionFile,'Summed Load');
title(sprintf('%s; %s',ConversionFile,'load vs time'))
grid on
grid minor

% Make a choice to apply the savitzky-golay filter (If very noisy apply
% filter)
Choice = input('Do you want to apply the filter? Y or N: ','s')

if Choice == 'Y'
    % Apply the filter below if the data is very noisy
    loadcellsumtrim = sgolayfilt(loadcellsumtrim,2,41);

    %Plot the trimmed summed data with filter
figure('units','normalized','outerposition',[0 0 1 1])
plot(t,loadcellsumtrim,'linewidth',2)
xlabel('t')
ylabel('N')
set(gca,'XTick',0:100:length(loadcell1));
```

```
PlotTitle2 = sprintf('%s; %s',ConversionFile,'Summed Load');
title(sprintf('%s; %s',ConversionFile,'load vs time'))
grid on
grid minor
else Choice == 'N'
    %If not leave as is
    loadcellsumtrim=loadcellsumtrim;
end

%% Have user enter the intervals where the two maxes are located
%Prompt0 = 'How many spikes are there on this plot?  ';
NumSpikes = 2; % input(Prompt0);
Mmax=zeros(1,NumSpikes);
tmax=zeros(1,NumSpikes);
firstMaxbegin=zeros(1,NumSpikes);
firstMaxend=zeros(1,NumSpikes);
for i=1:NumSpikes

    Prompt1 = 'Enter beginning of first maximum interval: ';
    firstMaxbegin(i) = input(Prompt1);
    Prompt2 = 'Enter end of first maximum interval: ';
    firstMaxend(i) = input(Prompt2);

   [Mmax(i),tmax(i)] =
max(loadcellsumtrim(firstMaxbegin(i):firstMaxend(i)));
end

% Selecting the maximums from the array you created to get velocity,
% example for a tire it would be 1 and 2. For a bomb and you knew the
% distance between the front and read bogey wheel it would be 2 and 5.
% Prompt1 ='Enter the number from left to right of the 1st spike you
% want for velocity measurement: ';
firstspike = 1;% input(Prompt1);
% Prompt2 ='Enter the number from left to right of the 2nd spike you
% want for velocity measurement: ';
secondspike = 2;% input(Prompt2);

tm1f = tmax(firstspike)+firstMaxbegin(firstspike);
tm2f = tmax(secondspike)+firstMaxbegin(secondspike);

%% Caculate Velocity from time interval -- UPDATE AXLES for Vehicle

timeInt = tm2f-tm1f;
timeS = timeInt/2000;
axles = 286;
% axles = input('Enter distance do you want to use for velocity
% calculation (in centimeters): ');
Vms = axles/(100*timeS);  %% Vel in meters per second
Vmih = Vms*60*60/1609.34; %% Vel in miles per hour

VelTitle = sprintf('V = %.2f m/s ', Vms);

%% Put time into seconds
tS = t/2000;
```

```
%% Impulse calculation
% This filter works for always haveing 3 offsets 1 before the first
% event i.e tire/ ski / track, one between the first event and one
% after the last event
num_offsets=3;
%num_offsets= input('How many offsets are there on this plot? ');
for k=1:num_offsets
    Range1(k)=input('Enter beginning of range to calc Baseline: ' );
    Range2(k)=input('Enter end of range to calc Baseline: ' );
    Baseline(k)=mean(loadcellsumtrim(Range1(k):Range2(k)));

end
% Select Number of Loadcell ranges there are
for l=1:num_offsets
loadranges(l)= input('Enter end of the range to apply baseline
subtraction ' );
end

% This part might be able to be more general with a loop so we don't
% always have to have 3 offsets, with the time I have I couldn't find a
% way to put this in a loop that makes sense...
Part1=loadcellsumtrim(1:loadranges(1))-Baseline(1);
Part2=loadcellsumtrim(loadranges(1)+1:loadranges(2))-Baseline(2);
Part3=loadcellsumtrim(loadranges(2)+1:loadranges(3))-Baseline(3);

% With the baseline subtraction some values may becomes negative so we
% set them to zero
for h=1:length(Part1)
if Part1(h)<0
    Part1(h)=0;
else Part1(h)>0
    Part1(h)=Part1(h);
end
end
for h=1:length(Part2)
if Part2(h)<0
    Part2(h)=0;
else Part2(h)>0
    Part2(h)=Part2(h);
end
end
for h=1:length(Part3)
if Part3(h)<0
    Part3(h)=0;
else Part3(h)>0
    Part3(h)=Part3(h);
end
end

% Concatenate vectors to make one large vector again, this will be the
% final vector we calculate Impulse with.
loadcellsumtrimCAT=[Part1(:); Part2(:); Part3(:)];
```

```
%Calculate impulse element wise
for i=1:length(loadcellsumtrimCAT)-1

Impulse(i)=((loadcellsumtrimCAT(i)+loadcellsumtrimCAT(i+1))/2)*(1/2000)
;
end

%Sum all elements of Impulse to get a total impulse from the passby.
ImpulseFinal=sum(Impulse);

plot(Impulse)

%% Select the Impulse file where you are storing the data
% info.
currentFile = uigetfile('*.xlsx', 'Select file to process:');
currentFileName = currentFile(1:end-5);

% Get the existing names of sheets in the Excel workbook.
[status,sheets] = xlsfinfo(currentFile);
sheets = [sheets 'Other'];

% Ask the user which Sheet to put the data on. If the vehicle is not
% listed yet, allow the user to select "Other". Then ask for the user
% to provide an appropriate name for the vehicle so that we can make a
% new sheet for it in the Excel file.
[sel,okay] = listdlg('PromptString', 'Select the Vehicle',...
    'SelectionMode','single','ListString',sheets);
if sel == length(sheets)
    vPrompt = 'Please enter the vehicle type (Mattracks, Tires, or
Bomb): ';
    Vsheet = input(vPrompt, 's');
else
    Vsheet = sheets(sel);
end

% If you will be adding to an existing sheet, read the data from that
% sheet in so you know where the blank rows start.
if sel < length(sheets)
    [num,txt,raw] = xlsread(currentFile, char(Vsheet));
    SSrows = size(txt,1)+1;
    SSaddRow = SSrows(1)+2;
    StartCell = sprintf('A%d',SSaddRow);
    StartDataCell = sprintf('B%d',SSaddRow);okay
    StartDataCellNums = sprintf('B%d',SSaddRow+5);
else
    StartCell = 'A1';
    StartDataCell = 'B1';
    StartDataCellNums = 'B6';
end

% Find where the blank rows start and define 2 rows down as your start
% point.

%% Test vals (won't be needed when plugged into bigger file)
```

```
%Vehic = 'Snowbuster 65';
%ConversionFile = 'Snowbuster12';
%Vms = 100;
%Vmih = 5;
StressTimes = (firstMaxbegin+tmax)/2000;
%Stress = [100, 200, 300, 400, 500];

% Make Column and Row Titles
Tc = {'Vehicle';'File';'Date';'Velocity (m/s)';'Velocity (mph)'...
     ;'Impulse (Ns)'};

% Make partial column for file ID values
Mdc = {Vehic; ConversionFile; Dt; Vms; Vmih;ImpulseFinal};
%MdcVs = [StressTimes; Mmax];

xlswrite(currentFile, Tc, char(Vsheet), StartCell);
xlswrite(currentFile, Mdc, char(Vsheet), StartDataCell);
%xlswrite(currentFile, MdcVs, char(Vsheet), StartDataCellNums)
```

APPENDIX D

LOAD CELL DATA SHEETS

The following images show the data sheets for all load cells used. Numbers written on the top right of the pages indicate the load cell number as arranged on the load cell array. The label “1” appears on two data sheets because damage to during Year 1 necessitated replacement of Load Cell 1 between Year 1 and Year 2.

OMEGA ENGINEERING INC.

LOAD CELL
FINAL CALIBRATION

0.00 - 500.00 LBS
Excitation 10.000 Vdc

Job: WHM5315
Model: LC304-500
Date: 12/8/2015
Calibrated: 0.00 - 500.00 LBS

Serial: 337710
Tested By: ED
Temperature Range: +60 to +160 F
Specfile: LC304

Force LBS	Unit Data mVdc	Normalized Data
0.00	- 0.015	0.000
250.00	10.488	10.503
500.00	21.062	21.077
250.00	10.500	10.515
0.00	- 0.017	- 0.002

Balance	- 0.015	mVdc
Sensitivity	21.077	mVdc
In Resist	379.30	Ohms
Out Resist	352.80	Ohms
59K Shunt	14.875	mVdc

Change at 0.00 LBS (-INPUT to -OUTPUT)

Calibration Factors:
Sensitivity = 2.108 mV/V 59K Shunt = 1.488 mV/V

ELECTRICAL LEAKAGE: PASS
ELECTRICAL WIRING/CONNECTOR: RED = +INPUT (EXC)
BLACK = -INPUT (EXC)
GREEN = +OUTPUT
WHITE = -OUTPUT

This Calibration was performed using Instruments and Standards that are traceable to the United States National Institute of Standards Technology.

S/N	Description	Range	Reference	Cal Cert
	10001b Reference STD	0 - 500.00 LBS	C-2692	C-2692
3146A40859	HP34401A DMM UUT	Unit Under Test	C-2412	C-2412

Q.A. Representative : Ed Suchman Jr

Date: 12/8/2015

This transducer is tested to & meets published specifications. After final calibration our products are stored in a controlled stock room & considered in bonded storage. Depending on environment & severity of use factory calibration is recommended every one to three years after initial service installation date.
COMMENTS: FINAL TEST.

Omega Engineering Inc., One Omega Drive, Stamford, CT 06907
http://www.omega.com email: info@omega.com phone (800) 826-6342

O M E G A E N G I N E E R I N G I N C.

LOAD CELL
FINAL CALIBRATION

0.00 - 500.00 LBS
Excitation 10.000 Vdc

New

Job: WHM6152 Serial: 347529
Model: LC304-500 Tested By: ED
Date: 1/21/2016 Temperature Range: +60 to +160 F
Calibrated: 0.00 - 500.00 LBS Specfile: LC304

Force LBS	Unit Data mVdc	Normalized Data
0.00	- 0.126	0.000
250.00	10.315	10.441
500.00	20.736	20.862
250.00	10.323	10.449
0.00	- 0.129	- 0.003

Balance	- 0.126	mVdc
Sensitivity	20.862	mVdc
In Resist	377.60	Ohms
Out Resist	352.30	Ohms
59K Shunt	14.849	mVdc

Change at 0.00 LBS (-INPUT to -OUTPUT)

Calibration Factors:
Sensitivity = 2.086 mV/V 59K Shunt = 1.485 mV/V

ELECTRICAL LEAKAGE: PASS
ELECTRICAL WIRING/CONNECTOR: RED = +INPUT (EXC)
BLACK = -INPUT (EXC)
GREEN = +OUTPUT
WHITE = -OUTPUT

This Calibration was performed using Instruments and Standards that are traceable to the United States National Institute of Standards Technology.

S/N	Description	Range	Reference	Cal Cert
	10001b Reference STD	0 - 500.00 LBS	C-2692	C-2692
3146A40859	HP34401A DMM UUT	Unit Under Test	C-2412	C-2412

Q.A. Representative : Ed Suchman Jr Date: 1/21/2016

This transducer is tested to & meets published specifications. After final calibration our products are stored in a controlled stock room & considered in bonded storage. Depending on environment & severity of use factory calibration is recommended every one to three years after initial service installation date.
COMMENTS: FINAL TEST.

Omega Engineering Inc., One Omega Drive, Stamford, CT 06907
http://www.omega.com email: info@omega.com phone (800) 826-6342

O M E G A E N G I N E E R I N G I N C.

LOAD CELL
FINAL CALIBRATION

2

0.00 - 500.00 LBS
Excitation 10.000 Vdc

Job: WHM5315
Model: LC304-500
Date: 12/8/2015
Calibrated: 0.00 - 500.00 LBS

Serial: 342051
Tested By: ED
Temperature Range: +60 to +160 F
Specfile: LC304

Force LBS	Unit Data mVdc	Normalized Data
0.00	- 0.141	0.000
250.00	10.149	10.290
500.00	20.554	20.695
250.00	10.170	10.311
0.00	- 0.142	- 0.001

Balance	- 0.141	mVdc
Sensitivity	20.695	mVdc
In Resist	377.40	Ohms
Out Resist	352.20	Ohms
59K Shunt	14.877	mVdc

Change at 0.00 LBS (-INPUT to -OUTPUT)

Calibration Factors:
Sensitivity = 2.070 mV/V 59K Shunt = 1.488 mV/V

ELECTRICAL LEAKAGE: PASS
ELECTRICAL WIRING/CONNECTOR: RED = +INPUT (EXC)
BLACK = -INPUT (EXC)
GREEN = +OUTPUT
WHITE = -OUTPUT

This Calibration was performed using Instruments and Standards that are traceable to the United States National Institute of Standards Technology.

S/N	Description	Range	Reference	Cal Cert
	10001b Reference STD	0 - 500.00 LBS	C-2692	C-2692
3146A40859	HP34401A DMM UUT	Unit Under Test	C-2412	C-2412

Q.A. Representative : Ed Suchman Jr Date: 12/8/2015

This transducer is tested to & meets published specifications. After final calibration our products are stored in a controlled stock room & considered in bonded storage. Depending on environment & severity of use factory calibration is recommended every one to three years after initial service installation date.
COMMENTS: FINAL TEST.

Omega Engineering Inc., One Omega Drive, Stamford, CT 06907
http://www.omega.com email: info@omega.com phone (800) 826-6342

O M E G A E N G I N E E R I N G I N C.

3

LOAD CELL
FINAL CALIBRATION

0.00 - 500.00 LBS
Excitation 10.000 Vdc

Job: WHM5315
Model: LC304-500
Date: 12/8/2015
Calibrated: 0.00 - 500.00 LBS

Serial: 342028
Tested By: ED
Temperature Range: +60 to +160 F
Specfile: LC304

Force LBS	Unit Data mVdc	Normalized Data
0.00	- 0.087	0.000
250.00	11.193	11.280
500.00	22.506	22.593
250.00	11.208	11.295
0.00	- 0.090	- 0.003

Balance	- 0.087	mVdc
Sensitivity	22.593	mVdc
In Resist	376.70	Ohms
Out Resist	352.10	Ohms
59K Shunt	14.862	mVdc

Change at 0.00 LBS (-INPUT to -OUTPUT)

Calibration Factors:
Sensitivity = 2.259 mV/V 59K Shunt = 1.486 mV/V

ELECTRICAL LEAKAGE: PASS
ELECTRICAL WIRING/CONNECTOR: RED = +INPUT (EXC)
BLACK = -INPUT (EXC)
GREEN = +OUTPUT
WHITE = -OUTPUT

This Calibration was performed using Instruments and Standards that are traceable to the United States National Institute of Standards Technology.

S/N	Description	Range	Reference	Cal Cert
	10001b Reference STD	0 - 500.00 LBS	C-2692	C-2692
3146A40859	HP34401A DMM UUT	Unit Under Test	C-2412	C-2412

Q.A. Representative : Ed Suchman Jr Date: 12/8/2015

This transducer is tested to & meets published specifications. After final calibration our products are stored in a controlled stock room & considered in bonded storage. Depending on environment & severity of use factory calibration is recommended every one to three years after initial service installation date.
COMMENTS: FINAL TEST.

Omega Engineering Inc., One Omega Drive, Stamford, CT 06907
http://www.omega.com email: info@omega.com phone (800) 826-6342

4

O M E G A E N G I N E E R I N G I N C.

LOAD CELL
FINAL CALIBRATION

0.00 - 500.00 LBS
Excitation 10.000 Vdc

Job: WHM5315
Model: LC304-500
Date: 12/8/2015
Calibrated: 0.00 - 500.00 LBS

Serial: 342020
Tested By: ED
Temperature Range: +60 to +160 F
Specfile: LC304

Force LBS	Unit Data mVdc	Normalized Data
0.00	0.050	0.000
250.00	9.419	9.369
500.00	18.891	18.841
250.00	9.447	9.397
0.00	0.052	0.002

Balance	0.050	mVdc
Sensitivity	18.841	mVdc
In Resist	378.70	Ohms
Out Resist	353.10	Ohms
59K Shunt	14.952	mVdc

Change at 0.00 LBS (-INPUT to -OUTPUT)

Calibration Factors:
Sensitivity = 1.884 mV/V 59K Shunt = 1.495 mV/V

ELECTRICAL LEAKAGE: PASS
ELECTRICAL WIRING/CONNECTOR: RED = +INPUT (EXC)
BLACK = -INPUT (EXC)
GREEN = +OUTPUT
WHITE = -OUTPUT

This Calibration was performed using Instruments and Standards that are traceable to the United States National Institute of Standards Technology.

S/N	Description	Range	Reference	Cal Cert
	1000lb Reference STD	0 - 500.00 LBS	C-2692	C-2692
3146A40859	HP34401A DMM UUT	Unit Under Test	C-2412	C-2412

Q.A. Representative : Ed Suchman Jr. Date: 12/8/2015

This transducer is tested to & meets published specifications. After final calibration our products are stored in a controlled stock room & considered in bonded storage. Depending on environment & severity of use factory calibration is recommended every one to three years after initial service installation date.
COMMENTS: FINAL TEST.

Omega Engineering Inc., One Omega Drive, Stamford, CT 06907
http://www.omega.com email: info@omega.com phone (800) 826-6342

O M E G A E N G I N E E R I N G I N C.

5

LOAD CELL
FINAL CALIBRATION

0.00 - 500.00 LBS
Excitation 10.000 Vdc

Job: WHM5315
Model: LC304-500
Date: 12/8/2015
Calibrated: 0.00 - 500.00 LBS

Serial: 342050
Tested By: ED
Temperature Range: +60 to +160 F
Specfile: LC304

Force LBS	Unit Data mVdc	Normalized Data
0.00	0.053	0.000
250.00	10.562	10.509
500.00	21.154	21.101
250.00	10.567	10.514
0.00	0.048	- 0.005

Balance	0.053	mVdc
Sensitivity	21.101	mVdc
In Resist	378.90	Ohms
Out Resist	352.60	Ohms
59K Shunt	14.887	mVdc

Change at 0.00 LBS (-INPUT to -OUTPUT)

Calibration Factors:
Sensitivity = 2.110 mV/V 59K Shunt = 1.489 mV/V

ELECTRICAL LEAKAGE: PASS
ELECTRICAL WIRING/CONNECTOR: RED = +INPUT (EXC)
BLACK = -INPUT (EXC)
GREEN = +OUTPUT
WHITE = -OUTPUT

This Calibration was performed using Instruments and Standards that are traceable to the United States National Institute of Standards Technology.

S/N	Description	Range	Reference	Cal Cert
	10001b Reference STD	0 - 500.00 LBS	C-2692	C-2692
3146A40859	HP34401A DMM UUT	Unit Under Test	C-2412	C-2412

Q.A. Representative : Ed Suchman Jr Date: 12/8/2015

This transducer is tested to & meets published specifications. After final calibration our products are stored in a controlled stock room & considered in bonded storage. Depending on environment & severity of use factory calibration is recommended every one to three years after initial service installation date.
COMMENTS: FINAL TEST.

Omega Engineering Inc., One Omega Drive, Stamford, CT 06907
http://www.omega.com email: info@omega.com phone (800) 826-6342

O M E G A E N G I N E E R I N G I N C.

6

LOAD CELL
FINAL CALIBRATION

0.00 - 500.00 LBS
Excitation 10.000 Vdc

Job: WHM5315
Model: LC304-500
Date: 12/8/2015
Calibrated: 0.00 - 500.00 LBS

Serial: 342030
Tested By: ED
Temperature Range: +60 to +160 F
Specfile: LC304

Force LBS	Unit Data mVdc	Normalized Data
0.00	0.286	0.000
250.00	11.002	10.716
500.00	21.784	21.498
250.00	11.015	10.729
0.00	0.284	- 0.002

Balance	0.286	mVdc
Sensitivity	21.498	mVdc
In Resist	377.50	Ohms
Out Resist	353.00	Ohms
59K Shunt	15.004	mVdc

Change at 0.00 LBS (-INPUT to -OUTPUT)

Calibration Factors:
Sensitivity = 2.150 mV/V 59K Shunt = 1.500 mV/V

ELECTRICAL LEAKAGE: PASS
ELECTRICAL WIRING/CONNECTOR: RED = +INPUT (EXC)
BLACK = -INPUT (EXC)
GREEN = +OUTPUT
WHITE = -OUTPUT

This Calibration was performed using Instruments and Standards that are traceable to the United States National Institute of Standards Technology.

S/N	Description	Range	Reference	Cal Cert
	10001b Reference STD	0 - 500.00 LBS	C-2692	C-2692
3146A40859	HP34401A DMM UUT	Unit Under Test	C-2412	C-2412

Q.A. Representative : Ed Suchman Jr Date: 12/8/2015

This transducer is tested to & meets published specifications. After final calibration our products are stored in a controlled stock room & considered in bonded storage. Depending on environment & severity of use factory calibration is recommended every one to three years after initial service installation date.
COMMENTS: FINAL TEST.

Omega Engineering Inc., One Omega Drive, Stamford, CT 06907
http://www.omega.com email: info@omega.com phone (800) 826-6342

7

O M E G A E N G I N E E R I N G I N C.

LOAD CELL
FINAL CALIBRATION

0.00 - 500.00 LBS
Excitation 10.000 Vdc

Job: WHM5585 Serial: 342026
Model: LC304-500 Tested By: ED
Date: 12/8/2015 Temperature Range: +60 to +160 F
Calibrated: 0.00 - 500.00 LBS Specfile: LC304

Force LBS	Unit Data mVdc	Normalized Data
0.00	- 0.018	0.000
250.00	9.783	9.801
500.00	19.661	19.679
250.00	9.791	9.809
0.00	- 0.017	0.001

Balance	- 0.018	mVdc	
Sensitivity	19.679	mVdc	
In Resist	377.70	Ohms	
Out Resist	352.00	Ohms	
59K Shunt	14.857	mVdc	Change at 0.00 LBS (-INPUT to -OUTPUT)

Calibration Factors:
Sensitivity = 1.968 mV/V 59K Shunt = 1.486 mV/V

ELECTRICAL LEAKAGE: PASS
ELECTRICAL WIRING/CONNECTOR: RED = +INPUT (EXC)
BLACK = -INPUT (EXC)
GREEN = +OUTPUT
WHITE = -OUTPUT

This Calibration was performed using Instruments and Standards that are traceable to the United States National Institute of Standards Technology.

S/N	Description	Range	Reference	Cal Cert
	10001b Reference STD	0 - 500.00 LBS	C-2692	C-2692
3146A40859	HP34401A DMM UUT	Unit Under Test	C-2412	C-2412

Q.A. Representative : Ed Suchman Jr Date: 12/8/2015

This transducer is tested to & meets published specifications. After final calibration our products are stored in a controlled stock room & considered in bonded storage. Depending on environment & severity of use factory calibration is recommended every one to three years after initial service installation date.
COMMENTS: FINAL TEST.

Omega Engineering Inc., One Omega Drive, Stamford, CT 06907
http://www.omega.com email: info@omega.com phone (800) 826-6342

OMEGA ENGINEERING INC.

LOAD CELL
FINAL CALIBRATION

0.00 - 500.00 LBS
Excitation 10.000 Vdc

Job: WHM5315
Model: LC304-500
Date: 12/8/2015
Calibrated: 0.00 - 500.00 LBS

Serial: 342046
Tested By: ED
Temperature Range: +60 to +160 F
Specfile: LC304

Force LBS	Unit Data mVdc	Normalized Data
0.00	0.146	0.000
250.00	10.521	10.375
500.00	20.996	20.850
250.00	10.542	10.396
0.00	0.147	0.001

Balance	0.146	mVdc
Sensitivity	20.850	mVdc
In Resist	377.40	Ohms
Out Resist	352.80	Ohms
59K Shunt	14.933	mVdc

Change at 0.00 LBS (-INPUT to -OUTPUT)

Calibration Factors:
Sensitivity = 2.085 mV/V 59K Shunt = 1.493 mV/V

ELECTRICAL LEAKAGE: PASS
ELECTRICAL WIRING/CONNECTOR: RED = +INPUT (EXC)
BLACK = -INPUT (EXC)
GREEN = +OUTPUT
WHITE = -OUTPUT

This Calibration was performed using Instruments and Standards that are traceable to the United States National Institute of Standards Technology.

S/N	Description	Range	Reference	Cal Cert
	10001b Reference STD	0 - 500.00 LBS	C-2692	C-2692
3146A40859	HP34401A DMM UUT	Unit Under Test	C-2412	C-2412

Q.A. Representative : Ed Suchman Jr Date: 12/8/2015

This transducer is tested to & meets published specifications. After final calibration our products are stored in a controlled stock room & considered in bonded storage. Depending on environment & severity of use factory calibration is recommended every one to three years after initial service installation date.
COMMENTS: FINAL TEST.

Omega Engineering Inc., One Omega Drive, Stamford, CT 06907
http://www.omega.com email: info@omega.com phone (800) 826-6342

9

O M E G A E N G I N E E R I N G I N C.

LOAD CELL
FINAL CALIBRATION

0.00 - 500.00 LBS
Excitation 10.000 Vdc

Job: WHM5315
Model: LC304-500
Date: 12/8/2015
Calibrated: 0.00 - 500.00 LBS

Serial: 334700
Tested By: ED
Temperature Range: +60 to +160 F
Specfile: LC304

Force LBS	Unit Data mVdc	Normalized Data
0.00	0.098	0.000
250.00	9.222	9.124
500.00	18.398	18.300
250.00	9.225	9.127
0.00	0.101	0.003

Balance	0.098	mVdc
Sensitivity	18.300	mVdc
In Resist	378.10	Ohms
Out Resist	352.50	Ohms
59K Shunt	14.911	mVdc

Change at 0.00 LBS (-INPUT to -OUTPUT)

Calibration Factors:
Sensitivity = 1.830 mV/V 59K Shunt = 1.491 mV/V

ELECTRICAL LEAKAGE: PASS
ELECTRICAL WIRING/CONNECTOR: RED = +INPUT (EXC)
BLACK = -INPUT (EXC)
GREEN = +OUTPUT
WHITE = -OUTPUT

This Calibration was performed using Instruments and Standards that are traceable to the United States National Institute of Standards Technology.

S/N	Description	Range	Reference	Cal Cert
	10001b Reference STD	0 - 500.00 LBS	C-2692	C-2692
3146A40859	HP34401A DMM UUT	Unit Under Test	C-2412	C-2412

Q.A. Representative : Ed Suchman Jr Date: 12/8/2015

This transducer is tested to & meets published specifications. After final calibration our products are stored in a controlled stock room & considered in bonded storage. Depending on environment & severity of use factory calibration is recommended every one to three years after initial service installation date.
COMMENTS: FINAL TEST.

Omega Engineering Inc., One Omega Drive, Stamford, CT 06907
http://www.omega.com email: info@omega.com phone (800) 826-6342

O M E G A E N G I N E E R I N G I N C.

10

LOAD CELL
FINAL CALIBRATION

0.00 - 500.00 LBS
Excitation 10.000 Vdc

Job: WHM5315 Serial: 342042
Model: LC304-500 Tested By: ED
Date: 12/8/2015 Temperature Range: +60 to +160 F
Calibrated: 0.00 - 500.00 LBS Specfile: LC304

Force LBS	Unit Data mVdc	Normalized Data
0.00	0.045	0.000
250.00	10.826	10.781
500.00	21.654	21.609
250.00	10.823	10.778
0.00	0.050	0.005

Balance	0.045	mVdc	
Sensitivity	21.609	mVdc	
In Resist	377.80	Ohms	
Out Resist	353.10	Ohms	
59K Shunt	14.868	mVdc	Change at 0.00 LBS (-INPUT to -OUTPUT)

Calibration Factors:
Sensitivity = 2.161 mV/V 59K Shunt - 1.487 mV/V

ELECTRICAL LEAKAGE: PASS
ELECTRICAL WIRING/CONNECTOR: RED = +INPUT (EXC)
BLACK = -INPUT (EXC)
GREEN = +OUTPUT
WHITE = -OUTPUT

This Calibration was performed using Instruments and Standards that are traceable to the United States National Institute of Standards Technology.

S/N	Description	Range	Reference	Cal Cert
	1000lb Reference STD	0 - 500.00 LBS	C-2692	C-2692
3146A40859	HP34401A DMM UUT	Unit Under Test	C-2412	C-2412

Q.A. Representative : Ed Eschman Jr Date: 12/8/2015

This transducer is tested to & meets published specifications. After final calibration our products are stored in a controlled stock room & considered in bonded storage. Depending on environment & severity of use factory calibration is recommended every one to three years after initial service installation date.
COMMENTS: FINAL TEST.

Omega Engineering Inc., One Omega Drive, Stamford, CT 06907
http://www.omega.com email: info@omega.com phone (800) 826-6342

OMEGA ENGINEERING INC.

11

LOAD CELL
FINAL CALIBRATION

0.00 - 500.00 LBS
Excitation 10.000 Vdc

Job: WHM4986 Serial: 342049
Model: LC304-500 Tested By: WF
Date: 11/17/2015 Temperature Range: +60 to +160 F
Calibrated: 0.00 - 500.00 LBS Specfile: LC304

Force LBS	Unit Data mVdc	Normalized Data
0.00	- 0.082	0.000
250.00	10.150	10.232
500.00	20.467	20.549
250.00	10.175	10.257
0.00	- 0.081	0.001

Balance	- 0.082	mVdc	
Sensitivity	20.549	mVdc	
In Resist	377.80	Ohms	
Out Resist	352.00	Ohms	
59K Shunt	14.849	mVdc	Change at 0.00 LBS (-INPUT to -OUTPUT)

Calibration Factors:
Sensitivity = 2.055 mV/V 59K Shunt = 1.485 mV/V

ELECTRICAL LEAKAGE: PASS
ELECTRICAL WIRING/CONNECTOR: RED = +INPUT (EXC)
BLACK = -INPUT (EXC)
GREEN = +OUTPUT
WHITE = -OUTPUT

This Calibration was performed using Instruments and Standards that are traceable to the United States National Institute of Standards Technology.

S/N	Description	Range	Reference	Cal Cert
	10001b Reference STD	0 - 500.00 LBS	C-2692	C-2692
3146A40859	HP34401A DMM UUT	Unit Under Test	C-2412	C-2412

Q.A. Representative : William Fleeter Date: 11/17/2015

This transducer is tested to & meets published specifications. After final calibration our products are stored in a controlled stock room & considered in bonded storage. Depending on environment & severity of use factory calibration is recommended every one to three years after initial service installation date.
COMMENTS: FINAL TEST.

Omega Engineering Inc., One Omega Drive, Stamford, CT 06907
http://www.omega.com email: info@omega.com phone (800) 826-6342

O M E G A E N G I N E E R I N G I N C.

12

LOAD CELL
FINAL CALIBRATION

0.00 - 500.00 LBS
Excitation 10.000 Vdc

Job: WHM5315 Serial: 342019
Model: LC304-500 Tested By: ED
Date: 12/8/2015 Temperature Range: +60 to +160 F
Calibrated: 0.00 - 500.00 LBS Specfile: LC304

Force LBS	Unit Data mVdc	Normalized Data
0.00	- 0.007	0.000
250.00	10.317	10.324
500.00	20.682	20.689
250.00	10.310	10.317
0.00	- 0.014	- 0.007

Balance	- 0.007	mVdc	
Sensitivity	20.689	mVdc	
In Resist	378.10	Ohms	
Out Resist	352.70	Ohms	
59K Shunt	14.827	mVdc	Change at 0.00 LBS (-INPUT to -OUTPUT)

Calibration Factors:
Sensitivity = 2.069 mV/V 59K Shunt - 1.483 mV/V

ELECTRICAL LEAKAGE: PASS
ELECTRICAL WIRING/CONNECTOR: RED = +INPUT (EXC)
BLACK = -INPUT (EXC)
GREEN = +OUTPUT
WHITE = -OUTPUT

This Calibration was performed using Instruments and Standards that are traceable to the United States National Institute of Standards Technology.

S/N	Description	Range	Reference	Cal Cert
	10001b Reference STD	0 - 500.00 LBS	C-2692	C-2692
3146A40859	HP34401A DMM UUT	Unit Under Test	C-2412	C-2412

Q.A. Representative : Ed Eschman Jr Date: 12/8/2015

This transducer is tested to & meets published specifications. After final calibration our products are stored in a controlled stock room & considered in bonded storage. Depending on environment & severity of use factory calibration is recommended every one to three years after initial service installation date.
COMMENTS: FINAL TEST.

Omega Engineering Inc., One Omega Drive, Stamford, CT 06907
http://www.omega.com email: info@omega.com phone (800) 826-6342

APPENDIX E

ARAMIS

Throughout the first field-testing season, a variety of LED light configurations were tried in an attempt to minimize glare while maximizing light on the Plexiglas. Researchers started with “puck” type lights that could be tilted in different directions, but determined that more light was needed. LED light strips that could be turned on and off with a remote control were then added, reducing the amount of time that lights in the box were on and therefore reducing battery needs. However, these still created a slight glare that caused analysis problems in Aramis. Finally, an additional LED tube light setup was added. Experimentation with lighting setups continued into Year 2, when an LED spotlight was added.

To create visual points that Aramis could track, paint was sprayed onto the wall with spray bottles. Occasionally due to spray bottles freezing, the paint was flicked from the spray tube end onto the snow wall. Toward the end of the study, a stiff-bristled brush was dipped in paint, then its bristles flicked toward the wall to create a speckled pattern. Once paint was applied to the snow wall, it typically froze quickly so Plexiglas could be placed against it without smearing the paint.

During the last trip for pass-by testing, temperatures in the park were warmer and snow in the top several centimeters of the road had liquid in it. This meant that the paint mixed with the melted water and turned the top centimeters of snow into a uniform grey color rather than retaining the black speckles. This rendered subsurface videos taken in these conditions unusable since Aramis could not pick out points in the grey area.

Processing the images using Aramis was accomplished back at Montana State University. This involved importing all of the images from a certain pass into Aramis, having Aramis calculate a start point which it could track during the entire series, having Aramis calculate and analyze all strain, and then viewing different types of strain that Aramis calculated. For most of the videos processed, researchers planned to look at vertical (Y) strain, horizontal (X) strain, and shear angle. For some videos that Aramis was not reading properly, brightness and/or contrast were adjusted on the images.

APPENDIX F

ACCELEROMETER PROCESSING

Many researchers both within the field of engineering and in other fields make use of accelerometers. Common applications include measurements of seismic activity for use by structural engineers and, more recently, measurements of physical activity for use by laypeople in activity-trackers such as FitBits and by researchers conglomerating and analyzing this data.

Accelerometers yield data on acceleration, typically expressed in gs. Integration of acceleration readings gives velocity, and a second integration gives displacement. However, this procedure results in velocity and displacement numbers that contain an implausible drifting throughout the duration of the measurement (Yang and others, 2006). There are several identified reasons contributing to this drift (Yang and others, 2006), and researchers have worked to better understand these factors (Moschas and others, 2015). In 2008, Stiros published a study on the propagation of error in these integrations. Yang and others (2006) provides an overview of these methods, and proposes a data correction procedure involving a correction curve (using a least-squares method to find the equation for the curve) and a windowed filter that corrects for long-period oscillations. Researchers often use this type of progression (least squares and then filtering) to remove noise from their data (Zhang and others, 2016), but there does not appear to be one predominant procedure for removing noise. For the current research, the method proposed by Yang et. al seems to be appropriate and effective. The method of data filtering used in this project follows the steps proposed in Yang and others (2006), except that no Fourier Transform was applied in this processing.

Data from accelerometers was collected using a cDAQ and LabView, and then processed using MATLAB. LabView created data files with in the form of large tables, with each column listing readings for one accelerometer. The accelerometer channel is listed on the top of the column and identifies which accelerometer's readings are listed. Prior to testing, voltage readings corresponding to baseline, 1-g (gravity) readings were obtained for each axis of each accelerometer. These voltages were then used to find the gs/Volt conversion for each axis of each accelerometer.

For each day of testing, a "conversion" file was created in which the location (depth in the road; center or side of the track) of each accelerometer during testing was identified using the name of the channel on which the accelerometer was read. This file listed the conversion factors associated with each accel axis.

The MATLAB code written to process the accelerometer files imports the raw data from LabView and the conversion file for the particular testing day. MATLAB finds the correct conversion factor for each channel and associates that channel's data with the accelerometer's location during testing. The conversion factor is used to convert all raw voltage readings into gs. MATLAB then displays a graph of this so that the user may select approximately where the acceleration event begins and ends in the data. Points outside of this selected window are assumed to represent zero baseline. From this point; an average of these baseline values is determined for each accelerometer and subtracted out from the other readings for that particular accelerometer. This gives the minimally-processed accelerometer readings. A filter

is then applied to convert all accelerometer readings with an absolute value below 0.02 to zero. This is intended to cut down on noise seen in the accelerometer data.

The acceleration values are numerically integrated to give approximate velocity values. MATLAB then find points before the beginning and after the end of the acceleration event by looking for a certain number of zeros before and after the event. The readings between these beginning and end values then become the velocity values that need to be corrected for drift. The velocities prior to and after the event are calculated, and the slope of velocity drift based on the difference between these velocities and the time over which the event occurs is calculated. Then these slopes are subtracted out from the accelerometer readings within the event window, giving accelerometer readings that have been corrected for the common problem of drift. The MATLAB code then numerically integrates these corrected numbers once to find velocity and again to find displacement.

Corrected acceleration, velocity, and displacement data is all output into both excel sheets and graphs, and in this form data can be analyzed for insight into vehicle impacts.

The following pages show the MATLAB code used to process the accelerometer data. This code uses the raw data from LabView, combined with an Excel file that lists the position and orientation of each accelerometer on this particular test day, to find acceleration, velocity, and displacement values. The code asks for user input to trim the files. It outputs an Excel file containing all of the processed data values and jpg images showing graphs of all of these values versus time, organized by accelerometer positions.

```
%% File to go through accelerometer files and convert
% voltages to gs, then integrate for velocity and displacement.

clear
close all
clc

%% Select files to be used in processing (accel data, conversion file)
% and pull in raw data.

% Get file with conversion numbers specific to the accels, info on
% accel location/orientation for the particular test.
ConversionFile = uigetfile('*.xlsx','Select conversion file:');
B = readtable(ConversionFile);
C = table2struct(B);

% Select file to process.
currentFile = uigetfile('*.xlsx', 'Select file to process:');
currentFileName = currentFile(1:end-5);

% Get data from Excel worksheet (tab 2)
[num,txt,raw] = xlsread(currentFile, 'Measured Data');

%% Set up header information layout to be used in processed output.
% Make cell for channel names.
Nms = {};
% Make double for conversion values used.
ConvRates = [];
% Make cell for orientation of accels.
Orients = {};
% Make cell for depth of accels.
Depths = {};
% Make cell for position of accels.
Positions = {};
% Make double for row in graph matrix.
PlotRows = [];
% Make double for column in graph matrix.
PlotCols = [];
% Make cell for positive direction description
PosDirs = {};

%% Loop through all columns and make big array with the pertinent raw
data.

% Decide on Number of Columns Needed (get rid of NAs by making their
% conversion number equal to 0).
L = 0;
for i = 1:length(txt)
% Find the conversion factor for the channel specified in the column
% name.
    Conv = 0;
    for j = 1:length(C)
```

```
        if strcmp(C(j).Name, txt(i))
            Conv = C(j).Conversion;
        end
    end
    % Add a column for any rows with a non-zero conversion factor.
    if Conv ~= 0
        L = L+1;
    end
end

% Set up a matrix for all of the accel measurements converted to gs.
Gvals = [];

% Go through each column of raw data to find appropriate header
% information and, find acceleration data, and convert acceleration to
% gs.

for i = 1:length(txt)
    Conv = 0;
    % Find the correct header information for the channel, if not "NA".
    for j = 1:length(C)
        if strcmp(C(j).Name, txt(i))
            Nm = C(j).Name;
            Conv = C(j).Conversion;
            Orient = C(j).Orientation;
            Depth = C(j).Depth;
            Position = C(j).Position;
            PlotRow = C(j).PlotRow;
            PlotCol = C(j).PlotCol;
            PosDir = C(j).PosPoints;
        end
    end
    % Get the raw readings from the column and convert them to gs.
    if Conv ~= 0
        % Make vector of the column's raw values
        colvals = num(:,i);
        % Make a new vector of the column's converted values
        colvalsGs = colvals*Conv;
        % Add the header values for this column to the collected
        % values.
        Nms = [Nms {Nm}];
        ConvRates = [ConvRates Conv];
        Orients = [Orients {Orient}];
        Depths = [Depths {Depth}];
        Positions = [Positions {Position}];
        Gvals = [Gvals colvalsGs];
        PlotRows = [PlotRows PlotRow];
        PlotCols = [PlotCols PlotCol];
        PosDirs = [PosDirs {PosDir}];
        % Plot the current values
        scatter(1:length(colvalsGs),abs(colvalsGs))
        hold on

    end
```

```
end

hold off

% Ask user where to trim this file.
begPrompt = 'Please enter the beginning trim value (at least 1): ';
begin = input(begPrompt);

endPrompt = 'Please enter the ending trim value: ';
ending = input(endPrompt);

% Number of points in trimmed data
Trimmed = ending-begin+1;

% And make a vector of time values in seconds:
Tvals = zeros(Trimmed,1);
for i = 1:Trimmed
    Tvals(i) = i;
end
Tvals = Tvals/5000;

% Make a matrix for dT values (for t(j)-t(j-1))
dTs = zeros(length(Tvals),1);
for i = 2:length(dTs)
    dTs(i) = Tvals(i)-Tvals(i-1);
end

%% Subtract Baseline out from Acceleration

% Prep for the final values
GvalsInt = zeros(Trimmed,L);
GvalsFin = zeros(Trimmed,L);

% Another for loop through columns to subtract out the baseline accel
% readings
for i = 1:L

% Find average of points outside of trim area.
    preData = Gvals(1:begin,i);
    postData = Gvals(ending:length(Gvals),i);
    allnonData = [preData; postData];
    Baseline = mean(allnonData);

% Extract the values within the trim area
    GvalsDataRaw = Gvals(begin:ending,i);

% Subtract out the baseline as determined by the average
    GvalsData = GvalsDataRaw - Baseline;

% Add converted, normalized data into final matrix
    GvalsInt(1:length(GvalsInt),i) = GvalsData;
    for n = 1:length(GvalsData)
        if abs(GvalsInt(n,i)) <= 0.02
```

```
            GvalsInt(n,i) = 0;
        end
    end
end

%% Find Initial Velocity Values from Acceleration

% Find the average acceleration value between i and i-1, to use for
% numeric integration
SumGi = zeros(size(GvalsInt));
SumGi(2:size(SumGi,1), :) = GvalsInt(2:size(GvalsInt,1),:)...
    +GvalsInt(1:size(GvalsInt,1)-1,:);
AvgGi = SumGi/2;

% Multiply each row by 9.81 and the appropriate dt to get change in
% velocity (m/s) from the previous point
VvalsChgi = zeros(size(AvgGi));
for i = 1:size(VvalsChgi,1)
    %% There was a "*9.81*" between AvgGi(i,:) and dTs(i) but I am
     % taking
    %% it out experimentally (this change in vel will be G*s)
    VvalsChgi(i,:) = AvgGi(i,:)*dTs(i);
end

% Use the change in velocity numbers to get the velocity at each time
VvalsUncor = zeros(size(AvgGi));
for i = 2:size(VvalsUncor,1)
    VvalsUncor(i,:) = VvalsUncor(i-1,:)+VvalsChgi(i,:);
end


% Find section that will need velocity correction based on number zeros
% desired.
% How many zeros do you want to find to decide that it's the start of
% the real acceleration?
numzers = 200;
% Make a matrix to store the beginning and end filter numbers for each
% channel.
FixRg = zeros(2,L);
for i = 1:L

% Find the beginning and end of the section that will need correcting
% (last 0 before action and first 0 after action)
    for n = (numzers+1):length(GvalsInt)
        if (GvalsInt(n,i)~=0) && (isequal(GvalsInt(n-numzers:n-
1,i),zeros(numzers,1)))
            FixRg(1,i) = n-1;
            break
        end
    end

    if FixRg(1,i) == 0
        FixRg(1,i) = 1;
    end
```

```
    for n = (length(GvalsInt)-numzers-1):-1:1
        if (GvalsInt(n,i)~=0) &&
(isequal(GvalsInt(n+1:n+numzers,i),zeros(numzers,1)))
            FixRg(2,i) = n+1;
            break
        end
    end

    if FixRg(2,i) == 0
        FixRg(2,i) = length(GvalsInt);
    end

end

% Find the slope of drift of the velocity (in G*s/s), using the
% velocity at the
% beginning and end of the acceleration range, using the range found
% above.

VelChgInRg = zeros(1,L);
Slopes = zeros(1,L);
for i = 1:L
    VelChgInRg(1,i)=VvalsUncor(FixRg(2,i),i)-VvalsUncor(FixRg(1,i),i);
    Slopes(1,i)=VelChgInRg(1,i)/(Tvals(FixRg(2,i))-Tvals(FixRg(1,i)));
end

% Now subtract these slopes out from the accelerations in the relevant
% range to get the final accelerations.

for i = 1:L
   for n = 1:length(GvalsData)
       if n <= FixRg(1,i)
           GvalsFin(n,i) = GvalsInt(n,i);
       elseif n >= FixRg(2,i)
           GvalsFin(n,i) = GvalsInt(n,i);
       else
           GvalsFin(n,i) = GvalsInt(n,i)-Slopes(1,i);
       end
   end
end

%% Then Continue on to Graph Accel and Integrate

for i = 1:L

% Plot the current values on a big sheet with room for all accels
    Rws = max(PlotRows);
    Cls = max(PlotCols);
    Posit = (PlotRows(i)-1)*Cls+PlotCols(i);
    subplot(Rws,Cls,Posit)
    plot(Tvals, GvalsFin(:,i))
    axis([0 inf -0.1 0.1])
```

```
    xlabel('Time, seconds')
    ylabel('Acceleration, Gs')
    set(gca, 'Fontsize',7)
    PlotTitle1 = sprintf('%s; %s',currentFileName,char(Orients(i)));
    PlotTitle2 = sprintf('%s cm Depth, Track %s',char(Depths(i)),...
                 char(Positions(i)));
    FinalTitle = {PlotTitle1,PlotTitle2};
    title(FinalTitle)
    hold on
end

PlotName = sprintf('%sAccelPlots.jpg', currentFileName);
set(gcf, 'PaperUnits', 'Inches');
set(gcf, 'PaperPosition', [0 0 17 11]);
saveas(gcf, PlotName);
hold off

close(gcf)

% Write acceleration data to Excel
OutFile = sprintf('%sProc', currentFileName);
sheet = 'AccelSheet';

% Make a Legend Column and put into spreadsheet
Legend = [{'Channel'}; {'ConversionRate'}; {'Depth'};
{'Orientation'};...
    {'Position'}; {'PositivePoints'}];
xlRange = 'A1';
xlswrite(OutFile,Legend,sheet,xlRange);

% Compile all header info and put into spreadsheet
Header = [Nms; num2cell(ConvRates); Depths; Orients; Positions;
PosDirs];
xlRange = 'B1';
xlswrite(OutFile,Header,sheet,xlRange);

% Then finally the values
xlRange = 'B7';
xlswrite(OutFile,GvalsFin,sheet,xlRange);
%% VELOCITY
% Find the average acceleration value between i and i-1, to use for
% numeric integration
SumG = zeros(size(GvalsFin));
SumG(2:size(SumG,1), :) = GvalsFin(2:size(GvalsFin,1),:)...
    +GvalsFin(1:size(GvalsFin,1)-1,:);
AvgG = SumG/2;

% Multiply each row by 9.81 and the appropriate dt to get change in
% velocity (m/s) from the previous point
VvalsChg = zeros(size(AvgG));
for i = 1:size(VvalsChg,1)
    VvalsChg(i,:) = AvgG(i,:)*9.81*dTs(i);
end
```

```
% Use the change in velocity numbers to get the velocity at each time
VvalsFin = zeros(size(AvgG));
for i = 2:size(VvalsFin,1)
    VvalsFin(i,:) = VvalsFin(i-1,:)+VvalsChg(i,:);
end

% Another for loop through columns to plot them
for i = 1:size(VvalsFin,2)

% Plot the current values
    Rws = max(PlotRows);
    Cls = max(PlotCols);
    Posit = (PlotRows(i)-1)*Cls+PlotCols(i);
    subplot(Rws,Cls,Posit)
    plot(Tvals, VvalsFin(:,i))
    axis([0 inf -inf inf])
    xlabel('Time, seconds')
    ylabel('Velocity, m/s')
    set(gca, 'Fontsize',7)
    PlotTitle1 = sprintf('%s; %s',currentFileName,char(Orients(i)));
    PlotTitle2 = sprintf('%s cm Depth, Track %s',...
                 char(Depths(i)),char(Positions(i)));
    FinalTitle = {PlotTitle1,PlotTitle2};
    title(FinalTitle)
    hold on
end

PlotName = sprintf('%sVelPlots.jpg', currentFileName);
% PDF attempt: PdfName = sprintf('%sPlots.pdf', currentFileName);
set(gcf, 'PaperUnits', 'Inches');
set(gcf, 'PaperPosition', [0 0 17 11]);
saveas(gcf, PlotName);
% Pdf Attempt: print(PdfName,'-dpdf','-fillpage');
hold off

close(gcf)

% Write velocity data to Excel
sheet = 'VelSheet';

% Put legend column into spreadsheet
xlRange = 'A1';
xlswrite(OutFile,Legend,sheet,xlRange);

% Put header information into spreadsheet
xlRange = 'B1';
xlswrite(OutFile,Header,sheet,xlRange);

% Then finally the values
xlRange = 'B7';
xlswrite(OutFile,VvalsFin,sheet,xlRange);

%% DISPLACEMENT
```

```
% Make a matrix for avg velocity values between i and i-1, to use for
% numeric integration
SumV = zeros(size(VvalsFin));
SumV(2:size(SumV,1), :) = VvalsFin(2:size(VvalsFin,1),:)...
    +VvalsFin(1:size(VvalsFin,1)-1,:);
AvgV = SumV/2;

% Prep a matrix of values for the change in displ., then the final
displ.
DvalsChg = zeros(size(VvalsFin));

% Make a vector to hold the final displacement for each channel
Dends = [];

% Multiply each row by the appropriate dt to get change in displ, and
then
% 1000 to make the displacement unit millimeters
for i = 1:size(DvalsChg,1)
    DvalsChg(i,1:size(DvalsChg,2)) = AvgV(i,:)*dTs(i)*1000;
end

% Use the change in disp numbers to get the disp at each time
DvalsFin = zeros(size(AvgV));
for i = 2:size(DvalsFin,1)
    DvalsFin(i,:) = DvalsFin(i-1,:)+DvalsChg(i,:);
end

for i = 1:size(DvalsFin,2)
    Dend = DvalsFin(length(DvalsFin),i);
    Dends = [Dends Dend];
end

% Another for loop through columns
for i = 1:size(DvalsFin,2)

% Plot the current values
    Rws = max(PlotRows);
    Cls = max(PlotCols);
    Posit = (PlotRows(i)-1)*Cls+PlotCols(i);
    subplot(Rws,Cls,Posit)
    plot(Tvals, DvalsFin(:,i))
    axis([0 inf -inf inf])
    xlabel('Time, seconds')
    ylabel('Displacement, mm')
    set(gca, 'Fontsize',7)

    PlotTitle1 = sprintf('%s; %s',currentFileName,char(Orients(i)));
    PlotTitle2 = sprintf('%s cm Depth, Track %s',char(Depths(i)),...
                 char(Positions(i)));
    FinalTitle = {PlotTitle1,PlotTitle2};
    title(FinalTitle)
    hold on
```

```
end

PlotName = sprintf('%sDispPlots.jpg', currentFileName);
% PDF attempt: PdfName = sprintf('%sPlots.pdf', currentFileName);
set(gcf, 'PaperUnits', 'Inches');
set(gcf, 'PaperPosition', [0 0 17 11]);
saveas(gcf, PlotName);
% Pdf Attempt: print(PdfName,'-dpdf','-fillpage');
hold off

% Write displacement data to Excel
sheet = 'DispSheet';

% Put legend column into spreadsheet
xlRange = 'A1';
xlswrite(OutFile,Legend,sheet,xlRange);

% Put header information into spreadsheet
xlRange = 'B1';
xlswrite(OutFile,Header,sheet,xlRange);

% Then finally the values
xlRange = 'B7';
xlswrite(OutFile,DvalsFin,sheet,xlRange);

%% Summary Data

%%% Summarize Acceleration Data

% Max/min
Amax = max(GvalsFin);
Amin = min(GvalsFin);

% Switches from Pos to Neg
Aswitch = zeros(1,L);
for i = 1:L
    for n = 2:length(Tvals)
        if GvalsFin(n-1,i)<0 && GvalsFin(n,i)>=0
            Aswitch(1,i) = Aswitch(1,i)+1;
        elseif GvalsFin(n-1,i)>=0 && GvalsFin(n,i)<0
            Aswitch(1,i) = Aswitch(1,i)+1;
        end
    end
end

%%% Summarize Velocity Data

% Max/Min
Vmax = max(VvalsFin);
Vmin = min(VvalsFin);

% Switches from Pos to Neg
Vswitch = zeros(1,L);
```

```
for i = 1:L
    for n = 2:length(Tvals)
        if VvalsFin(n-1,i)<0 && VvalsFin(n,i)>=0
            Vswitch(1,i) = Vswitch(1,i)+1;
        elseif VvalsFin(n-1,i)>=0 && VvalsFin(n,i)<0
            Vswitch(1,i) = Vswitch(1,i)+1;
        end
    end
end

%%% Summarize Velocity Data

% Max/Min
Dmax = max(DvalsFin);
Dmin = min(DvalsFin);

% Switches from Pos to Neg
Dswitch = zeros(1,L);
for i = 1:L
    for n = 2:length(Tvals)
        if DvalsFin(n-1,i)<0 && DvalsFin(n,i)>=0
            Dswitch(1,i) = Dswitch(1,i)+1;
        elseif DvalsFin(n-1,i)>=0 && DvalsFin(n,i)<0
            Dswitch(1,i) = Dswitch(1,i)+1;
        end
    end
end


Legend2 = [{'AccelMax'}; {'AccelMin'}; {'AccelSwitch'}; {'VelMax'};...
    {'VelMin'}; {'VelSwitch'}; {'DispMax'}; {'DispMin'};
{'DispSwitch'};...
    {'DispFinal'}];

SummDat = [Amax; Amin; Aswitch; Vmax; Vmin; Vswitch; Dmax; Dmin;...
    Dswitch; Dends];

% Write displacement data to Excel
sheet = 'Sheet1';

% Put legend column into spreadsheet
xlRange = 'A1';
xlswrite(OutFile,Legend,sheet,xlRange);

% Put header information into spreadsheet
xlRange = 'B1';
xlswrite(OutFile,Header,sheet,xlRange);

% Then legend 2
xlRange = 'A7';
xlswrite(OutFile,Legend2,sheet,xlRange);

% Then finally the values
```

```
xlRange = 'B7';
xlswrite(OutFile,SummDat,sheet,xlRange);
```

APPENDIX G

ACCELEROMETER DATA SHEETS

The following data sheets are for the model of accelerometers used in this project, Analog Devices ADXL 327. These data sheets are not unique to the particular accelerometer, but are generic for the model.

Small, Low Power, 3-Axis ±2 *g* Accelerometer

ADXL327

FEATURES

3-axis sensing
Small, low profile package
  4 mm × 4 mm × 1.45 mm LFCSP
Low power: 350 µA typical
Single-supply operation: 1.8 V to 3.6 V
10,000 *g* shock survival
Excellent temperature stability
Bandwidth adjustment with a single capacitor per axis
RoHS/WEEE lead-free compliant

APPLICATIONS

Cost-sensitive, low power, motion- and tilt-sensing applications
  Mobile devices
  Gaming systems
  Disk drive protection
  Image stabilization
  Sports and health devices

GENERAL DESCRIPTION

The ADXL327 is a small, low power, complete 3-axis accelerometer with signal conditioned voltage outputs. The product measures acceleration with a minimum full-scale range of ±2 *g*. It can measure the static acceleration of gravity in tilt-sensing applications, as well as dynamic acceleration, resulting from motion, shock, or vibration.

The user selects the bandwidth of the accelerometer using the C_X, C_Y, and C_Z capacitors at the X_{OUT}, Y_{OUT}, and Z_{OUT} pins. Bandwidths can be selected to suit the application with a range of 0.5 Hz to 1600 Hz for X and Y axes and a range of 0.5 Hz to 550 Hz for the Z axis.

The ADXL327 is available in a small, low profile, 4 mm × 4 mm × 1.45 mm, 16-lead, plastic lead frame chip scale package (LFCSP_LQ).

FUNCTIONAL BLOCK DIAGRAM

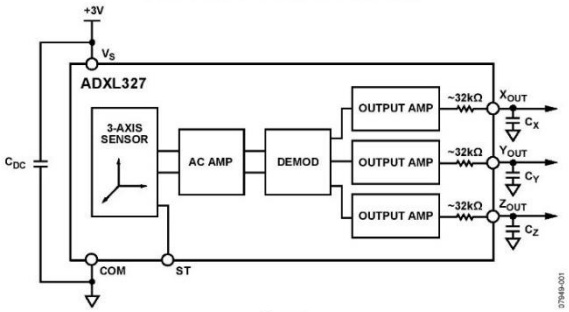

Figure 1.

Rev. 0
Information furnished by Analog Devices is believed to be accurate and reliable. However, no responsibility is assumed by Analog Devices for its use, nor for any infringements of patents or other rights of third parties that may result from its use. Specifications subject to change without notice. No license is granted by implication or otherwise under any patent or patent rights of Analog Devices. Trademarks and registered trademarks are the property of their respective owners.

One Technology Way, P.O. Box 9106, Norwood, MA 02062-9106, U.S.A.
Tel: 781.329.4700 www.analog.com
Fax: 781.461.3113 ©2009 Analog Devices, Inc. All rights reserved.

ADXL327* PRODUCT PAGE QUICK LINKS

Last Content Update: 02/23/2017

COMPARABLE PARTS

View a parametric search of comparable parts.

EVALUATION KITS

- ADXL327 Breakout Board

DOCUMENTATION

Application Notes

- AN-1057: Using an Accelerometer for Inclination Sensing
- AN-688: Phase and Frequency Response of iMEMS® Accelerometers and Gyros

Data Sheet

- ADXL327: Small, Low Power, 3-Axis ±2 *g* Accelerometer Data Sheet

DESIGN RESOURCES

- ADXL327 Material Declaration
- PCN-PDN Information
- Quality And Reliability
- Symbols and Footprints

DISCUSSIONS

View all ADXL327 EngineerZone Discussions.

SAMPLE AND BUY

Visit the product page to see pricing options.

TECHNICAL SUPPORT

Submit a technical question or find your regional support number.

DOCUMENT FEEDBACK

Submit feedback for this data sheet.

This page is dynamically generated by Analog Devices, Inc., and inserted into this data sheet. A dynamic change to the content on this page will not trigger a change to either the revision number or the content of the product data sheet. This dynamic page may be frequently modified.

TABLE OF CONTENTS

Features ... 1
Applications ... 1
General Description ... 1
Functional Block Diagram ... 1
Revision History ... 2
Specifications ... 3
Absolute Maximum Ratings ... 4
ESD Caution ... 4
Pin Configuration and Function Descriptions ... 5
Typical Performance Characteristics ... 6
Theory of Operation ... 10
Mechanical Sensor ... 10
Performance ... 10
Applications Information ... 11
Power Supply Decoupling ... 11
Setting the Bandwidth Using C_X, C_Y, and C_Z ... 11
Self Test ... 11
Design Trade-Offs for Selecting Filter Characteristics: The Noise/BW Trade-Off ... 11
Use with Operating Voltages Other Than 3 V ... 11
Axes of Acceleration Sensitivity ... 12
Layout and Design Recommendations ... 13
Outline Dimensions ... 14
Ordering Guide ... 14

REVISION HISTORY

8/09—Revision 0: Initial Version

SPECIFICATIONS

T_A = 25°C, V_S = 3 V, C_X = C_Y = C_Z = 0.1 µF, acceleration = 0 *g*, unless otherwise noted. All minimum and maximum specifications are guaranteed. Typical specifications are not guaranteed.

Table 1.

Parameter	Conditions	Min	Typ	Max	Unit
SENSOR INPUT	Each axis				
Measurement Range		±2	±2.5		*g*
Nonlinearity	Percent of full scale		±0.2		%
Package Alignment Error			±1		Degrees
Interaxis Alignment Error			±0.1		Degrees
Cross Axis Sensitivity[1]			±1		%
SENSITIVITY (RATIOMETRIC)[2]	Each axis				
Sensitivity at X_{OUT}, Y_{OUT}, Z_{OUT}	V_S = 3 V	378	420	462	mV/*g*
Sensitivity Change Due to Temperature[3]	V_S = 3 V		±0.01		%/°C
ZERO *g* BIAS LEVEL (RATIOMETRIC)					
0 *g* Voltage at X_{OUT}, Y_{OUT}	V_S = 3 V	1.3	1.5	1.7	V
0 *g* Voltage at Z_{OUT}	V_S = 3 V	1.2	1.5	1.8	V
0 *g* Offset vs. Temperature			±1		m*g*/°C
NOISE PERFORMANCE					
Noise Density X_{OUT}, Y_{OUT}, Z_{OUT}			250		µ*g*/√Hz rms
FREQUENCY RESPONSE[4]					
Bandwidth X_{OUT}, Y_{OUT}[5]	No external filter		1600		Hz
Bandwidth Z_{OUT}[5]	No external filter		550		Hz
R_{FILT} Tolerance			32 ± 15%		kΩ
Sensor Resonant Frequency			5.5		kHz
SELF TEST[6]					
Logic Input Low			+0.6		V
Logic Input High			+2.4		V
ST Actuation Current			+60		µA
Output Change at X_{OUT}	Self test 0 to 1	−210	−450	−850	mV
Output Change at Y_{OUT}	Self test 0 to 1	+210	+450	+850	mV
Output Change at Z_{OUT}	Self test 0 to 1	+210	+770	+1400	mV
OUTPUT AMPLIFIER					
Output Swing Low	No load		0.1		V
Output Swing High	No load		2.8		V
POWER SUPPLY					
Operating Voltage Range		1.8		3.6	V
Supply Current	V_S = 3 V		350		µA
Turn-On Time[7]	No external filter		1		ms
TEMPERATURE					
Operating Temperature Range		−40		+85	°C

[1] Defined as coupling between any two axes.
[2] Sensitivity is essentially ratiometric to V_S.
[3] Defined as the output change from ambient-to-maximum temperature or ambient-to-minimum temperature.
[4] Actual frequency response controlled by user-supplied external filter capacitors (C_X, C_Y, C_Z).
[5] Bandwidth with external capacitors = 1/(2 × π × 32 kΩ × C). For C_X, C_Y = 0.003 µF, bandwidth = 1.6 kHz. For C_Z = 0.01 µF, bandwidth = 500 Hz. For C_X, C_Y, C_Z = 10 µF, bandwidth = 0.5 Hz.
[6] Self test response changes cubically with V_S.
[7] Turn-on time is dependent on C_X, C_Y, C_Z and is approximately 160 × C_X or C_Y or C_Z + 1 ms, where C_X, C_Y, C_Z are in µF.

ABSOLUTE MAXIMUM RATINGS

Table 2.

Parameter	Rating
Acceleration (Any Axis, Unpowered)	10,000 *g*
Acceleration (Any Axis, Powered)	10,000 *g*
V_S	−0.3 V to +3.6 V
All Other Pins	(COM − 0.3 V) to (V_S + 0.3 V)
Output Short-Circuit Duration (Any Pin to Common)	Indefinite
Temperature Range (Powered)	−55°C to +125°C
Temperature Range (Storage)	−65°C to +150°C

Stresses above those listed under Absolute Maximum Ratings may cause permanent damage to the device. This is a stress rating only; functional operation of the device at these or any other conditions above those indicated in the operational section of this specification is not implied. Exposure to absolute maximum rating conditions for extended periods may affect device reliability.

ESD CAUTION

ESD (electrostatic discharge) sensitive device. Charged devices and circuit boards can discharge without detection. Although this product features patented or proprietary protection circuitry, damage may occur on devices subjected to high energy ESD. Therefore, proper ESD precautions should be taken to avoid performance degradation or loss of functionality.

PIN CONFIGURATION AND FUNCTION DESCRIPTIONS

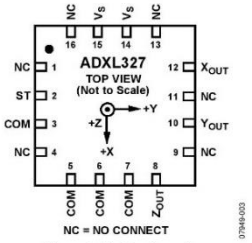

Figure 2. Pin Configuration

Table 3. Pin Function Descriptions

Pin No.	Mnemonic	Description
1	NC	No Connect (or Optionally Ground)
2	ST	Self Test
3	COM	Common
4	NC	No Connect
5	COM	Common
6	COM	Common
7	COM	Common
8	Z_{OUT}	Z Channel Output
9	NC	No Connect (or Optionally Ground)
10	Y_{OUT}	Y Channel Output
11	NC	No Connect
12	X_{OUT}	X Channel Output
13	NC	No Connect
14	V_S	Supply Voltage (1.8 V to 3.6 V)
15	V_S	Supply Voltage (1.8 V to 3.6 V)
16	NC	No Connect
EP	Exposed pad	Not internally connected. Solder for mechanical integrity.

TYPICAL PERFORMANCE CHARACTERISTICS

N > 1000 for all typical performance plots, unless otherwise noted.

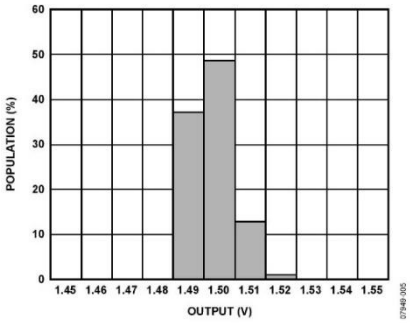

Figure 3. X-Axis Zero g Bias at 25°C, V_S = 3 V

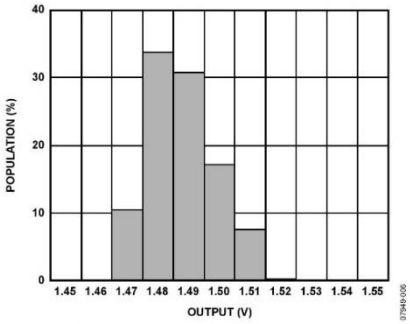

Figure 4. Y-Axis Zero g Bias at 25°C, V_S = 3 V

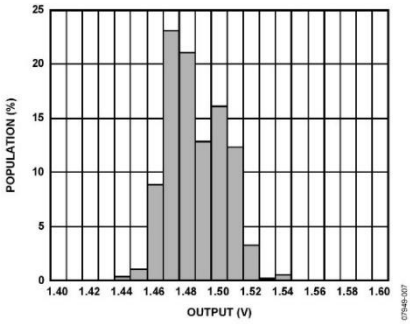

Figure 5. Z-Axis Zero g Bias at 25°C, V_S = 3 V

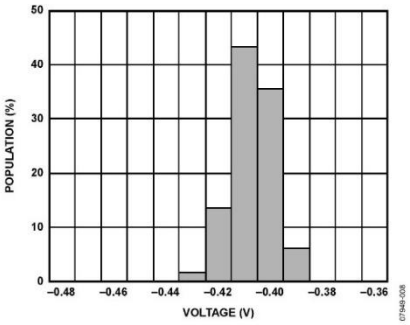

Figure 6. X-Axis Self Test Response at 25°C, V_S = 3 V

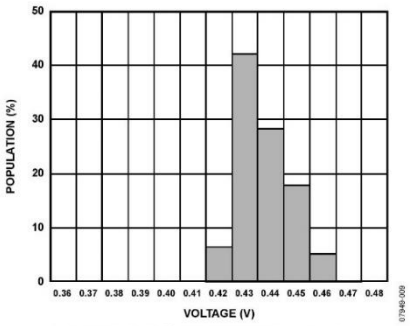

Figure 7. Y-Axis Self Test Response at 25°C, V_S = 3 V

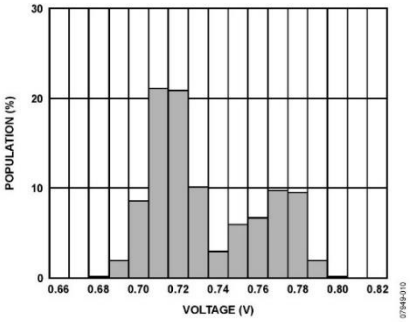

Figure 8. Z-Axis Self Test Response at 25°C, V_S = 3 V

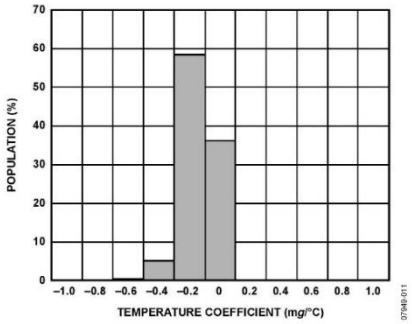

Figure 9. X-Axis Zero g Bias Temperature Coefficient, $V_S = 3$ V

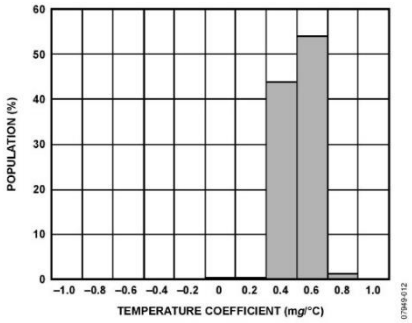

Figure 10. Y-Axis Zero g Bias Temperature Coefficient, $V_S = 3$ V

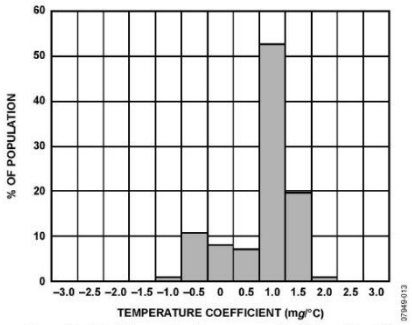

Figure 11. Z-Axis Zero g Bias Temperature Coefficient, $V_S = 3$ V

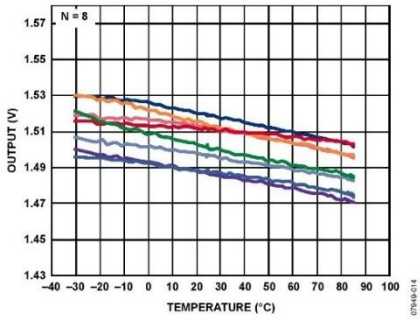

Figure 12. X-Axis Zero g Bias vs. Temperature, Eight Parts Soldered to PCB

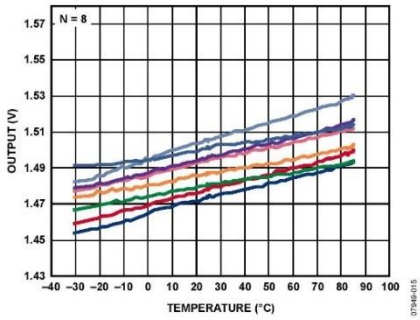

Figure 13. Y-Axis Zero g Bias vs. Temperature, Eight Parts Soldered to PCB

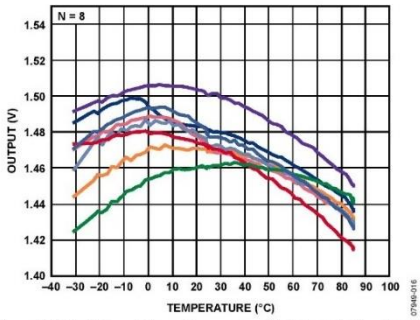

Figure 14. Z-Axis Zero g Bias vs. Temperature, Eight Parts Soldered to PCB

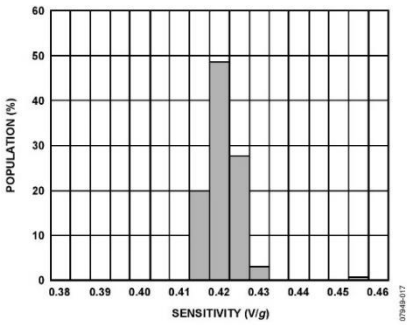

Figure 15. X-Axis Sensitivity at 25°C, V_S = 3 V

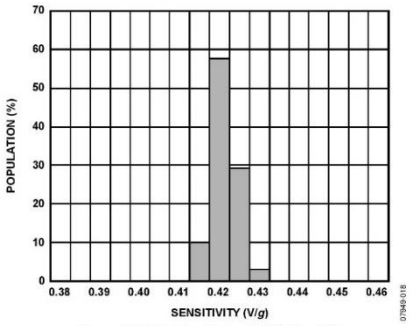

Figure 16. Y-Axis Sensitivity at 25°C, V_S = 3 V

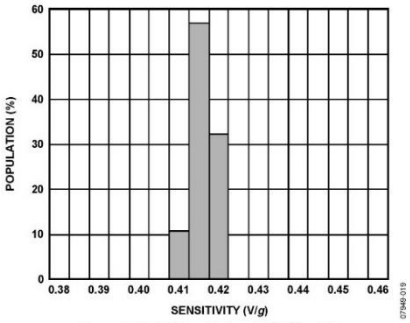

Figure 17. Z-Axis Sensitivity at 25°C, V_S = 3 V

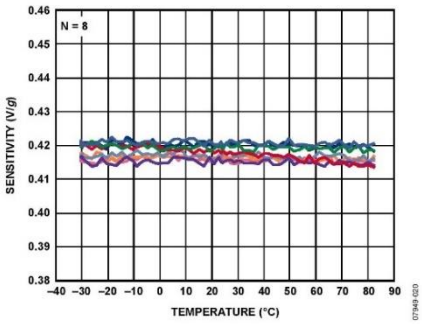

Figure 18. X-Axis Sensitivity vs. Temperature, Eight Parts Soldered to PCB, V_S = 3 V

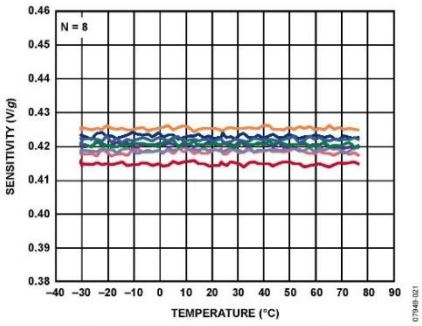

Figure 19. Y-Axis Sensitivity vs. Temperature, Eight Parts Soldered to PCB, V_S = 3 V

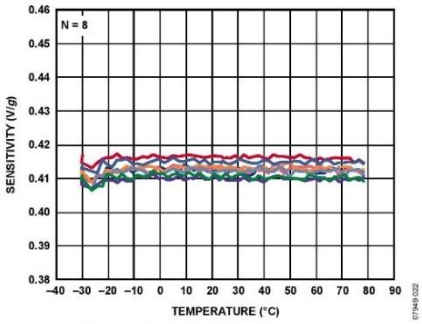

Figure 20. Z-Axis Sensitivity vs. Temperature, Eight Parts Soldered to PCB, V_S = 3 V

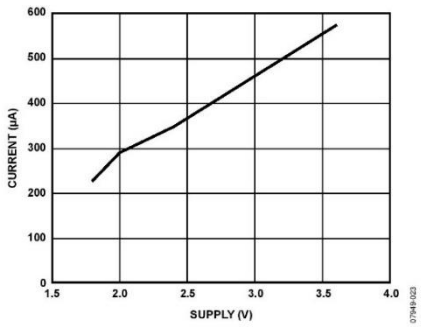

Figure 21. Typical Current Consumption vs. Supply Voltage

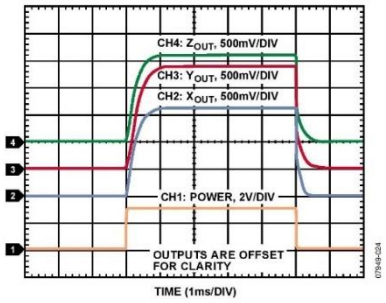

Figure 22. Typical Turn-On Time, $V_S = 3$ V
$C_X = C_Y = C_Z = 0.0047$ µF

THEORY OF OPERATION

The ADXL327 is a complete 3-axis acceleration measurement system. The ADXL327 has a measurement range of ±2 *g* minimum. It contains a polysilicon surface micromachined sensor and signal conditioning circuitry to implement an open-loop acceleration measurement architecture. The output signals are analog voltages that are proportional to acceleration. The accelerometer can measure the static acceleration of gravity in tilt sensing applications, as well as dynamic acceleration, resulting from motion, shock, or vibration.

The sensor is a polysilicon surface micromachined structure built on top of a silicon wafer. Polysilicon springs suspend the structure over the surface of the wafer and provide a resistance against acceleration forces. Deflection of the structure is measured using a differential capacitor that consists of independent fixed plates and plates attached to the moving mass. The fixed plates are driven by 180° out-of-phase square waves. Acceleration deflects the moving mass and unbalances the differential capacitor resulting in a sensor output whose amplitude is proportional to acceleration. Phase-sensitive demodulation techniques are then used to determine the magnitude and direction of the acceleration.

The demodulator output is amplified and brought off-chip through a 32 kΩ resistor. The user then sets the signal bandwidth of the device by adding a capacitor. This filtering improves measurement resolution and helps prevent aliasing.

MECHANICAL SENSOR

The ADXL327 uses a single structure for sensing the X, Y, and Z axes. As a result, the three axes sense directions are highly orthogonal with little cross-axis sensitivity. Mechanical misalignment of the sensor die to the package is the chief source of cross-axis sensitivity. Mechanical misalignment can, of course, be calibrated out at the system level.

PERFORMANCE

Rather than using additional temperature compensation circuitry, innovative design techniques ensure that high performance is built-in to the ADXL327. As a result, there is neither quantization error nor nonmonotonic behavior, and temperature hysteresis is very low (typically <3 m*g* over the −25°C to +70°C temperature range).

APPLICATIONS INFORMATION

POWER SUPPLY DECOUPLING

For most applications, a single 0.1 μF capacitor, C_{DC}, placed close to the ADXL327 supply pins adequately decouples the accelerometer from noise on the power supply. However, in applications where noise is present at the 50 kHz internal clock frequency (or any harmonic thereof), additional care in power supply bypassing is required because this noise can cause errors in acceleration measurement. If additional decoupling is needed, a 100 Ω (or smaller) resistor or ferrite bead can be inserted in the supply line. Additionally, a larger bulk bypass capacitor (1 μF or greater) can be added in parallel to C_{DC}. Ensure that the connection from the ADXL327 ground to the power supply ground is low impedance because noise transmitted through ground has a similar effect as noise transmitted through V_S.

SETTING THE BANDWIDTH USING C_X, C_Y, AND C_Z

The ADXL327 has provisions for band limiting the X_{OUT}, Y_{OUT}, and Z_{OUT} pins. Capacitors must be added at these pins to implement low-pass filtering for antialiasing and noise reduction. The 3 dB bandwidth equation is

$$f_{-3\,dB} = 1/(2\pi(32\ k\Omega) \times C_{(X,\,Y,\,Z)})$$

or more simply

$$f_{-3\,dB} = 5\ \mu F/C_{(X,\,Y,\,Z)}$$

The tolerance of the internal resistor (R_{FILT}) typically varies as much as ±15% of its nominal value (32 kΩ), and the bandwidth varies accordingly. A minimum capacitance of 0.0047 μF for C_X, C_Y, and C_Z is recommended in all cases.

Table 4. Filter Capacitor Selection, C_X, C_Y, and C_Z

Bandwidth (Hz)	Capacitor (μF)
1	4.7
10	0.47
50	0.10
100	0.05
200	0.027
500	0.01

SELF TEST

The ST pin controls the self test feature. When this pin is set to V_S, an electrostatic force is exerted on the accelerometer beam. The resulting movement of the beam allows the user to test whether the accelerometer is functional. The typical change in output is −1.08 *g* (corresponding to −450 mV) in the X axis, +1.08 *g* (+450 mV) on the Y axis, and +1.83 *g* (+770 mV) on the Z axis. This ST pin can be left open circuit or connected to common (COM) in normal use.

Never expose the ST pin to voltages greater than V_S + 0.3 V. If this cannot be guaranteed due to the system design (for instance, there are multiple supply voltages), then a low V_F clamping diode between ST and V_S is recommended.

DESIGN TRADE-OFFS FOR SELECTING FILTER CHARACTERISTICS: THE NOISE/BW TRADE-OFF

The selected accelerometer bandwidth ultimately determines the measurement resolution (smallest detectable acceleration). Filtering can be used to lower the noise floor to improve the resolution of the accelerometer. Resolution is dependent on the analog filter bandwidth at X_{OUT}, Y_{OUT}, and Z_{OUT}.

The output of the ADXL327 has a typical bandwidth greater than 500 Hz. The user must filter the signal at this point to limit aliasing errors. The analog bandwidth must be no more than half the analog-to-digital sampling frequency to minimize aliasing. The analog bandwidth can be further decreased to reduce noise and improve resolution.

The ADXL327 noise has the characteristics of white Gaussian noise, which contributes equally at all frequencies and is described in terms of μg/√Hz (the noise is proportional to the square root of the accelerometer bandwidth). The user should limit bandwidth to the lowest frequency needed by the application to maximize the resolution and dynamic range of the accelerometer.

With the single-pole roll-off characteristic, the typical noise of the ADXL327 is determined by

$$rms\ Noise = Noise\ Density \times (\sqrt{BW \times 1.6})$$

Often, the peak value of the noise is desired. Peak-to-peak noise can only be estimated by statistical methods. Table 5 is useful for estimating the probabilities of exceeding various peak values, given the rms value.

Table 5. Estimation of Peak-to-Peak Noise

Peak-to-Peak Value	% of Time That Noise Exceeds Nominal Peak-to-Peak Value
2 × rms	32
4 × rms	4.6
6 × rms	0.27
8 × rms	0.006

USE WITH OPERATING VOLTAGES OTHER THAN 3 V

The ADXL327 is tested and specified at V_S = 3 V; however, it can be powered with V_S as low as 1.8 V or as high as 3.6 V. Note that some performance parameters change as the supply voltage is varied.

The ADXL327 output is ratiometric; therefore, the output sensitivity (or scale factor) varies proportionally to the supply voltage. At V_S = 3.6 V, the output sensitivity is typically 500 mV/*g*. At V_S = 2 V, the output sensitivity is typically 289 mV/*g*.

The zero *g* bias output is also ratiometric; therefore, the zero *g* output is nominally equal to V_S/2 at all supply voltages.

The output noise is not ratiometric but is absolute in volts; therefore, the noise density decreases as the supply voltage increases. This is because the scale factor (mV/*g*) increases while the noise voltage remains constant. At V_S = 3.6 V, the X- and Y-axis noise density is typically 200 μg/√Hz, while at V_S = 2 V, the X- and Y-axis noise density is typically 300 μg/√Hz.

Self test response in *g* is roughly proportional to the square of the supply voltage. However, when ratiometricity of sensitivity is factored in with supply voltage, the self test response in volts is roughly proportional to the cube of the supply voltage.

For example, at V_S = 3.6 V, the self test response for the ADXL327 is approximately −780 mV for the X axis, +780 mV for the Y axis, and +1330 mV for the Z axis. At V_S = 2 V, the self test response is approximately −130 mV for the X axis, +130 mV for the Y axis, and −220 mV for the Z axis.

The supply current decreases as the supply voltage decreases. Typical current consumption at V_S = 3.6 V is 375 μA, and typical current consumption at V_S = 2 V is 300 μA.

AXES OF ACCELERATION SENSITIVITY

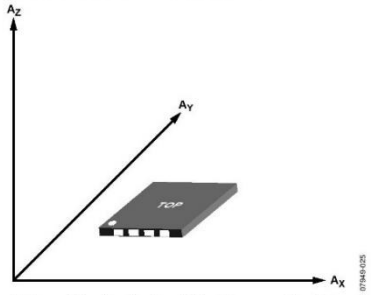

Figure 23. Axes of Acceleration Sensitivity (Corresponding Output Voltage Increases When Accelerated Along the Sensitive Axis)

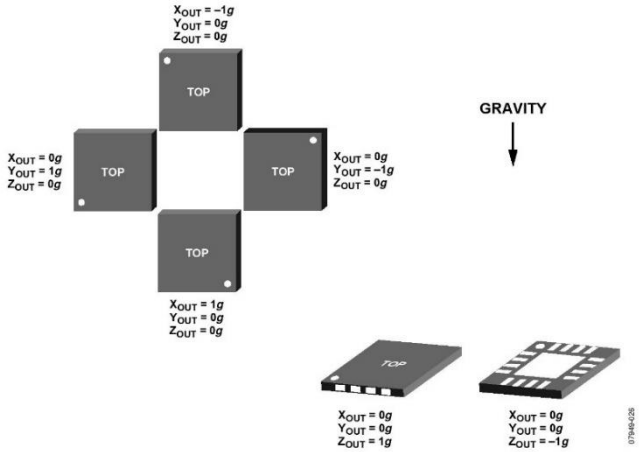

Figure 24. Output Response vs. Orientation to Gravity

LAYOUT AND DESIGN RECOMMENDATIONS

The recommended soldering profile is shown in Figure 25, followed by a description of the profile features in Table 6. The recommended PCB layout or solder land drawing is shown in Figure 26.

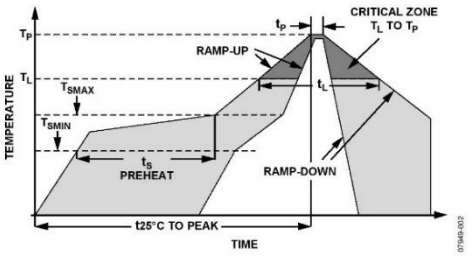

Figure 25. Recommended Soldering Profile

Table 6. Recommended Soldering Profile

Profile Feature	Sn63/Pb37	Pb-Free
Average Ramp Rate (T_L to T_P)	3°C/sec maximum	3°C/sec maximum
Preheat		
Minimum Temperature (T_{SMIN})	100°C	150°C
Maximum Temperature (T_{SMAX})	150°C	200°C
Time (T_{SMIN} to T_{SMAX}), t_S	60 sec to 120 sec	60 sec to 180 sec
T_{SMAX} to T_L		
Ramp-Up Rate	3°C/sec maximum	3°C/sec maximum
Time Maintained Above Liquidous (T_L)		
Liquidous Temperature (T_L)	183°C	217°C
Time (t_L)	60 sec to 150 sec	60 sec to 150 sec
Peak Temperature (T_P)	240°C + 0°C/−5°C	260°C + 0°C/−5°C
Time Within 5°C of Actual Peak Temperature (t_P)	10 sec to 30 sec	20 sec to 40 sec
Ramp-Down Rate	6°C/sec maximum	6°C/sec maximum
Time 25°C to Peak Temperature	6 minutes maximum	8 minutes maximum

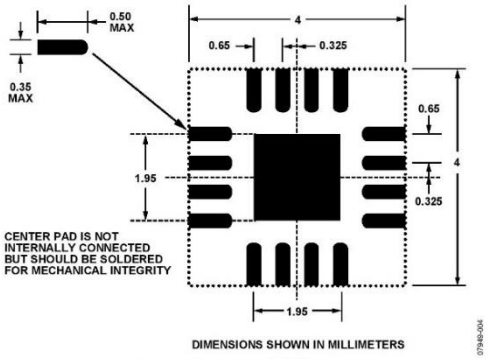

Figure 26. Recommended PCB Layout

OUTLINE DIMENSIONS

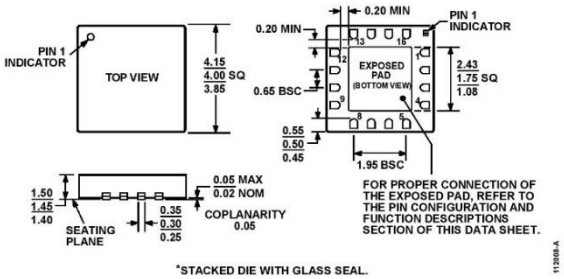

Figure 27. 16-Lead Lead Frame Chip Scale Package [LFCSP_LQ]
4 mm × 4 mm Body, 1.45 mm Thick Quad
(CP-16-5a)*
Dimensions shown in millimeters

ORDERING GUIDE

Model	Measurement Range	Specified Voltage	Temperature Range	Package Description	Package Option
ADXL327BCPZ[1]	±2 *g*	3 V	−40°C to +85°C	16-Lead LFCSP_LQ	CP-16-5a
ADXL327BCPZ–RL[1]	±2 *g*	3 V	−40°C to +85°C	16-Lead LFCSP_LQ	CP-16-5a
ADXL327BCPZ–RL7[1]	±2 *g*	3 V	−40°C to +85°C	16-Lead LFCSP_LQ	CP-16-5a
EVAL-ADXL327Z[1]				Evaluation Board	

[1] Z = RoHS Compliant Part.

APPENDIX H

ACCELEROMETER CDAQ DATA SHEETS

The following pages show the specifications sheet for the cDAQ used to record send accelerometer readings to LabView. This specifications sheet is generic for the model of cDAQ and not specific to the individual unit.

SPECIFICATIONS

NI cDAQ™-9188

8-Slot, Ethernet CompactDAQ Chassis

Definitions

Warranted specifications describe the performance of a model under stated operating conditions and are covered by the model warranty.

Characteristics describe values that are relevant to the use of the model under stated operating conditions but are not covered by the model warranty.

- *Typical* specifications describe the expected performance met by a majority of the models.
- *Nominal* specifications describe parameters and attributes that may be useful in operation.

Specifications are *Typical* unless otherwise noted.

Conditions

Specifications are valid at 25 °C unless otherwise noted.

Analog Input

Input FIFO size	127 samples per slot
Maximum sample rate[1]	Determined by the C Series module or modules
Timing accuracy[2]	50 ppm of sample rate
Timing resolution[2]	12.5 ns
Number of channels supported	Determined by the C Series module or modules

[1] Performance dependent on type of installed C Series module and number of channels in the task.
[2] Does not include group delay. For more information, refer to the documentation for each C Series module.

Analog Output

Number of channels supported	
Hardware-timed task	
Onboard regeneration	16
Non-regeneration	Determined by the C Series module or modules
Non-hardware-timed task	Determined by the C Series module or modules
Maximum update rate	
Onboard regeneration	1.6 MS/s (multi-channel, aggregate)
Non-regeneration	Determined by the C Series module or modules
Timing accuracy	50 ppm of sample rate
Timing resolution	12.5 ns
Output FIFO size	
Onboard regeneration	8,191 samples shared among channels used
Non-regeneration	127 samples per slot
AO waveform modes	Non-periodic waveform, periodic waveform regeneration mode from onboard memory, periodic waveform regeneration from host buffer including dynamic update

Digital Waveform Characteristics

Waveform acquisition (DI) FIFO	
Parallel modules	511 samples per slot
Serial modules	63 samples per slot
Waveform generation (DO) FIFO	
Parallel modules	
Slots 1 to 4	2,047 samples per slot
Slots 5 to 8	1,023 samples per slot

Serial modules	63 samples per slot

Note When parallel modules in a digital task are in slots 1 through 4, FIFO is 2,047 samples per slot for all slots. When any parallel module in a digital task is in slots 5 through 8, FIFO is 1,023 samples per slot for all eight slots.

Digital input sample clock frequency	
Streaming to application memory	System-dependent
Finite	0 MHz to 10 MHz
Digital output sample clock frequency	
Streaming from application memory	System-dependent
Regeneration from FIFO	0 MHz to 10 MHz
Finite	0 MHz to 10 MHz
Timing accuracy	50 ppm

General-Purpose Counters/Timers

Number of counters/timers	4
Resolution	32 bits
Counter measurements	Edge counting, pulse, semi-period, period, two-edge separation, pulse width
Position measurements	X1, X2, X4 quadrature encoding with Channel Z reloading; two-pulse encoding
Output applications	Pulse, pulse train with dynamic updates, frequency division, equivalent time sampling
Internal base clocks	80 MHz, 20 MHz, 100 kHz
External base clock frequency	0 MHz to 20 MHz
Base clock accuracy	50 ppm
Output frequency	0 MHz to 20 MHz
Inputs	Gate, Source, HW_Arm, Aux, A, B, Z, Up_Down
Routing options for inputs	Any module PFI, chassis PFI, analog trigger, many internal signals
FIFO	Dedicated 127-sample FIFO

Frequency Generator

Number of channels	1
Base clocks	20 MHz, 10 MHz, 100 kHz
Divisors	1 to 16 (integers)
Base clock accuracy	50 ppm
Output	Any chassis PFI or module PFI terminal

Module PFI Characteristics

Functionality	Static digital input, static digital output, timing input, and timing output
Timing output sources[3]	Many analog input, analog output, counter, digital input, and digital output timing signals
Timing input frequency	0 MHz to 20 MHz
Timing output frequency	0 MHz to 20 MHz

Chassis PFI Characteristics

Maximum input or output frequency	1 MHz
Cable length	3 m (10 ft)
Cable impedance	50 Ω
PFI 0, PFI 1 connectors	BNC
Power-on state	High impedance

[3] Actual available signals are dependent on type of installed C Series module.

Table 1. Input/Output Voltage Protection

Voltage	Minimum	Maximum
Input	-20 V	25 V
Output	-15 V	20 V

Maximum operating conditions[4]	
I_{OL} output low current	8 mA maximum
I_{OH} output high current	-8 mA maximum

Table 2. DC Input Characteristics

Voltage	Minimum	Maximum
Positive going threshold	1.43 V	2.28 V
Negative going threshold	0.86 V	1.53 V
Hysteresis	0.48 V	0.87 V

Table 3. DC Output Characteristics

Voltage	Conditions	Minimum	Maximum
High	—	—	5.25 V
	Sourcing 100 µA	4.65 V	—
	Sourcing 2 mA	3.60 V	—
	Sourcing 3.5 mA	3.44 V	—
Low	Sinking 100 µA	—	0.10 V
	Sinking 2 mA	—	0.64 V
	Sinking 3.5 mA	—	0.80 V

Digital Triggers

Source	Any chassis PFI or module PFI terminal
Polarity	Software-selectable for most signals

[4] Stresses beyond those listed under *Maximum operating conditions* may cause permanent damage to the chassis.

Analog input function	Start Trigger, Reference Trigger, Pause Trigger, Sample Clock, Sample Clock Timebase
Analog output function	Start Trigger, Pause Trigger, Sample Clock, Sample Clock Timebase
Counter/timer function	Gate, Source, HW_Arm, Aux, A, B, Z, Up_Down

Module I/O States

At power-on	Module-dependent. Refer to the documentation for each C Series module.

Network Interface

Network protocols	TCP/IP, UDP
Network ports used	HTTP:80 (configuration only), TCP:3580; UDP:5353 (configuration only), TCP:5353 (configuration only); TCP:31415; UDP:7865 (configuration only), UDP:8473 (configuration only)
Network IP configuration	DHCP + Link-Local, DHCP, Static, Link-Local
High-performance data streams	7
Data stream types available	Analog input, analog output, digital input, digital output, counter/timer input, counter/timer output, NI-XNET[5]
Default MTU size	1500 bytes
Jumbo frame support	Up to 9000 bytes

[5] When a session is active, CAN or LIN (NI-XNET) C Series modules use a total of two data streams regardless of the number of NI-XNET modules in the chassis.

Ethernet

Network interface	1000 Base-TX, full-duplex; 1000 Base-TX, half-duplex; 100 Base-TX, full-duplex; 100 Base-TX, half-duplex; 10 Base-T, full-duplex; 10 Base-T, half-duplex
Communication rates	10/100/1000 Mbps, auto-negotiated
Maximum cabling distance	100 m/segment

Power Requirements

Caution The protection provided by the NI cDAQ-9188 chassis can be impaired if it is used in a manner not described in the *NI cDAQ-9181/9184/9188/9191 User Manual*.

Note Some C Series modules have additional power requirements. For more information about C Series module power requirements, refer to the documentation for each C Series module.

Note Sleep mode for C Series modules is not supported in the NI cDAQ-9188.

Voltage input range	9 V to 30 V
Maximum power consumption[6]	15 W

Note The maximum power consumption specification is based on a fully populated system running a high-stress application at elevated ambient temperature and with all C Series modules consuming the maximum allowed power.

Power input connector	2 positions 3.5 mm pitch mini-combicon screw terminal with screw flanges, Sauro CTMH020F8-0N002
Power input mating connector	Sauro CTF020V8, Phoenix Contact 1714977, or equivalent

[6] Includes maximum 1 W module load per slot across rated temperature and product variations.

Physical Characteristics

Weight (unloaded)	Approximately 900 g (31.7 oz)
Dimensions (unloaded)	254.0 mm × 88.1 mm × 58.9 mm (10.00 in. × 3.47 in. × 2.32 in.) Refer to the following figure.
Screw-terminal wiring	
Gauge	0.5 mm^2 to 2.1 mm^2 (20 AWG to 14 AWG) copper conductor wire
Wire strip length	6 mm (0.24 in.) of insulation stripped from the end
Temperature rating	85 °C
Torque for screw terminals	0.20 N · m to 0.25 N · m (1.8 lb · in. to 2.2 lb · in.)
Wires per screw terminal	One wire per screw terminal
Connector securement	
Securement type	Screw flanges provided
Torque for screw flanges	0.20 N · m to 0.25 N · m (1.8 lb · in. to 2.2 lb · in.)

If you need to clean the chassis, wipe it with a dry towel.

Figure 1. NI cDAQ-9188 Dimensions

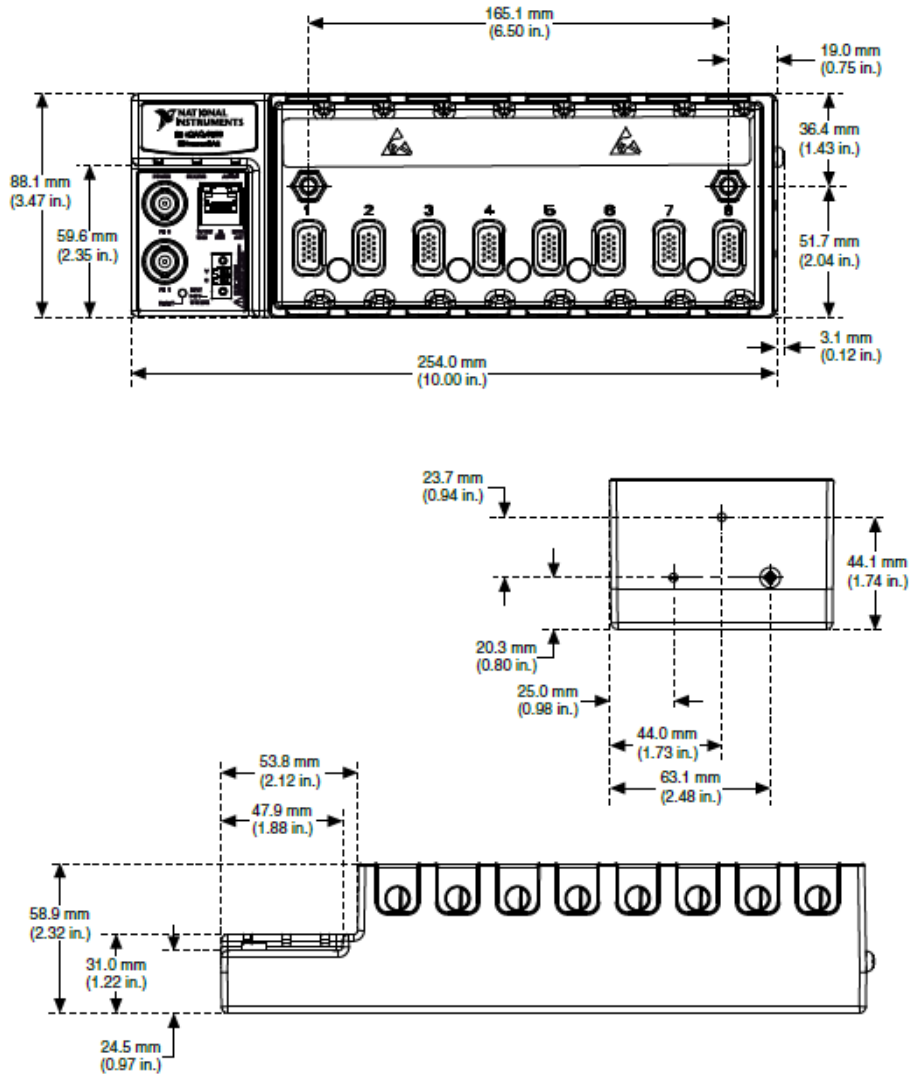

Safety Voltages

Connect only voltages that are within these limits.

V terminal to C terminal	30 V maximum, Measurement Category I

Measurement Category I is for measurements performed on circuits not directly connected to the electrical distribution system referred to as MAINS voltage. MAINS is a hazardous live electrical supply system that powers equipment. This category is for measurements of voltages from specially protected secondary circuits. Such voltage measurements include signal levels, special equipment, limited-energy parts of equipment, circuits powered by regulated low-voltage sources, and electronics.

Caution Do not connect the system to signals or use for measurements within Measurement Categories II, III, or IV.

Note Measurement Categories CAT I and CAT O (Other) are equivalent. These test and measurement circuits are not intended for direct connection to the MAINs building installations of Measurement Categories CAT II, CAT III, or CAT IV.

Environmental

Operating temperature (IEC 60068-2-1 and IEC 60068-2-2)	-20 °C to 55 °C[7]

Caution To maintain product performance and accuracy specifications when the ambient temperature is between 45 and 55 °C, you must mount the chassis horizontally to a metal panel or surface using the screw holes or the panel mount kit. Measure the ambient temperature at each side of the CompactDAQ system 63.5 mm (2.5 in.) from the side and 25.4 mm (1.0 in.) from the rear cover of the system. For further information about mounting configurations, go to `ni.com/info` and enter the Info Code `cdaqmounting`.

Storage temperature (IEC 60068-2-1 and IEC 60068-2-2)	-40 °C to 85 °C
Ingress protection	IP 30
Operating humidity (IEC 60068-2-56)	10% to 90% RH, noncondensing
Storage humidity (IEC 60068-2-56)	5% to 95% RH, noncondensing
Pollution Degree (IEC 60664)	2
Maximum altitude	5,000 m

Indoor use only.

[7] When operating the NI cDAQ-9188 in temperatures below 0 °C, you must use the PS-15 power supply or another power supply rated for below 0 °C.

Hazardous Locations

U.S. (UL)	Class I, Division 2, Groups A, B, C, D, T4; Class I, Zone 2, AEx nA IIC T4
Canada (C-UL)	Class I, Division 2, Groups A, B, C, D, T4; Class I, Zone 2, Ex nA IIC T4
Europe (ATEX) and International (IECEx)	Ex nA IIC T4 Gc

Shock and Vibration

To meet these specifications, you must direct mount the NI cDAQ-9188 system and affix ferrules to the ends of the terminal lines.

Operational shock	30 g peak, half-sine, 11 ms pulse (Tested in accordance with IEC 60068-2-27. Test profile developed in accordance with MIL-PRF-28800F.)
Random vibration	
Operating	5 Hz to 500 Hz, 0.3 g_{rms}
Non-operating	5 Hz to 500 Hz, 2.4 g_{rms} (Tested in accordance with IEC 60068-2-64. Non-operating test profile exceeds the requirements of MIL PRF-28800F, Class 3.)

Safety and Hazardous Locations Standards

This product is designed to meet the requirements of the following electrical equipment safety standards for measurement, control, and laboratory use:

- IEC 61010-1, EN 61010-1
- UL 61010-1, CSA C22.2 No. 61010-1
- EN 60079-0:2012, EN 60079-15:2010
- IEC 60079-0: Ed 6, IEC 60079-15; Ed 4
- UL 60079-0; Ed 6, UL 60079-15; Ed 4
- CSA 60079-0:2011, CSA 60079-15:2012

Note For UL and other safety certifications, refer to the product label or the *Online Product Certification* section.

Electromagnetic Compatibility

This product meets the requirements of the following EMC standards for electrical equipment for measurement, control, and laboratory use:

- EN 61326-1 (IEC 61326-1): Class A emissions; Basic immunity
- EN 55011 (CISPR 11): Group 1, Class A emissions
- EN 55022 (CISPR 22): Class A emissions
- EN 55024 (CISPR 24): Immunity
- AS/NZS CISPR 11: Group 1, Class A emissions
- AS/NZS CISPR 22: Class A emissions
- FCC 47 CFR Part 15B: Class A emissions
- ICES-001: Class A emissions

Note In the United States (per FCC 47 CFR), Class A equipment is intended for use in commercial, light-industrial, and heavy-industrial locations. In Europe, Canada, Australia and New Zealand (per CISPR 11) Class A equipment is intended for use only in heavy-industrial locations.

Note Group 1 equipment (per CISPR 11) is any industrial, scientific, or medical equipment that does not intentionally generate radio frequency energy for the treatment of material or inspection/analysis purposes.

Note For EMC declarations and certifications, and additional information, refer to the *Online Product Certification* section.

CE Compliance CE

This product meets the essential requirements of applicable European Directives, as follows:

- 2014/35/EU; Low-Voltage Directive (safety)
- 2014/30/EU; Electromagnetic Compatibility Directive (EMC)
- 2014/34/EU; Potentially Explosive Atmospheres (ATEX)

Online Product Certification

Refer to the product Declaration of Conformity (DoC) for additional regulatory compliance information. To obtain product certifications and the DoC for this product, visit *ni.com/certification*, search by model number or product line, and click the appropriate link in the Certification column.

Environmental Management

NI is committed to designing and manufacturing products in an environmentally responsible manner. NI recognizes that eliminating certain hazardous substances from our products is beneficial to the environment and to NI customers.

For additional environmental information, refer to the *Minimize Our Environmental Impact* web page at *ni.com/environment*. This page contains the environmental regulations and directives with which NI complies, as well as other environmental information not included in this document.

Waste Electrical and Electronic Equipment (WEEE)

EU Customers At the end of the product life cycle, all NI products must be disposed of according to local laws and regulations. For more information about how to recycle NI products in your region, visit *ni.com/environment/weee*.

电子信息产品污染控制管理办法（中国 RoHS）

中国客户 National Instruments 符合中国电子信息产品中限制使用某些有害物质指令(RoHS)。关于 National Instruments 中国 RoHS 合规性信息，请登录 `ni.com/environment/rohs_china`。(For information about China RoHS compliance, go to `ni.com/environment/rohs_china`.)

Information is subject to change without notice. Refer to the *NI Trademarks and Logo Guidelines* at `ni.com/trademarks` for information on NI trademarks. Other product and company names mentioned herein are trademarks or trade names of their respective companies. For patents covering NI products/technology, refer to the appropriate location: **Help»Patents** in your software, the `patents.txt` file on your media, or the *National Instruments Patent Notice* at `ni.com/patents`. You can find information about end-user license agreements (EULAs) and third-party legal notices in the readme file for your NI product. Refer to the *Export Compliance Information* at `ni.com/legal/export-compliance` for the NI global trade compliance policy and how to obtain relevant HTS codes, ECCNs, and other import/export data. NI MAKES NO EXPRESS OR IMPLIED WARRANTIES AS TO THE ACCURACY OF THE INFORMATION CONTAINED HEREIN AND SHALL NOT BE LIABLE FOR ANY ERRORS. U.S. Government Customers: The data contained in this manual was developed at private expense and is subject to the applicable limited rights and restricted data rights as set forth in FAR 52.227-14, DFAR 252.227-7014, and DFAR 252.227-7015.

© 2013—2017 National Instruments. All rights reserved.

370086C-01 March 17, 2017

APPENDIX I

PROFILOMETER DATA PROCESSING

Profilometer data was recorded through photographs and post-processed using these photos.

For each profilometer reading, the clearest picture of this reading was selected. The vertical position of each individual profilometer pole was recorded. The position was determined by identifying at which colored stripe on each pole the profilometer's metal crossbar was positioned. Each colored stripe is approximately 1 cm tall, and poles are spaced at approximately 2 cm center-to-center. Figure I.1 shows this process.

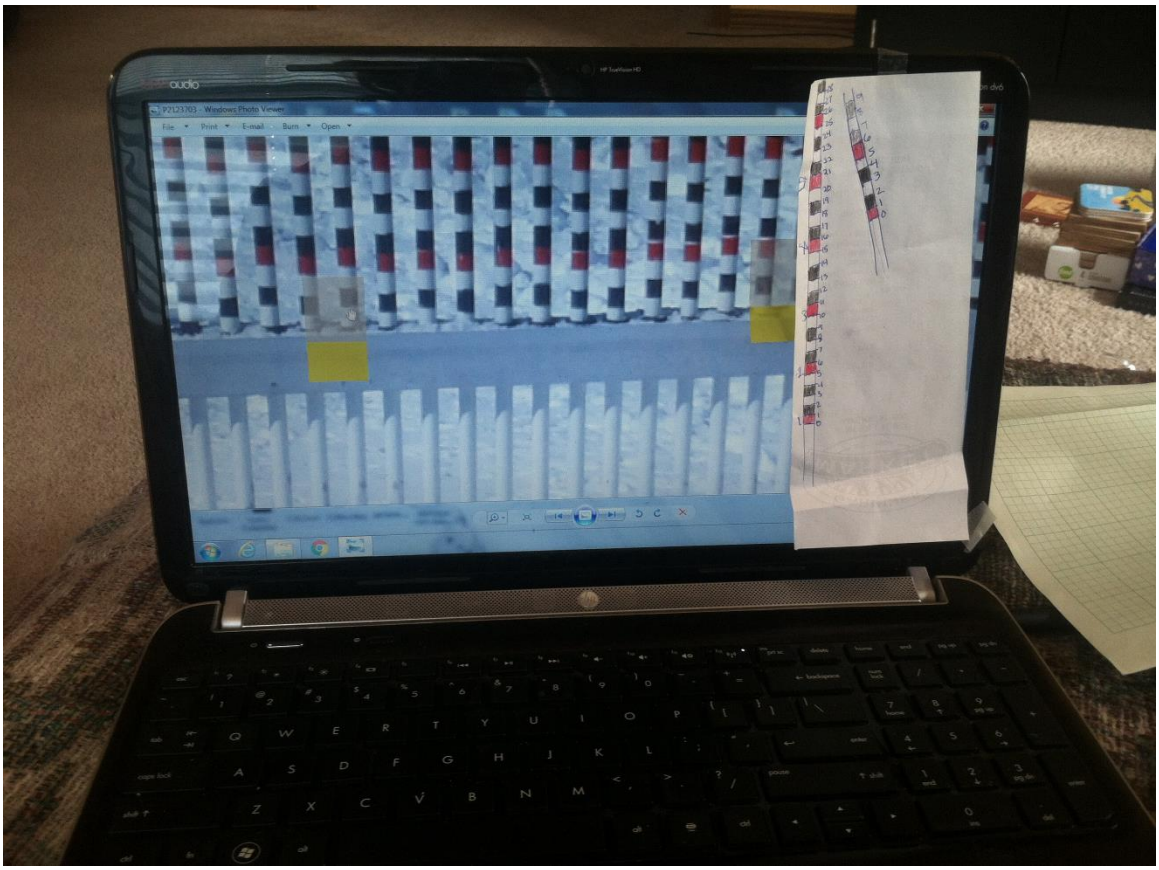

Figure I.1. Profilometer picture processing

To determine whether each pole's position indicated a level above, below, or even with the flat road surface, the photo was examined and poles outside of the area affected by the vehicle passage were identified. The vertical positions of these poles were then assumed to represent the flat road baseline that would be represented by entire profile if the vehicle had not passed. The positions of these "baseline" poles were then plotted together in Excel, and a best-fit linear equation was determined. This linear equation represented the untouched, flat road surface. Finding this line rather than just averaging the vertical positions of the baseline poles helped to correct for any accidental tilt of the profilometer, as no level was used when it was positioned.

After a baseline profile had been established, the theoretical baseline vertical position for all poles was determined based on their horizontal positions along the profiometer. The actual vertical position of all of the poles was then compared with the theoretical vertical position. This comparison showed whether the vehicle passage had caused the road surface to lower (a rut) or raise (a windrow, generally next to the rut). This difference could be quantified in cm, and then multiplied by 2 cm (the width between poles) to show the approximate area represented by this change.

Using this method, the area displaced by vehicle pass-bys could be quantified. Area displaced both below and above the baseline road surface was computed, and were totaled to give the "total area displaced" number used in the results of this study.